The control of transpiration in olive and almond: mechanisms under drought conditions

Celia M. Rodríguez Domínguez

Universidad de Sevilla

Facultad de Biología

Departamento de Biología Vegetal y Ecología

Tesis Doctoral / PhD Thesis

THE CONTROL OF TRANSPIRATION IN OLIVE AND

ALMOND: MECHANISMS UNDER DROUGHT CONDITIONS

Dña. Celia M. Rodríguez Domínguez

Directores

Dr. Alfonso de Cires Segura

Profesor Titular de Universidad de Sevilla

Dpto. Biología Vegetal y Ecología

Dr. Antonio Díaz Espejo

Científico Titular del CSIC

Instituto de Recursos Naturales

y Agrobiología de Sevilla (IRNAS)

Universidad de Sevilla

Facultad de Biología

Departamento de Biología Vegetal y Ecología

Tesis Doctoral / PhD Thesis

THE CONTROL OF TRANSPIRATION IN OLIVE AND ALMOND: MECHANISMS UNDER DROUGHT CONDITIONS

Tesis Doctoral presentada por Dña. Celia M. Rodríguez Domínguez, en satisfacción de los requisitos necesarios para optar al grado de Doctora por la Universidad de Sevilla, bajo la dirección y tutorización de

Directores

Dr. Alfonso de Cires Segura

Profesor Titular de Universidad de Sevilla

Dpto. Biología Vegetal y Ecología

Dr. Antonio Díaz Espejo

Científico Titular del CSIC

Instituto de Recursos Naturales

y Agrobiología de Sevilla (IRNAS)

Tutora

Doctoranda

Dra. Elena Fernández Boy

Profesora Titular de Universidad de Sevilla

Dpto. Cristalografía, Mineralogía y Química Agrícola

Dña. Celia M. Rodríguez Domínguez

NOTA: Según la Normativa vigente en la Universidad de Sevilla a 10 de abril de 2014 para optar a la Mención Internacional del Título de Doctor (Acuerdo 9.1/CG- 19-4-2012), aunque la presente Tesis será escrita en su totalidad en inglés, el resumen (p. 29) y las conclusiones (p. 205) serán también redactados en español.

A mis padres

Contents

Figures

Tables

Most used abbreviations and symbols

Symbol or Abbreviation	Description	Units
ABA	Abscisic acid	-
A_L	Leaf area	m^{-2} tree^{-1}
A_N	Net CO_2 assimilation rate	$\mu mol\ m^{-2}\ s^{-1}$
A_R	Root area	m^2 tree^{-1}
c_a	Ambient CO_2 concentration	$\mu mol\ mol^{-1}$
c_i	Intercellular CO_2 concentration	$\mu mol\ mol^{-1}$
D_a	Air vapor pressure deficit	kPa
DI	Deficit irrigation	-
DOY	Day of year	-
E	Leaf transpiration rate	mmol H_2O $m^{-2}\ s^{-1}$
E_p	Plant transpiration per leaf area	mmol $m^{-2}\ s^{-1}$
ET_c	Crop evapotranspiration	mm
ET_o	Potential evapotranspiration	mm
F_a	Attenuation factor of the leaf transfer function	-
g_c	Canopy conductance	mol $m^{-2}\ s^{-1}$
GCM	General circulation model	-
g_m	Mesophyll conductance to CO_2	mol $m^{-2}\ s^{-1}$
g_s	Stomatal conductance	mol $m^{-2}\ s^{-1}$
HPV	Heat-pulse velocity	-
IA	Irrigation amounts	L tree^{-1} day^{-1}
IN	Irrigation needs	mm
J_{max}	Maximum potential electron transport rate	$\mu mol\ m^{-2}\ s^{-1}$
K	Leaf-specific hydraulic conductance	mmol $m^{-2}\ s^{-1}$ MPa^{-1}
K_c	Crop coefficient	-
K_r	Reduction coefficient related to the percentage of ground covered by the crop	-
LAI	Leaf area index	m^2 leaf area m^{-2} ground

		area
m	Epidermal mechanical advantage	-
M	Net epidermal mechanical advantage	-
P	Precipitation	mm
P_c	Leaf turgor pressure	kPa
P_{clamp}	External clamp pressure	kPa
P_e	Epidermal turgor pressure	MPa
P_g	Guard cell turgor pressure	MPa
PLC	Percentage loss of conductivity	%
P_p	Leaf patch output pressure	kPa
PPFD	Photosynthetic photon flux density	$\mu mol\ m^{-2}\ s^{-1}$
Q	Sap flux in the trunk	$L\ h^{-1}$
R_d	Non-photorespiratory CO_2 release	$\mu mol\ m^{-2}\ s^{-1}$
RDI	Regulated deficit irrigation	-
RLD	Root length density	$cm\ cm^{-3}$
R_p or R	Plant hydraulic resistance	$MPa\ mmol^{-1}$ $m^2\ s$
R_s	Solar global radiation	$W\ m^{-2}$
SF	Sap flow	-
SWC	Soil water content	$m^3\ H_2O\ m^{-3}$ soil
T_a	Air temperature	ºC
TDV	Trunk diameter variation	-
T_l	Leaf temperature	°C
$V_{c,max}$	Maximum carboxylation rate	$\mu mol\ m^{-2}\ s^{-1}$
VPD	Air vapor pressure deficit	kPa
Δw	Leaf-air H_2O mole fraction gradient	$mmol\ mol^{-1}$
Γ^*	Photorespiratory CO_2 compensation point	$\mu mol\ mol^{-1}$
Ψ_e	Epidermal water potential	$-MPa$
Ψ_g	Guard cell water potential	$-MPa$
Ψ_{leaf}	Leaf water potential	$-MPa$
Ψ_{md}	Leaf water potential at midday	$-MPa$
Ψ_{pd}	Leaf water potential at predawn	$-MPa$

Ψ_s	Soil water potential	$-$MPa
Ψ_{stem}	Stem water potential at midday	$-$MPa
α	Guard cell advantage	-
β	Hydromechanical/biochemical response parameter	[mmol ATP m^{-2}]$^{-1}$
χ	Turgor-to-conductance scaling factor	mol air m^{-2} s^{-1} MPa^{-1}
π	Bulk leaf osmotic pressure	MPa
π_d	Leaf osmotic pressure at dawn	MPa
π_e	Epidermal osmotic pressure	MPa
π_g	Guard cell osmotic pressure	MPa
θ_v	Volumetric soil water content	m^3 H$_2$O m^{-3} soil
τ	ATP concentration in photosynthesising cells	mmol ATP m^{-2}

Chapter 1

Introduction,

Summary

and

Objectives

Stomatal key role in the control of transpiration

The balance among uptake, transport and water release in the leaf was an essential event that the early land plants, *ca.* 400 million years ago, learned to control. The transition to the terrestrial life represented one of the greatest challenges for plant survival in particular and life evolution in general. Basal land non-vascular plant groups (liverworts) were astomatous, they do not possess true stomata, but their gametophyte presented air pores to take up CO_2 from the high-saturated atmosphere (Graham *et al.*, 1995; Rudall *et al.*, 2013). Still, these tiny pores were not able to regulate the equilibrium between water loss and carbon gain, necessary for photosynthetic functioning, and then, restricting their habitats (Woodward, 1998). The origin of stomata allowed early land non-vascular plants (mosses) to regulate transpirational water loss during taking up the essential substrate for photosynthesis. Stomatal regulation became progressively more effective as hydraulic systems and development of rhizoids and roots evolved in vascular and seed plant lineages. The early-diverging vascular plants presented simpler stomatal control than seed plants (Brodribb & McAdam, 2011). Many different signals, from intracellular to environmental, are involved in the response of a still poorly understood stomatal physiology. The interaction between passive and active processes in the stomatal behavior as regulators of leaf water balance is one of the main reasons of the high stomatal control complexity in seed plants (Buckley *et al.*, 2003; Buckley, 2005). Active processes are highly sensitive to the phytohormone abscisic acid (Brodribb & McAdam, 2011) that seems to be a transition from passive control of leaf hydration after the divergence of ferns (McAdam & Brodribb, 2012). This stomatal evolution enabled seed plants to rise and colonize a wider range of terrestrial habitats in the planet. Furthermore, this event makes stomata, through controlling transpiration, the major gates for carbon and water balance of the plant and global scales (Hetherington & Woodward, 2003).

Stomata are minute pores mainly located in the lower epidermis of the leaves (abaxial surface) and bounded by a pair of specialized guard cells. These guard cells play a vital role by regulating the opening and closing of the stomata through increasing or declining, respectively, their turgor pressures. This dynamic gas exchange between the leaves and the atmosphere represents a key process for CO_2 and water fluxes, and is strongly linked with plant productivity since stomata control transpiration and photosynthetic CO_2 uptake (Jones & Tardieu, 1998). Environmental factors such as light intensity and quality, temperature, water vapor concentration in the air, leaf water status, and intracellular CO_2 concentrations are sensed by guard cells, integrating all of these signals into well-defined stomatal responses. Water uptake by the roots is carried through the vascular system of the plant (xylem) to the cell walls of the mesophyll, where it evaporates into the sub-stomatal cavity. Water vapor is released by diffusion through the stomatal pores in the process called transpiration. Despite some cuticular transpiration exists, most leaf transpiration occurs through the pores of stomata. Only a small percentage (~2 %) of the water absorbed by roots is used by the plant to supply growth or to play in the biochemical machinery for photosynthesis or other metabolic processes (Taiz & Zeiger, 2010). When the water is evaporated, a large tension (negative hydrostatic pressure) is developed, pulling water through the xylem. This mechanism, established over 100 years ago as the 'cohesion-tension theory of sap ascent', explains water movements through plants relying on basic physical properties of water and on some assumptions: the high cohesive forces of water are necessary to sustain large tensions in the xylem water columns; when a critical tension is reached in the xylem vessels, the soil-plant-atmosphere-continuum (SPAC) that water forms is broken by the process called 'cavitation', resulting in gas-filled, non-functional vessels or 'embolism'; transpiration lowers the leaf water potentials, causing water to move up; and, finally, the sun provides the energy needed for that movement, by increasing the temperature of both leaf and the air surrounding, and driving the evaporation of water. But, this

theory has been recently criticized, generating still a fervent debate (Steudle, 2001; Angeles *et al.*, 2004; Zimmermann *et al.*, 2004).

Stomatal conductance (g_s) is the conductance associated with diffusion of gases (CO_2 and water vapor) through the stomatal pore. Four hundred water molecules are lost from leaves per molecule of CO_2 fixed by photosynthesis (Taiz & Zeiger, 2010). Thus, when soil water availability is scarce, a trade-off between avoiding dehydration and allowing sufficient CO_2 fixation for photosynthesis is raised. As a consequence of the stomatal control of transpiration, photosynthetic limitations appear. Traditionally analyzed in terms of 'stomatal' and 'non-stomatal' limitations (Flexas & Medrano, 2002), at the present, photosynthetic limitations under drought conditions are composed of 'difusional', consisted of g_s and mesophyll conductance (g_m) to CO_2, and 'non-difusional' or 'biochemical' limitations, integrated in metabolic changes of the ribulose-1,5-bisphosphate carboxylase/oxygenase (Rubisco) related to the photosynthetic capacity of the plant (Flexas *et al.*, 2013). A quantitative estimation of the relative significance of g_s, g_m and the maximum capacity for carboxylation ($V_{c,max}$) in limiting net photosynthesis (A_N) has been proposed by Grassi & Magnani (2005). The control of transpiration by stomata in both wild and cultivated plants has been proved in many studies (Irvine *et al.*, 1998; Franks, 2004), including olive (Fernández *et al.*, 1997; Moriana *et al.*, 2002; Testi *et al.*, 2006) and almond species (Klein *et al.*, 2001; Romero & Botía, 2006).

In response to environmental changes, g_s is controlled by plant and soil hydraulics being down-regulated to prevent runaway xylem embolisms (Sperry *et al.*, 2002). Furthermore, water deficit strongly stimulates abscisic acid (ABA) biosynthesis by roots and leaves and influences g_s mediating stomatal closure (Davies & Zhang, 1991; Sauter *et al.*, 2001; Holbrook *et al.*, 2002; Bauer *et al.*, 2013). Because stomata are the gatekeepers of terrestrial photosynthetic gas exchange, they become a crucial component in all of the

above processes and understanding their dynamic behavior is imperative to comprehend the control of transpiration by plants.

The control of transpiration in precision agriculture

Understanding the basis of the control of transpiration is crucial in precision agriculture within a context of global changing conditions and restrictive water availability. The Mediterranean basin is recognized as one of the major areas where agriculture was originated, with the first domestication events occurring in the Fertile Crescent about 12 000 years ago (Zeder, 2008), followed by the spread of agricultural practices along the European and African Mediterranean shores. This expansion of agriculture was the consequence of two main advantages over the nomadic lifestyle of hunter-gatherers (Smith, 2001). First, the increment of food yield per fertile land area allowed maintaining a greater human population. And second, these novel food producing societies were sedentary and could store the accumulated surplus, resulting in the development of new technologies and stratified societies evolving to what we know at the present-day. Since these early events of plant domestication, humans have developed different methods to hold up and enhance those advantages. Among these new techniques, the emergence of irrigation to avoid water deficits that reduced production was crucial for a constant provision to a continuously larger human population. The current increase of cultivated areas promoted by the expansion in human population and thus, a higher demand for food, has led irrigated agriculture to be the largest consumer of water in the world, becoming up to 80 % in arid and semiarid environments (Fereres & Soriano, 2007). This causes a diminution of water availability for other sectors of the society, which is exacerbated with the effects of the climate change, further accentuated in areas with Mediterranean climate. More frequent and severe drought combined with high temperatures has been recognized as a potential impact of global warming on agriculture. Rainfall

will become more unpredictable and extreme weather events, such as heat waves and floods, will occur more frequently (IPCC, 2013). In this context, implementation of more efficient irrigation strategies is compulsory to reduce agricultural water use, to make water resources more sustainable and, at the same time, to meet the food needs of a growing population. Furthermore, the idea of increasing crop yield per unit of cultivated area has turned into maximizing 'water productivity' or 'water use efficiency', i.e. amount of yield produced per unit of water used.

In order to improve water productivity in agriculture, continuous search of new precision irrigation techniques and strategies has motivated during the last decades several and insightful studies (Fereres *et al.*, 2003; Morison *et al.*, 2008; Jacobsen *et al.*, 2012). The use of drip irrigation techniques has the main advantages over other techniques of water savings, due to improvements in water circulation, increasing fertilizer use efficiency and decreasing soil salinity. Moreover, this irrigation technique coupled with applying deficit irrigation (DI) seems to be the most suitable strategy for a rational use of water in fruit tree orchards in arid and semiarid areas (Fereres *et al.*, 2003). DI is defined as the amount of water supplied to the orchard below its water needs. An optimal management of DI can allow considerable water savings without causing negative impacts in production and even, at times, improving quality. However, mismanagement of DI strategies may cause water deficits in periods when plants are more sensitive to water stress, reducing both production and productive life span of the orchard (Fereres & Evans, 2006). Thus, the application of regulated deficit irrigation (RDI) that Chalmers *et al.* (1981) and Mitchell & Chalmers (1982) started to use in peach orchards proved that it was possible to reduce the water use without penalizing production. RDI is defined as the reduction or withdraw of water supply in plant phenological periods in which the orchard is more tolerant to water deficits, imposing a controlled water stress. This irrigation strategy seems to be the most advisable tool to

improve water use efficiency and orchard yield in semiarid conditions (Boyer, 1996).

Over the last two decades, the RDI strategy has been extensively investigated, still increasing, in the main fruit tree crops, such as citrus (González-Altozano & Castel, 2003; Pérez-Pérez *et al.*, 2008), almond (Romero *et al.*, 2004; Girona *et al.*, 2005; Goldhamer *et al.*, 2006), olive (Giorio *et al.*, 1999; Iniesta *et al.*, 2009; Fernández *et al.*, 2013), peach (Dichio *et al.*, 2007), vine (McCarthy, 1997; Cifre *et al.*, 2005; Santesteban *et al.*, 2011), or plum trees (Intrigliolo & Castel, 2010). But, knowing when, how much and how to apply this irrigation strategy is still a pending and challenging task not only for orchard managers, but especially for the scientific community. It depends on the species, and even on the variety within a species, and on the soil and weather conditions of the orchard location. In the present Thesis, we will focus on two high resistance species to drought typical from Mediterranean climate: olive and almond.

Physiological and agronomical features of two Mediterranean species under drought: olive and almond

Drought and water stress

Water is one of the main abiotic factors, together with light, temperature and mineral elements in the soil, influencing and constraining plant physiological and biochemical behavior (Taiz & Zeiger, 2010). Land plants have been coping with drought and water stress since they first left the seas and colonized dry land. 'Water deficit' (insufficient water availability) occurs in most natural and agricultural environments and is mainly caused, but not only, by short to long periods without precipitations. 'Drought' can be defined as the meteorological period in which partial or none precipitation events happen, resulting in soil dehydration, diminution of soil water

reservoirs and, hence, in plant water deficit. Indeed, this environmental dynamic state is considered to be the most frequent cause of water stress in plants (Boyer, 1982). 'Water stress' is a functional and structural plant response to low water availability condition. This situation of water deficit is not only provoked by rainfall scarcity, but also, and overall in Mediterranean climate, by the combination of high temperatures, light intensities and atmospheric demand. All of these environmental factors cause a large variety of effects in soil and plants, altering most of their physiological processes. After a heavy rainfall or an abundant irrigation event and once excess water has been allowed to drain away, the water content of a soil reaches 'field capacity'. As soil dries down, its hydraulic conductivity decreases and the 'permanent wilting point' can eventually be reached, i.e. the soil water content at which plants cannot regain turgor upon rehydration (usually at about -1.5 MPa, but it depends on the species). At this point, water delivery to the roots is too slow to allow the overnight rehydration of plants that have wilted during the day (Taiz & Zeiger, 2010). The control of irrigation occurs between field capacity and wilting point, and it is in this range of available water where most of the plant regulation and physiological response to water stress occurs. Normally, the first symptoms of water stress in plants are cellular dehydration, inhibition of cell expansion and reduction in cell turgor, that result in reduction of stomatal opening to prevent desiccation (Flexas & Medrano, 2002). Stomatal closure in response to dehydration is almost always an active, energy-dependent process rather than a passive one (Buckley, 2005). Abscisic acid (ABA) mediates the solute loss from guard cells that is triggered by a decrease in the water content of the leaf and induces stomatal closure under water stress conditions. Subsequently, photosynthesis is unavoidably reduced due to decreased CO_2 availability at chloroplast level. When water stress becomes more severe, photosynthetic capacity is reduced (through decreasing carboxylation efficiency), xylem dysfunctions are induced, osmotic adjustment (net accumulation of solutes to lower water potential during drought periods) appear or disruption of phloem function occur.

An understanding of the impact, mechanisms and traits underlying drought tolerance is essential to improve water productivity. But first, it is necessary to understand some concepts. Plant species differ widely in their capacity to cope with drought. Response mechanisms to drought are mainly divided in 'avoidance' and 'resistance' behaviors that profoundly depend on the plant capacity to maintain water status (Kozlowski & Pallardy, 2002; Tyree *et al.*, 2002). Within the mechanisms of drought resistance two types of responses can be distinguished: 'desiccation avoidance' and 'desiccation tolerance'. Desiccation-avoiding responses (through increasing access to water and reducing water loss) include leaf shedding and changes in leaf orientations, early stomatal closure, sunken stomata, low cuticular conductance (through abundant leaf waxes), enhanced water storage in plant sinks, strong development of palisade mesophyll, low resistance to water flow in vascular tissues, deep roots and extensive root growth. Desiccation-tolerance responses (through physiological changes that allow continued water transport, gas exchange and cell survival at low water content) usually involve osmotic adjustment, changes in elasticity of tissues, decreased vulnerability of xylem to embolism and molecular-level changes. Olive and almond are considered to be drought resistant species, but the mechanisms to cope with water stress are different between them.

Olive

Olive (*Olea europaea* L.; Oleaceae) is a common crop of the Mediterranean basin and native to the coastal areas of the eastern Mediterranean. Olive on crop probably started 6000 years ago, when the first olive growers began to select from the surrounding wild olive forests significantly better individuals due to their productivity, fruit size and oiliness, and adaptation to the environment. Vegetative propagation has maintained the characteristics of those initially selected cultivars that constituted the first varieties (Barranco, 2001). The Mediterranean climatic region is characterized by long periods of drought during the dry season (from May to September) when temperature

and atmospheric demand are high, and a mild wet season from October to April. At present, of the estimated total of 9.5 million ha of olive orchards in the world (producing 20.8 million t), two-thirds (6 million ha) are extended through the Mediterranean region. Spain has the largest area (2.09 million ha), and is also the largest producer of table olives and olive oil (total 8.01 million t), comprising olive oil over 90 % of the production (FAO, 2012). Its capacity to grow and produce acceptable yields under severe drought conditions, and the increased demand for olive products, especially olive oil, driven by health-related benefits (Hu, 2003), have led in the last decades to an expansion of olive orchards and to an increasing of studies on olive biology and growing (Fernández, 2014b). Although olive is considered to be drought-resistant, it responds well to irrigation, which in fact can improve yield (Iniesta *et al.*, 2009). A correct equilibrium between water scarcity in arid and semi-arid areas producing olives, and sustainable irrigation strategies is necessary to maintain good production and quality (Carr, 2013). For that purpose, it is essential to disentangle the physiological mechanisms of olive tree to respond and adapt to water stress and how to use this knowledge to improve crop management practices (Fernández & Moreno, 1999).

According to Rapopport (2001), the olive tree under cultivation can attain a height of 4-5 m maintained by pruning. Canopy is normally rounded, almost lobed, and their branches tend to make it fairly dense. Pruning practices are designed to allow light to penetrate into the canopy and to promote fruiting sites. The canopy shape is of considerable importance since it can modify CO_2 assimilation rate and water use efficiency (Diaz-Espejo *et al.*, 2002) and, hence, it can affect vegetative and reproductive developments. Olive is considered a xerophytic evergreen and sclerophyllous tree species and therefore, it has morphological and physiological characteristics that confer it high capacity to resist water stress (Fernández, 2014b). The growth and reproductive olive biennial cycle contributes to alternate bearing, with years of intense fruiting tending to be

followed by years of restricted flowering and reduced crop load. Leaf upper, adaxial surface is covered by a waxy cuticle. Palisade parenchyma usually consists of two-to-three highly packed layers of elongated cells, and spongy mesophyll anatomy greatly depends on leaf water status (Ehrenberger *et al.*, 2012b). In the lower, abaxial surface of the leaf, stomata are covered by a dense network of trichomes, providing a very effective control of transpiration (Connor, 2005). Under dry conditions stem develops a thick cork layer covering the living bark tissues, thus protecting against sun-burning. Below the bark there is the phloem, the cambium, and the xylem. Narrow xylem vessels with low hydraulic conductivity reduce risk of embolism and allow olive to withstand water potentials below turgor loss point with minor xylem embolisms (Torres-Ruiz *et al.*, 2013a). This low vulnerability to embolisms is different depending on the plant organ. Thus, hydraulic segmentation (Zimmermann, 1983; Tyree *et al.*, 1993) occurs in olive (Torres-Ruiz *et al.*, 2013b), as in other Mediterranean species (Martínez-Vilalta *et al.*, 2002), making leaves effective in reducing whole-plant transpiration and, hence, in avoiding the spread of embolism in other plant organs. The olive root system is adapted to water scarcity, and its depth, shape and lateral extension will be dependent on the plant variety and on the type, aeration and water content of the soil (Fernández *et al.*, 1991). For olive trees with localized irrigation, the greatest root length densities of fine ($\varnothing < 0.5$ mm), active roots, are found in wetted soil volumes close to the drippers, with a favorable balance between air and water for root growing. In dual soils, characterized by a sandy top layer and a clayey bottom layer of high resistance to penetration, roots may only explore the top layer, and penetrate deeper layers due to soil cracks and favorable aeration when soil dries (Diaz-Espejo *et al.*, 2012). Water supply, tree age, plant density and soil characteristics greatly affect the root/canopy ratio, being usually larger in rain-fed than in irrigated olive trees (Fernández *et al.*, 1991). Furthermore, the well-known capacity of olive to take up water from drying soils may be allowed by physiological mechanisms aiming to maintain turgor pressure, such as osmotic and elastic adjustments

(Fernández, 2014b). Stomatal closure mediated by chemical and hydraulic signals is still a matter of debate (Schachtman & Goodger, 2008; Pantin *et al.*, 2012; Christmann *et al.*, 2013; Dodd, 2013; Franks, 2013). Drought-induced ABA from roots and long-distance signaling are dominated by complex mechanisms (Davies & Zhang, 1991). Some authors argue that stomata mostly respond to ABA generated in the leaf, rather than in the roots (Bauer *et al.*, 2013). Recently the response of stomata to soil drying seems to depend mostly on hydraulic signals rather than on chemical signals in olive, especially under saturating light and high evaporative demand (e.g., at midday, Diaz-Espejo *et al.*, 2012). Therefore, a good election of the irrigation techniques and strategies has important effects on how olive trees behave in arid and semi-arid conditions, where water for irrigation is scarce.

During the last years, new olive growing systems designed for improving short-term crop performance have been developed and gradually implemented. Among them, hedgerow olive orchards with high plant densities, also called super-high-density orchards (plant densities close to 2000 trees ha^{-1}), have been gaining importance, occupying nowadays more than 40 000 ha worldwide (Gómez-del-Campo, 2013). Besides early yield after planting, these orchards are designed for high yield when the crop is established, compact bearing, self-fertility, limited vigor and mechanization, especially during harvesting (Rius & Lacarte, 2010). Among the large list of olive tree cultivars, cv. 'Arbequina' is well adapted to these far-extended commercial orchards and it has been the cultivar in which our studies have been focused during the last four years. Olive responds well to deficit irrigation, since it is well-adapted to stressed conditions and has a marked productive response to favorable water supplies. In Mediterranean regions, potential evapotranspiration (ET$_o$) range from 1000 to 1400 mm year^{-1}, and crop evapotranspiration (ET$_c$), from 560 to 800 mm year^{-1} depending on environmental conditions, crop characteristics, and orchard management (Fernández & Moreno, 1999). Considering that mean annual precipitations values are lower than 600 mm and irrigation needs in super-high-density

orchards may increase to 5000 m^3 ha^{-1}, deficit irrigation strategies and precision irrigation techniques seem to be unavoidable to achieve the maximum water productivity (WP, net income per unit water used, Kijne *et al.*, 2003). Regulated deficit irrigation (RDI), in which water supplies equal irrigation needs in the phases of the growing cycle when the crop is more sensitive to water stress, and they are markedly reduced for the rest of the cycle, can be an effective option. Indeed, applying RDI to hedgerow olive orchards can be adequate not only to increase WP, but also to avoid problems derived from excessive vigor and to improve oil quality (García *et al.*, 2013).

Almond

Almond (*Prunus dulcis* (Mill.) D.A. Webb (syn. *Amygdalus communis* L. and *Prunus communis* Archang; Rosaceae)) is considered a drought-resistant species typical from Mediterranean regions (De Herralde *et al.*, 2003), whose production, profitability and water productivity is highly dependent on irrigation supply during the growing season (Egea *et al.*, 2010). It is capable to withstand frequent periods of low soil moisture accompanied by high evaporative demand and high air temperature. Moreover, almond plantations have an important role in fighting desertification and providing products for human consumption, such as almond kernels and oil which is used in confectionery, and also in pharmaceutical and cosmetic preparations (Rouhi *et al.*, 2007). Historically, almond trees have played a key cultural and economic role in Mediterranean human communities (Delplancke *et al.*, 2013). Nowadays, the annual world almond production exceeds 1.9 million t (FAO, 2012). After olive and grapevine, it is the third important woody crop in cultivated areas in Spain with *ca.* 550 000 ha (AEA, 2011). Spain is the Mediterranean country that has the greatest production of almonds and is ranked second in the world, accounting for 17 % of world production, being the main competitor of USA (Romero *et al.*, 2004a). Almond has traditionally been cultivated in marginal and dry areas with no irrigation and

low productivity. The good yield response to irrigation reported for this nut tree species (Torrecillas *et al.*, 1988; Hutmacher *et al.*, 1994), together with the aim of maintaining low water consumption in the semiarid regions of the Mediterranean coast, have stimulated the application of RDI strategies. RDI has been applied successfully in almond (Romero *et al.*, 2004a) to enhance WP with no or minor penalty on crop yield and fruit quality. A large body of studies has shown that there are advantages in reducing irrigation at the time of the lowest water stress sensitivity (kernel filling). This stage occurs when the evaporative demand is highest (summer season) and coincides with dry mass accumulation in the seed (kernel). Meanwhile, applying full irrigation during the most stress-sensitive times (spring season) is considered critical to avoid water stress. This stage is characterized by the flowering phase, the rapid vegetative development phase and the post-harvest phase (Goldhamer & Viveros, 2000; Romero *et al.*, 2004a, b; Girona *et al.*, 2005; Goldhamer *et al.*, 2006). Therefore, one of the prerequisites for valuation and further implementation of best RDI management practices is a detailed knowledge of almond physiological responses to abiotic stresses, while accounting for leaf age, plant phenology and fruit load (Nortes *et al.*, 2009).

Almond is a winter-deciduous, woody-perennial nut tree species. Like other Mediterranean species, e.g. olive, the adaptation of almond to water stress is owed to various physiological and morphological drought tolerance mechanisms. But also, as other perennial trees, is able to induce dormancy of actively growing tissues in order to cope with unfavorable environmental conditions occurring during autumn and winter (Barros *et al.*, 2012). One of the most common and earliest events responding to water deficits under field conditions is, as commented above, stomatal closure to prevent water loss (Escalona *et al.*, 1999; Chaves *et al.*, 2002). But this provokes a reduction in daily carbon assimilation at the leaf level as well, decreasing the net carbon gain in the long-term by the whole plant. Thus, plants in general and the almond in particular, have other mechanisms as well to survive in arid

areas. These mechanisms include a high resistant xylem, a capacity for osmotic adjustment, changes in the elastic properties of cells and tissues, the onset of leaf abscission, and the presence of a deeply penetrating root system (Torrecillas *et al.*, 1988; Goldhamer & Viveros, 2000; Matos *et al.*, 2004; Romero *et al.*, 2004c; Cochard *et al.*, 2008). Evergreen species (olive) have been more associated with desiccation tolerance, since they mostly retain their leaves throughout the dry season, being active at low soil water potentials and including adaptations to reduce xylem cavitation (such as small vessels, high stem density) and to minimize water loss (small leaf size, low specific leaf area – leaf area to dry mass ratio – and low transpiration rates). By contrast, desiccation avoidance has been more associated with deciduous species, like almond, which are able to drop their leaves when soil water potentials decline during dry seasons (Tomlinson *et al.*, 2013). Thus, comparing with the olive tree, the almond tree avoids dry periods, and hence, it may be able to sustain high photosynthetic rates when conditions are favorable for growth (Higgins *et al.*, 1992). But, water-stressed almond trees have been reported to have lower water-use efficiency than other fruiting species (Romero *et al.*, 2004c). This behavior can probably be related to the 'spendthrift' feature of this species when water is plentiful. Almond leaves are also hypostomatous. Unlike evergreen sclerophyllous leaves (olive), deciduous malacophyllous leaves (almond) commonly exhibit increased intercellular air spaces and surface area-to-volume ratio, and a less strongly developed palisade mesophyll (Marchi *et al.*, 2008).

Knowledge about how water stress can modify the functioning in the almond tree is needed, because it is likely to affect almond yield determinants. Almond physiological processes, such as photosynthesis and transpiration depend on the rapidity, severity and duration of the drought event. Like in olive, in field-grown almond trees under RDI, the daily patterns of gas exchange show a strong stomatal control of transpiration throughout the day with a maximum in stomatal conductance and

photosynthesis in the early morning, at low vapour pressure deficit and temperature, and a progressive decrease at midday and early afternoon (Romero & Botía, 2006). Romero *et al.* (2004c) reported a significant reduction in the photosynthetic capacity of young branches of almond trees under pre-harvest conditions of mild to moderate soil water deprivation, whereas the accumulation of dry matter in the kernel was little affected compared with the fully irrigated trees. Thus, dry matter accumulation stage is one of the processes that are least sensitive to water stress. But, under more severe environmental conditions (pre-dawn leaf water potential < –2 MPa), reduced leaf surface area as a result of excessive abscission, lower leaf growth and lower photosynthetic rates could become important factors limiting CO_2 uptake (Romero *et al.*, 2004c).

Current methods of irrigation scheduling and plant-based sensing to monitor water stress

The advent of precision irrigation methods such as drip irrigation has played a major role in reducing the water required in agricultural crops, but has highlighted the need for new methods of accurate irrigation scheduling and control. As already commented above, RDI seems to be the most recommended strategy to improve water-use efficiency and yield in orchards under arid and semi-arid conditions (Boyer, 1996), gaining also in sustainability for these areas where high competition for water resources (i.e. urban, tourism, industrial, agriculture) occurs, especially in summer. But, this irrigation strategy requires a precise maintenance of water status within a narrow range of tolerance. Any excess in the irrigation doses applied will counterbalance the advantage of the RDI in terms of water-use efficiency, meanwhile any under-application can lead to severe yield or quality losses. At present, three major methods of irrigation scheduling exist. The first of them, uses the evolution of soil water status to decide the irrigation frequency. This method includes techniques to measure (i) soil

water potential (tensiometers, psychrometers, etc.) and (ii) soil water content (gravimetric, capacitance, time-domain reflectometry, etc.), and also (iii) a soil water balance approach, in which changes in soil water status over a period are given by the difference between inputs (irrigation, precipitation) and losses (runoff, drainage, crop evapotranspiration). Although these methods of irrigation scheduling are easy to apply in the field and some sensors (especially capacitance and time-domain probes) can be automated, the high spatial and temporal soil heterogeneity is considered the main constraint and makes their use in agricultural practice very difficult (Jones, 2004). Moreover, it requires good knowledge of root distribution and relative density, with the limitation that uncertainty increases when the wetted soil volume varies in three dimensions, as it does in drip irrigation (Ortuño *et al.*, 2010).

A second approach is based on meteorological variables for estimating crop reference evapotranspiration (ET_o) and for calculating crop water requirements or crop evapotranspiration (ET_c), corrected by a crop coefficient (K_c) and a reduction coefficient (K_r) related to the degree of orchard floor covered by plant (Allen *et al.*, 1998):

(1.1) $ET_c = ET_o\, K_c\, K_r$.

ET_o is the evaporative demand of the atmosphere and corresponds to the evapotranspiration of a standard grass cover, plague and disease-free, and 10 - 15 cm height. This method, also called the FAO approach, has been successful worldwide because of its good level of precision and robustness combined with the fact that it is easy to use and transferable to farmers. However, the specific information on tree crops that it contains (K_c, K_r) is scarce and is based on relatively few research reports (Orgaz *et al.*, 2006). K_c differs considerably between herbaceous and tree crops. It is linked with easily detectable phenological stages, which occur only seasonally in the first case. In deciduous trees, besides seasonally changes, K_c is also affected by additional factors such as canopy architecture, tree density, pruning

practices, crop load, irrigation method, and soil surface management. In evergreen trees, active throughout the year, a longer irrigation season than deciduous tree species is required, increasing the complexity in the determination of K_c. Furthermore, this crop coefficient method is subject to the serious problem that errors are cumulative over time, so regular recalibration is needed (Jones, 2004). In summary, the main disadvantage of this method is that crop coefficients need to be adjusted empirically, which makes difficult their extrapolation to a wide range of different crops and climates unless specific experiments are conducted.

A potential problem with every soil and meteorological-based approach is that many features of the plant physiology respond directly to changes in water status in the plant tissues, rather than to changes in the bulk soil water status or in the atmosphere. Thus, plant-based methods have increased in interest, since plant measurements have the advantage of integrating the soil and atmospheric water status, as well as the response of the plant to the surrounding conditions (Jones, 2004). It is often difficult to determine precisely where in the soil-plant system it is appropriate to measure because of the feedbacks involving control of water status. These feedbacks mean that it is often difficult to disentangle or break the correlations between, for example, soil and leaf water potentials that result from conventional hydraulic signaling (Jones, 2007). Potential plant-based indicators include direct measurements of some aspects of plant water status as well as measurements of a number of plant processes that are known to respond sensitively to water deficits. Jones (2004) revised in detail advantages and disadvantages of plant-based methods, pointing out to potential opportunities for use of plant-based stress sensing as the basis for irrigation scheduling. In general, the use of any plant-based indicator for irrigation scheduling requires the definition of plant water stress threshold values, beyond which irrigation is necessary. However, identifying these reference values is rather complicated, because it requires extensive knowledge of the physiological mechanisms involved in the response to water stress and its

ultimate effect on production. Although these methods have several advantages and have been widely used in research, there are still a number of practical difficulties for implementing their use in commercial orchards (for a review on this topic, see Fernández, 2014a).

Conventional plant-based methods to monitor water stress include leaf and stem water potentials (Naor *et al.*, 2006), stomatal conductance, shoot length growth and leaf area. Even though there was often homeostasis of leaf water potential between different soil moisture regimes, rapid temporal fluctuations are often observed as a function of environmental conditions (such as passing clouds). This makes the interpretation of leaf water potential as an indicator of irrigation-need doubly unsatisfactory (Jones, 1990). As a partial solution for that, stem water potential at midday (measured on leaves enclosed in darkened plastic bags for some time before measurement and allowed to equilibrate with the xylem water potential) has been proposed as a more robust indicator of water status (Shackel *et al.*, 2000). Furthermore, pre-dawn leaf water potential has been used as an estimator of the soil water potential. All water potentials are measured with a Scholander-type chamber (Scholander *et al.*, 1965) and hence, are highly invasive, destructive and time consuming. Less invasive methods are stomatal conductance, shoot growth and leaf area measurements. Nevertheless, they are still largely time and labor consuming. None of these traditional plant-based methods are suitable for automatic and continuous measurements. Thus, in the last decades, new water stress monitoring methods have been developed for non-destructive, automatic and continuous data recording, easily implemented with data transmission systems for a nearly real time access to the collected records from a remote computer. Most of them are highly sensitive and capable of working under field conditions for long periods of time, meeting most of the criteria for both reliable monitoring of water stress and irrigation scheduling (Jones, 2004; Fernández, 2014a). Among these methods, those based on measurements or estimations of sap flow, trunk diameter variation and leaf

turgor pressure are the most widely studied. Sap flow (SF) methods have a potential for *in situ* determinations of plant water consumption and transpiration dynamics (www.wgsapflow.com). Because SF rates are expected to be sensitive to water deficits and especially to stomatal closure, the use of SF measurements for irrigation scheduling has been tested in a diverse range of crops, including comparisons with other water stress indicators (Fernández *et al.*, 2001, 2008b; Intrigliolo & Castel, 2006; Ortuño *et al.*, 2006; Conejero *et al.*, 2007). Although changes in transpiration rate estimated by sap flow are largely determined by changes in stomatal aperture, transpiration is also influenced by other environmental conditions such as atmospheric water demand, and reference trees are often used to cancel-out the effect of environmental variables (Fernández *et al.*, 2008b, 2011a). The usefulness of trunk diameter variation (TDV) records both for monitoring water stress and scheduling irrigation has been evaluated for a great number of species (Intrigliolo & Castel, 2006b; Fernández & Cuevas, 2010; Ortuño *et al.*, 2010), and comparative studies between TDV and other water stress indicators have also been made (Ehrenberger *et al.*, 2012a; Cuevas *et al.*, 2013). TDV devices are relatively easy to install, their outputs are quite sensitive to water stress and can be continuously and automatically recorded. However, the TDV outputs are affected by seasonal growth patterns, crop load, plant age and size, and other factors besides water stress (Fernández & Cuevas, 2010). Thus, continuous readjustments are needed along the irrigation season. Furthermore, detailed interpretations of TDV signals require strong knowledge on plant physiology to disentangle the role of each trait on the trunk variation. The leaf patch clamp pressure probe, or ZIM probe (Zimmerman *et al.*, 2008) is a relatively novel plant-based sensor able to record automatically and continuously the so-called leaf patch output pressure (P_p), which is inversely correlated with the leaf turgor pressure (P_c), when P_c > ca. 50 kPa (Rüger *et al.*, 2010; Ehrenberger *et al.*, 2012a, 2012b), a variable closely related to leaf water potential and stomatal conductance (Ache *et al.*, 2010). It has been used in several plant species and crops to precisely monitor water stress (Westhoff *et al.*, 2009; Rüger *et al.*,

2010; Fernández *et al.*, 2011b; Lee *et al.*, 2012; Bramley *et al.*, 2013). Furthermore, this variable is one of the physiological variables recognized to be among the most sensitive to water stress (Jones, 2004, 2007), although it still requires intense evaluation under field conditions to prove its applicability. The present Thesis dedicates three Chapters (4, 5 and 6) to the study of this plant-based sensor. Moreover, Chapter 4 combines these probe signals with a process-based stomatal conductance model (see next section).

Modeling leaf gas exchange: the quest for the right model

Once recognized the crucial role of stomatal functioning in the control of transpiration and fluxes of CO_2 between the leaf and the atmosphere, modeling stomatal conductance (g_s) would be one of the most effective and valuable tools for improving our understanding of the regulation of stomatal conductance to changing environmental conditions and to water stress, as well as for integration, simulation and prediction purposes (Damour *et al.*, 2010). Indeed, a trustworthy modeling of g_s is also required for successful modeling of plant transpiration, necessary for designing more efficient and water-saving cropping systems. This is especially suitable in fruit trees where a low decoupling factor exists (Jarvis & McNaughton, 1986). Under these conditions, there is a high coupling of leaves and canopies to atmospheric conditions and, as a consequence, a high importance of the aerodynamic conductance in controlling water flux from vegetation to atmosphere decreases. Thus, stomata strongly control transpiration rates. The boundary layer reduces this effect, i.e. as the ratio of boundary layer conductance to stomatal conductance decreases (or, in other words, the boundary layer resistance increases comparing to stomatal resistance), the decoupling factor increases. The coupling to the atmosphere of fruit tree canopies is modulated daily from wind velocity, incoming radiation and evaporative demand, and seasonally from a high influence of

the water deficit endured by trees (Aranda *et al.*, 2012). This translates in the latter that transpiration becomes highly dependent on the sensitivity of stomata to changes in water vapour deficit of atmosphere. Although global models are very useful to accurately predict and assess impacts of climate change on carbon and water cycles, they are generally incapable of disentangling the mechanisms through which stomata respond to environmental conditions, especially water stress, which has become the real Achilles´ heel in g_s modeling. Therefore, including accurate predictions of plant gas exchange with stomatal conductance models at the leaf level are needed to implement these models (Egea *et al.*, 2011b; Buckley & Mott, 2013).

The majority of stomatal modeling approaches at leaf level are empirical (data-based), based on statistical correlations between environmental or internal factors and g_s, or semi-empirical, built on physiological hypotheses, but still combined with empirical functions, and very few are really mechanistic (process-based). Nevertheless, both empirical and mechanistic approaches are difficult to completely separate, since even the most empirical models are at least partially mechanistic and even the most detailed mechanistic models must resort to empiricism at some scale (Buckley & Mott, 2013). There is also another approach for modeling g_s: economic- or optimization-based. This approach is focused on why stomata behave as they do leading into the optimization of carbon gain *versus* water loss, and how that behavior impacts other aspects of plant form and function (the so-called stomatal optimization theory) (Cowan & Farquhar, 1977). Responses of stomata to environmental factors have been extensively described (Jarvis, 1976; Jones, 1992; Monteith, 1995). These responses are mediated from short to long distances by many internal signals such as hormones, reactive oxygen species (ROS), CO_2 concentration in the leaf intercellular space and hydraulic signals (Hetherington & Woodward, 2003). However, the links between environmental conditions, how they are sensed and translated into the whole plant functioning and how they end up into

stomatal responses, are still poorly elucidated. Disentangling these mechanisms and relationships will help to develop more integrative approaches of stomatal responses to environmental influences where possible couplings and interactions could be taken into account. A particularly powerful approach might be to parameterize plant and leaf models of hydraulic function, such as the SACC model of Sperry *et al.* (1998, 2002), concurrently with a stomatal model. However, the main challenge remains incorporating the effect of water stress in the models, gaining in the capacity to simulate plant functioning under limited water supply conditions (Damour *et al.*, 2010; Egea *et al.*, 2011b). This section reviews the most used g_s models, mainly focusing on empirical and mechanistic approaches capable to account for multiple environmental influences with special attention to water stress conditions.

The stomatal conductance model or combinations of models selected will depend on the final intended use and objectives of the research. Empirical models are often numerically simpler than mechanistic models, and they are more recommended for those users who want to combine them within a larger model of global or canopy level processes. More mechanistic models are often more mathematically complex, but the physical and biochemical basis in which they fall on allow their use for investigating the cellular and sub-cellular processes involved in environmental sensing, signal transduction, and ion movements (Buckley & Mott, 2013). Among the empirical models, the 'Jarvis' model (Jarvis, 1976) is a simplistic modeling approach based on the observed responses of g_s to environmental factors. This multiplicative model of environmental influences integrates responses to irradiance (PPFD), leaf temperature (T_l), air vapor pressure deficit (VPD), CO_2 concentration in the air (c_a) and leaf water potential (Ψ_{leaf}), assuming that each response is independent of the others. Following modifications expressed these responses as reduction factors of a maximal stomatal conductance ($g_{s,max}$) related to stomatal closure or limiting g_s:

(1.2) $g_s = g_{s,max} \, f(\text{PPFD}) \, f(T_l) \, f(\text{VPD}) \, f(c_a) \, f(\Psi_{leaf})$ $f \in [0,1]$.

Although these limiting factor-based approaches can explain 95 % of the observed variation of g_s, interactive effects between environmental factors are not taken into account and their empiricisms make necessary new parameterization for each new environmental condition. However, they have been successfully tested in the field (e.g. olive or walnut trees) linking with the biochemical model of photosynthesis of Farquhar *et al.* (1980) and incorporating the effect of soil water deficit (Le Roux *et al.*, 1999; Diaz-Espejo *et al.*, 2006). Furthermore, its modular structure makes it easy to include into larger models, such as general circulation models (GCM) (Egea *et al.*, 2011b), and explains its still wide use by the scientific community.

One of the most widely used empirical models is the 'BWB' model (Ball *et al.*, 1987) and variations thereof. This coupled photosynthesis-stomatal conductance model is basically based on the correlation usually found between g_s and A_N. It is able to describe the stomatal response to light, humidity and CO_2, being g_s described as a function of net photosynthesis (A_N), CO_2 concentration at the surface of the leaf (c_s), the relative humidity at the surface of the leaf (h_s) and the residual stomatal conductance when A_N is zero (g_0):

(1.3) $g_s = g_0 + m \dfrac{A_N h_s}{c_s}$,

where *m* is an empirical parameter that varies among leaves and among different water stress conditions. As it can be observed from the Equation (1.3), *m* is the slope of the commonly linear relationship between g_s and A_N. It is also widely used in canopy models and GCMs (Egea *et al.*, 2011b). Since stomata do not respond directly to c_s *per se*, but rather to CO_2 concentration in the intercellular spaces (c_i) (Mott, 1988), for predicting purposes, the so-called 'supply function of CO_2 diffusion rate' must be coupled to a model of A_N (Farquhar *et al.*, 1980):

(1.4) $\quad g_s = 1.6 \dfrac{A_N}{c_s\left(1 - \dfrac{c_i}{c_s}\right)}$.

Leuning (1990, 1995) proposed modified versions of the 'BWB' model to enhance its physiological meaning. Thus, CO_2 compensation point (Γ^*) is taken into account, subtracting from c_s, to prevent A_N from becoming negative at low c_s, which could lead to negative g_s values. Later, the relative humidity term (h_s) was replaced with an inverse hyperbolic response to the leaf-to-air vapour pressure deficit (VPD): $1/(1 + VPD/D_0)$, where D_0 is an empirical parameter. Indeed, Mott & Parkhurst (1991) demonstrated experimentally that stomatal responses to humidity are really responses to water-loss rates (transpiration), and thus showed that stomata sense leaf transpiration rate (E) rather than air humidity. Furthermore, the hyperbolic relationship between g_s and VPD also arises in mechanistic models from the effect of transpiration on turgor pressures of cells in the stomatal complex (e.g. Dewar, 2002; Gao *et al.*, 2002; Buckley *et al.*, 2003). The revised versions can be summarized as:

(1.5) $\quad g_s = g_0 + m \dfrac{A_N}{(c_s - \Gamma^*)\left(1 + \dfrac{VPD}{D_0}\right)}$.

'BWB' and 'Leuning' models are still extensively used. This is mainly because they both represent a good compromise between ease-to-use, explicative power and predictive accuracy in various experimental conditions. Although these models have been implemented to simulate g_s in water stress conditions (e.g. introducing a function of soil water content or a function of ABA or Ψ_{leaf}), they are still rather empirical and hence, based on observed relationships which lead to complicated simulations in a wide range of environmental conditions.

With a better understanding of plant physiological mechanisms involved in the response to water stress and as a powerful tool to improve it, process-based models have been proposed (Buckley & Mott, 2013). Some of them are based on the effects of leaf water potentials and xylem ABA concentrations on g_s (Gutschick & Simonneau, 2002). Others use hydraulic models, where water flux through the whole tree equals transpiration, to simulate g_s. In these approaches, the hydraulic tree architecture is represented by different organs, from the roots to the leaves, and specific hydraulic conductivities for each organ are estimated (Sperry *et al.*, 1998). But none of these mentioned mechanistic models consider at the same time the whole combination of stimuli that influence g_s: hydraulic and non-hydraulic factors. 'Hydromechanical' models aim to integrate g_s as a function of water balance and turgor regulation of guard cells. This approach has led to the emergence of common issues that account for the influences of guard cell and epidermal turgor pressures (P_g and P_e) on g_s. Both P_g and P_e are related to water potential (Ψ) and osmotic pressure (π), by the standard expression of plant-water relations: $P_g = \Psi_g + \pi_g$, and $P_e = \Psi_e + \pi_e$ (taking the convention that osmotic pressure is positive). Some assume that the differences between both P_g and P_e govern stomatal movements, and that stomatal response to water loss is mediated by a feedback mechanism (the so-called 'hydropassive feedback') where transpiration causes diminution of water potential and reduces P_g, leading to stomatal closure (Dewar, 2002). On the other hand, for other hydromechanical models, stomata respond simply through the direct effect of low water potential on P_g (Gao *et al.*, 2002). Although these two approaches can simulate the effects of water stress, none of them consider the effect of P_e on g_s, i.e. the mechanical advantages of epidermal cells over guard cells (Franks *et al.*, 1998). This implies that:

(1.6) $g_s = \chi \left(P_g - m P_e \right),$

where $\chi > 0$ is a proportionality constant accounting stomatal size and density and $m \geq 0$ (dimensionless) is the epidermal mechanical advantage. Buckley *et al.* (2003) dealt with this issue in a model ('BMF' model) based on leaf, plant and stomatal water relations. In addition, they proposed an alternative 'hydroactive feedback' hypothesis where guard cell osmotic pressure is actively regulated in proportion to P_e (which acts as a sensor for changes in leaf water status) and to the ATP concentration of photosynthesising cells (which acts as a sensor for light and CO_2). Thereby, g_s is linked to photosynthetic activity:

$$(1.7) \qquad \pi_g = \pi_e + \beta \tau P_e ,$$

where β is a scaling factor and τ is ATP concentration in photosynthesising cells that can be simulated using the model of Farquhar & Wong (1984). When combined with a steady state model for liquid phase water flow from the soil to the leaf ($E = K(\Psi_s - \Psi_{leaf})$, where E is transpiration rate, K is leaf-specific hydraulic conductance, and Ψ_s and Ψ_{leaf} are soil and leaf water potentials, respectively), Equations (1.6) and (1.7) lead to:

$$(1.8) \qquad g_s = \chi \frac{\alpha K(\Psi_s + \pi)}{K + \chi \alpha \text{VPD}} ,$$

where π is bulk leaf osmotic pressure and $\alpha = \beta \tau - m + 1$. Important features of this model have to be highlighted. The use of m enables a better simulation of g_s variations with VPD, namely the transient opening with increasing VPD which results from rapid, hydropassive responses, and the subsequent closure associated with the slower, hydroactive, energy-dependent osmotic response. Moreover, abscisic acid (ABA) effects can be introduced in the model. Buckley *et al.* (2003) showed that β could be interpreted as the ratio of the specific rates of active ion uptake and passive ion efflux in guard cells. Considering that the flux of ions entering the guard cells is ABA dependent, one would expect β, and therefore the parameter

α, to decline as ABA concentration increases. Moreover, the most interesting advantage is that the parameters used in this model have explicit physiological meaning. Reviews on this topic (Damour *et al.*, 2010; Egea *et al.*, 2011b) recognized the potential of this model, but noted the difficulty in applying it, due to its high number of parameters. More and more mechanistic models are expected to appear as new information is acquired, aiming to bridge the gap between mechanistic and empirical models. In the present Thesis (Chapters 2, 3 and 4), this model will be parsed in more detail and will be slightly simplified with the aim of validating it in the field under water stress conditions. It will be suggested as well as a powerful tool not only for prediction, but also as a generator of new working hypothesis.

Resumen

En la presente Tesis se han utilizado una amplia gama de técnicas experimentales y análisis de modelización para estudiar los mecanismos fisiológicos involucrados en el control de la transpiración y aplicar los conocimientos adquiridos en la optimización del riego de cultivos de árboles frutales. Dos enfoques principales fueron utilizados para enlazar el conocimiento fisiológico emergente con la búsqueda de un manejo adecuado del riego en estos cultivos: sensores basados en medidas en plantas y modelos con base fisiológica o mecanísticos. En el Capítulo 2 se evaluó la regulación de los mecanismos que subyacen al control de la transpiración en una plantación de olivos en seto bajo condiciones de riego deficitario, combinando (i) el modelo hidráulico basado en las conductancias hidráulicas tanto del suelo como de la planta (Sperry *et al.*, 1998), el modelo hidromecánico del control del estoma por balance hídrico (Buckley *et al.*, 2003, o modelo 'BMF') y (iii) sondas de flujo de savia para validar los modelos con medidas independientes. En el Capítulo 3 se llevó a

cabo un estudio más detallado y cuantitativo de las respuestas estomáticas a la sequía impuesta a plantas de almendro en macetas. Para lograr tal propósito, el modelo 'BMF' fue aplicado a medidas ecofisiológicas obtenidas *in situ* y fue usado como plataforma para separar el papel que diversos factores tienen en las limitaciones hidráulicas y no hidráulicas de la conductancia estomática. En el Capítulo 4, y de nuevo a partir del modelo 'BMF', se derivaron cambios absolutos de presión de turgencia de la hoja para evaluar la aplicabilidad de sensores de presión de turgencia de reciente aparición. Estos sensores se han descrito en la literatura como herramientas adecuadas para monitorizar el estado hídrico de plantas, ya que las señales obtenidas se relacionan con la presión de turgencia de las hojas. Además, en este estudio se exploró el comportamiento estomático y las variables fisiológicas que determinan el estado hídrico de la planta dentro de un contexto de la copa de árboles de olivo (hojas de sol y hojas de sombra). A partir de estos estudios, se sugirió que estos sensores de presión de turgencia de las hojas son una herramienta con un gran potencial para el seguimiento del estrés hídrico en el campo, por lo que se han dedicado dos capítulos más a estudiar y evaluar su aplicabilidad directa en cultivos bajo condiciones de riego deficitario. Primero, en el Capítulo 5 se demostró la correlación inversa que existe entre las señales obtenidas a partir de las sondas de presión de turgencia en hojas y la presión de turgencia real de las mismas, medida a partir de sondas de presión de turgencia celular. Gracias a este estudio, distintos estados observados en la dinámica de las señales de salida de estas sondas tanto en plantas de olivo bajo condiciones de laboratorio como en árboles bajo condiciones de campo, se han propuesto como posibles indicadores de estrés hídrico para la programación del riego. Además, el análisis teórico del funcionamiento de estas sondas ha mostrado que otros factores, distintos a la presión de turgencia de las hojas, están influenciando en la señal de salida cuando las hojas tienen una presión de turgencia muy baja (cercana al punto de pérdida de turgencia). Finalmente, en el Capítulo 6 se evaluó la aplicación agronómica de estas sondas para la programación de riego en una plantación de olivos bajo diferentes

regímenes de agua y se compararon con medidas simultáneas de flujo de savia. Los datos sugirieron que tensiones de corto rango en el sistema vascular fueron los responsables de la elevación del agua por la planta y que la toma de agua a partir de los reservorios de la planta debe jugar un papel importante en el abastecimiento de agua a las hojas. Además, también se evaluó la potencialidad de estas sondas como posible alternativa a medidas con la cámara de presión Scholander para el seguimiento del estado hídrico de la planta.

Summary

The physiological mechanisms involved in the control of transpiration through a wide range of experimental techniques and modeling analyses have been studied in this Thesis. Two main approaches were used to link the arising physiological knowledge to proper management of irrigation in fruit tree species orchards: plant-based sensors and process-based models. Chapter 2 evaluated the regulation of the mechanisms behind the control of transpiration in olive trees under water deficit irrigation, combining (i) the hydraulic model based on soil and plant hydraulic conductance (Sperry *et al.*, 1998), (ii) the hydromechanical model of the control of stomata by water balance (Buckley *et al.*, 2003, or 'BMF' model) and (iii) sap flow probes to validate the models with independent measurements. In Chapter 3 a more detailed and quantitative study of the stomatal response to soil drought in almond pots is presented. To achieve that purpose, the 'BMF' model was applied to ecophysiological measurements and used as a platform for separating the role of several factors related to hydraulic and non-hydraulic limitations of stomatal conductance. Then, in Chapter 4, absolute changes in leaf turgor pressure were derived from the 'BMF' model to assess the diurnal changes of the outputs of the recently developed leaf turgor pressure-related probe. In that study, the stomatal behavior and the

physiological variables determining the plant water status within the canopy was explored as well. This plant-based sensor was presented as a potential tool to monitor tree water stress in the field and two more chapters were dedicated to study and evaluate its applicability in more detail. First, Chapter 5 demonstrated the inverse correlation between the outputs of the leaf turgor pressure-related probe and the leaf turgor pressure measured with the cell turgor pressure probe in olive leaves. Different states of the probe output curves identified in young potted olive plants under laboratory conditions and in adult olive trees under field conditions were proposed as potential indicators of water stress for irrigation scheduling purposes. Furthermore, theoretical analyses showed that other factors rather than leaf turgor pressure affected the probe signals at very low leaf turgor pressure (close to turgor loss point). And finally, Chapter 6 evaluated the potential use of the probes for irrigation scheduling in olive trees under different water regimes concomitantly with sap flow probes. The data suggested that short-range tension forces were responsible for water lifting and that water uptake from water storage reservoirs in the plant must play an important role in the supply of water to the leaves. Potentiality of the probe as a suitable alternative to the Scholander pressure chamber measurements to monitor plant water status was also assessed.

Objectives

Water demand from plants mainly depends on environmental variables, leaf area and stomatal control. Soil and plant hydraulics, root area and soil water content influences the water supply aiming to equal water demand. Under this context, stomata play an essential role in controlling not only transpiration, but also CO_2 assimilation by photosynthesis. The present Thesis is focused on understanding the mechanisms underlying the regulation of water loss in two important crop woody trees (olive and almond) under soil and atmospheric drought. Achieving this knowledge will help to improve irrigation management by keeping crops within favorable transpiration rates and hence, CO_2 assimilation rates and production. For that purpose, two main approaches were used and combined to explore their potentialities: plant-based sensors and process-based models. Firstly, plant-based sensors reflect the integration response of soil and atmospheric effects on plant behavior, but challenges remain on interpreting these output signals. And secondly, owing to the large concomitant factors that influence the plant response to drought, process-based models can be powerful tools to understand and integrate all the physiological functions. In this case, challenges remain on obtaining more mechanistic approaches without complicating their mathematical structures.

To achieve the above general objective, the following specific goals were pursued:

∴ To evaluate the use of process-based models in a hedgerow olive tree orchard under regulated deficit irrigation for improving our knowledge of water use by this crop tree and for translating it to a more suitable irrigation management.

∴ To develop and test a novel model-based integrative approach to examine and quantify the control of stomatal conductance during soil

drought by hydraulic and non-hydraulic factors in almond plants. This will help us to comprehend more in detail the stomatal response to soil drought.

∴ To use the process-based model of stomatal conductance tested in this study, for deriving leaf turgor pressure and assessing the outputs of a leaf turgor pressure-related probe. The combined use of both model and plant sensor is expected to raise new insights into the regulation of plant water use by stomatal conductance under drought conditions and within the canopy.

∴ To study in more detail, experimentally and theoretically, the output dynamics of the leaf turgor pressure-related probe in olive plants under laboratory and field conditions. A good interpretation of these outputs will help us to enhance the potentiality of the probes as indicators of plant water status.

∴ To assess the agronomical applicability of the leaf turgor pressure-related probe combining with sap flow measurements for (i) a better understanding of the dynamics of water stress in a hedgerow olive tree orchard under regulated deficit irrigation and (ii) for evaluating the potential of the probes as a tool for irrigation scheduling. An evaluation of the probe as a suitable alternative to the pressure chamber to monitor plant water status will also be performed.

Chapter 2

Towards a more mechanistic model of water use:

A case study in olive

Introduction

The main challenge for precision agriculture in fruit trees in arid and semi-arid environments is the optimal management of irrigation. Two main approaches are being widely used with that purpose: the crop coefficient approach, also known as the FAO-56 approach, based on the Penman-Monteith equation to calculate the atmospheric demand and on the use of crop coefficients adapted to the orchard conditions (Allen *et al.*, 1998); and the use of plant-based methods for a precise monitoring of the trees' water stress (Fernández & Cuevas, 2010). In the first case, large uncertainties arise when equations are applied in different scenarios where soil conditions, phenological stages, orchard age, etc. vary (Pardossi and Incrocci, 2011). On top of that, the use of monthly values of the crop coefficient limits the temporal precision of this approach (Fernández & Moreno, 1999). The need for deficit irrigation in most fruit trees orchards (Fereres & Soriano, 2007; Ruiz-Sanchez *et al.*, 2010) has driven substantial development of plant-based methods in recent decades. These methods can be used for the continuous and automatic monitoring of plant water stress, so they have a potential for high precision irrigation. A variety of sensors are used, including those related to measurements of sap flow (Fernández *et al.*, 2008b), trunk diameter variations (Fernández & Cuevas, 2010; Ortuño *et al.*, 2010), leaf turgor pressure (Fernández *et al.*, 2011b), water content in the trunk (Nadler & Tyree, 2008), electric water potential (Oyarce & Gurovich, 2011) and canopy temperature (Jones, 1999). Plant-based methods have the potential advantage of measuring the plant's response to the prevailing environmental conditions. The outputs, therefore, have a physiological basis, although their interpretation and application present challenges. Using these outputs to generate a measure of the degree of stress suffered by the plant, in order to apply management decisions, remains the main challenge.

However, another approach has received some attention as well: physiologically based models. Modeling plant transpiration requires

successful modeling of stomatal conductance, especially in fruit trees with a low decoupling factor (Jarvis & McNaughton, 1986) where transpiration is effectively controlled by stomata. Models of stomatal conductance have been approached from empirical (Jarvis, 1976; Ball *et al.*, 1987; Leuning, 1995) and mechanistic points of view (Jarvis & Davies, 1998; Dewar, 2002; Gao *et al.*, 2002; Buckley *et al.*, 2003; Peak & Mott, 2011). However, the main challenge remains incorporating the effect of water stress in the models (Damour *et al.*, 2010; Egea *et al.*, 2011b). In addition to the importance of stomatal conductance, another key variable usually ignored in modeling fruit tree transpiration, and directly related to water stress and drought, is soil and plant hydraulic conductivity. Soil and xylem conductivity both decrease under hydraulic tension, and these decreases can be described well with physically based 'unsaturated conductivity curves' (for soil) or 'vulnerability curves' (for xylem). Improving the representation of soil and xylem hydraulics in models of crop water use is necessary to achieve a mechanistic link between soil water availability and canopy water use (Sperry *et al.*, 2002). The present study will assess the ability of two process-based models – the Sperry *et al.* (1998, hereafter SACC) model of hydraulic limits and the Buckley *et al.* (2003, hereafter BMF) model of stomatal conductance – to inform management of water use in a hedgerow olive orchard. Our results demonstrate the central role played by the rhizosphere in the hydraulic limitation of transpiration in this orchard. This limitation can be partially managed by farmers if leaf area (pruning practices) and number of drippers in the irrigation system are modified. Moreover, our results show how much both hydraulic and non-hydraulic signals are involved in the control of transpiration by stomata.

Material and methods

Study site and orchard characteristic

The experiments were made in 2011 at the Sanabria orchard, a hedgerow olive commercial orchard at 25 km to the west of Seville, southwest Spain (37°15´N, −5°48´W). The trees, 5-year-old *Olea europaea* L. 'Arbequina', were planted at 4 m × 1.5 m (1667 trees ha^{-1}). They had a single trunk with branches from 0.6 to 0.7 m above ground and the rows, 2.40 m tall and 1.96 m wide, run N–NE to S–SW. The area has a Mediterranean climate, with a mild, wet season from October to April and a hot, dry season for the rest of the year. Yearly average precipitation (P) and potential evapotranspiration (ET_o) are 525.9 mm and 1542.4 mm, respectively (period 2002–2011).

   The experimental design was a randomized complete block design with four 12 m × 16 m plots per treatment. Each plot contained 8 central trees surrounded by 24 border trees. All measurements were made on the central trees of each plot. Two irrigation treatments were imposed in the orchard: a Control treatment where irrigation fulfilled tree water demand; and a regulated deficit irrigation treatment in which only 30% of the water added to control was applied (30RDI). The irrigation amounts (IA) supplied to this treatment varied according to the sensitivity to water stress of the crop at each phenological stage. Daily irrigation to replace 100% of the irrigation needs (IN) was calculated as IN = ET_c − P_e, where ET_c is the crop evapotranspiration and P_e the effective precipitation (75% of P recorded by the weather station in the orchard). Daily ET_c values were calculated as ET_c = K_c K_r ET_o, where K_c is the crop coefficient and K_r is a coefficient related to the percentage of ground covered by the crop. We used the K_c values derived by Fernández *et al.* (2006a) for an orchard of similar characteristics, with a slightly greater canopy volume than that of the present orchard (0.76 in May; 0.70 in June; 0.63 in July and August; 0.72 in September; 0.77 in October; 1.07 in November) and we calculated a K_r value of 0.75 after Fereres & Castel (1981). Daily values of the FAO-56 Penman-Monteith ET_o

were collected from a nearby standard weather station belonging to the Agroclimatic Information Network of the *Junta de Andalucía*. Water for irrigation was supplied by a system consisting of one drip line per tree row with a 2 L h^{-1} dripper every 0.5 m with, and one caudalimeter per treatment to record the applied IAs. We used an irrigation controller (Agronic 2000, Sistemes Electrònics PROGRÉS, S.A., Lleida, Spain) for supplying the calculated INs. From June 7 to June 13, all trees in the orchard received enough water to match the crop water requirements. From June 14, day of year (DOY) 165, to October 24 (DOY 297), the 30RDI treatment was imposed in the orchard. All trees were fertilized by injecting a 8N-3P-8K + 0.05 % B + 0.05 % Fe solution into the irrigation system, once a week throughout the irrigation season. The amounts of fertilizers were enough to cover the tree requirements.

Root and leaf area measurements

To study root distributions, two soil trenches 1.5 m wide, 1.5 m deep and 3.5 m long were opened in July 2011, one in the Control treatment and one in the 30RDI treatment. Trenches were dug with a backhoe, and then the faces were squared and smoothed with a shovel. Using a 1 m × 1 m grid fixed on the trench face with nails, intersection root density (number of intersections per unit area) was counted in each grid unit of the trench wall face. A water spray bottle was used to highlight the roots to facilitate the identification of root ends. After counting all roots, a total of 17 soil samples with size 200 cm^3 were removed by soil coring. Samples were transferred to the laboratory, where roots were washed from the soil samples and analyzed. All the roots were scanned with a WinRhizo LA 1600 scanner with a resolution of 300 dots per inch, and analyzed with the WinRhizo software (Régent Instruments, Quebec, Canada). Distribution of roots diameters and root length were measured. Root length density (RLD) was calculated from root length and soil volume sampled.

Leaf area (A_L) was measured in each plot on the same days that the water status of the trees was monitored, i.e. once every two weeks during the irrigation season. Measurements were made at dawn with a LAI-2200 Plant Canopy Analyzer (Li-Cor, Inc., Lincoln, NE, USA). We followed the measurement strategy proposed by Villalobos *et al.* (1995) for olive orchards. Briefly, eight points per plot were measured in each of the four plots per treatment. In each plot, four points were measured just underneath the tree row, where LAI is maximum (LAI_{max}), and other four points were measured in the midpoint between two rows where LAI is minimum (LAI_{min}). The average LAI (LAI_{avg}) was calculated using the fraction of ground cover (GC) as a weighting factor ($LAI_{avg} = LAI_{max} GC + LAI_{min} (1-GC)$). The average tree A_L was calculated as LAI_{avg} multiplied by the ground area per plot and dividing by the number of trees in the plot.

Soil water status and physical properties

In every plot we installed two access tubes for a Profile probe (Delta-T Devices Ltd, Cambridge, UK) at 0.5 m from the tree trunk and 0.1 m and 0.4 m, respectively, from the nearest dripper. Measurements of volumetric soil water content (θ_v, $m^3\ m^{-3}$) in each access tube were made 1 - 2 times per week, at 0.1, 0.2, 0.3, 0.4, 0.6 and 1.0 m depths. The Profile probe was calibrated *in situ*, by comparing the values derived from the Profile probe readings with θ_v values measured with TDR probes (TDR FOM/mts, Institut of Agrophysics, Lubin, Poland).

Cores of undisturbed soil were extracted from 0.1 to 1.0 m depth in cylinders (2.5 cm long and 5 cm diameter) to determine textural characteristics and dry bulk soil density (ρ). Two contrasted soil layers were identified. This soil has a 0.6 m deep top layer with an average textural composition of 77.7 % sand, 2.2 % silt and 20.1 % clay, and $\rho = 1.73$ kg m^{-3}. Below 0.6 m there is a less porous soil layer with average textural values of 60.9 % sand, 2.0 % silt and 37.1 % clay, and $\rho = 1.82$ kg m^{-3}.

Undisturbed soil cores were used to determine θ_v at -0.033 MPa using a 0.1-MPa porous ceramic pressure plate (Soil Moisture Equipment Corp., Santa Barbara, CA, USA) and -1.5 MPa by using a 1.5-MPa porous ceramic pressure plates with compressed air (Soil Moisture Equipment Corp., Santa Barbara, CA, USA). Values of residual θ_v (θ_{resid}), saturated θ_v (θ_{sat}), retention curve parameters (α, n) and soil hydraulic conductivity at saturation (K_{sat}) were estimated by using the Rosetta model (Schaap *et al.*, 2001). α is related to the inverse of the air entry suction and n is a measure of the pore-size distribution. Rosetta model is based on van Genuchten model. Inputs to Rosetta were textural characteristics, ρ, and θ_v at -0.033 MPa and -1.5 MPa.

Plant water status

The time course of tree water status was monitored by measuring the leaf water potential at predawn (Ψ_{pd}) and midday (Ψ_{md}), and the midday stem water potential (Ψ_{stem}), once every two weeks during the whole irrigation season. Measurements were made with a Scholander-type pressure chamber (PMS Instrument Company, Albany, Oregon, USA) on one leaf per tree from two representative trees per plot ($n = 8$). For Ψ_{pd} and Ψ_{md} we sampled the 4th or 5th leaf below the apex of peripheral twigs at about 1.5 - 1.9 m above ground. They were healthy, fully developed, sun-exposed leaves facing east. For Ψ_{stem} we sampled leaves from the inner part of the canopy. These leaves were wrapped in aluminum foil *ca.* 2 h before the measurements to ensure hydraulic equilibration with stem xylem water.

Osmotic pressure (π) was measured on the same days as water potentials. At dawn, five leaves per plot were sampled, cleaned with a damp paper towel, packed in aluminum foil and immediately frozen in liquid nitrogen. These leaves were stored in a freezer until analysis. The expressed sap from each leaf was extracted according to Callister *et al.* (2006). π was then determined with a thermocouple psychrometer with six standard C-52

sample chambers (Wescor Inc., Logan, UT, USA) connected to a datalogger (PSYPRO, Wescor Inc.). The measurements were carried out under constant temperature conditions. For each sample, one paper disc soaked with 10 µl of the expressed sap was loaded into the sample chamber. A waiting time of 15 min was determined for sample equilibrium.

Xylem vulnerability

Xylem vulnerability was studied in current year olive shoots. The vulnerability to xylem cavitation was determined by the bench-top technique (Tyree & Dixon, 1986; Sperry & Tyree, 1988). Briefly, 1.5 m long branches were sampled under water from different representative olive trees, wrapped in plastic bags with wet paper towel inside to prevent water loss and transported to the lab where they were left to dry out on the bench. During the drying process, repeated measurements of xylem water potential and percentage loss of conductivity (PLC) were made. For PLC measurement, 30-mm long segments were sampled under water from the current-year shoots of the collected branches and connected to a XYL´EM apparatus (Bronkhorst, Montigny les Cormeilles, France) for determining their hydraulic conductivity (K). K was determined with a filtered (0.22 µm) 50 mM KCl solution at 3 kPa until a steady-stated K was attained. Segments were then flushed at 150 kPa for 20 min to remove the embolisms and K measured again for determining the maximum K (K_m). The PLC was then calculated as:

$$(2.1) \quad PLC = 100 \times \left(1 - \frac{K}{K_m} \right).$$

Leaf gas exchange and sap flow

Measurements of stomatal conductance (g_s) were made with a Li-6400 open flow single pass gas exchange system using a standard 2 cm × 3 cm leaf chamber (Li-Cor Inc., Lincoln, NE, USA) at the hours of maximum

stomatal conductance, from *ca.* 08:00 to 09:00 GMT. For these measurements, two healthy, fully developed, sun-exposed leaves per tree and treatment were sampled (8 leaves per treatment). Chamber conditions were set to match ambient conditions of CO_2 concentration, radiation and temperature.

On April 14 we installed heat-pulse velocity (HPV) probes (Tranzflo NZ Ltd., Palmerston North, New Zealand) for sap flow measurements by the T_z heat-pulse method (Green *et al.*, 2003). One representative tree per plot was instrumented in three plots per treatment (30RDI and Control). Two sets of probes were installed into the trunk of each tree. Each set had two temperature probes, located at 5 mm upstream and 10 mm downstream of a linear heater probe. Each temperature probe had four thermocouples, at 5, 12, 22 and 35 mm below the cambium. One set of HPV probes faced east and the other west, and the minimum distance between the two sets was approximately 0.1 m. Heat pulses (60 J; 60 W over 1 s) were applied once every 30 min. Both the firing of the heat pulses and the recording of the outputs from the probes was made by a CR10X Campbell datalogger (Campbell Scientific Inc, North Logan, USA). The system worked continuously from April 27 to October 30, 2011.

The method was validated for olive by Fernández *et al.* (2006b). We followed their procedure for processing the HPV outputs. The resulting values of each set of probes were averaged to derive the sap flux in the trunk (Q, L h^{-1}), as well as the plant water consumption per leaf area (E_p, mmol m^{-2} s^{-1}).

Canopy conductance (g_c) was estimated from E_p and air vapour pressure deficit (VPD), assuming a complete coupling between canopy and atmosphere (Jarvis & McNaughton, 1986; Moreno *et al.*, 1996), as:

$$(2.2) \qquad g_c = \frac{E_p}{VPD}.$$

The hydraulic resistance of the plant (R_p) was calculated as:

$$(2.3) \quad R_p = \frac{\Delta \Psi}{E_p},$$

where $\Delta \Psi$ is the difference between Ψ_{md} and Ψ_{pd}.

SACC model

The SACC model (Sperry *et al.*, 1998) is based on the biophysics of water flow through the porous media of soil and xylem. A comprehensive overview of the model can be found in Sperry *et al.* (1998, 2002). A brief description is provided here. Water flow rate through vegetation (E_p) is predictable from the hydraulic conductance of the media ($K[\Psi]$) and the difference between the soil water potential of the rooting zone (Ψ_{sr}) and the xylem pressure in the plant canopy (Ψ_{pc}):

$$(2.4) \quad E_p = K(\Psi)(\Psi_{sr} - \Psi_{pc}).$$

The hydraulic conductance is a declining function of Ψ as a result of soil drying and xylem cavitation. The $K(\Psi)$ function for soil is well characterized for soil types (Campbell, 1985), and the Ψ gradient across the rhizosphere is assessed from the ratio of absorbing root area per leaf area ($A_R{:}A_L$). The $K(\Psi)$ function of xylem is the 'vulnerability curve' which can be measured on stems and roots (Alder *et al.*, 1996). The SACC model solves for E_p as a function of rooting depth, profile of Ψ_s, vulnerability curves, and Ψ_{pc} (Sperry *et al.*, 1998). The utility of the SACC model is to provide a mechanistic, predictable, and species-specific link between Ψ_{sr} and g_c. The link is chiefly influenced by the rooting profile and the vulnerability curve: species that are resistant to cavitation or that tap reliable soil water respond with less sensitivity to soil drought than vulnerable or shallow-rooted species. However, the model also predicts the critical fluxes and pressures at

hydraulic failure where the soil-plant hydraulic continuum is severed by dynamic water stress (Sperry *et al.* 1998). In this study we focus on this last application of the model.

BMF model

The BMF model (Buckley *et al.*, 2003) is based on the observed dependence of stomatal aperture on turgor pressures of stomatal guard cells and adjacent epidermal cells, and on the effect of stomatal transpiration on those turgor pressures, via bulk leaf water potential. The model assumes that guard cell osmotic pressure is actively regulated to seek a 'target' value that is proportional to both epidermal turgor pressure and the concentration of ATP in photosynthesising cells (τ). τ is a function of irradiance, intercellular CO_2 concentration and photosynthetic, as discussed below. Additional parameters in the model include soil water potential (Ψ_s), leaf osmotic pressure (π), plant hydraulic resistance (R), VPD, net epidermal mechanical advantage (M), a scaling factor that includes effects of stomatal density (χ) and a parameter that describes sensitivity to epidermal turgor and ATP concentration (β). The model predicts stomatal conductance (g_s) as:

$$(2.5) \quad g_s = \frac{\chi(\beta\tau - M)(\Psi_s + \pi)}{1 + \chi(\beta\tau - M)R\text{VPD}} \, .$$

Preliminary work showed that qualitative predictions of g_s were insensitive to the value of M, a parameter that is very difficult to measure, so for simplicity we set $M = 0$. This further allowed the product $\chi\beta$ to be treated as a single parameter. Parameters in the model were either measured as described above (Ψ_s, π, and VPD), fitted by least-squares ($\chi\beta$ and R), or simulated (τ). The concentration of ATP (τ) was calculated using the model of Farquhar & Wong (1984), which is based on the photosynthesis model of Farquhar *et al.* (1980). Parameters of the Farquhar *et al.* model specific for

olive were measured by gas exchange, as described by Diaz-Espejo *et al.* (2006). The model for ATP (τ) predicts a roughly hyperbolic increase of τ with increasing irradiance, and a negative response of τ to intercellular CO_2 concentration that is steeper at high light, consistent with laboratory studies of stomatal responses to light and CO_2 (e.g., Buckley *et al.*, 2003; Messinger *et al.*, 2006). Buckley *et al.* (2003) discussed in detail the rationale for using this model, and its implications for predicting stomatal responses to light and CO_2.

Results

Meteorological and soil data

Fig. 2.1 shows the time courses of main environmental variables and IAs for three different periods of the olive growing season. Left panels (Fig. 2.1 A, D, G, J) represent the period in which irrigation was supplied daily in both treatments, although with lower IAs in 30RDI. In the central panels (Fig. 2.1 B, E, H, K), irrigation in 30RDI was reduced to once per week, meanwhile in Control it continued in a daily basis. In the last period showed by the right panels (Fig. 2.1 C, F, I, L) irrigation frequency to 30RDI was increased to twice per week. θ_v values in 30RDI echoed the irrigation events (Fig. 2.1 G-I). During the first period water supply was enough to keep θ_v at nearly constant values, which increased with depth. However, the amplitude of their fluctuations decreased with depth (Fig. 2.1 G). During the other periods, irrigation events affected the first 0.3 m of soil only. At 0.4 m θ_v remained close to 0.1 m^3 m^{-3}. No changes were detected at 0.6 m and 1.0 m depth, where θ_v was close to saturation all along the season. Table 2.1 shows the textural characteristics in the soil orchard, defining a sandy loam soil layer for the first 0.6 m, and then a sandy clay layer around 0.6 and

downwards. Despite the large percentage of sand in both layers, the small differences in clay content produced large differences in their hydraulics properties. During most of the irrigation season, the radiation regime showed a constant pattern along the periods reaching maximum daily values of 1000 W m^{-2}, with seldom exceptions of partially cloudy days (Fig. 2.1 A-C). Daily maximum VPD was always higher than 2 kPa (Fig. 2.1 D-F), and most frequently close to 5 kPa, with peak values close to 6 kPa. Air temperature reached maximum values of 39 °C.
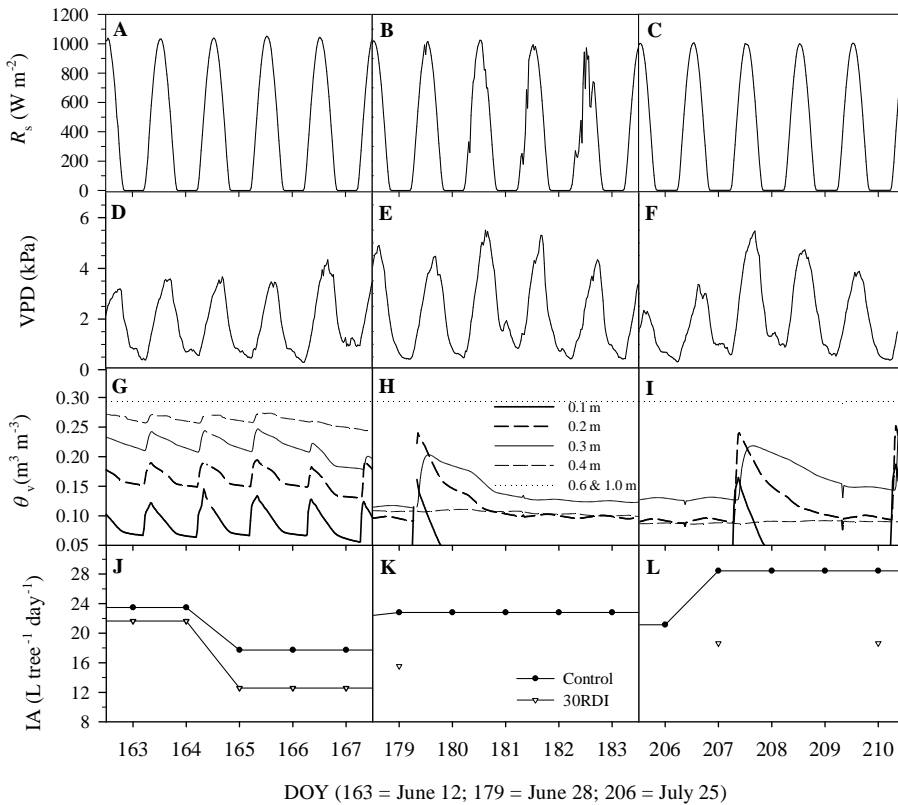
Fig. 2.1. Time courses of solar radiation (R_s), air vapour pressure deficit (VPD), volumetric soil water content (θ_v) in 30RDI, and irrigation amounts (IA) on three periods of the irrigation season at the experimental orchard. Left panels (A, D, G, J) represent a period of

time in which irrigation was applied daily; central panels (B, E, H, K) represent an early stage of the stress period when irrigation to 30RDI was applied once per week; right panels (C, F, I, L) represent the last days of the irrigation season, when irrigation to 30RDI turned into twice per week. DOY = day of year.

Table 2.1. Soil textural and physical properties obtained by the Rosetta software. ρ = soil bulk density (kg m^{-3}), θ_{33} = volumetric soil water content at field capacity (m^3 m^{-3}); θ_{2500} = volumetric soil water content at wilting point; θ_{resid} = residual volumetric soil water content (m^3 m^{-3}); θ_{sat} = saturated volumetric soil water content; α = parameter related to the inverse of the air entry suction (cm^{-1}); n = parameter related to the pore-size distribution (unitless); K_s = saturated hydraulic conductivity (cm day^{-1}).

Depth	Sand	Clay	Silt	ρ	θ_{33}	θ_{2500}	θ_{resid}	θ_{sat}	$\log_{10}(\alpha)$	$\log_{10}(n)$	$\log_{10}(K_s)$
0-0.6	77.7	20.1	2.2	1.73	0.16	0.09	0.038	0.34	-1.53	0.123	1.68
0.6-1.0	60.9	37.1	2.0	1.82	0.24	0.14	0.041	0.33	-1.61	0.119	1.86

Roots distribution and leaf area

A linear correlation was found between RLD and intersection root density on the trench walls. The slope was 2.47 after the intercept was forced to pass through zero. Root distribution observed on trench walls followed a pattern related to irrigation wet bulb locations in both Control and 30RDI treatments (Fig. 2.2). No roots were found below 0.45 m. Root length density measured in soil core samplings reached a maximum value of 1.4 cm cm^{-3} in points inside wet bulbs. Wet bulbs were observed to have a volume of *ca.* 0.04 m^3. Since each tree had three drippers, the total volume of wet soil was 0.12 m^3. Assuming a radius for the fine roots of 0.25 mm, an average 2.65 m^2 of root area (A_R) was calculated. The distribution of roots shown in Fig. 2.3 helped us to determine the effective depth of available water for the trees. The value of 0.45 m matched well with the seasonal evolution of θ_v at 0.4 m (and above) and at 0.6 m (and below) showed in

Fig. 2.1 G-I. Another evidence for the absence of roots below 0.45 m can be inferred from the constant value of θ_v, close to saturation, measured all along the season. This value did not decrease even when θ_v at 0.4 m presented values as low as 0.12 m^3 m^{-3}. An upper limit of 0.1 m was also set on the view of the low values measured at this shallow depth, close to residual. Values of θ_v were turned into Ψ_s by using soil physical parameters shown in Table 2.1. A single value of Ψ_s was obtained from the integration of θ_v from 0.2 to 0.4 m, and compared to the values of Ψ_{pd} measured in those trees, obtaining a good agreement (see Extra Fig. 2.1 in Appendix I).
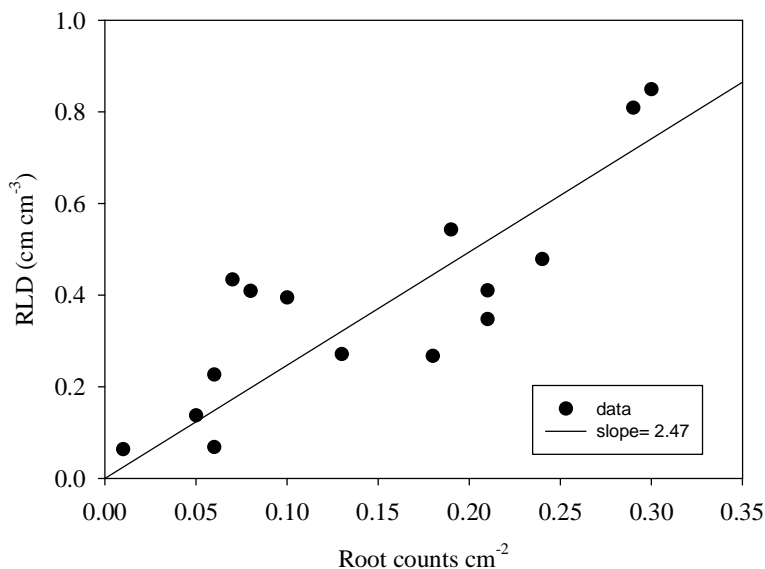
Fig. 2.2. Relationship between root length density (RLD) and root intersection on the trench wall per unit of surface. Data correspond to both Control and 30RDI treatments. r^2 = 0.65 was significant at a value of $P < 0.01$.

Despite significant differences of A_L between treatments at the beginning of the growing season, the high growing rate of 30RDI trees

during spring allowed them to catch up Control trees by the time the daily irrigation was still on (Fig. 2.4). At this time of the year A_L was on average 7.25 m^2 per tree, meaning a LAI in the orchard of 1.43. However, Control trees grew again from mid July, up to maximum value of 12.3 m^2 in October. This growing period was not observed in the 30RDI trees, which showed a constant A_L all over the studied period. Assuming no changes in A_R in 30RDI during this period, A_R:A_L was calculated as 0.38.
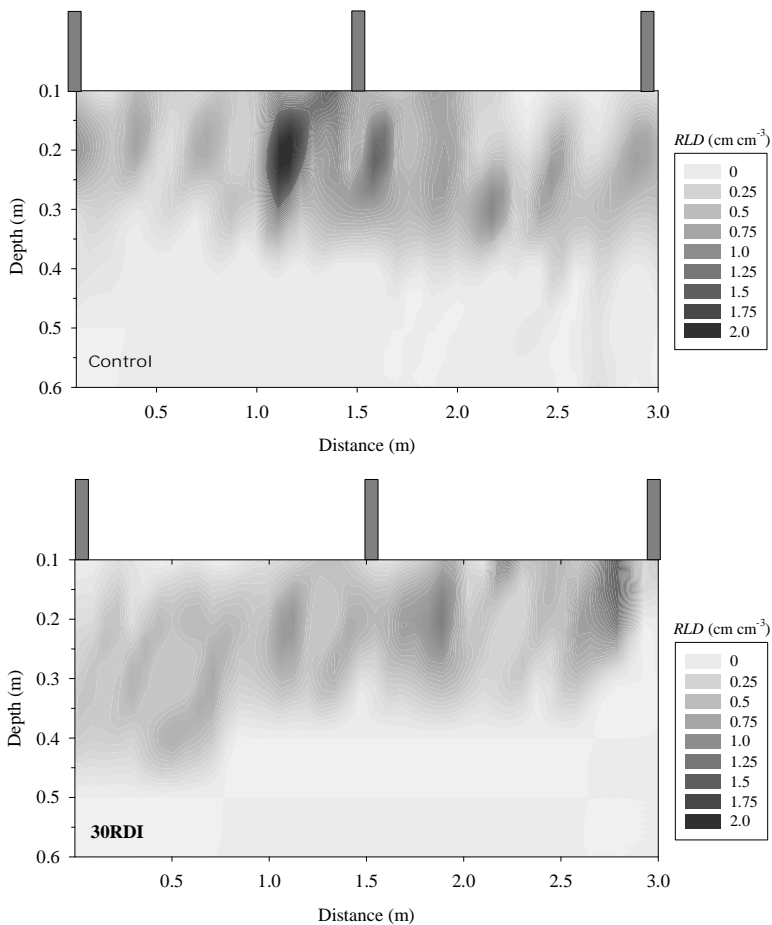
Fig. 2.3. Spatial distribution of root length density (RLD) on a trench wall in both the Control and 30RDI treatment. RLD values were calculated from the relationship shown in Fig. 2.2. Vertical bars on the upper horizontal line represent the tree trunks.
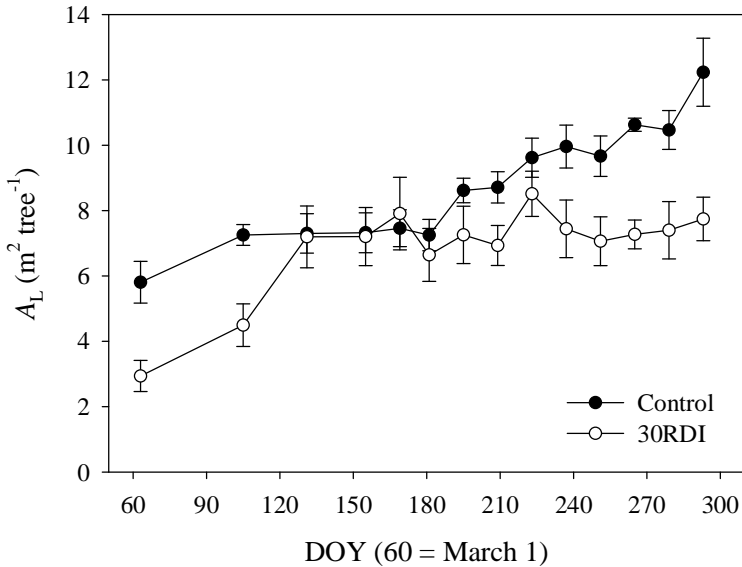
Fig. 2.4. Seasonal courses of tree leaf area (A_L) for the two irrigation treatments. DOY = day of year.

Plant water status, leaf gas exchange and transpiration

Full water availability in the soil for the Control trees was indirectly assessed on the view of the high values of Ψ_{pd} measured along the growing season (Table 2.2). However, 30RDI trees presented a minimum value of -1.5 MPa on DOY 209. Proportionally, Ψ_{md} showed a clear difference between treatments as soon as the irrigation frequency changed to once or twice per week in 30RDI, getting to a minimum value of -2.96 MPa on July 28, DOY 209 (Table 2.2). At the same time, g_s showed nearly constant maximum values in Control trees along the season, meanwhile more than 3-fold lower g_s values were measured in 30RDI trees at the end of the studied period

(Table 2.2). These data matched well with E_p estimated from sap flow, shown in Fig. 2.5. This figure shows a period in which irrigation was applied daily to both treatments, although with slightly lower IAs to 30RDI, and the period in which the maximum stress was observed. During the first period, very close E_p were measured in both treatments, the small differences reflecting likely the different IAs mentioned above. However, a clear drop of more than 5-fold in 30RDI was observed during the second period plotted. In this period the E_p cycles of stress and recovery following irrigation were clear. R_p increased in both treatments during summer (Table 2.2). However, in Control trees R_p increased 1.4-fold, while in 30RDI trees the increase was over 8-fold.

Table 2.2. Seasonal evolution of main physiological variables in both Control and regulated deficit irrigation trees (30RDI). Ψ_{pd} = pre-dawn leaf water potential; Ψ_{md} = midday leaf water potential; g_s = stomatal conductance (mol m^{-2} s^{-1}); R_p= plant hydraulic resistance (MPa mmol^{-1} m^2 s). Each value represents the average of 8 replicates ± SE. Asterisk indicates significant differences between treatments on each date (*t*-student, $P < 0.05$).

Variable	Treatment	DOY 165 (Jun 14)	181 (Jun 30)	209 (Jul 28)	223 (Aug 11)
Ψ_{pd}	Control	−0.20 (0.04)	−0.31 (0.05)*	−0.37 (0.02)*	−0.30 (0.03)*
	30RDI	−0.15 (0.03)	−0.50 (0.03)*	−1.53 (0.15)*	−1.09 (0.11)*
Ψ_{md}	Control	−0.99 (0.14)	−1.33 (0.13)	−1.37 (0.19)*	−1.07 (0.12)*
	30RDI	−0.77 (0.14)	−1.80 (0.23)	−2.96 (0.10)*	−2.50 (0.19)*
g_s	Control	0.222 (0.01)	0.193 (0.01)*	0.215 (0.02)*	0.229 (0.02)*
	30RDI	0.233 (0.01)	0.098 (0.01)*	0.069(0.01)*	0.069 (0.01)*
R_p	Control	0.53 (0.12)	0.59 (0.08)*	0.64 (0.12)*	0.74 (0.12)*
	30RDI	0.47 (0.10)	2.03 (0.37)*	4.49 (0.82)*	4.10 (0.57)*
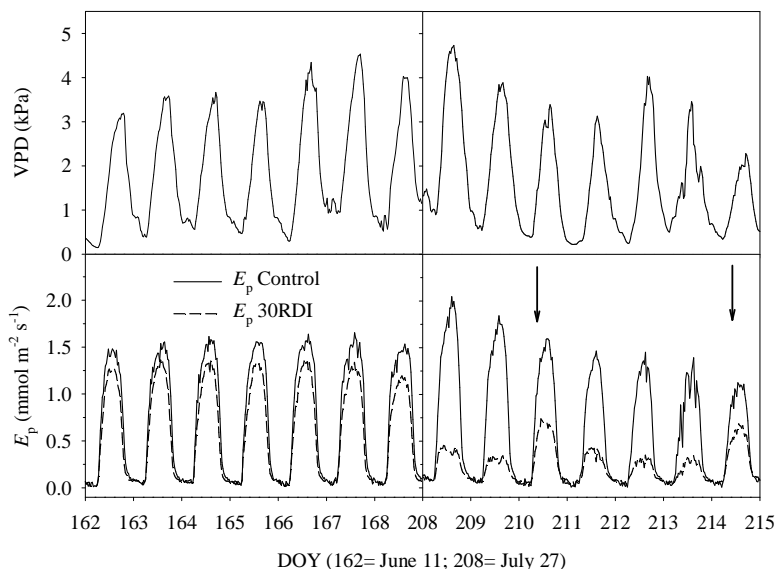
Fig. 2.5. Time courses of air vapour pressure deficit (VPD) and transpiration estimated from sap flow measurements (E_p). Graphs on the left shows a period previous to the 30RDI treatment, when all trees in the orchard were daily irrigated. Graphs on the right correspond to days on which the 30RDI trees were irrigated twice per week. Arrows indicate irrigation events during this second period. DOY = day of year.

SACC model

Soil and plant hydraulic properties are the main determinants of the hydraulic limits for a species in a particular soil. Fig. 2.6A shows the relationship between K_s and Ψ_s based on the Van Genuchten equation. Despite of its high sand content, the orchard soil behaves more similar to a typical clay or silt soil, rather than a sandy soil. However, its high sand content makes it have 25-fold greater K_s than clay at $\Psi_s = 0$ MPa, and 13-fold smaller K_s at $\Psi_s = -1.0$ MPa. Xylem vulnerability curves (Fig. 2.6B)

show that olive is quite resistant to embolism. A PLC of 24 % was found at $\Psi_{stem} = -3.0$ MPa, the minimum Ψ_{stem} measured in the field site that year. The Ψ_{stem} at which 50 % of K is lost (P_{50}) was -5.0 MPa. A complete loss of K (P_{100}) was only achieved at values lower than -15 MPa. By comparison, grapevine – another woody crop considered to be well-adapted to semi-arid conditions – showed a P_{50} of -2.8 MPa, and a P_{100} around -5 MPa.
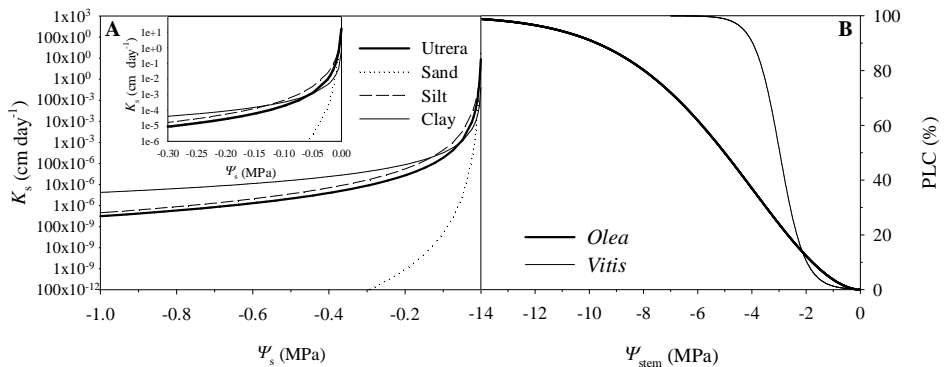
Fig. 2.6. (A) Relationship between soil matric potential (Ψ_s) and soil hydraulic conductivity (K_s) for the Sanabria orchard soil at the top 0.6 m. The inset allows for a closer comparison of K_s at the highest Ψ_s. The small percentage of clay allows the maintenance of higher K_s than pure sand as Ψ_s decreases. Meanwhile the large percentage of sand of this soil allows for a high K_s at $\Psi_s = 0$. (B) Comparison of curves of vulnerability to cavitation of two species with contrasting resistance: *Olea* and *Vitis*. Data for *Vitis* was obtained from Choat *et al.* (2010). PLC data were fit with the Weibull equation: $1 - e^{-(\frac{-\psi}{d})^c}$. *Olea*, $d = 6.13$, $c = 1.81$; *Vitis*, $d = 2.97$, $c = 2.2$.

This information, together with A_R and A_L, was used to build the 'envelope' of water use proposed by Sperry *et al.* (1998, 2002). The difference between the actual transpiration and the envelope is called the safety margin, and it is reduced as Ψ_s is lower. Fig. 2.7 shows four different envelopes: two for olive and two for grapevine. In addition, actual data of

E_p *vs* Ψ_s were obtained from sap flow and continuous measurements of θ_v in the orchard and included in the plot for comparison. Data fit well under the olive envelope (thick line) for most of the range of Ψ_s. For very low values of Ψ_s data were above the limits. This could be due to uncertainty in Ψ_s arising from integration over three layers of heterogeneous soil moisture. A large safety margin is evident between the envelope at $A_R{:}A_L$ measured in the orchard at high Ψ_s. However, this margin is severely reduced at Ψ_s close to -3 MPa. For grapevine, a similar value of $A_R{:}A_L$ reduces the envelope notably, indicating that grapevine could not sustain the E_p values measured for olive. A three-fold increase in $A_R{:}A_L$ increased the safety margin, emphasizing the differences in within-plant hydraulic limitation in the two species.
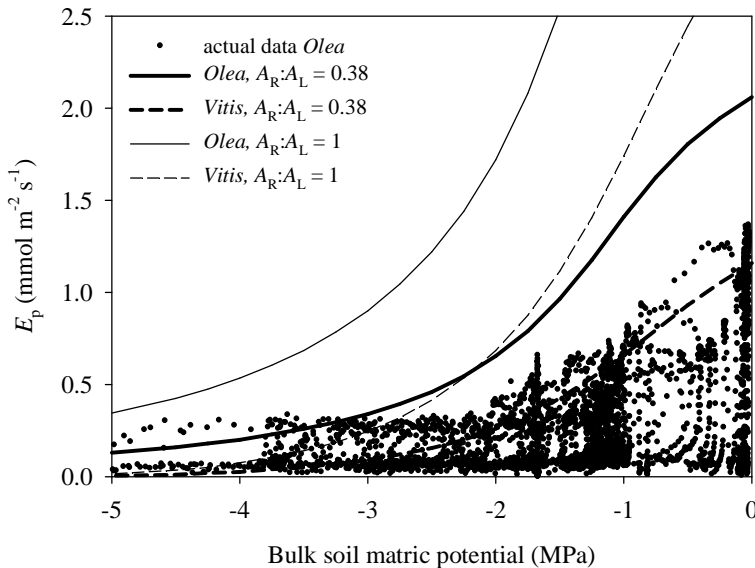
Fig. 2.7. Results of plant transpiration (E_p) simulated by the SACC model for two species of contrasting vulnerability to caviation: *Olea*, resistant, and *Vitis*, sensitive. All simulations were made for the soil conditions of our experimental orchard. Lines represent the hydraulic limit to transpiration fitted both by the rhizosphere and xylem. Simulation were made for two different root-leaf area ratios ($A_R{:}A_L$). The lower $A_R{:}A_L$ value, 0.38, is the

actual value measured in the experimental orchard. Data points represent the actual E_p derived from sap flow measurements in the orchard.

The model can be used to simulate the effect of pruning intensity (changing A_L) or the impact of the number of drippers (changes in volume of wet soil and therefore A_R) in E_p. As expected, the increase in LAI decreases E_p (Fig. 2.8A), assuming that A_R keeps constant (through changes in RLD, since the volume of soil is limited). If LAI is doubled, maximum E_p is halved. An increase in the number of wet drippers from 3 to 5 would nearly compensate for an increase in LAI. Since each dripper generates a wet bulb in the soil of 0.3 m in diameter, and each tree is 1.5 m apart from neighbors, five drippers is the maximum number that a line can hold.
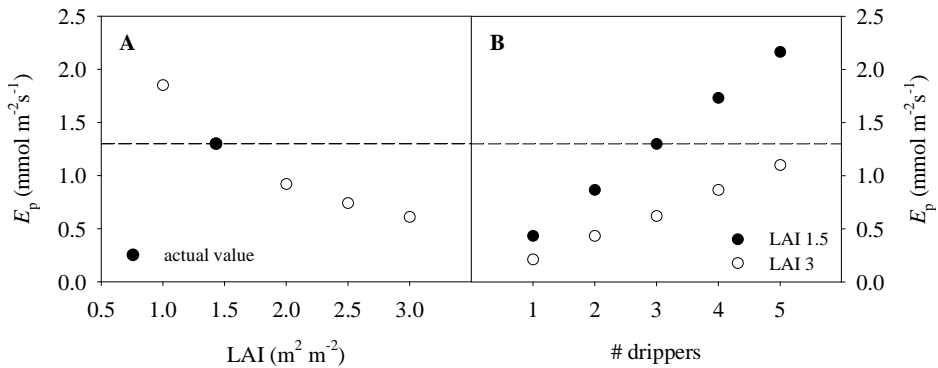
Fig. 2.8. Modeling exercise with the SACC model under well-irrigated conditions. (A) Effect of increasing leaf area index (LAI) on transpiration rate (E_p). Close circles represent the actual values measured in our experimental orchard. We assumed a constant root length density when LAI increased. Simulation was made for three drippers (total volume of wet soil = 0.12 m³). (B) Effect of increasing number of drippers on E_p, for two different LAIs. We assumed a greater root area when the number of drippers, and therefore the volume of wet soil, increased. It was assumed that root distribution followed the pattern shown in Fig. 2.3.

BMF model

g_c values estimated from sap flow measurements are plotted in Fig. 2.9 for the days leaf gas exchange and leaf water potential were measured (Table 2.2). The use of g_c values allowed us to have complete series of diurnal evolution of a close surrogate of g_s to apply the model. On DOY 165 (June 14) during the period of daily irrigation in 30RDI, no significant differences were observed between treatments. However, differences emerged as the soil dried out. A 4-fold decrease in 30RDI g_c compared to Control g_c values was observed on DOY 209 (July 28). The model fit well to measure g_c on all dates shown and in both treatments. The model was able to reproduce the two peaks measured on at the beginning of DOY 181 (June 30). The seasonal evolution of the three parameters of the model is plotted in Fig. 2.10. π was measured and input to the model. Fig. 2.10A shows identical osmotic adjustment (change in π with Ψ_s) in both treatments despite their differences in Ψ_{md}. Tree hydraulics showed differences between treatments (Fig. 2.10B). These differences were evident from DOY 181, and especially later on, when a 3-fold increase in R of 30RDI was estimated by the model (which was fitted by least squares). Control trees showed a nearly steady value of R along the season. $\chi\beta$ (also fitted by least squares) showed a similar seasonal trend in both treatments (Fig. 2.10C), except on DOY 223 (August 11) when a small recovery was obtained in Control. The model always predicted higher values for Control than for 30RDI.
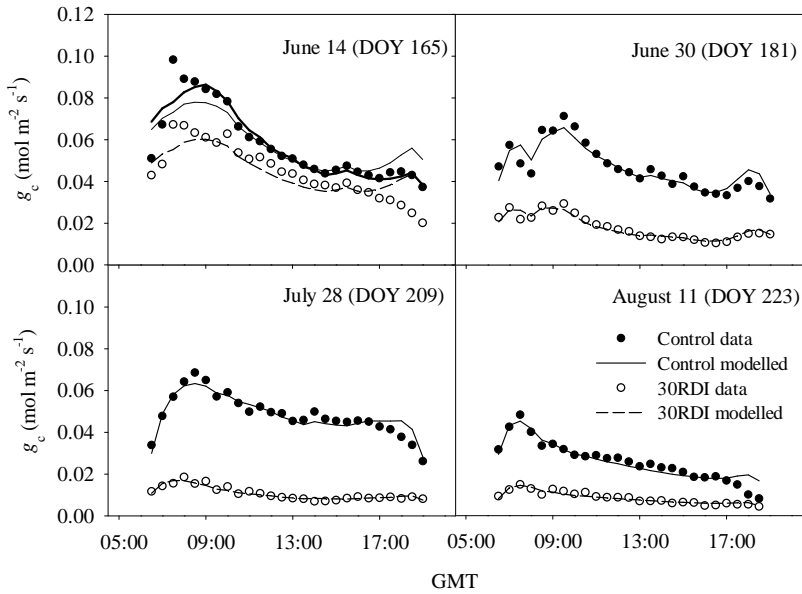
Fig. 2.9. Simulation of the evolution of canopy conductance (g_c) by the BMF model, for both Control (close circles) and 30RDI (open circles) trees. Points represent actual g_c data derived from sap flow measurements made in the orchard every half-hour. The lines represent the simulated values. The thicker line on DOY 165 shows the result of the model with a variable soil matric potential (Ψ_s) as mentioned in the text. Similar results were obtained for the 30RDI trees on that day, but the line has not been included for clarity. The input meteorological data was obtained from the weather station located in the orchard, and Ψ_s was estimated from predawn leaf water potential.
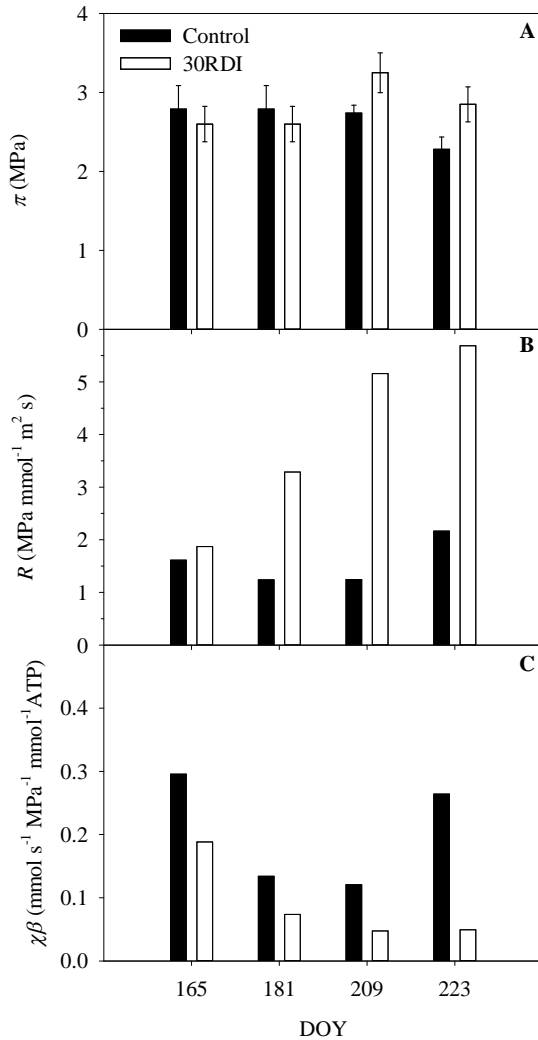
Fig. 2.10. Values of the BMF parameters for the four days in which we measured leaf gas exchange and leaf water potential (see Table 2.2). (A) Measured osmotic pressure of leaves (π, $n = 8$). (B) Soil-to-leaf hydraulic conductance (R). (C) Sensitivity of the hydroactive mechanism of response of guard cells to turgor pressure ($\chi\beta$). This parameter is potentially related to ABA. Both R and $\chi\beta$ were modeled parameters.

Discussion

The use of models with a mechanistic basis has a strong attraction for scientists working on the control of transpiration by plants under water stress conditions and on irrigation scheduling. There are numerous interacting processes involved in the acclimation of plants to water stress (Chaves *et al.*, 2002; McDowell *et al.*, 2008; Neumann, 2008). The integration of all the involved mechanisms is challenging, in particular the coordination of responses at different scales, from the stomata to the whole plant and their interaction with the soil. Mechanistic models help to describe the processes across the scales, including the soil and plant hydraulic resistance, and the leaf/tissue scale of stomatal regulation. The results obtained in this work are very encouraging for understanding and interpreting the behaviors usually observed in fruit woody plants during acclimation to drought. We have used process-based models to describe the main physiological changes observed in a hedgerow olive orchard under regulated deficit irrigation in southern Europe during an irrigation season, and to put these responses in the context of local climate and soil characteristics.

Physiological response to water stress

Transpiration was steady in both treatments during the first period, during which irrigation was applied daily, and despite wide variation in VPD. This indicates strong stomatal regulation (Fig. 2.5, left panel). Therefore, we can conclude that a maximum E_p of 1.7 mmol m^{-2} s^{-1} and 1.3 mmol m^{-2} s^{-1} are the limits for Control and 30RDI respectively at this time of the season. When the irrigation frequency decreased to once or twice per week in 30RDI (Fig. 2.5, right panel), E_p decreased and showed a cycle of recovery and down-regulation that agreed well with the irrigation events. Even on days when irrigation was applied, E_p did not fully recover. Moreover, on DOY 208 (July 27) a maximum E_p of 2 mmol m^{-2} s^{-1} was achieved in Control, i.e. 17 % higher than in the first period studied. Two questions arise from the observation of these data: 1) Why was the response of

30RDI trees to irrigation so dynamic in comparison to other findings reported for olive under deficit irrigation (DI) and even under dry-farming conditions (Fernández *et al.*, 2008c)? 2) What is limiting E_p in Control trees during early summer in comparison to late summer?

Our recent research in a nearby olive orchard may help to answer the first question. Palomo *et al.* (2002) and Fernández *et al.* (2003) worked with 'Manzanilla' olive trees at La Hampa orchard, at 15 km southwest of Seville, and found a slower reduction in E_p, in trees under DI and dry-farming conditions, than the measured in this study (Sanabria orchard). The simplest explanation is that water depletion from soil was slower and the access to soil water was larger in the La Hampa study than in the present (Sanabria) study. This is supported by the high Ψ_{pd} values measured in summer in non-irrigated trees at La Hampa, and by the slow decrease of E_p even in periods of several weeks without any water supply (Fernández *et al.*, 2008c). Trees at La Hampa are older than at Sanabria (45- *vs* 5-years old) and of bigger size (50 m² *vs* 12 m² A_L), but lower LAI (1 m² m⁻² vs 1.43 m² m⁻²). However, the main difference between these orchards involves the soil and rhizosphere. The soil at La Hampa is deeper (up to 2 m deep) and roots of non-irrigated trees explore a greater volume of soil, *ca.* 32 m³ (Fernández *et al.* 1991, 2008a) than in Sanabria. The average RLD is about 0.2 cm cm⁻³ (Fernández *et al.*, 1991). This suggests A_R = 100 m², and therefore an A_R:A_L = 3.34 vastly greater than the A_R:A_L = 0.38 estimated for Sanabria and than the value of 1.0 used for the simulation in Fig. 2.7. The low A_R:A_L value for Sanabria is due to the shallow establishment of the rhizosphere in the soil profile. Roots were not found below 0.45 m, and most of them were enclosed in the wet bulbs (Fig. 2.3). When dry, the deeper layer of soil, richer in clay, shows a high resistance to penetration. When wet, the low hydraulic conductivity favored hypoxia conditions, which it is known to restrict olive root growth (Fernández & Moreno, 1999). The θ_v values that were almost continuously near saturation in this layer were probably not amenable to root growth. The slope of the relationship between RLD and

intersection point density in the trench wall, close to 2 (Fig. 2.2), suggests an isotropic root growth, i.e. roots grew in all directions of space (López-Zamora *et al.*, 2002). This is what it can be expected from a localized irrigation system where most of the roots are concentrated in the wet bulbs and nearby regions (Pires *et al.*, 2011). In addition to this, olive trees at Sanabria are relatively young and have been growing under drip irrigation conditions since planting. Therefore, they have acclimated their root development to this spatial availability of water. Moreover, the soil's high sand content makes K_s very sensitive to changes in the soil moisture (Fig. 2.6), i.e. small changes in θ_v produces large changes in K_s. These two circumstances – a reduced rhizosphere and very coarse soil – make transpiration very dependent on the frequency and amount of irrigation events, due to the low buffer capacity of the soil.

The answer to the second question, what limits E_p in Control trees in early summer, is partly implicit in the preceding discussion. Although E_p was higher in Control trees on DOY 208 (July 27) than on DOY 167 (June 16), g_c reached a higher peak value early in the morning on DOY 167 than on DOY 208 (data not shown). Differences in VPD values were not significant, but their diurnal shape was; the difference arose from greater g_c at mid-day on DOY 208 when VPD was maximum. This was probably due to the greater irrigation applied on DOY 208 (28 L tree^{-1}) *vs* on DOY 167 (18 L tree^{-1}), which could have led to large differences, both in Ψ_s and K_s, in this sensitive soil. The agronomical implications for this observation might be negligible, but the analysis of this observation will help us to explore the sensitivity of the BMF model later on.

The seasonal evolution of g_s measured in sunlit leaves (Table 2.2), shows that while the stomata of the Control trees remained fully open, that of the 30RDI trees was reduced by half soon after the frequency of irrigation decreased to once per week. By the end of the summer g_s was reduced more than 3-fold. g_s was strongly correlated with Ψ_{md} down to 0.1 mol m^{-2} s^{-1},

but below this point the response became less steep. Olive has been reported as a near-isohydric species (Cuevas *et al.*, 2010), able to maintain nearly constant Ψ_{md} under varying evaporative demand, whereas our data indicate substantial changes in Ψ_{md} under varying Ψ_s. Our results, then, are more in agreement with those of Tognetti *et al.* (2009), who concluded that olive had an anisohydric behavior under the conditions of their study. Our findings, however, are not contradictory with those of Cuevas *et al.* (2010). Hacke *et al.* (2000) demonstrated that the isohydric and anisohydric behaviors depend on the type of soil where the plant grows. Loamy soils favor isohydric behavior meanwhile sandy soils do anisohydric. This is related to the hydraulic limits imposed by soil and plant, which will be seen in detail in the next section.

Results from a hydraulic model

Are there hydraulic constraints for transpiration in our olive orchard, and if so, are they due to soil or plant? The SACC model (Sperry *et al.*, 1998) is uniquely suited to answer this question. Some species can maintain transpiration and survive at very low Ψ_s, like *Artemisia tridentata* (Kolb & Sperry, 1999), while others, like *Betula occidentalis*, cannot (Sperry *et al.*, 2002). Similarly, plants growing on nearby soils of different characteristics, like the case of a *Pinus taeda* stand planted on a patchy soil (Hacke *et al.*, 2000), showed very different canopies and patterns in water use. The model predicts a water use envelope that sets the limit for transpiration as a function of Ψ_s; beyond this limit, the plant would suffer catastrophic failure of its hydraulic system. As far as we know, this model has not yet been applied to woody fruit trees or to the management of irrigation. The discussion above highlights the role of our orchard's soils in setting hydraulic limits on water use. Fig. 2.7 shows the water use envelope for trees with a root to leaf area ratio (A_R:A_L) of 0.38 (our trees at Sanabria), in comparison to actual data. The measured E_p was below the boundary line over the entire range of Ψ_s measured. Exceptionally, some points at low Ψ_s

are above the line; however this can be explained by the inaccuracy in the estimation of a single bulk value of Ψ_s while attempting to represent the whole soil profile. This is especially true in soils that have very heterogeneous θ_v distribution due to drip irrigation, like the one at Sanabria. Despite this, the performance of the model is good, and explains our data satisfactorily. The difference between the model and the actual transpiration is wider at high Ψ_s than at lower ones. In other words, there is a larger safety margin at high Ψ_s than at low ones, where actual values of E_p get closer to the envelope. This was already observed by Sperry *et al.* (1998, 2002) in other species. In general, our conditions of sandy soil with a shallow root system favor the existence of a low $A_R{:}A_L$, which "pushes" the envelope to actual values of E_p at relatively high Ψ_s.

Most plants usually do not modify the vulnerability of their hydraulic system in response to drought (Maherali & DeLucia, 2000; Cornwell *et al.*, 2007; Fichot *et al.*, 2010), although some species have been reported to do so (Kolb & Sperry, 1999; Beikircher & Mayr, 2008; Fichot *et al.*, 2010). Of course, they cannot modify the soil texture either. The main variable that plants regulate to influence the shape of the water use envelope is the $A_R{:}A_L$. Fig. 2.7 shows how an increase from $A_R{:}A_L$ = 0.38 to 1 makes transpiration approach the critical E_p at Ψ_s much lower than −3 MPa. For a species like olive with a high resistance to xylem cavitation, an increase in $A_R{:}A_L$ allows the plant to function at extremely low Ψ_s without reaching the permanent wilting point. A value of $A_R{:}A_L$ = 3.34 was calculated at La Hampa orchard, indicating no limitation by the rhizosphere in that location. The stomatal control of actual E_p shown in Fig. 2.7 agrees with measurements of g_s at the leaf level. At Ψ_s = −1.5 MPa g_s was 0.69 mol m^{-2} s^{-1}. And in the previous year, 2010, Ψ_s dropped to −3 MPa for a g_s of 0.048 mol m^{-2} s^{-1} (data not published), which indicates a nearly total stomata closure. We must be aware of the lack of information about A_R evolution, in contrast to the well described evolution of A_L. This could modify slightly

the value of 0.38 estimated. We think, however, that the bias is not important since the volume of soil for active growing is limited to wet bulbs, where we have measured RLD values close to the maximum values reported by olive orchards under drip irrigation (Fernández *et al.*, 1991).

The effect of greater xylem vulnerability can be evaluated with grapevine simulations (Figs. 6 and 7). Grapevines planted at Sanabria and with an A_R:A_L = 0.38 would not be able to maintain the same E_p as olive. Assuming a potential E_p of 1.3 mmol m^{-2} s^{-1}, similar to that for olive in this study, and considering that the safety margin is maintained at high Ψ_s despite the decreasing water use envelope (Sperry *et al.*, 2002, Fig. 2.3), maximum E_p would be reduced by half. Increasing A_R:A_L to 1.0 eliminates this limitation at high Ψ_s, and allows grapevine to approach the extraction limit of around −5 MPa imposed by the xylem. Changes in A_R:A_L could be achieved not only by increasing A_R but also by decreasing A_L. Some species like *Quercus canariensis* and *Q. faginea*, typical of our latitudes, are semi-deciduous, i.e. their leaves drop in summer, which reduces A_L. In some species adapted to arid environments the reduction of A_L in summer can be extremely severe, provoking leafless branches (Miranda *et al.*, 2010).

Contrary to what happens in plants under natural conditions, farmers can modify the A_R:A_L ratio by changing both A_R and A_L. Fig. 2.8 shows a simulation of the impact of a changing LAI on E_p if A_R is kept constant. E_p is decreased by 50 %. In olive, as in most crops, yield is directly related to water transpired by the plant (Moriana *et al.*, 2003; Fereres & Soriano, 2007). The simulation rests on two assumptions. One is that A_R is maintained, which is likely due to the limitation of volume of wet soil imposed by localized irrigation and the high RLD already found. The second assumption is that the increment in E_p with increasing LAI is not dependent on a different percentage of sunny and shaded leaves. We did not consider, in the simulation, that increasing LAI enhances the number of shaded leaves *vs* sunny leaves. But if that effect is taken into account, the

assumption also holds, as Fernández *et al.* (2008a) demonstrated using a multilayer radiation interception model. The simulation in Fig. 2.8 shows an important impact of the pruning management in the orchard, and sets an optimal LAI value for an irrigation system with three drippers per tree. However, larger yield will be obtained from larger LAI, since more shoots are able to carry fruits. On the other side, the reduction in E_p due to the increasing LAI could have a negative impact on yield. Currently, we have no answer to this trade-off. However, farmers can influence A_R to compensate for increasing values of A_L. The question is: how many drippers do we need to install per tree to recover E_p (to that at previous values of LAI) if we double LAI? The answer can be assessed by the model changing the volume of soil wetted by a dripper and considering steady RLD. The double LAI is nearly compensated by increasing the number of drippers from three to five.

A model for the actual transpiration

We have seen how the SACC model can predict hydraulic limits based on plant and soil characteristics, and how it can be applied to orchard management. However, this model was not designed to predict diurnal courses of actual transpiration, unless the diurnal course of leaf water potential is input as well. Additional insights can be gained by simulating stomatal responses to atmospheric demand and soil water deficit. In canopies well coupled to the atmosphere most of the transpiration is driven by VPD (Jarvis & McNaughton, 1986). This is the case of olive tree orchards (Moreno *et al.*, 1996; Tognetti *et al.*, 2009). An important characteristic of well coupled canopies is that g_s exerts a strong control of transpiration. This means that if we can model g_s satisfactorily, we can predict E_p. Traditionally, the most widely used g_s models have been those of Jarvis (1976) and Leuning (1995). However, these models, although able to mimic the stomatal response in most simulations, have difficulty simulating the effect of water stress (Vico & Porporato, 2008; Egea *et al.*, 2011b).

Several attempts have been made to consider the response of stomata to a drying soil, for instance by including the effect of ABA (Gutschick & Simonneau, 2002), which has been reported to act as a chemical signal from roots to leaves. Egea *et al.* (2011) found a suitable solution by including a soil moisture dependent function to account for the effects of water stress on g_s. The hydromechanical model proposed by Buckley *et al.* (2003) (BMF) has not been widely applied yet and it has an advantage over most others in that its parameters have explicit physiological meaning. Recent reviews on this topic (Damour *et al.*, 2010; Egea *et al.*, 2011b) recognized the potential of this model, but noted the difficulty in applying it, due to its high number of parameters. Our results show we were able to apply and validate a slightly simplified form of this model.

We estimated canopy conductance (g_c) from sap flow data as a surrogate of g_s (Fig. 2.9) in order to obtain long time series of this variable. Values of g_c compared well with g_s measurements made at the leaf level. In these same trees, g_s measured in sunny and shaded leaves were on average 0.23 mol m^{-2} s^{-1} and 0.07 mol m^{-2} s^{-1}, respectively. Assuming a fraction of sunny leaf area between 0.2 and 0.3 (based on measurements by Moreno *et al.*, 1996, lowered from their value of 0.3 to account for mutual shading in hedgerows), the g_c value obtained is very similar to the value estimated from leaf gas exchange. The BMF model fitted our data quite well in both treatments as soil dried out (Fig. 2.9). The model's real strength, however, is that it allowed us to analyze the physiological parameters obtained (Fig. 2.10). In our case, only two parameters of three were fitted. The seasonal evolution of π shows that similar osmotic adjustment occurred in both treatments. This was especially strong in Control on DOY 209 since Ψ_{md} was only -1.37 MPa. Osmotic adjustment has been interpreted as a mechanism for maintaining leaf turgor pressure when Ψ_{md} is reduced to withdraw water from drying soils (Dichio *et al.*, 2006). In the case of 30RDI this explanation fits perfectly. Ψ_{md} on DOY 209 was as low as -2.96 MPa

and $\pi = -3.03$ MPa. Therefore, another explanation is required for the osmotic accumulation observed in the Control treatment. One possibility is accumulation of photosynthates, which would build up a high π to facilitate the transport of assimilates to phloem. The theory of passive loading to phloem for the primary photoassimilates, sucrose and sugar alcohols, could explain this increase in π independently of a response to water stress (Rennie & Turgeon, 2009). Species accumulating mannitol, like olive (Flora & Madore, 1993), use this strategy preferentially, probably because it requires no energy (Reidel *et al.*, 2009). This explanation agrees well with the activation of growing in Control trees from DOY 190 (July 9) (Fig. 2.4). Although this hypothesis deserves further experimental study, it might have important implications in the identification of the growth inhibition threshold for olive, and the determination of optimal water potentials for managing irrigation.

One parameter fitted by the model is plant hydraulic resistance, R (Fig. 2.10B). The small increase in R observed in Control trees was expected, since Ψ_s did not exceed -0.4 MPa in the whole period, and Ψ_{md} was never lower than -1.4 MPa. On the contrary, 30RDI experienced a progressive increase in R, in agreement with the decrease in Ψ_s. The seasonal pattern of both treatments fits well to data of R_p shown in Table 2.2. Differences in absolute values of both variables also highlight the importance of the soil component included in R: these differences increased as soil dried out, as suggested by Sperry (2000). Similar values of R_p and its seasonal evolution have been reported previously for olive (Tognetti *et al.*, 2009), as well as for other Mediterranean tree species like *Quercus rotundifolia* (David *et al.*, 2004), but we have not found in literature such a marked difference between controls and stressed plants under field conditions as in this study. The likely explanation for this behavior is the small $A_R{:}A_L$ in our olive trees. The reduced IAs and low irrigation frequency in 30RDI affected the hydraulic capacity of the plant. Despite this constraint in A_R, Control plants did not

experience important changes in their R. The daily irrigation with sufficient IAs was enough to maintain a nearly steady maximum E_p. However, it is important to note that the increase in R in 30RDI looks disproportionate to the PLC predicted by the vulnerability curve on Fig. 2.6. PLC on this figure refers only to shoot xylem vulnerability to cavitation, while R comprises the soil-to-leaf continuum. This means that the increase in R arose elsewhere in the plant, likely roots or leaves. Indeed, the vulnerability to cavitation has been reported to be higher in both roots (Alder *et al.*, 1996; Kolb & Sperry, 1999) and leaves (Brodribb & Holbrook, 2003; Zufferey *et al.*, 2011), than in the xylem. Vulnerability to cavitation in petiole and leaf lamina have been recognized in recent years to play an important role in stomatal regulation (e.g., Guyot *et al.*, 2011).

The other fitted parameter, $\chi\beta$, represents the sensitivity of guard cells to changes in turgor pressure. Unlike R, $\chi\beta$ showed clear seasonal dynamics in both treatments (Fig. 2.10C). $\chi\beta$ includes the effect of guard cell solute efflux, so it should decline in response to hormonal signals from drying roots, like ABA (Buckley, 2005). This is consistent with the inferred seasonal patterns. $\chi\beta$ also includes the effect of stomatal size and density, which were similar between treatments in this study (data not shown). Our data suggest that the putative drought signal was stronger in 30RDI for most dates. On DOY 165 $\chi\beta$ was one third as high in Control than in 30RDI, before declining to a minimum in both treatments on DOY 209 and then recovering on DOY 223. The main conclusion is that the stomatal sensitivity to leaf water status was regulated seasonally not only in 30RDI, but also in well-irrigated Control trees – suggesting that $\chi\beta$ is not primarily regulated by soil moisture (nor, by inference, by ABA signals from droughted roots) in this species. This is consistent with some research suggesting that ABA is synthesized primarily in leaves, rather than in roots (Holbrook *et al.*, 2002; Christmann *et al.*, 2005), and that the travel time of

ABA in woody species may be too great for it to serve as a rapid long distance signal (Perks *et al.*, 2002).

To sum up this section, application of the BMF model to our data suggests that stomata in olive are regulated seasonally by something other than purely hydraulic signals, and that this occurs not only in droughted but also in well-watered trees. These signals might be chemical (for example ABA, nitric oxide, reactive oxygen species, etc.; Jiang & Zhang, 2001; Neill, 2007), or physical (for example electric signals, Stahlberg *et al.*, 2001; Oyarce & Gurovich, 2011). Additionally, hydraulic capacity of plants receiving only 30 % of water supplied to Control is severely affected under our conditions of climate, soil and irrigation strategy. In any case, the BMF model can serve as a useful research tool to understand the mechanisms behind observations, and as a platform to accommodate experimental knowledge from the literature.

Conclusions

The use of two process-based models helped us to advance understanding of water use by an olive orchard planted in hedgerow. The SACC model confirmed that the main limitation in the water use by olive trees in this orchard was in their rhizosphere. The limited volume of wet soil, determined by the number of drippers, reduced the ratio of root to leaf area. This reduction imposed a large hydraulic limitation to transpiration as bulk soil water potential decreased. The model was able to predict the impact of soil type, ratio of root and leaf areas on the limit of extraction of water by the plant. This has important practical implications for pruning and irrigation management, as the model can be used to assess the impact of changes in leaf area and number of drippers. Increasing the number of drippers from the actual three to five would be necessary to compensate for

two-fold increment in leaf area if the goal were to keep maximum transpiration values. The BMF model simulated satisfactorily the actual canopy conductance on several dates through the summer, both in well-watered and water stressed plants. Plants of both water treatments made similar osmotic adjustment. However, soil-to-leaf hydraulic resistance in stressed plants increased more than 4-fold during the summer. A potential involvement of regulating signals, other than purely hydraulics, was evident in both treatments, although our data suggests that these signals were themselves regulated by something other than soil water status.

Chapter 3

The contribution of hydraulic and non-hydraulic factors to suppression of stomatal conductance during soil drought: A case study in almond.

Introduction

Leaf stomata regulate the trade-off between carbon gain and water loss in leaves. The stomatal response to soil drought greatly impacts crop production and ecosystem function across the globe (Hetherington & Woodward, 2003), yet this response remains poorly understood. One reason is the sheer complexity of stomatal control – stomata respond to a wide range of environmental parameters that vary greatly across time scales, and they are also affected by numerous endogenous processes. The traditional approach of experimental biologists when faced with such daunting complexity is to focus on a single question, and to frame that question as a dichotomy between two alternative and mutually exclusive hypotheses. One curious phenomenon that has been studied by this dichotomous approach is 'isohydric' behavior – a marked reduction in stomatal conductance that is sufficient to prevent decline in mid-day minimum leaf water potential despite a large decline in soil water potential during soil drought in some species. In this case, a dichotomy is typically drawn between hydraulic and non-hydraulic mechanisms to explain isohydry. One view holds that the negative feedback response of stomata to leaf water status is sufficient to explain the phenomenon (Sperry *et al.*, 2002; Buckley, 2005; Brodribb & Cochard, 2009). The opposing view is that negative feedback alone cannot produce true homeostasis, and that chemical signals such as abscisic acid (ABA) generated during soil drought are required to cause sufficient reduction in stomatal conductance to produce isohydry (Davies & Zhang, 1991; Tardieu & Simonneau, 1998; Dodd, 2005). The conflict between these two viewpoints has dominated discussion of stomatal regulation for decades, yet shows no sign of abating (Schachtman & Googer, 2008; Dodd *et al.*, 2012; Pantin *et al.*, 2012; Brodribb & McAdam, 2013; Franks, 2013).

The objective of this study was to present and demonstrate a new approach to examining and quantifying the mechanistic basis of stomatal

response to soil drought. In this approach, a process-based model of stomatal conductance is applied to measurements of conductance and other environmental and biophysical data, and the model is then used as a platform for separating the roles of various factors in a way that cannot be achieved by experiment alone. The main advantage of using a model in this way is that it embraces the complexity of the system, rather than attempting to circumvent it by dichotomizing the system. We chose the stomatal conductance model of Buckley, Mott & Farquhar (2003) for this purpose, because most other models currently used to study stomatal control are essentially empirical or phenomenological (Jarvis, 1976; Ball, Woodrow & Berry, 1987; Leuning, 1995), in the sense that their structures were chosen to represent emergent properties of stomatal behavior rather than the biophysical processes that underlie that behavior (Buckley & Mott, 2013). We developed a simplified form of this model that contains fewer parameters and is thus easier to apply and to study, and we applied it to field measurements of stomatal response to soil drought in almond.

Material and Methods

Experimental conditions

The experiment occurred in 2012 at an orchard near Seville, Spain (37° 15′ N, −5° 48′ W). In early 2011, one-year almond seedlings (*Prunus dulcis* (Mill.) D. A. Webb cv. Guara) were transplanted to 50-L pots containing a soil (*Arenic Albaqualf*, USDA 2010) with 69.3 % sand, 28.6 % clay and 2.1 % silt (Fernández *et al.*, 2011b). Volumetric soil water content estimated by the Rosetta model (Schaap *et al.*, 2001), were 0.194 m^3 m^{-3} for field capacity (matric potential -0.03 MPa) and 0.118 m^3 m^{-3} at wilting point (-2.5 MPa). Twenty pots were placed in two rows oriented north to south, with 1.5 m between rows and 1 m between plants. Pots were insulated with foam. A

slow-release fertilizer (5 g pot^{-1} of Floranid® Permanent, NPK 16+7+15+2 MgO, Compo, BASF, Ludwigshafen, Germany) was applied every 40 days. Measurements occurred on three days: August 15, 21 and 31.

The site's climate is Mediterranean: hot and dry from May to September and mild and wet for the rest of the year. Air temperature (T_a) and relative humidity (RH) were recorded by probes (ZIM Plant Technology GmbH, Hennigsdorf, Germany) near the pots, and used to estimate leaf-air H_2O mole fraction gradient (Δw). Photosynthetic photon flux density (PPFD) was monitored by a Li-190 Quantum Sensor (LI-COR, Lincoln, NE) located 3 m above the plants.

Irrigation and soil water status

The irrigation system consisted of one drip line per row with three drippers per pot (6 L h^{-1} per pot). Irrigation was regulated with a controller (Agronic 2000, Sistemes Electrònics PROGRÉS, S.A., Lleida, Spain). Pots were irrigated in 2011 with 1.5 L pot^{-1} day^{-1}, and in 2012 with 1.5 L pot^{-1} day^{-1} until July. From late July through mid-August, irrigation was increased to 10 L pot^{-1} day^{-1}. Two irrigation treatments were applied during the experiment in August 2012: 1) Control (well watered, WW) pots were irrigated to keep soil water content (SWC) near field capacity. 2) Deficit irrigated (water stressed, WS) pots were gradually stressed by withholding irrigation, such that SWC was 19% lower than in WW on 21 August and 64% lower on 31 August. Volumetric soil water content (SWC) was monitored with time domain reflectometry (TDR) probes (TDR FOM/mts, Institute of Agrophysics, Lubin, Poland). Two probes (7 cm and 10 cm depth) equidistant from the stem were inserted in three pots per row.

Plant water status and gas exchange

On the three measurement days (August 15, 21 and 31), leaf water potential (Ψ_{leaf}) and gas exchange were measured every 1.5 hours from 5:30 to 19:00

GMT. Water potentials were measured with a Scholander-type pressure chamber (PMS, Albany, Oregon) on two leaves per plant and three plants per treatment. For Ψ_{leaf}, sun-exposed, healthy, fully developed leaves of representative current-year branches were measured.

Stomatal conductance to H_2O (g_s) was measured on two leaves per plant (similar to leaves chosen for Ψ_{leaf} measurements) and four plants per treatment, using an open flow gas exchange system with a 2×3 cm chamber (Li-6400, LI-COR). Chamber radiation and temperature matched ambient and CO_2 concentration was controlled at 390 μmol mol^{-1} by a 6400-01 CO_2 injector (LI-COR).

On the same dates, leaves were sampled at predawn and mid-day for osmotic pressure (π) measurements. One mature, full expanded leaf per plant in four plants per treatment were cleaned, packed in aluminum foil and immediately frozen in liquid nitrogen. One 7-mm diameter disc per leaf was sampled between the midrib and margin with a cork borer, punctured 15-20 times with forceps to speed equilibration and immediately loaded in a C-52 thermocouple psychrometer chamber (Wescor Inc., Logan, UT) connected to a datalogger (PSYPRO, Wescor). Equilibrium was reached in ~30 min. We corrected π using the regression model of Bartlett *et al.* (2012) to account for apoplastic dilution and wall solute enrichment.

Photosynthetic response curves

Seven A-c_i response curves (response of net CO_2 assimilation rate, A, to intercellular CO_2 concentration, c_i) per treatment were determined between 9:00 and 13:00 GMT over the experimental period. Measurements were performed at ambient temperature, saturating PPFD (2000 μmol m^{-2} s^{-1}) and ambient CO_2 concentration (c_a) between 50 and 1700 μmol mol^{-1}. After steady-state photosynthesis was achieved, the response of A to varying c_i was measured by lowering c_a stepwise from 400 to 50 μmol mol^{-1}, returning

to 400 $\mu mol\ mol^{-1}$, and then increasing c_a stepwise from 400 to 1700 μmol mol^{-1}. Each A-c_i curve comprised 15 measurements, each made after at least 3 min at each c_a. Parameters of the photosynthesis model of Farquhar *et al.* (1980) were derived for each curve using the method of Ethier & Livingston (2004) to fit three parameters by non-linear least squares regression (Table 3.1): mesophyll conductance (g_m), maximum carboxylation rate ($V_{c,max}$) and maximum potential electron transport rate (J_{max}) (we found no evidence of triose-phosphate utilization limitation, TPU, in our data, so we did not consider this limitation). Other parameters were taken from the literature. Rubisco kinetic parameters and the photorespiratory CO_2 compensation point (Γ^*) were taken from Bernacchi *et al.* (2002). Non-photorespiratory CO_2 release (R_d) and its temperature dependence was taken from Egea *et al.* (2011a). $V_{c,max}$, J_{max} and g_m were normalized to 25 °C using published temperature responses for almond (Egea *et al.*, 2011a).

Table 3.1. Maximum carboxylation rate ($V_{c,max}$), maximum potential electron transport rate (J_{max}) and mesophyll conductance (g_m) measured at the beginning and end of the experiment. Standard errors in brackets (n = 4). Different letters indicate significant differences (Multiple comparisons on significant effects from linear mixed model, $P <$ 0.05).

Experimental period	Treat.	$V_{c,max}$ $\mu mol\ m^{-2}\ s^{-1}$		J_{max} $\mu mol\ m^{-2}\ s^{-1}$		g_m $mol\ m^{-2}\ s^{-1}$	
Beggining	WW	185.43	(8.11)[a]	207.10	(18.85)[a]	0.15	(0.03)[b]
	WS	197.97	(56.33)[a]	182.77	(5.47)[ab]	0.26	(0.03)[c]
Ending	WW	185.73	(13.99)[a]	174.35	(12.14)[ab]	0.08	(0.01)[a]
	WS	186.56	(25.96)[a]	152.79	(11.11)[b]	0.08	(0.01)[a]

Four PPFD response curves per treatment were performed using a LED Light Source (Li-6400-02B, LI-COR) connected to the Li-6400, between 9:00 and 13:00 GMT, by reducing PPFD from 2500 $\mu mol\ m^{-2}\ s^{-1}$ to

darkness in 15 steps. Temperature and CO_2 were 28-32 °C and 390 μmol mol^{-1}, respectively. Maximum A (A_{max}, μmol m^{-2} s^{-1}), the curvature parameter (θ, dimensionless) and maximum quantum yield of CO_2 (α, the initial slope of A versus PPFD, dimensionless) were determined by least squares curve fitting to a non-rectangular hyperbola. Parameter values ($\theta = 0.71$ and $\phi = 4\alpha = 0.20$ electrons $photon^{-1}$, where ϕ is the effective maximum quantum yield of electrons) were similar between treatments.

ABA extraction, purification and quantification

Predawn and mid-day leaves were sampled as for π measurements. Leaf ABA was measured by the liquid chromatography-electrospray/tandem mass spectrometry method of Gómez-Cadenas *et al.* (2002). Samples of *ca.* 400 mg of frozen leaf tissue, with midribs removed, were milled with liquid nitrogen and homogenized and extracted in 5 ml of distilled water. An aliquot of 50 μL of 2-ppm deuterated abscisic acid (dABA) was added as an internal standard. Samples were centrifuged (26000 min^{-1}; 7 min; 8 °C), supernatants were acidified to pH 3.0 (150 μL acetic acid 30 % (v/v)) and leaf extracts were 2-times partitioned with 3 mL of diethyl ether. Organic phases were collected in test tubes and totally evaporated providing a gaseous nitrogen flow. Tube walls were washed with 1 mL diethyl ether and desiccated again. Dry residues were re-suspended in 500 μL methanol, completed to a total volume of 1 mL with Milli-Q quality (reverse osmosis) water and filtered through 25 mm diameter polypropylene membrane syringe filter (ø 0.2 μm, VWR® International, Pennsylvania). Analyses were performed using an Agilent 1290 Infinity HPLC system (Agilent Technologies Inc., CA) coupled with an electrospray/tandem mass spectrometer (3200 QTRAP® LC/MS/MS System, AB SCIEX, Framingham, MA) and data were processed with mass spectrometry software (Analyst® Software, AB SCIEX). Leaf ABA was normalized by fresh weight (FW, g).

Statistical analysis

We used linear mixed models to analyze effects of irrigation treatment (as a fixed factor) on SWC, Ψ_{leaf}, g_s, K, n, π, leaf ABA concentrations, $V_{c,max}$, J_{max} and g_m. We used random factors when necessary to describe our experimental design (leaf within pot for Ψ_{leaf} and g_s, and soil water content probe within pot for SWC). Variables were transformed to improve normality or to fix non-constant variance in residuals when needed. Models were fitted by restricted maximum likelihood (REML) in R (package 'nlme R'; Pinheiro *et al.*, 2012). Multiple-comparison analyses were conducted when an overall significant effect was detected ($\alpha = 0.05$).

BMF model of stomatal conductance

We used a modified form of the stomatal conductance model originally presented by Buckley *et al.* (2003) (hereafter, the BMF model) to examine the mechanistic basis of observed changes in g_s. This model is based on leaf, plant and stomatal water relations, and the hypothesis that guard cell osmotic pressure is actively regulated in proportion to epidermal turgor pressure (which acts as a sensor for changes in leaf water status) and to the ATP concentration of photosynthesising cells (which acts as a sensor for light and CO_2). In the Appendix II, we present the model in greater detail, and we derive the following modified form of the model:

$$(3.1) \quad g_s = \frac{naK(\Psi_s + \pi)}{K + na\Delta w},$$

where K is leaf-specific hydraulic conductance, Ψ_s is soil water potential, π is bulk leaf osmotic pressure and Δw is leaf to air water vapor mole fraction gradient. n and a capture non-hydraulic effects: a is mesophyll ATP concentration expressed relative to its maximum value and n is a lumped parameter representing other non-hydraulic factors:

(3.2) $n \equiv \chi \beta \tau_m$, and

(3.3) $a \equiv \tau / \tau_m$,

where τ is ATP concentration in photosynthesising cells. The parameters embedded in n are χ, a proportionality factor that scales guard and epidermal cell turgor pressures to g_s; β, a proportionality factor that scales the product of τ and epidermal turgor to changes in guard cell osmotic pressure; and τ_m, the maximum τ (the total pool of adenylates, ADP + ATP). We simulate τ with the model of Farquhar & Wong (1984), which was derived from the photosynthesis model of Farquhar *et al.* (1980) and is presented in detail in the Appendix II.

Buckley *et al.* (2003) showed that β could be interpreted as the ratio of the specific rates of active ion uptake and passive ion efflux in guard cells. Because abscisic acid (ABA) affects guard cells by stimulating passive efflux (Hetherington, 2001), one would expect β – and therefore the parameter n in the modified model – to decline as ABA concentration increases.

Equation (3.1) was derived from the BMF model based on several assumptions, namely that the osmotic gradient from guard to epidermal cells, not to the apoplast, is the target for active regulation; that the resistance from epidermal to guard cells is negligible compared to the resistance from the soil to the epidermis; that epidermal and bulk leaf osmotic pressure are similar; and that the response of g_s to PPFD is homogeneous (Extra Fig. 3.1 in Appendix II). These assumptions are discussed in greater detail in the Appendix II.

Attributing changes in stomatal conductance to factors in the BMF model

We parsed changes observed in g_s between 21 and 31 August in the WS treatment into changes due to individual factors in Equation (3.1) using the following expression:

$$(3.4) \quad \delta g_s = \frac{\partial g_s}{\partial n} \delta n + \frac{\partial g_s}{\partial a} \delta a + \frac{\partial g_s}{\partial K} \delta K + \frac{\partial g_s}{\partial \psi_s} \delta \psi_s + \frac{\partial g_s}{\partial \pi} \delta \pi + \frac{\partial g_s}{\partial \Delta w} \delta \Delta w.$$

The percent contribution of a factor was computed by dividing it by the sum of all of contributions and multiplying by 100 (details in Appendix II).

Stomatal limitations

Jones (1985) and Grassi & Magnani (2005) proposed delineating the limitations on photosynthesis in terms relatives partial derivatives of A with respect to various limiting factors, which has proven useful for attributing differences in photosynthesis to those factors. The same concept can be applied to Equation (3.1) to compute the *hydraulic* and *non-hydraulic limitations to stomatal conductance*, γ_h and γ_{nh}, respectively. We define the hydraulic limitation to be that due to investments (or lack thereof) in hydraulic conductance, K ($\gamma_h = \partial \ln g_s / \partial \ln K$), and the non-hydraulic limitation as that due to limitations in the product na ($\gamma_{nh} = \partial \ln g_s / \partial \ln\{na\}$). These derivatives are:

$$(3.5) \quad \gamma_h \equiv \frac{\partial \ln g_s}{\partial \ln K} = \frac{na}{K/\Delta w + na}, \text{ and}$$

$$(3.6) \quad \gamma_{nh} \equiv \frac{\partial \ln g_s}{\partial \ln na} = \frac{K/\Delta w}{K/\Delta w + na} = 1 - \gamma_h.$$

Note that if one chose instead to define γ_{nh} in relation to either n or a alone, the same expression would arise:

$$(3.7) \quad \frac{\partial \ln g_s}{\partial \ln n} = \frac{\partial \ln g_s}{\partial \ln a} = \frac{K/\Delta w}{K/\Delta w + na} \; .$$

Results

Soil water content (SWC) was similar between the well-watered (WW) and water-stressed (WS) treatments during the first two measurement cycles (on 15 and 21 Aug), but declined significantly in WS during the third cycle (31 Aug) as compared to WW (Fig. 3.1A - C). Evaporative demand (Δw) was greatest on 21 Aug (exceeding 70 mmol mol^{-1}), but was also quite high during the third cycle (Fig. 3.1G - I). Despite the high Δw on 21 Aug, leaves in both treatments were able to maintain stomatal conductance at levels similar to 15 Aug, when Δw was much lower (Fig. 3.2B). However, the lower SWC in WS on 31 Aug led to a large decline in both g_s and predawn leaf water potential (Fig. 3.2A).
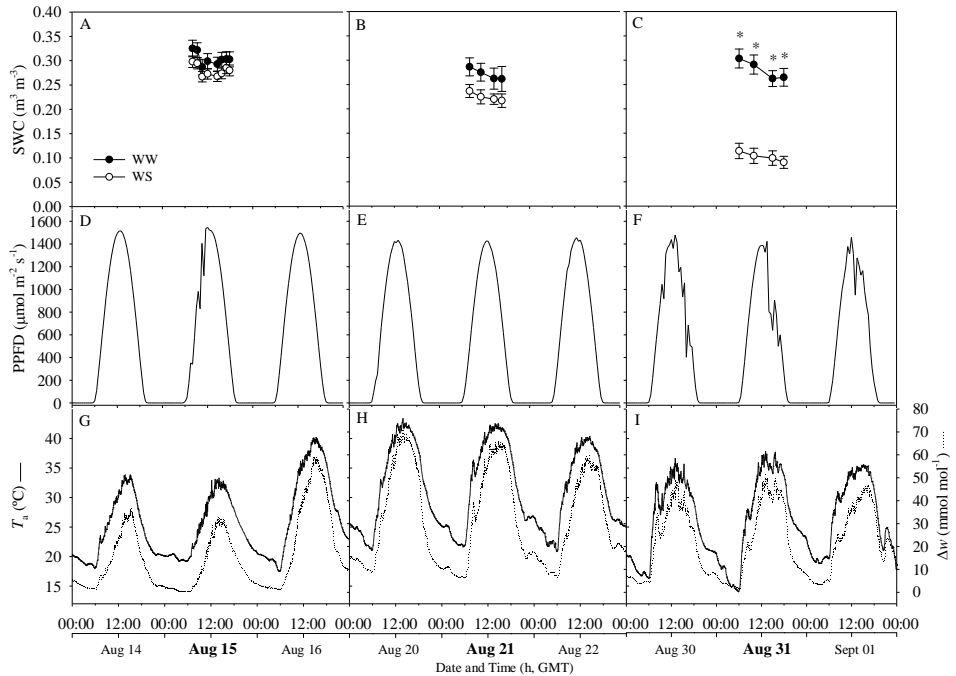
Fig. 3.1. Time courses of soil water content (SWC) measured on the experimental dates, and photosynthetic active photon flux density (PPFD), air temperature (T_a) and leaf to air water vapor mole fraction gradient (Δw) on three experimental periods. Central dates of each panel correspond to daily measurement dates (August 15, 21 and 31). SWC is represented for the two irrigation treatments supplied: well watered treatment (WW) and water stressed treatment (WS). Error bars on SWC represent standard errors, $n = 6$. Asterisks indicate statistically significant differences between treatments ($P < 0.001$).
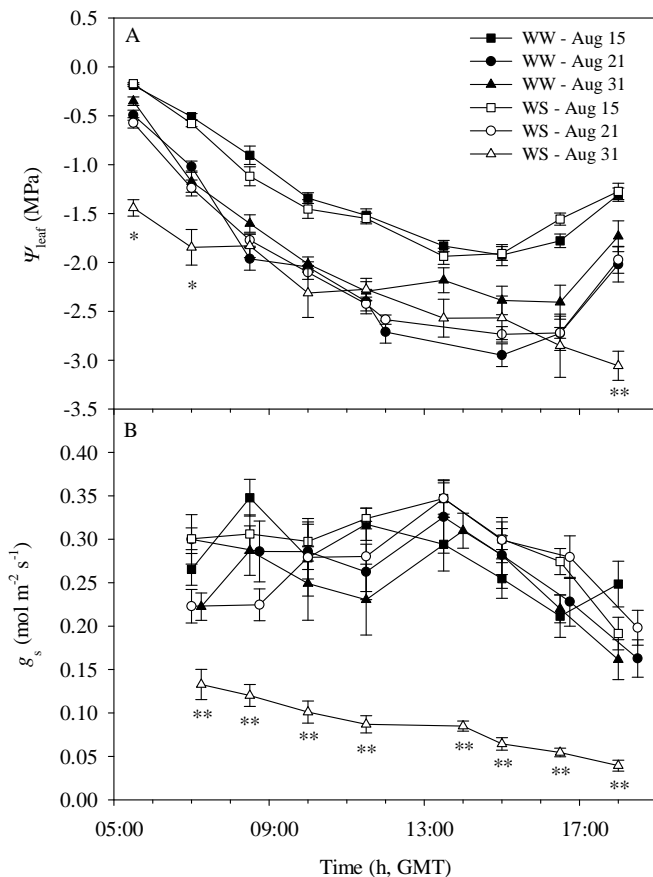
Fig. 3.2. Diurnal courses of (A) leaf water potential (Ψ_{leaf}) and (B) stomatal conductance (g_s) on the three experimental dates. Error bars show standard errors for $n = 6$ (Ψ_{leaf}) and $n = 8$ (g_s). Asterisks indicate statistically significant differences between treatments on August 31 (* $= 0.01 < P < 0.05$, ** $= P < 0.01$). GMT = Greenwich Mean Time.

Therefore, we focused on what caused the decline in g_s in the WS treatment between 21 and 31 Aug. We investigated the physiological causes of this decline by a combination of measurements and inference. The measurements included predawn leaf water potential as a proxy for soil water potential (Ψ_s), leaf osmotic pressure (π), PPFD, Δw, and leaf abscisic acid concentration ([ABA]) at predawn and mid-day. The inferential

approach entailed fitting the BMF model (Equation 3.1) to our data to infer changes in two fitted parameters – leaf hydraulic conductance (K) and the lumped parameter of non-hydraulic factors (n) – and using the model to separate the contributions of each factor in the model to the observed decline in g_s. We expected that n would decline but K would remain constant during this decline, so that n would emerge as the major driver of declining g_s. Our rationale was twofold: first, diurnal minimum leaf water potential was similar between treatments and days (Fig. 3.2A), suggesting any additional loss of hydraulic conductivity on 31 Aug would be minimal; and second, the parameter n contains embedded within it the parameter β (Equation 3.2), which captures the effect of passive, outward-rectifying osmotic solute loss from guard cells – the main process believed to mediate stomatal closure in response to the biochemical drought signal ABA (see Appendix II).
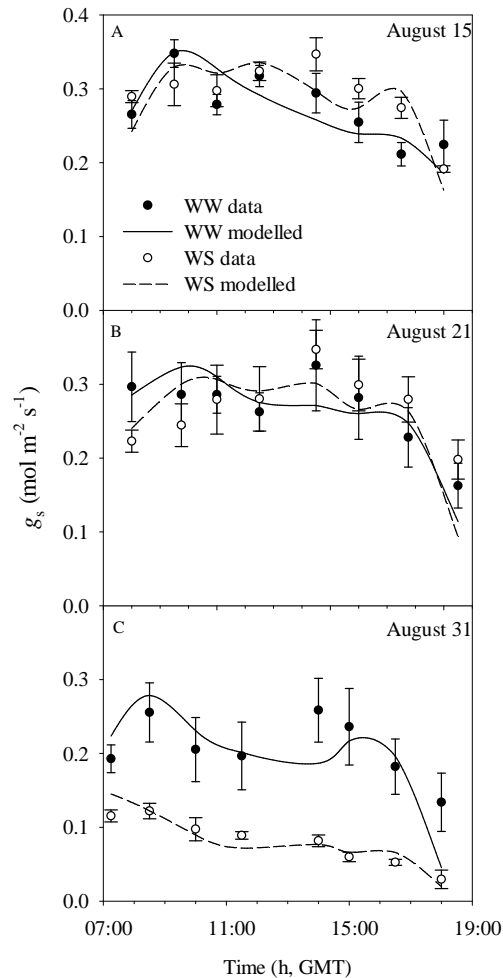
Fig. 3.3. Evolution of g_s data (points) and g_s fitted with the BMF model (lines) on the three experimental dates during the study. For g_s data we used $n = 8$. Error bars show standard errors.

The model was able to reproduce diurnal variations in g_s across the study period, as well as the decline in g_s in WS on 31 Aug (Fig. 3.3). Trends in Ψ_s, PPFD and Δw differed: Ψ_s was lower in WS on 31 Aug than in other treatments and days (Fig. 3.2A), but neither PPFD, Δw nor π differed

significantly between 21 and 31 Aug (Fig. 3.1B, C; Fig. 3.4C). *K* was similar between treatments on 21 Aug but declined on 31 Aug by 54 % in WS and 22 % in WW (Fig. 3.4B). Conversely, the non-hydraulic term *n* declined on 31 Aug, as expected, but by a greater degree in WW (71 %) than in WS (26 %), which contradicted our expectations. To assess whether these variations in *n* were paralleled by changes in biochemical drought signals, we compared them to trends in leaf [ABA]. Mid-day [ABA] was similar in all cases except WS on 31 Aug, when it increased (Fig. 3.5B). Conversely, pre-dawn ABA was greater in WW than in WS on 21 Aug (Fig. 3.5A), despite the similar conditions between both treatments, but this pattern was reversed on 31 Aug, when pre-dawn ABA was greater in WS than in WW (Fig. 3.5A). Overall, g_s was negatively correlated with [ABA] (Fig. 3.6A, B), as expected, but the parameter *n* was not (Fig. 3.6C, D), contrary to expectations.
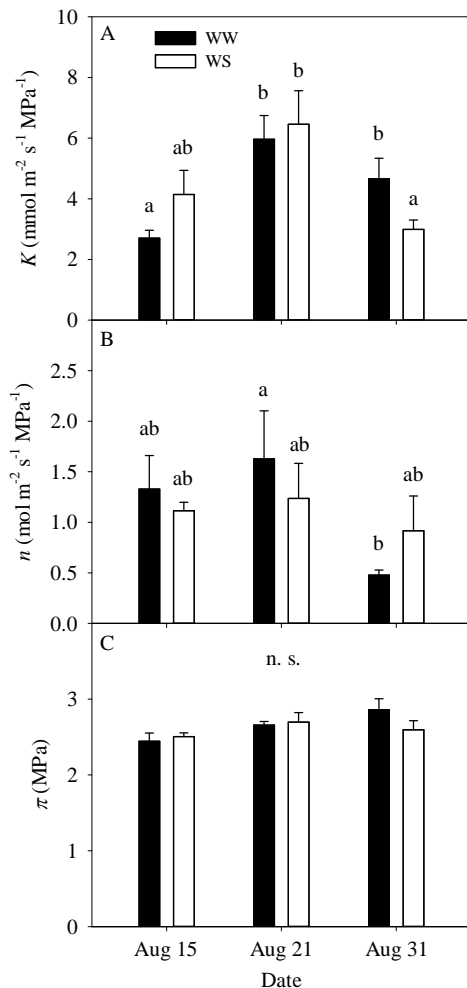
Fig. 3.4. Values of the parameters obtained by adjusting the BMF model to g_s data on the three experimental dates. (A) Soil-to-leaf hydraulic conductance (K). (B) The model parameter that captures non-hydraulic effects (n). Both K and n were fitted parameters. (C) Leaf osmotic pressure (π). Error bars are standard errors ($n = 4$). Different letters indicate statistically significant differences ($P < 0.05$).
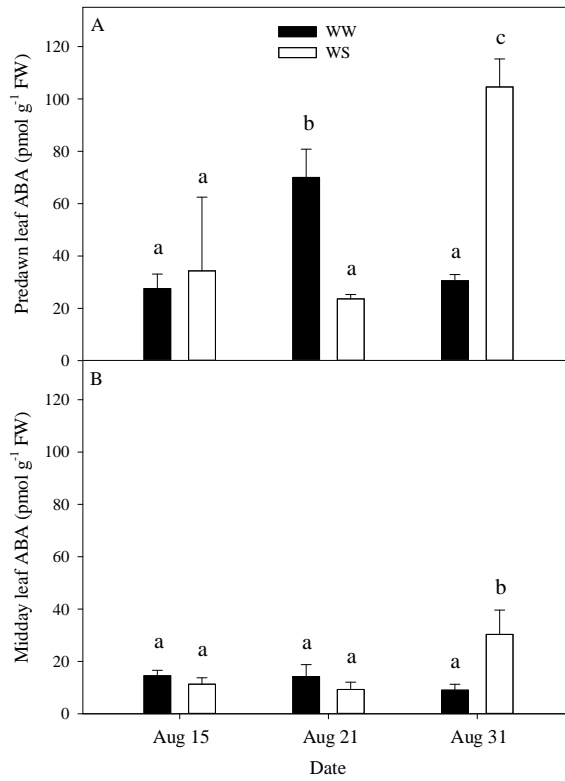
Fig. 3.5. Leaf abscisic acid (ABA) concentrations from leaves sampled at (A) predawn and (B) mid-day on experimental dates. Error bars show standard errors ($n = 4$) and different letters indicate statistically significant differences ($P < 0.05$).
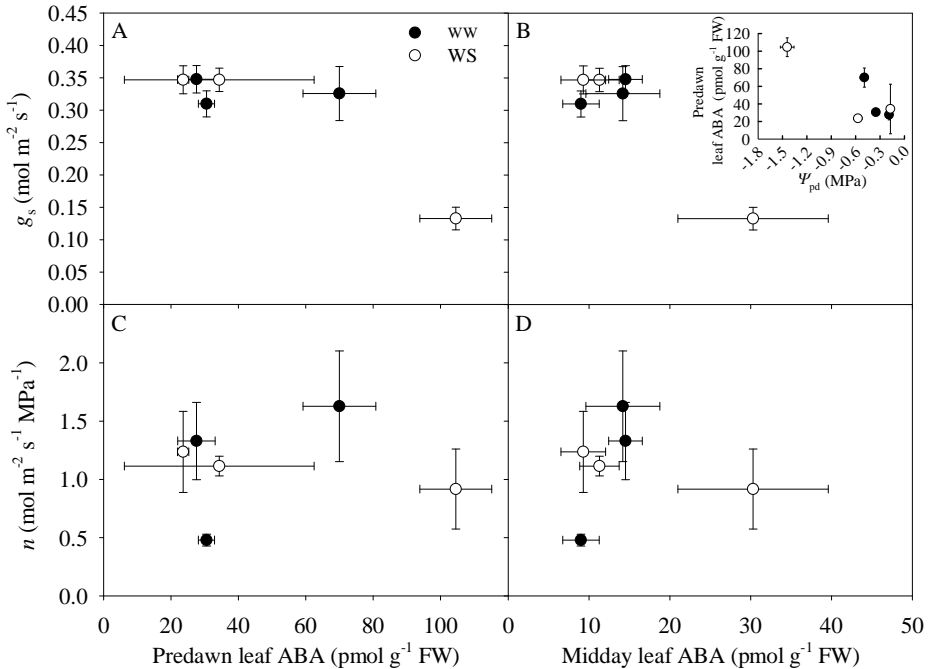
Fig. 3.6. Relationships between predawn leaf abscisic acid (ABA) and (A) stomatal conductance, g_s, and (B) the BMF model parameter that captures non-hydraulic effects, n, estimated by fitting the model. Inset shows the relationship between predawn leaf water potential (Ψ_{pd}) and predawn leaf ABA. Error bars are standard errors.

To gain further insight into the cause of the decline in g_s in WS on 31 Aug, we used the model to attribute this decline in g_s to factors in the model (Fig. 3.7) (Equation 3.4; details in Appendix II). We found that, on average over the day, 46 % of the decline in g_s was attributable to the decline in K, and 38 % to the decline in Ψ_s, whereas only 7 % was attributable to the decline in the non-hydraulic parameter n (Fig. 3.7). (The other non-hydraulic factor in the model, relative ATP concentration (a), actually increased by 2 %, due to a small increase in chloroplastic CO_2 concentration resulting from the decrease in g_s itself).
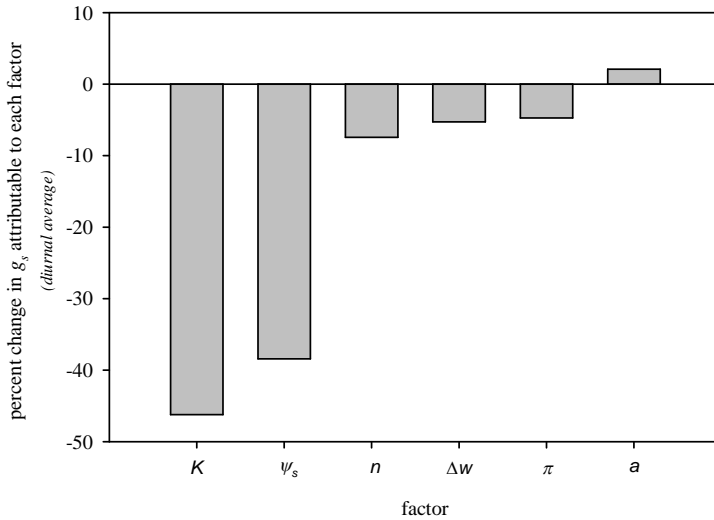
Fig. 3.7. Attribution of the change in stomatal conductance observed between 21 and 31 August in the water-stressed (WS) treatment to changes in BMF model parameters (expressed as diurnal averages of the percent changes in g_s attributable to each factor): the model parameter that captures non-hydraulic effects other than ATP concentration, n; relative ATP concentration, a; leaf-air water vapour mole fraction gradient, Δw; leaf osmotic pressure, π; soil water potential, Ψ_s; leaf specific hydraulic conductance, K. Calculation of these changes is described in greater detail in Appendix II.

To understand why the model attributed more control to hydraulic factors despite the large increase in mid-day leaf [ABA], and to provide a more general tool for assessing hydraulic vs non-hydraulic contributions to stomatal regulation in future work, we computed the *relative limitations* of g_s by hydraulic and non-hydraulic factors (γ_h and $\gamma_{nh} = 1 - \gamma_h$; Equations 3.5 and 3.6; Fig. 3.8). γ_{nh}, which represents the degree to which non-hydraulic factors control stomatal conductance, was large only at the shoulders of the day, when neither PPFD (which controls a in Equations 3.5 and 3.6) nor evaporative demand were yet maximal. By contrast, the hydraulic limitation to stomatal conductance, γ_h, was large during the middle of the day, when PPFD and Δw are both very high. The non-hydraulic limitation actually

declined in WS between 21 and 31 Aug, and was greater in WW than in WS on 31 Aug.
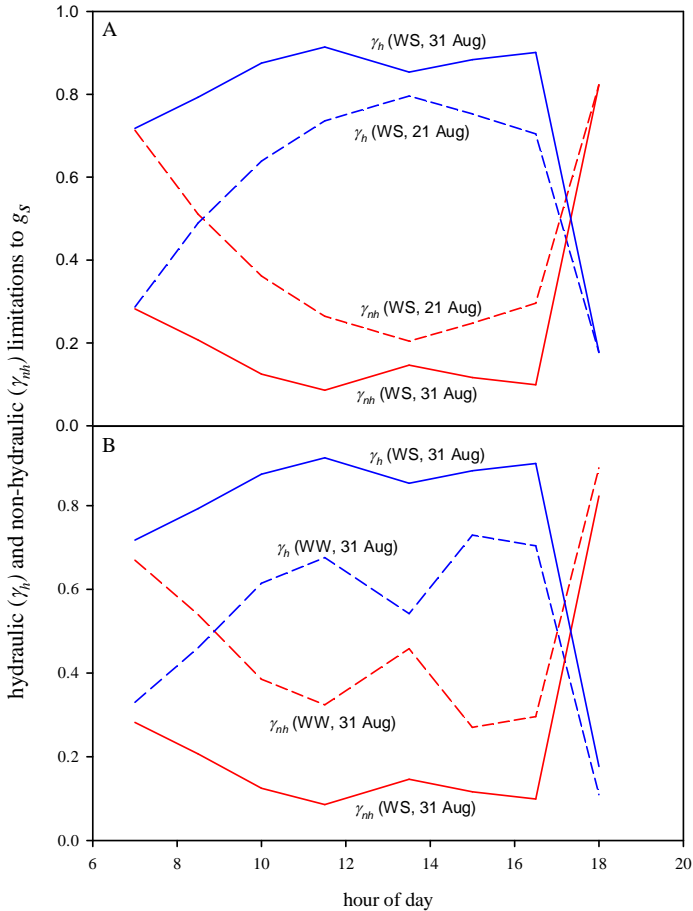
Fig. 3.8. Hydraulic and non-hydraulic limitations to stomatal conductance ($\gamma_h = K/(K + na\Delta w)$, blue lines; and $\gamma_{nh} = na\Delta w/(K + na\Delta w)$, red lines; where n is a lumped parameter representing non-hydraulic influences on g_s other than ATP concentration, a is relative photosynthetic ATP concentration, Δw is the leaf-air water vapour mole fraction gradient and K is leaf specific hydraulic conductance), compared between (A) 21 and 31 Aug in the water-stressed treatment (WS), and (B) the well-watered (WW) and WS treatments on 31 Aug, showing that soil drought increased the hydraulic limitation and decreased the non-hydraulic limitation of stomatal conductance.

Discussion

We observed the archetypical 'isohydric' behaviour in almond – i.e., a pattern in which a decline in stomatal conductance during soil drought prevents significant further decline of minimum daily leaf water potential. Both hydraulic and chemical signals have previously been proposed to explain this pattern, but there is no consensus about which is most important (Tardieu & Simonneau, 1998; Christmann *et al.*, 2007). Our novel model-based approach allowed us to parse the decline in g_s into contributions from several different biophysical factors. This approach concluded that, in our experiments in almond, most of the decline in g_s could be explained by changes in hydraulic factors. However, it also showed that two different hydraulic factors – leaf specific hydraulic conductance and soil water potential itself – were of similar importance, and our analysis also attributed part of the decline to changes in the model parameter that captures effects of biochemical drought signals on guard cell function.

These results highlight the fact that no single factor, hydraulic or otherwise, is likely to explain isohydry. This questions the usefulness of seeking to identify only a single overarching explanation by testing two mutually exclusive hypotheses. That approach has led to occasionally acrimonious controversy while deflecting attention from the potential inherent in a more integrative, formal and quantitative approach to attributing cause in stomatal behaviour. Although our results suggest a greater role for hydraulic than non-hydraulic factors in the single instance that we studied, it seems likely that the degree of hydraulic *vs* non-hydraulic control would differ if we were to apply our approach to a different species, or a different set of environmental conditions. Thus, the more important conclusion that we wish to emphasise from this study is that one is not

constrained to the 'binary' approach of competing alternative hypotheses, and that in fact a more integrative approach is more informative.

Response to water stress in almond

The imposition of soil water deficit on WS plants produced a large decrease in g_s on 31 Aug which reduced transpiration enough to maintain minimum daily Ψ_{leaf} at a constant value of around -2.7 MPa, similar to the value observed before soil drought. We found that leaf [ABA] at mid-day increased coincident with the decline in g_s, and that [ABA] at predawn was negatively correlated to Ψ_s. Similar results have led other authors to suggest that under soil water deficit, roots synthesise ABA, which is delivered in the transpiration stream to guard cells where it induces ion efflux, thus reducing stomatal aperture (Tardieu & Davies, 1992; Dodd *et al.*, 2010). It has been argued that such signals are necessary because a negative feedback response of g_s to Ψ_{leaf} cannot produce true homeostasis in Ψ_{leaf}. A counter-argument is that homeostasis could result if the gain of the negative feedback were amplified by a reduction in hydraulic conductance (Oren *et al.*, 1999; Buckley & Mott, 2002b; Buckley, 2005).

Although we did observe a 35% decline in hydraulic conductance coincident with the decline in g_s, it is not self-evident whether this should be sufficient to produce isohydry. Therefore, we developed a novel and formal approach, based on the stomatal conductance model of Buckley *et al.* (2003) (the BMF model), to address this question. Despite the recognized potential of this model (Damour *et al.*, 2010; Egea *et al.*, 2011b), it has not been widely applied in field experiments, partly because it has many parameters that are difficult to estimate. To overcome this limitation, we simplified the model to produce a modified form with just three parameters (Equation 3.1), which fitted our data reasonably well. We then used a differential analysis of Equation (3.1) to estimate the relative contribution of changes in K and ABA (the effect of which is embedded in the parameter n in Equation 3.1),

as well as other biophysical factors in the model, to the observed decline in g_s. That analysis concluded that the decline in K was responsible for nearly half (46 %) of the decline in g_s, whereas the decline in the ABA-related parameter n was responsible for only 8 %. Most of the remaining 44 % was attributable to the direct effect of reduced Ψ_s (38 %), with small effects due to π, Δw and irradiance.

Why, then, did the increase in [ABA] at mid-day apparently not exert greater control over stomatal conductance? To help answer that question, we computed the relative limitations to stomatal conductance due to hydraulic vs non-hydraulic factors, symbolised as γ_h and γ_{nh}, respectively (Equations 3.5 and 3.6). These limitations are directly analogous to the relative photosynthetic limitations proposed by Jones (1985) and developed further by Grassi & Magnani (2005). An unexpected insight of this limitations analysis was that non-hydraulic factors generally exert very little control over g_s during the middle of the day. The reason is that γ_{nh} is a decreasing function of irradiance and Δw (Equation 3.6: $\gamma_{nh} = K/(K + na\Delta w)$, where a is the model parameter that increases in relation to irradiance, and n is the parameter that should decrease as [ABA] increases). Furthermore, any decrease in K that may occur during soil drought will further reduce the non-hydraulic limitation of g_s. In light of these insights, it is less surprising that our model analysis attributed little control to mid-day [ABA].

There are several reasons to suppose this conclusion may not apply broadly to most species. Firstly, both Δw and PPFD are quite high in our study sites in southern Spain (e.g., Δw often exceeds 70 mmol mol^{-1}), and this increases the control of g_s by hydraulic factors (γ_h, Equation 3.5). Secondly, the greatest driver of the decline in g_s in this study was a decline in K, yet because species differ widely in the vulnerability of K to reduced water potential, soil drought will affect K differently across species. Thirdly,

the BMF model does not represent a universal consensus about the mechanisms of stomatal regulation. In particular, the nature of the link between the negative feedback response to water status and the effect of ABA is poorly understood (Buckley & Mott, 2013). The model assumes guard cells actively modulate osmotic pressure in relation to water status – an hypothesis that is strongly supported by a great deal of circumstantial evidence (Buckley, 2005) but has never been tested directly. Thus, although we feel that this model is currently the best tool available for mechanistic analysis of stomatal regulation, failure of any of its assumptions could mitigate the conclusion of our analysis.

What is the role of ABA?

Our analysis complements a range of evidence that hydraulic responses may explain much of the regulation of stomatal conductance in relation to soil drought in some species (Fuchs & Livingston, 1996; Comstock & Mencuccini, 1998; Yao *et al.*, 2001). Nevertheless, we did observe large increases in leaf [ABA] at mid-day coincident with the decline in g_s, and some speculation is warranted concerning the role of this increase. The hypothesis that root-derived ABA regulates g_s during soil drought has been extensively studied and has even impacted agriculture, through irrigation strategies based on split-root-zone drying (Dodd *et al.*, 2008). However, this hypothesis has been challenged in tall trees (Perks *et al.*, 2002) and in experiments in which shoots were grafted onto rootstock deficient in ABA synthesis (Holbrook *et al.*, 2002; Christmann *et al.*, 2005). The latter authors concluded that most ABA synthesis was confined to the vasculature and guard cells. This was later confirmed and extended by Gálvez-Valdivieso *et al.* (2009), who found that most ABA synthesis was localised in the vascular parenchyma, where it activates a signalling network in neighbouring bundle sheath cells linked to hydrogen peroxide accumulation under high light. More recently, Pantin *et al.* (2012) showed that ABA reduces the conductivity of water flow pathways distal to the xylem, perhaps by

modulating aquaporin activity. Together, these results suggest an hypothesis: namely, that the decline in K in our experiments, which we concluded was responsible for nearly half of the decline in g_s, was in fact mediated at least in part by ABA – i.e, the hydraulic and non-hydraulic limitations may be more closely coupled than previously thought.

Conclusions

We found that stomatal closure leading to isohydric behaviour under soil drought in almond could be explained by a combination of both hydraulic and non-hydraulic factors, but that nearly half of the decline in g_s was attributable to a decline in hydraulic conductance, and over a third was attributable to the direct effect of reduced soil water potential. Our novel model-based approach to parsing changes in g_s into contributions of various biophysical factors has the potential to yield more insight than a traditional binary approach based on mutually exclusive alternative hypotheses.

Chapter 4

Combining a process-based model of stomatal conductance with leaf turgor pressure related probe measurements to study the regulation of plant water status and stomatal conductance under drought

Introduction

Precision irrigation in horticultural crops is highly demanded by farmers for an optimal water management worldwide. The use of plant-based sensors is in many cases the recommended option since plants are an integral component of the soil-plant-atmosphere continuum (Jones, 1999; Jones, 2004; Fernández *et al.*, 2008b; Nadler & Tyree, 2008; Fernández & Cuevas, 2010; Ortuño *et al.*, 2010; Oyarce & Gurovich, 2011). These sensors have to meet a number of criteria to better approach precise irrigation scheduling: being a reliable and sensitive water stress indicator, user-friendly, minimally invasive and suitable for automatically and continuously data collection and transmission throughout a whole irrigation season the most relevant (Jones, 2004; Fernández, 2014a). The recently developed leaf patch clamp pressure probe (LPCP probe) has proved to meet those criteria to precisely monitor water stress in several plant species and crops (Westhoff *et al.*, 2009; Rüger *et al.*, 2010a; Fernández *et al.*, 2011b; Lee *et al.*, 2012; Bramley *et al.*, 2013). Its output targets on turgor pressure (Rüger *et al.*, 2010a; Ehrenberger *et al.*, 2012a, 2012b), one of the physiological variables recognized to be among the most sensitive to water stress (Jones, 2004, 2007). Additionally, the applicability of leaf patch pressure probes has been extended to more specific studies in the regulation of physiological processes by the leaf water status (Ache *et al.*, 2010; Bauer *et al.*, 2013), increasing its potential to disentangle mechanisms of response to water stress.

Besides that, process-based models have been also suggested as a powerful tool to improve our understanding of plant physiological mechanisms involved in the response to water stress (Buckley & Mott, 2013). These models use physiological based parameters and have the strength to mechanistically simulate leaf and plant behaviors. In the present work, we used a process-based stomatal conductance model (BMF model, Buckley *et al.*, 2003) to estimate absolute changes in leaf turgor pressures. Turgor pressure of guard cells and surrounding epidermal cells determine

largely the stomatal aperture (Franks *et al.*, 2001; Buckley & Mott, 2002b), and in this sense the use of BMF model to estimate turgor pressure from stomatal conductance measurements seems highly appropriated. Our main objective was to assess whether the diurnal leaf turgor pressure changes derived from LPCP outputs agrees with the turgor pressure modeled by the BMF model. Additionally, the concomitant use of LPCP probes and the BMF model will be used to understand mechanisms of stomatal conductance regulation under water stress. Experiments were carried out in a hedgerow olive tree orchard under two water treatments. Measurements were conducted at different leaf locations within the canopy, aiming to explore the behavior of stomata and main physiological variables determining the plant water status under different microenvironments.

Material and methods

Experimental design

The experiment was conducted in 2012 in a commercial hedgerow olive orchard (*Olea europaea* L., *cv.* Arbequina) near Seville, Spain (37º 15′ N, −5º 48′ W). The orchard was planted with 1667 tree ha^{-1} in 2007. An experiment on irrigation started in 2010 (Fernández *et al.*, 2013). Preliminary data show that differences among leaves within individual canopies, not differences among individuals, give rise to most of the variation in stomatal behavior in our study species. As our goal was not to describe differences among treatments, but to explain the physiological basis in the response of LPCP probes observed in a wide range of values, we decided to replicate locations within the canopy rather than tree individuals. Therefore, one tree per treatment in two of the four considered treatments was selected to carry out the study. The irrigation treatments supplied were: Control (well watered, WW), with daily irrigation to replace 100 % of the maximum

potential crop evapotranspiration (ET_c); and a regulated deficit irrigation treatment (water stressed, WS), aimed to supply a total of 30 % ET_c, with changing irrigation intensities and frequency during the season. Details on both the calculation of ET_c and actual water supplies to each treatment are given in Fernández *et al.* (2013). The irrigation system consisted of one drip line per tree row with a 2 L h^{-1} dripper every 0.5 m. The soil in the orchard (*Arenic Albaqualf*, USDA 2010) had a sandy loam top layer of 0.6 m and a sandy clay layer downwards (Fernández *et al.*, 2013).

Soil and weather conditions

Volumetric soil water content (θ_v) was estimated from measurements with a Profile probe (Delta-T Devices Ltd, Cambridge, UK) installed at 0.1 m from a dripper of the WS treatment. The probe was connected to a CR1000 Campbell datalogger (Campbell Scientific Ltd., Shepshed, UK) for collecting records every 10 min. In the WW treatment, where daily irrigation was supplied, we used a Profile probe to measure θ_v once or twice per week, in two access tubes (at 0.1 and 0.4 from a dripper). In all cases θ_v was measured at 0.1, 0.2, 0.3, 0.4, 0.6 and 1.0 m depths. We averaged θ_v down to 0.4 m depth only, since Diaz-Espejo *et al.* (2012) did not find roots in the orchard below 0.45 m. This was confirmed in this study by constant θ_v at 0.6 and 1.0 m depth along the studied period. The Profile probe was calibrated *in situ* by Fernández *et al.* (2011b).

Weather variables were monitored by a Campbell weather station (Campbell Scientific Ltd., Shepshed, UK) installed in the centre of the experimental area. The meteorological sensors were installed at 3 m above the trees and average values of air temperature (T_a) and air vapour pressure deficit (VPD) were recorded every 30 min. Photosynthetic photon flux densities (PPFD) were monitored at the same time-step than stomatal conductance measurements (see below) with the photosynthetically active

radiation sensor integrated in the chamber of a Li-6400 (LI-COR, Lincoln, NE, USA).

Plant measurements

Three leaf positions within the tree canopy (east, shade and west) were explored in the WW, whereas only eastern ('sunny') and shaded leaves were used in the WS. Measurements were made on two days, June 25 and August 3.

Leaf water potential (Ψ_{leaf}) and leaf gas exchange were measured diurnally every 1.5 hours on the two experimental days. A Scholander-type pressure chamber (PMS Instrument Company, Albany, Oregon, USA) was used to measure Ψ_{leaf} from 5:30 to 19:00 Greenwich Mean Time (GMT) on three healthy, fully developed leaves per canopy position.

Stomatal conductance to H_2O (g_s) was measured on four leaves per canopy position using an open flow gas exchange system with a 2×3 cm chamber (Li-6400, LI-COR, Lincoln, NE, USA). Chamber radiation and temperature matched ambient and CO_2 concentration was controlled at 390 μmol mol^{-1} by a 6400-01 CO_2 injector (LI-COR).

On the same dates, leaves were sampled at dawn for osmotic pressure (π_d) measurements. Three mature, fully expanded leaves per position within the tree canopy were cleaned, packed in aluminum foil and immediately frozen in liquid nitrogen. One 7-mm diameter disc per leaf was sampled between the midrib and margin with a cork borer, punctured 15-20 times with forceps to speed equilibration and immediately loaded in a C-52 thermocouple psychrometer chamber (Wescor Inc., Logan, UT, USA) connected to a datalogger (PSYPRO, Wescor). Equilibrium time in the chambers was *ca.* 30 min. π_d measurements were corrected by using the regression model of Bartlett *et al.* (2012) to account for apoplastic dilution and wall solute enrichment.

Leaf patch clamp pressure probe

Relative changes in leaf turgor pressure were derived from *in situ* measurements with the non-invasive, online-monitoring leaf patch clamp pressure probe (hereafter, LPCP probe, ZIM Plant Technology GmbH, Hennigsdorf, Germany). The principle of the magnetic LPCP probe was described in detail by Zimmermann *et al.* (2008) and Westhoff *et al.* (2009). Briefly, a small patch of an intact leaf is used as a sensing element for measuring relative changes of turgor pressure in the entire leaf tissue. The leaf patch must be in hydraulic and osmotic equilibrium with its surrounding. Leaf is clamped between two metal pads in which two magnets are integrated. The lower pad contains a temperature-independent pressure sensor chip silicone-embedded. The magnetic pressure exerted on the leaf patch can be altered by changing the distance between the two magnets. Relative leaf turgor pressure is determined by measuring the pressure transfer function of the leaf patch, i.e. by measuring the output leaf patch pressure, P_p, upon application of a constantly kept external magnetic pressure (P_{clamp}). The attenuation of the applied external pressure and thus P_p depends on the magnitude of the turgor pressure of the leaf (P_c) which is opposed to P_{clamp}. That implies that P_p is low at high P_c and high at low P_c. Detailed analyses (Zimmermann *et al.*, 2008; Westhoff *et al.*, 2009; Ehrenberger *et al.*, 2012b) showed that P_p is a power function of P_c, being both parameters inversely coupled:

$$(4.1) \qquad P_p = \left(\frac{b}{aP_c + b} \right)^{\frac{1}{a}} F_a P_{clamp},$$

where *a* and *b* are leaf-specific, elastic constants and F_a is the attenuation factor which takes into account the turgor pressure independent losses due to the compressibility of the silicone of the sensor chip and of leaf-specific structural elements (e.g. air-filled spaces, cuticle and cell walls). F_a can be assumed to be constant down to very low turgor pressures (~50 kPa) and a

calculated value of 0.29 was obtained when P_p was calibrated with concomitant cell turgor pressure probe measurements in olive (Ehrenberger *et al.*, 2012b). The signals are sent wireless by transmitters (connected by cable with the probe) to a controller which transfers the data to a GPRS modem linked to an Internet server. P_p were collected every 5 min.

At the beginning of May, three LPCP probes per canopy position were installed. Details on the clamping procedure are given by Fernández *et al.* (2011b). The probes clamped on eastern and western leaves of the canopy were installed at about 1.5 m above ground, whereas probes on the shaded leaves were clamped at 0.5 m and in the inner portion of the canopy. To allow average the three LPCP probes of each position and comparison among them, a normalizing procedure of P_p was carried out since initial P_{clamp}, and thus P_p, in the turgescent state (early in the morning) can vary between leaves. The normalized P_p (P'_p; %) presented here are the results of applying:

$$(4.2) \qquad P_p^{'} = \frac{P_p - P_{min,1}}{P_{max,1} - P_{min,1}},$$

where P_p is the actual value of the probe, $P_{min,1}$ is the minimum value (maximum turgor pressure) reached at pre-dawn of the decided experimental day (1 = June 25; 2 = August 3) and $P_{max,1}$ is the maximum value (minimum turgor pressure) reached during the same day. P_p data were previously smoothed by using the 9-point FFT Filter routine in OriginPro 8.1 (OriginLab, Northampton, MA, USA).

Photosynthetic response curves

From two to five A-c_i response curves (response of net CO_2 assimilation rate, A, to intercellular CO_2 concentration, c_i) per canopy position and treatment were determined between 9:00 and 13:00 GMT over the experimental period. Measurements were performed at ambient

temperature, saturating PPFD (1600 μmol m^{-2} s^{-1}) and ambient CO_2 concentration (c_a) between 50 and 1500 μmol mol^{-1}. After steady-state photosynthesis was achieved, the response of A to varying c_i was measured by lowering c_a stepwise from 390 to 50 μmol mol^{-1}, returning to 390 μmol mol^{-1}, and then increasing c_a stepwise from 390 to 1500 μmol mol^{-1}. Each A-c_i curve comprised 16 measurements, each made after at least 3 min at each c_a. Parameters of the photosynthesis model of Farquhar *et al.* (1980) were derived for each curve using the method of Ethier & Livingston (2004) to fit three parameters by non-linear least squares regression (Table 4.1): mesophyll conductance (g_m), maximum carboxylation rate ($V_{c,max}$) and maximum potential electron transport rate (J_{max}) (we found no evidence of triose-phosphate utilization limitation, TPU, in our data, so we did not consider this limitation). Other parameters were taken from the literature. Rubisco kinetic parameters and the photorespiratory CO_2 compensation point (Γ^*) were taken from Bernacchi *et al.* (2002). Non-photorespiratory CO_2 release (R_d) and its temperature dependence was taken from Diaz-Espejo *et al.* (2006). $V_{c,max}$, J_{max} and g_m were normalized to 25 °C using temperature responses from Warren & Dreyer (2006).

Table 4.1. Maximum carboxylation rate ($V_{c,max}$), maximum rate of electron transport (J_{max}) and mesophyll conductance (g_m) measured along the experiment. Numbers between brackets show standard errors ($n = 2 - 5$). Different letters indicate significant differences (Multiple comparisons on significant effects from linear mixed model, $P <$ 0.05). When no letters were presented, non-significant differences were found.

Treatments and position	$V_{c,max}$ μmol m^{-2} s^{-1}		J_{max} μmol m^{-2} s^{-1}		g_m mol m^{-2} s^{-1}	
WW						
East	153.08	(15.59)[ab]	92.60	(6.65)	0.043	(0.007)
Shade	115.61	(13.22)[b]	75.50	(10.48)	0.036	(0.011)
West	117.50	(7.02)[b]	72.95	(3.10)	0.023	(0.003)
WS						
East	194.34	(20.27)[a]	116.30	(25.76)	0.058	(0.024)
Shade	127.37	(18.54)[ab]	54.33	(2.14)	0.023	(0.008)

From two to four PPFD response curves per canopy position and treatment were performed using a LED Light Source (Li-6400-02B, LI-COR) connected to the Li-6400, between 9:00 and 13:00 GMT, by reducing PPFD from 2000 μmol m^{-2} s^{-1} to darkness in 14 steps. Temperature and CO_2 were 28-32 °C and 390 μmol mol^{-1}, respectively. Maximum A (A_{max}, μmol m^{-2} s^{-1}), the curvature parameter (θ, dimensionless) and maximum quantum yield of CO_2 (α, the initial slope of A versus PPFD, dimensionless) were determined by least squares curve fitting to a non-rectangular hyperbola. Average parameter values obtained were: $\theta = 0.44 \pm$ 0.11; $\phi = 4\alpha = 0.33 \pm 0.02$ electrons photon^{-1} (where ϕ is the effective maximum quantum yield of electrons).

Process-based model of stomatal conductance

We used the stomatal conductance model originally presented by Buckley *et al.* (2003) (hereafter, the BMF model) to derive leaf turgor pressure for assessing LPCP probes measurements. This model is based on leaf, plant and stomatal water relations, and the hypothesis that guard cell osmotic pressure is actively regulated in proportion to epidermal turgor pressure (which acts as a sensor for changes in leaf water status) and to the ATP concentration of photosynthesising cells (which acts as a sensor for light and CO_2). We modified the original model deriving the following form:

$$(4.3) \qquad g_{s,model} = \frac{naK(\Psi_s + \pi)}{K + naVPD},$$

where K is leaf-specific hydraulic conductance, Ψ_s is soil water potential (assumed here as the pre-dawn Ψ_{leaf} measured in the field), π is bulk leaf osmotic pressure and VPD is air vapour pressure deficit. n and a capture non-hydraulic effects: a is mesophyll ATP concentration expressed relative to its maximum value and n is a lumped parameter representing other non-hydraulic factors:

$$(4.4) \qquad n \equiv \chi\beta\tau_m, \text{ and}$$

$$(4.5) \qquad a \equiv \tau/\tau_m,$$

where τ is ATP concentration in photosynthesising cells. The parameters embedded in n are χ, a proportionality factor that scales guard and epidermal cell turgor pressures to g_s; β, a proportionality factor that scales the product of τ and epidermal turgor to changes in guard cell osmotic pressure; and τ_m, the maximum τ (the total pool of adenylates, ADP + ATP). We simulate τ with the model of Farquhar & Wong (1984), which was derived from the photosynthesis model of Farquhar *et al.* (1980).

Buckley *et al.* (2003) showed that β could be interpreted as the ratio of the specific rates of active ion uptake and passive ion efflux in guard cells. Because abscisic acid (ABA) affects guard cells by stimulating passive efflux (Hetherington, 2001), one would expect β – and therefore the parameter *n* in the modified model – to decline as ABA concentration increases.

Equation (4.3) is a simplified form of the BMF model based on the following assumptions: the osmotic gradient from guard to epidermal cells, not to the apoplast, is the target for active regulation; the resistance from epidermal to guard cells is negligible compared to the resistance from the soil to the epidermis; and epidermal and bulk leaf osmotic pressure are similar.

One of the constraints embedded in the BMF model is the 'hydroactive feedback hypothesis' (Buckley, 2005; $\pi_g = \pi_e + \beta\tau P_e$, where π_g is the guard cell osmotic pressure, π_e is the epidermal cell osmotic pressure and P_e is the epidermal cell turgor pressure) which can be written as:

(4.6) $g_s = \chi\beta\tau\left(\psi_{leaf} + \pi\right),$

solving for π:

(4.7) $\pi = \dfrac{g_s}{\chi\beta\tau} - \Psi_{leaf} = \dfrac{g_s}{na} - \Psi_{leaf}.$

Equation (4.7) was used in the present work to estimate π with concurrent measurements of g_s, Ψ_{leaf} and c_i and modeled *na* on each time step. Parameters of photosynthetic capacity ($V_{c,max}$, J_{max} and g_m, Table 4.1) and diurnal measurements of c_i were used to calculate τ, embedded in the parameter *na*, meanwhile $\chi\beta$ were parameterize from fitting the BMF model to g_s data. The maximum π value obtained in each day was selected as input

in the BMF model. See Results section for further explanations on why π measured was not used.

Variable hydraulic conductance (K_{var}) was obtained by fitting g_s data to the BMF model at single measuring time solving Equation (4.3) as:

$$(4.8) \quad K_{var} = \frac{g_s \text{VPD}}{\Psi_s + \pi - \dfrac{g_s}{na}} \, .$$

The modeled leaf turgor pressure (P_{model}) was derived from the standard expression of plant water relation: $P_{model} = \Psi_{l,model} + \pi$, where $\Psi_{l,model}$ is the modeled leaf water potential estimated as:

$$(4.9) \quad \Psi_{l,model} = -\left(\frac{g_{s,model} \text{VPD}}{K} - \Psi_s \right),$$

and π is the maximum value estimated as indicated above.

Statistics

Linear mixed models were used to analyze effects of irrigation treatment (as a fixed factor) on Ψ_{leaf}, g_s, π, K, n and π_d. Leaf within position into the tree canopy was used as random factor when necessary to describe our experimental design. Homogeneity of variance and normality were tested and transformations were applied when needed. Models were fitted by restricted maximum likelihood (REML) in R (package 'nlme R'; Pinheiro *et al.*, 2012). When significant differences were obtained by ANOVA ($\alpha = 0.05$), multiple comparisons were conducted for groups of more than two levels (package 'multcomp'; Hothorn *et al.*, 2008).

Linear regression analyses for P'_p and Ψ_{leaf} relationships were made by using SigmaPlot 11.0 (Systat Software, Inc., California, USA).

Results

During the progress of the experiment, the WW treatment presented θ_v values around 0.25 m^3 m^{-3} (Fig. 4.1), which in the soil of this study means soil capacity. The lower irrigation dose in June and the weekly irrigation events in August were reflected in the θ_v pattern in the WS treatment. Maximum air temperature (T_a) over 35°C and maximum evaporative demand (VPD) over 5 kPa were observed in the two daily cycle measurements. Despite of the high VPD on June 25, sky was partially cloudy, and maximum PPFD did not exceed 600 μmol m^{-2} s^{-1} in the eastern sunny locations (Fig. 4.1E, F). Meanwhile, a maximum up to 800 μmol m^{-2} s^{-1} was recorded in the west sunny location. Clear skies on August 3 allowed for a maximum PPFD between 1200-1400 μmol m^{-2} s^{-1}. As expected, the irradiance peaked at a different time of the day in east and west sides of the canopy (Fig. 4.1G, H). In both June and August, PPFD inside the canopy was up to 10-fold lower than in the outer canopy.
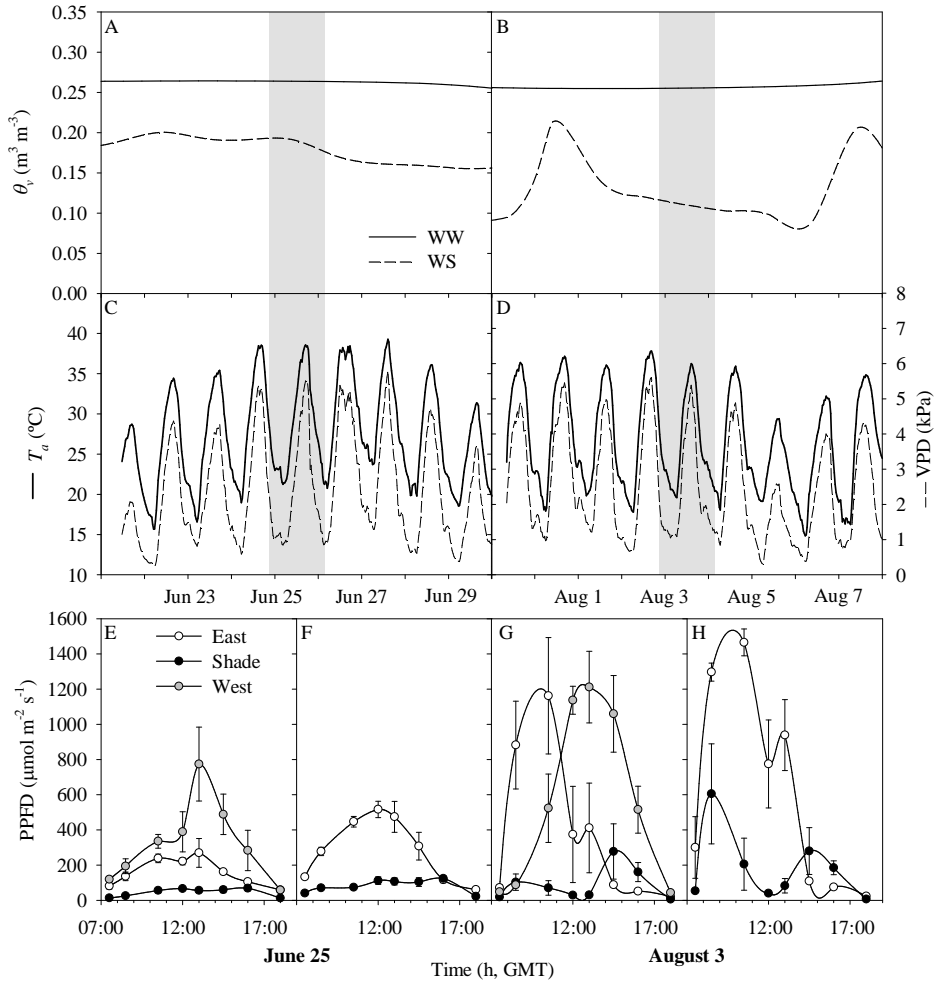
Fig. 4.1. Time courses of (A, B) volumetric soil water content (θ_v) measured on both well watered (WW) and water stressed (WS) treatments, (C, D) air temperature (T_a), air vapour pressure deficit (VPD) and (E, F, G, H) photosynthetically active photon flux density (PPFD) along the experiment. Panels (E) and (G) correspond to WW and (F) and (H) to WS treatments. Shaded areas indicate the two experimental dates, zoomed-in in the case of PPFD measurements. GMT = Greenwich Mean Time.

On June 25 the differences in Ψ_{leaf} between treatments and locations were small and only significant in the afternoon. But, the effect of different

water supply was clearly observed on August 3 with a significant drop in both predawn and minimum Ψ_{leaf} in WS leaves (Fig. 4.2A, B). Both sunny and shaded leaves presented a similar decline in Ψ_{leaf}, which reached values as low as -4.2 MPa, 3 MPa lower than the WW leaves. Accordingly, these severe water stressed conditions led to a strong stomatal closure (Fig. 4.2D). Clearly different g_s were observed between sunny and shaded leaves in both treatments, disappearing in the WS leaves once water stress was established in August (Fig. 4.2C, D). Furthermore, shaded leaves showed a more constant behavior along the studied period, and the main response to water stress came from sunny exposed leaves.
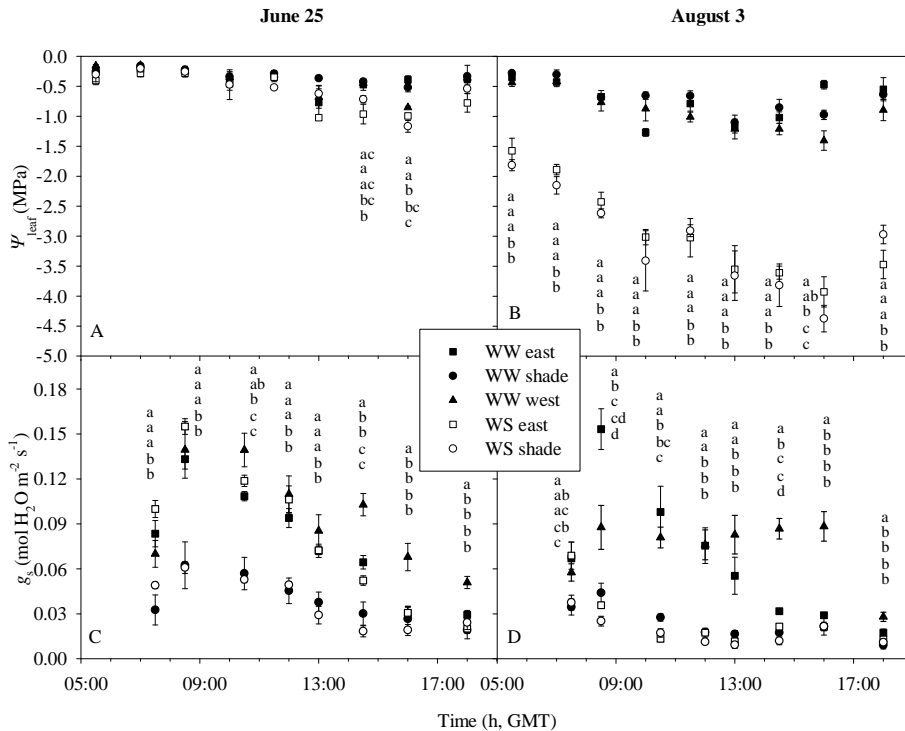
Fig. 4.2. Leaf water potential (Ψ_{leaf}, $-$MPa) and stomatal conductance (g_s, mol H_2O m^{-2} s^{-1}) measured in leaves from different locations within the canopy for the two water treatments (WW and WS) and on the two experimental dates. Error bars show standard errors for $n = 3$ (Ψ_{leaf}) and $n = 4$ (g_s). Different letters indicate significant differences

(Multiple comparisons on significant effects from linear mixed model, $P < 0.05$). When no letters were presented, non significant differences were found. GMT = Greenwich Mean Time.

The output of LPCP probes, although proportional to turgor pressure and Ψ_{leaf}, is dependent on clamping pressure and elastic properties of material clamped. This makes difficult averaging replicates. An example of the three probes installed in two locations in this study is shown in Fig. 4.3. WS leaves were chosen because of the wider range of Ψ_{leaf} shown, as well as both sunny and shaded locations. It can be observed that each probe varied in its offset, which motivated that probe readings were normalized following Equation (4.2). Measurements of Ψ_{leaf} are plotted on top of them for comparison (open symbols in Fig. 4.3). Significant negative linear relationships were obtained between P'_p and Ψ_{leaf} (Fig. 4.4), except in some cases where the correlation showed a hysteretic behavior. This phenomenon was clearly evident in both eastern and shaded leaves of the WS leaves on August 3 (Fig. 4.4B, D), but also slightly presented in eastern leaves in June (Fig. 4.4A). Although a linear relationship between P'_p and Ψ_{leaf} was observed in both treatments and dates, in the WS leaves the correlations were shifted to much lower values of Ψ_{leaf} in August. The WW leaves also presented a slight shift towards the same direction (note different range of X-axis in Fig. 4.4 between left and right panels).
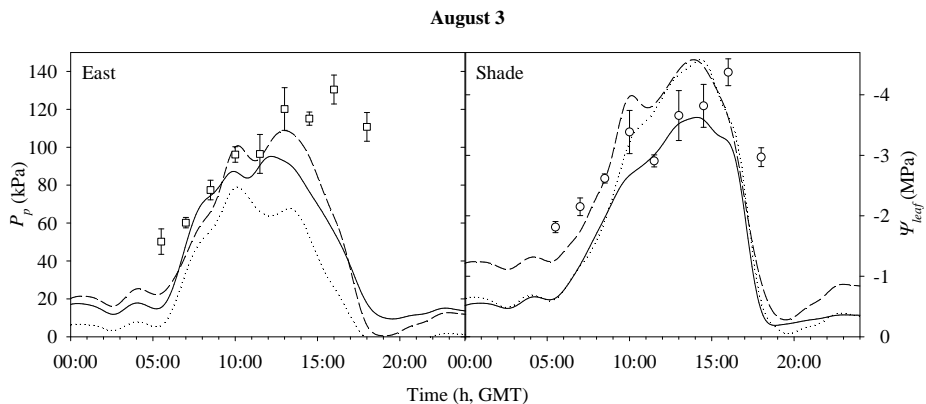
Fig. 4.3. Leaf patch clamp pressure (LPCP) probe actual recordings during August 3 in three eastern and shaded leaves of the WS tree (lines). Simultaneous leaf water potential (Ψ_{leaf}, $-\mathrm{MPa}$) measurements in the same canopy locations are also presented (open symbols). Error bars show standard errors for $n = 3$. GMT = Greenwich Mean Time.
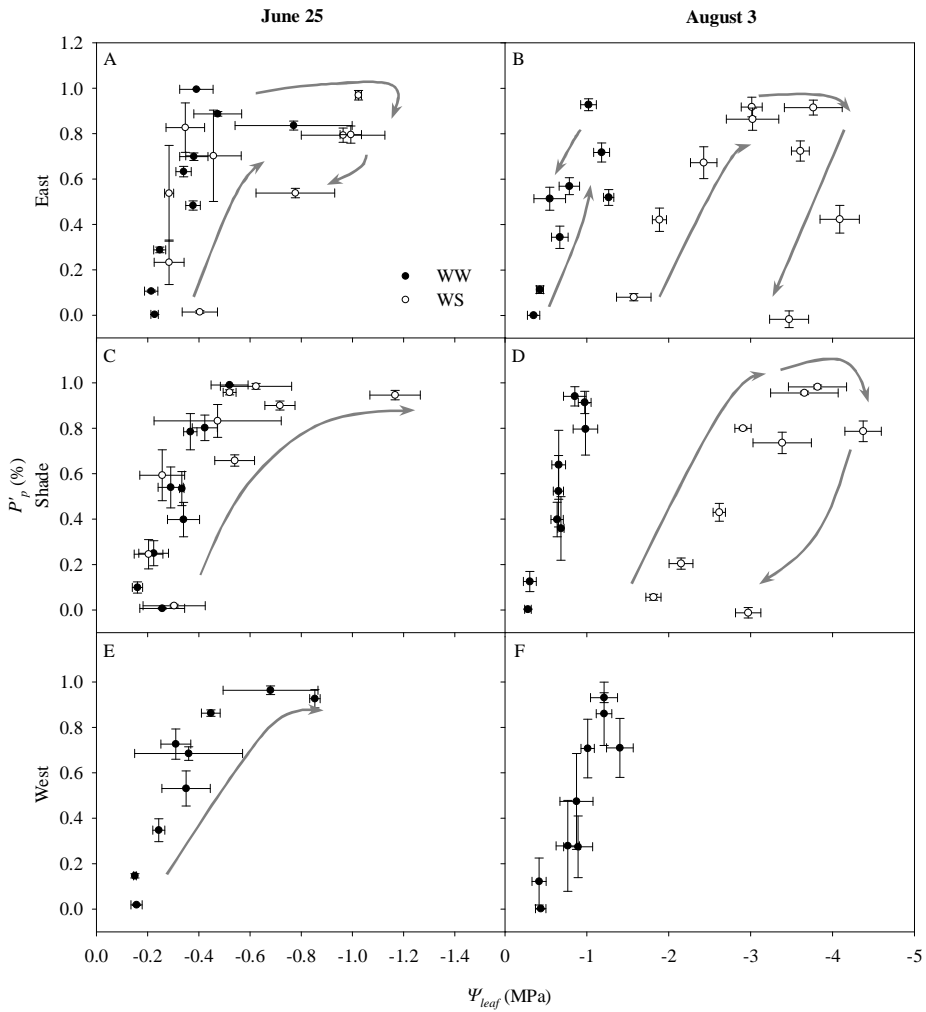
Fig. 4.4. Relationships between the normalized output leaf patch pressure (P'_p, %) and the leaf water potential (Ψ_{leaf}, $-$MPa) measured on the two experimental dates in different leaf locations within the canopy and for the two water treatments (WW and WS). Error bars show standard errors for $n = 3$. Gray arrows indicate the diurnal evolution of the measurements when hysteresis was observed.

The stomatal conductance model (BMF model) was used to estimate the diurnal progress of leaf turgor pressure (P_{model}), and to relate it to the P_p dynamics. Initially, the model was incapable of reproducing simultaneously

the diurnal behavior of both g_s and Ψ_{leaf}. This is a process-based model of stomatal conductance that, among several assumptions, uses a constant π during the day. Under the conditions of severe water stress experienced by the WS leaves, osmotic pressures measured at dawn (π_d; Table 4.2) were too low to reproduce the low Ψ_{leaf} measured in the afternoon (Fig. 4.2B). To solve that discrepancy, we used a maximum estimated π value based on Ψ_{leaf} as explained in M&M. Diurnal change of π has been reported by several authors (Girma & Krieg, 1992; Patakas & Noitsakis, 1999; Hummel *et al.*, 2010; Himmelsbach *et al.*, 2012), reaching increments of 0.5 - 1.4 MPa in olive to tolerate water stress periods maintaining photosynthetic activity (Dichio *et al.*, 2006). The BMF model satisfactorily captured the diurnal evolution observed in g_s in both treatments (Fig. 4.5) and produced parameters with full physiological meaning (Fig. 4.6). Accounting that π were estimated values from Ψ_{leaf}, a large osmotic adjustment was observed in both sunny and shaded leaves in WS from June to August (Fig. 4.6A). Soil-to-leaf hydraulic conductance (K) was quite constant for WW sunny leaves in both June and August, meanwhile in the WS leaves K decreased in August. Shaded leaves tended to have lower K than sunny ones, independently of water treatment, being larger the difference in August for WW, but disappearing in WS. However, the non-hydraulic term n did not have a distinguishable pattern. On June 25, a high variability was observed probably due to the cloudy weather conditions and due to the close relation of this parameter with PPFD through the embedded parameter τ. Despite of that, n mostly declined in August in both sunny and shaded leaves reaching lower values in the WS leaves. Although the goodness of fit of the BMF model presented in Fig. 4.5 (that assumed all the estimated parameters constant during the day) can be considered as good, still the model was not able to interpret some points at the onset and end of the day (e.g. Fig. 4.5A). To account for these discrepancies, we evaluated a dynamic diurnal variation in K (K_{var}) as a possible physiological mechanism not considered in the model at its current version. In order to achieve this, K_{var} was allowed to

change to fit g_s data to the BMF model output at very single measuring time. The new modeled g_s is not shown since simply matches perfectly with g_s data, but the diurnal evolution of K_{var} modeled is shown in Fig. 4.7. Results suggested that K changed during the day in both treatments. Additionally, K_{var} was plotted as a function of Ψ_{leaf} (Fig. 4.8).

Leaf turgor pressures modeled by the BMF model under a dynamic K were plotted against the normalized values of P_p (Fig. 4.9). Both variables were correlated and followed a power function. This power function was mainly observed in August.

Table 4.2. Osmotic pressures measured at dawn (π_d) on the two daily cycle measurements. Numbers between brackets show standard errors ($n = 3$). Different letters indicate significant differences (Multiple comparisons on significant effects from linear mixed model, $P < 0.05$).

Experimental period	Treatments and positions	π_d MPa	
June	WW		
	East	1.80	(0.08)[cb]
	Shade	1.50	(0.03)[b]
	West	1.91	(0.11)[cb]
	WS		
	East	2.48	(0.16)[a]
	Shade	2.18	(0.09)[ac]
August	WW		
	East	1.84	(0.09)[cb]
	Shade	2.00	(0.09)[ac]
	West	2.05	(0.15)[ac]
	WS		
	East	2.28	(0.05)[ac]
	Shade	2.23	(0.16)[ac]
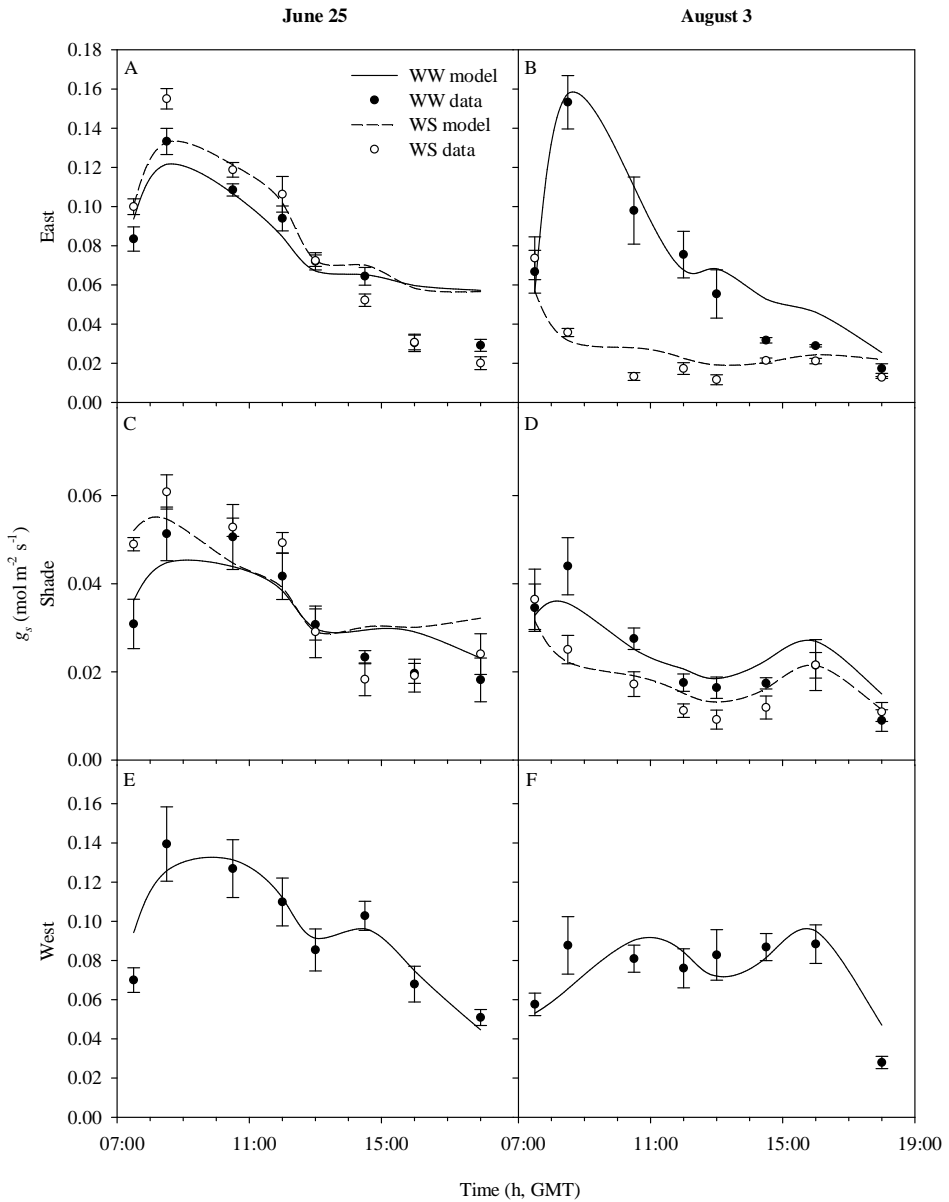
Fig. 4.5. Evolution of g_s data (points) and g_s fitted with the BMF model (lines) on the two experimental dates in different leaf locations within the canopy and for the two water treatments (WW and WS). Error bars show standard errors for $n = 4$ (g_s data). GMT = Greenwich Mean Time.
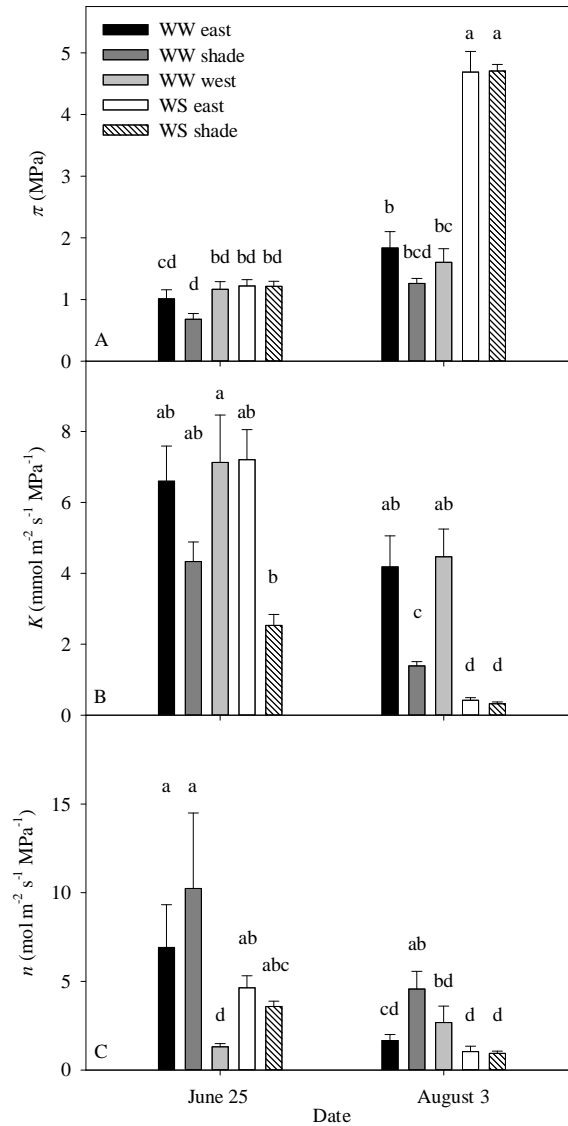
Fig. 4.6. Values of the parameters obtained by fitting the BMF model to g_s data on the two experimental dates in different leaf locations within the canopy and for the two water treatments (WW and WS). (A) Maximum leaf osmotic pressure (π) estimated from concurrent leaf water potential, meteorological and g_s data (see M&M for details). (B) Soil-to-leaf hydraulic conductance (K). (C) The non-hydraulic effects parameter (n). Error bars are standard errors for $n = 4$. Different letters indicate significant differences (Multiple

comparisons on significant effects from linear mixed model, $P < 0.05$).
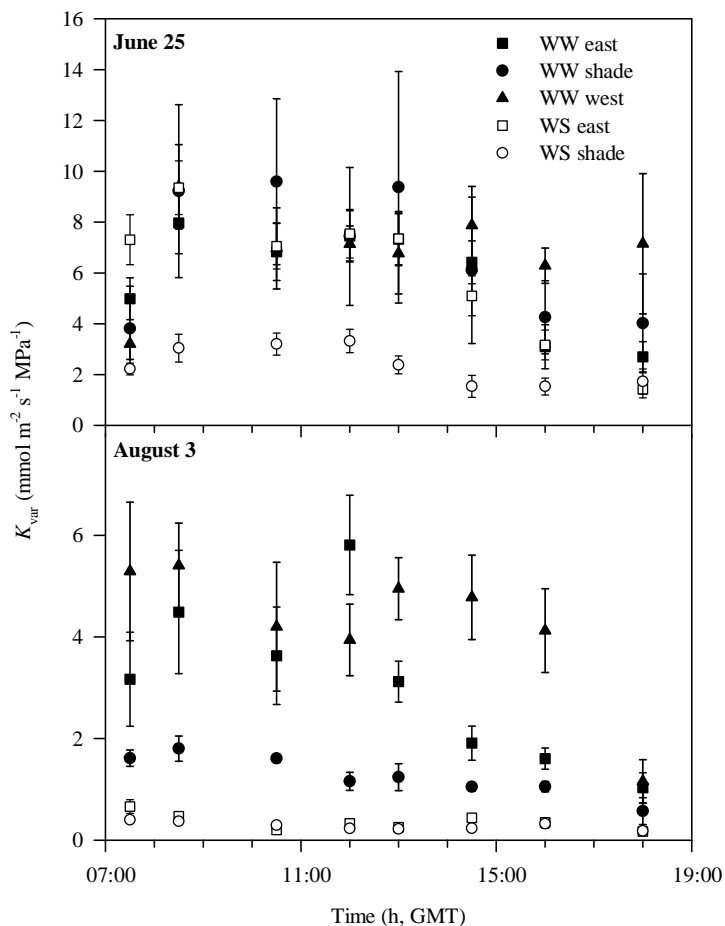
Fig. 4.7. Diurnal variation of soil-to-leaf hydraulic conductance (K_{var}) obtained by exactly fitting the BMF model to g_s data on the two experimental dates in different leaf locations within the canopy and for the two water treatments (WW and WS). Error bars are standard errors for $n = 4$.
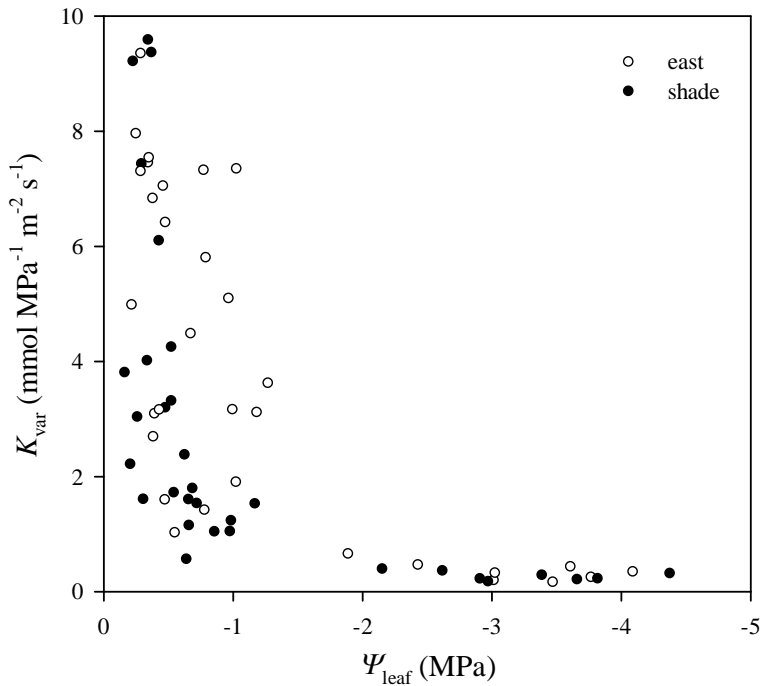
Fig. 4.8. Diurnal variation of soil-to-leaf hydraulic conductance (K_{var}) plotted against leaf water potential (Ψ_{leaf}) measured in eastern and shaded leaves and mixing the two water treatments and the two experimental dates. K_{var} values are the same than those presented in Fig. 4.6. Each point represents the average of $n = 4$ (K_{var}) and $n = 3$ (Ψ_{leaf}). Error bars are not presented for a clearer view of the figure.
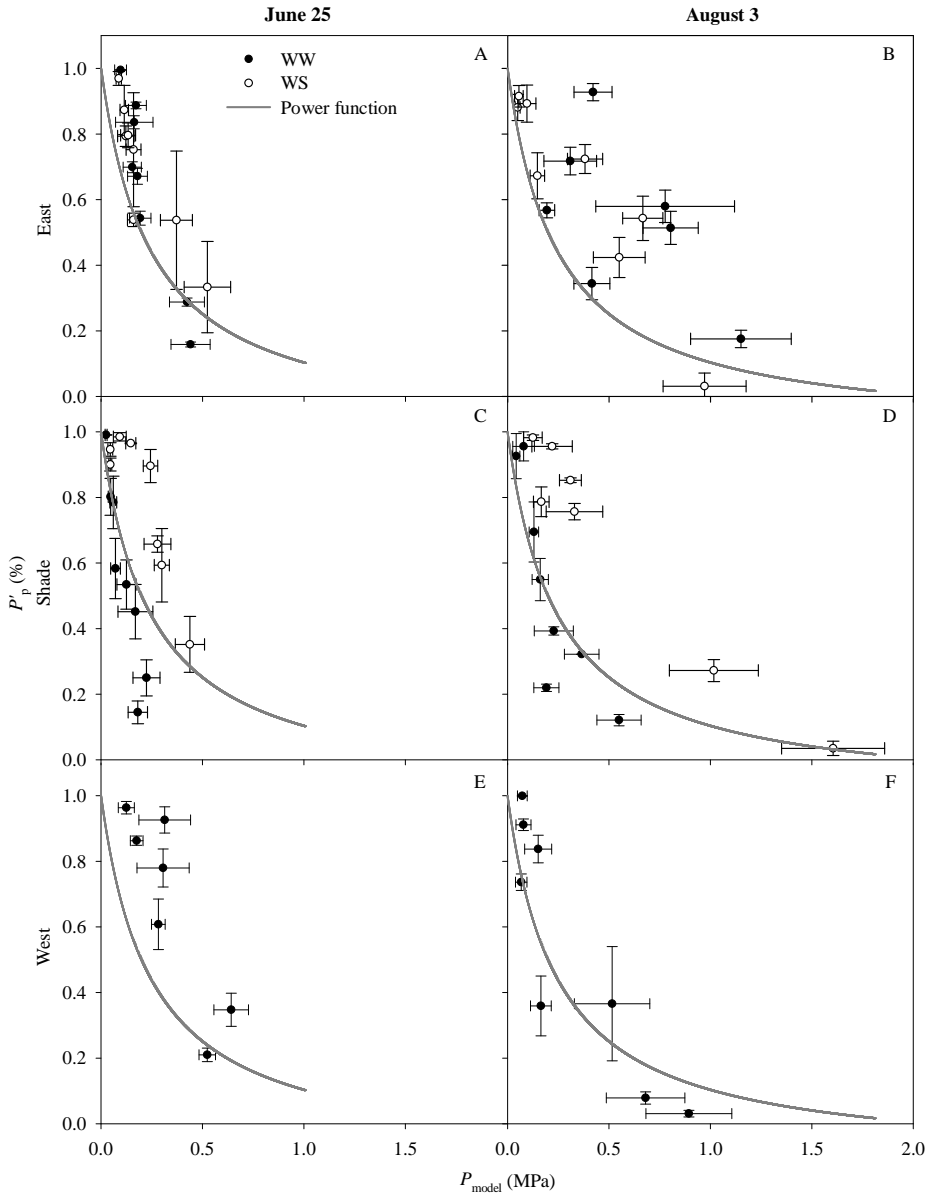
Fig. 4.9. Relationships between the normalized output leaf patch pressure (P'_p, %) and the absolute leaf turgor pressure modeled with the BMF model (P_{model}) on the two experimental dates in different leaf locations within the canopy and for the two water treatments (WW and WS). The power function presented (gray line) is the result of using the Equation (4.1) with a range between 0 and 2 MPa for P_c, $F_a = 0.29$, $P_{clamp} = 398$ kPa, $a = 1$, $b = 244$ kPa, and normalizing the P_p resulted by using the Equation (4.2).

Discussion

Leaf patch clamp pressure (LPCP) probes have been presented as promising tools in studies of ecophysiology of plant water stress. They are good surrogates of leaf turgor pressure, allowing for an automatic monitoring of this variable under field conditions. Turgor pressure is considered as one of the most sensitive variables of water stress in plants. For this reason it is a key target in understanding the mechanisms involved in the regulation of plant water status (Ache *et al.*, 2010), as well as in applied science like deficit irrigation scheduling (Fernández *et al.*, 2011b; Ehrenberger *et al.*, 2012b; Rodriguez-Dominguez *et al.*, 2012). However, although the LPCP probe has been compared with cell turgor pressure probe measurements in several species successfully (Zimmermann *et al.*, 2008, 2010; Westhoff *et al.*, 2009; Rüger *et al.*, 2010a; Ehrenberger *et al.*, 2012a), this has most of times been made under controlled conditions in the laboratory due to technical limitations under field conditions (Westhoff *et al.*, 2009; Rüger *et al.*, 2010b). In this study, we have found a good agreement between the output leaf patch pressure (P_p) and the turgor pressure estimated by a process-based model of stomatal conductance, showing the physiological reliability of this measurement for a long period of time under field conditions. As previously reported in other studies, this relationship was explained by a power function (Fig. 4.9). The reason for a power function has been explained elsewhere (Zimmermann *et al.*, 2008; Westhoff *et al.*, 2009; Ehrenberger *et al.*, 2012b) and it is based on losses of the external clamped pressure applied to the leaf, which are theoretically embedded in the term leaf-specific attenuation factor (Ehrenberger *et al.*, 2012b). These losses occur due to the compressibility and deformability of the silicone surrounding the sensor chip as well as the compressibility of the cuticle and other structural elements of the leaf (Westhoff *et al.*, 2009). The

relationship between P'_p and the turgor pressure modeled matched well with a previous comparison made with a cell turgor pressure probe in olive leaves (gray lines in Fig. 4.9), especially in the WW leaves. However, we found a shift toward a more positive value of turgor for leaves of the WS treatment, although data still showed the power relationship between both variables. The reasons for this shift can be a change in the elastic characteristics of the leaf patch clamped by the probe, which could have modified the leaf-specific attenuation factor (Ehrenberger *et al.*, 2012b). But we think that the most likely reason for explaining the difference between both treatments showed in Fig. 4.9 is related to the model output. Modeled turgor for the WS leaves was higher than that of the WW (Fig. 4.9D), which makes not much sense on the view of the severe water stress experienced by the WS treatment (Fig. 4.2B, D). The origin of the wrong performance of the BMF model might be due to the assumption of a constant π along the day. Diurnal active osmotic adjustment has been reported in several species (Marigo & Peltier, 1996; Xu *et al.*, 2007; Hummel *et al.*, 2010), including olive trees (Dichio *et al.*, 2006). In fact, this osmotic change was already pointed out by Rüger *et al.* (2010a) comparing cell turgor pressure measurements with leaf water potentials in *Citrus*, *Eucalyptus* and *Quercus*. This hypothesis is supported in our study by two evidences: 1) π modeled in the WS leaves in August was much higher than π measured at dawn (Fig. 4.6A; Table 4.2); and 2) the model output for Ψ_{leaf} was underestimated early in the morning (Ψ_{leaf} modeled was lower than measured), meanwhile a better agreement was found at noon and afternoon. To test for the feasibility of this hypothesis, which affects the WS leaves, we decreased π in the morning respect to π in the afternoon as much as necessary to obtain a good match between P_{model} and the leaf turgor pressures predicted by the power function presented (Fig. 4.9). An average decreasing of π modeled in the morning of 1.15 MPa ($\pm$ 0.54, n = 3) was obtained, which is in the same range of diurnal osmotic adjustment reported in olive in other studies (Dichio *et al.*, 2006).

The existence of an active osmotic adjustment was evident not only in a diurnal basis. Seasonally our results suggest an increase in π, especially large in the WS leaves (Fig. 4.6A). These differences were also observed at dawn in π measured (Table 4.2), although much modest. A consequence of this seasonal adjustment of π was likely the shift toward more negative values of Ψ_{leaf} in the relationship between P'_p and Ψ_{leaf} (Fig. 4.4). A similar conclusion was reached by Fernández *et al.* (2011b) some years before working with olive as well. The increase in π allows leaves to maintain turgor pressure at lower Ψ_{leaf} (Kramer & Boyer, 1995), as it can be interpreted from the output of the LPCP probes (Fig. 4.4). If this hypothesis is correct, it would suggest as well that the hysteresis found in August in the WS leaves was a consequence of the likely diurnal adjustment of π previously mentioned above: higher π in the afternoon than in the morning would produce an additional shift toward more negative values of Ψ_{leaf}, creating the hysteresis observed. This behavior was characterized by a plateau value when reaching maximum P'_p in the middle of the day. Indeed, this plateau can be detected in other cases on June 25 (e.g. WW western leaves or WS shaded leaves) (Fig. 4.4C, E). It has been suggested that this event occurs when leaf turgor pressure get close to zero (i.e. close to the turgor loss point), being the lowest value measurable by the LPCP probes (Westhoff *et al.*, 2009; Rüger *et al.*, 2010a). Again, a diurnal osmotic adjustment would help maintaining leaf turgor pressure and stomata opened with a lowering Ψ_{leaf}. Considering only the range of P'_p lower than 0.85, the regression coefficients were, on average, $r^2 = 0.76 \pm 0.06$ ($P < 0.05$, $n = 10$), reflecting the potential of the sensor to monitor leaf water status.

The results of this study have awarded us not only on the need of using a dynamic parameter π in the BMF model, especially under water stress. Fig. 4.7 and 4.8 suggest that K is also a highly dynamic parameter during the day and should be considered so for an adequate use and interpretation of model outputs. This conclusion is not surprising at all on the view of the

importance that leaf hydraulic conductance is acquiring in our understanding of the hydraulic system of plants (Brodribb & Holbrook, 2004; Lo Gullo *et al.*, 2005; Johnson *et al.*, 2009; Ounapuu & Sellin, 2013). Leaf hydraulic conductance can represent up to 80 % of total hydraulic conductance of plants (Sack & Holbrook, 2006), and it has been reported to be extremely vulnerable to cavitation, even at high water potentials as shown in Fig. 4.8. In fact, although it seems surprising that most of K can be lost at -1.5 MPa of Ψ_{leaf}, the relationship showed in Fig. 4.8 is identical to that reported recently for olive leaves (Torres-Ruiz *et al.*, 2013b). Therefore, K_{leaf} could be a candidate to explain the large decrease of K_{var} estimated in Fig. 4.7, although other part of the hydraulic system like roots might be also playing a role. The introduction of a variable K also allowed for a better prediction of Ψ_{leaf} by the model. The larger scattered relationship observed in the east position of the canopy (Fig. 4.8) could be explained by a seasonal adjustment of K_{leaf} to tolerate lower Ψ_{leaf}. This mechanism was already suggested by Martorell *et al.* (2014) working with grapevines, who suggested a process likely mediated by osmotic adjustment to explain the seasonal hydraulic plasticity. In our study, we found evidence that can point out to that mechanism as well: π increased from June to August in the WW eastern leaves (Fig. 4.6A), at the same time that a statistically significant increase in K_{var} (Student's *t*-test, $P = 0.01$) was obtained in the range of Ψ_{leaf} from -0.4 to -0.7 MPa ($n = 10$); This last point, could be interpreted as a mechanism to acclimate to water stress and facilitate water fluxes at lower Ψ_{leaf}.

The combination of LPCP probes and the BMF model at different locations within the canopy is of great value in our quest to understand the mechanisms and coordination among physiological variables in response to environmental stresses. So, our results show that despite of differences in water stress or PPFD regime, P'_p fluctuates in all cases in the same range of values of turgor pressure (Fig. 4.9). This suggests that leaves must be

regulating key physiological variables governing transpirational fluxes and leaf water status. The reduction of K observed in shaded leaves (Fig. 4.6B) seems to be of paramount importance in this regulation. Sunny leaves in comparison to shaded leaves are known to have, among other features, higher hydraulic capacity to balance water supply with higher evaporative demand, light intensities and temperatures (Nardini *et al.*, 2012). The coordinated reduction of K and g_s in different locations in the canopy helps the plant to maintain similar Ψ_{leaf} in all of them. This avoids disequilibrium of water potentials within the canopy and competition for water among them. The role of the non-hydraulic component of g_s regulation, represented in the BMF model by n, does not seem to play a role, although WS leaves presented always lower n than WW.

Conclusions

The present research has confirmed the potential of the LPCP probes as tools for an automatic monitoring of leaf turgor pressure under field conditions. The combined use with a process-based model of stomatal conductance open the door to new insights of the mechanisms involved in the regulation of leaf gas exchange and leaf water status under drought conditions. This study highlights the importance of considering in the future the dynamics of leaf osmotic potential and hydraulic conductance, both at a seasonal and daily scale. At the same time it is demonstrated the potential of mechanistic models as important tools in ecophysiology not only for prediction, but also as new working hypothesis generators.

Chapter 5

Leaf patch clamp pressure probes:

in situ measurement of turgor pressure

Introduction

Irrigation is the largest consumer of water in arid and semi countries. At present it is very often more cost-efficient for a farmer to over-irrigate than to risk the crop being stressed either early or at a later stage. However, it is well known (see e.g. Möller *et al.*, 2007; Netzer *et al.*, 2009) that proper management of irrigation can result in enhanced productivity and / or quality. Furthermore, as pressure on available fresh-water resources will increase dramatically in the future, farmers have to find ways of improving water use efficiency. Installation of sensors in the field, which measure the water demands of the crop or of fruit trees in real time over the entire vegetation period, provides a sustainable and therefore smart solution for reduction of water consumption. By using sensitive indicators, the effects of irrigation can be gauged, and thus optimized. Plant-based sensors that measure sap flow, diurnal changes in trunk diameter or leaf thickness, stem and leaf water potential, stomatal conductance, time domain reflectometry and / or canopy temperature have been suggested by several authors as feasible indicators for smart irrigation (Scholander *et al.*, 1965; Boyer, 1967; McBurney, 1988; Cardon *et al.*, 1994; Smith & Allen, 1996; Burgess *et al.*, 2000; Zweifel *et al.*, 2000, 2001; Fernández *et al.*, 2001, 2006b; Goldhamer & Fereres, 2001; Green *et al.*, 2003; Nadler *et al.*, 2003, 2006; Naor *et al.*, 2008). Routine implementation of these techniques in crop fields, orchards and forests, however, failed for several practical and technical reasons (see Blank *et al.*, 1995; Jones 2004).

There is convincing evidence that the non-invasive, Internet-based leaf patch clamp pressure (LPCP) probe recently introduced by Zimmermann *et al.* (2008) could meet the demands for precisely monitoring leaf water status of plants in real time. When clamped correctly, the probe measures relative changes in leaf turgor pressure, P_c. The measuring principle of the high-tech probe is quite simple. An external pressure, P_{clamp}, (generated by springs or – more elegantly – by magnets) is applied to a small patch of an intact leaf.

The pressure experienced by the cells is lower than P_{clamp} because of losses due to the compressibility and deformability of structural elements (such as the cuticle, cell walls and intercellular air spaces). The attenuation factor F_a for olive leaves is usually of the order of 0.2 - 0.3 and is assumed to be constant in the turgescent range of the leaf. Theory shows that the output pressure, P_p, sensed by the probe is dominated by the turgor pressure, P_c, of the cells. Both parameters are inversely coupled to each other. If the counter-acting turgor pressure is high (e.g. at pre-dawn), pressure transfer through the tissue is considerably attenuated; therefore, the output signal, P_p, is low. *Vice versa*, if the turgor pressure is low (e.g. at noon), a high P_p value is recorded. The prediction of the theoretically postulated power function relationship between P_p and P_c has been verified for many plant species, such as olive, grapefruit, grapevine, lianas, eucalypts, banana plants and oak trees, by concomitant P_p and leaf cell turgor pressure measurements using the minimal-invasive cell turgor pressure probe (Zimmermann *et al.*, 2008, 2009; Westhoff *et al.*, 2009; Rüger *et al.*, 2010a, b). These measurements were performed in a range of P_c values between *ca.* 50 and 550 kPa.

Case studies on several crop and fruit trees have shown that the profile of the diurnal curves of the output signals of the probe change in a characteristic manner upon ongoing drought, reflecting the increasing difficulty to compensate turgor pressure losses by water uptake. Several parameters, such as the rise time of the P_p values in the morning (= P_c loss), the peak P_p values at noon (= maximum P_c loss), the decrease rate of the P_p values during the afternoon (= recovery phase of P_c) and / or the P_p values reached during the night (= maximum P_c) are affected by water stress and can be used as sensitive indicators for irrigation.

When P_c drops below *ca.* 50 kPa, the P_p peak values measured at noon increase dramatically, quite often exceeding the recommended measuring range of the probe (up to 250 kPa). This increase is expected in the light of

the current theory and can be used (together with the other P_p parameters) as a clear-cut indication for severe water stress. Interestingly, olive trees (Ben-Gal *et al.*, 2010; Fernández *et al.*, 2011b) under field conditions show a reversal of the diurnal P_p curves upon approaching the plasmolytic point, i.e. at noon minimum P_p values were recorded, whereas peak P_p values occurred during the night. The reversal of the P_p curves was completely reversible, even after a long period of drought. Upon watering, the diurnal P_p changes measured usually on leaves are re-established within a very short time. The reversal of the P_p curves cannot explicitly be explained by the current theory, suggesting that the P_p signal is exclusively affected by P_c changes (Zimmermann *et al.*, 2008; Westhoff *et al.*, 2009; Rüger *et al.*, 2010a, b).

In this communication we show, theoretically, that the reversal of the P_p curves observed in olive trees can easily be explained by assuming that the attenuation factor, F_a, is no longer constant at P_c values close to zero due to an unfavorable ratio of air to water. Thus, at very low P_c values, F_a and not P_c is the dominant factor that affects the P_p signals. Fundamentals for the theoretical framework were diurnal P_p curves that were measured on small olive trees. These trees were subjected to several irrigation / non-irrigation regimes under constant laboratory conditions in order to exclude any effects of environmental factors on the P_p values.

Material and methods

Plants

Probe measurements were performed under laboratory conditions on *ca.* 2-m tall olive trees (*Olea europaea* L.) planted in *ca.* 30-L pots filled with soil. The trees were subjected to a 9.5-h light / 14.5-h dark regime. Ambient

temperature and relative humidity were kept constant at 23 °C and 55 %, respectively. The light irradiation was *ca.* 196 µmol s^{-1} m^{-2} at the top and *ca.* 55 µmol s^{-1} m^{-2} at 1-m height. Field experiments were made in 2010, in a hedgerow olive orchard with 4-year-old 'Arbequina' trees, close to Seville (37°15′N, −5°48′W). The tree rows were oriented north to south. Spacing between the rows was 4 m and between the trees 1.5 m (1667 trees ha^{-1}). The trees were, on average, 2.40-m tall and 2.12-m wide canopy. Some of the trees were subjected to a regulated deficit irrigation (RDI) treatment. The 60RDI treatments were scaled to a total irrigation amount of 60 % of the crop evapotranspiration (ET$_c$) demand.

Leaf patch clamp pressure (LPCP) probe

The measuring principle of the non-invasive, online-monitoring LPCP probe (commercial name: ZIM-probe) is described in details elsewhere (Zimmermann *et al.*, 2008, 2009; Westhoff *et al.*, 2009). Briefly, a relatively small patch of a leaf is used as a sensing element for turgor pressure changes in the entire leaf. To this end, the stomata in the patch must be closed; simultaneously, the patch must be in hydraulic contact with its surroundings. This is achieved by positioning of an intact leaf between two planar circular metal pads integrated into two magnets. The lower pad contains a receptacle for integration of the pressure sensor chip. Leaf turgescence is determined by measuring the pressure transfer function of the leaf patch, i.e. by measuring the output leaf patch pressure, P_p, upon application of a constantly maintained external clamp pressure, P_{clamp} (up to 400 kPa). P_{clamp} can be varied by changing the distance between the upper and lower magnet.

Probes, together with the components for telemetric and mobile network-based data transfer to the Internet, were purchased from the company ZIM Plant Technology GmbH (Hennigsdorf, Germany). Real-time recording of the LPCP probe data was provided by battery-powered

telemetric transmitters, which were connected by cable to up to three probes. These transmitters sent wireless data together with the transmitter ID-code every 5 min via ISM (433 MHz) to a control station that logged and transferred the data with time stamps to a GPRS (General Packet Radio Service) modem linked to an Internet server, which provides the data in real time in chart and table form.

For proper function of the LPCP probe it is necessary that there is a homogeneous contact between the leaf patch and the pads of the two magnets. Only under these conditions can the pressure transfer function and thus turgor pressure be measured (see below). In the case of an inhomogeneous contact (e.g. point contacts), the probe is measuring changes in leaf thickness, which results in P_p changes that are opposite to those induced by changes in turgor pressure. Changes in leaf thickness of plants subjected to water stress are much smaller than turgor pressure induced changes.

Cell turgor pressure probe

The principle of the cell turgor pressure probe is described in detail elsewhere (Tyerman *et al.*, 2004; Zimmermann *et al.*, 2004; Bramley *et al.*, 2007). The probe was inserted from the adaxial or abaxial side of the leaves into the parenchyma cells close to the midrib. The probe was inserted most likely into the spongy tissue because of the penetration depth of the microcapillary. Adaxial and abaxial measurements yielded similar results; therefore, the data were pooled. The cell turgor pressure probe was also used for the extraction of air from the leaves. To this end, the microcapillary filled with oil up to the very tip (under very small overpressure) was introduced perpendicular to the leaf surface. After release of tiny amounts of oil into the tissue, air – if present – could enter the tip.

Microscopy

Small fragments of leaf (2 mm^2) were fixed in 4 % glutaraldehyde dissolved in 0.1 M cacodylate buffer, pH 7.2, for 3 h at 4 °C and were post-fixed in 1 % OsO$_4$ solution for 2 h at 4 °C. Samples were dehydrated in a grade acetone series and embedded in Epon-812 (epoxy embedding medium; Sigma-Aldrich, St. Louis, MI, USA). Toluidine blue-stained semi-thin sections (0.5 μm) were viewed using a Leitz Aristoplan (Leica Mikroskopie and Systeme Gmbh, Wetzlar, Germany) light microscope.

Morphometric analysis

Forty cross-sections per group of treatments were investigated. The images were made with a digital camera (Leica DC-100, Leica Imaging Systems Ltd., Cambridge, England) and were analyzed using a Leica Q-win program. Data were statistically evaluated with the Student-Newman-Keuls test. A statistically significant difference was considered when $P \leq 0.0001$. Average data are given as mean ± standard error.

Results

Experimental

Fig. 5.1 shows part of a typical, long-term probe measurement on an olive tree subjected to several cycles of irrigation ∕ non-irrigation. About 4 days after stoppage of watering, the peak P_p values, which were reached at the end of the light phase (05:00 h), increased continuously over the following days, indicating continuous turgor pressure, P_c, loss. After some days, the increase in the peak P_p values was also accompanied by an increase of the P_p values during the dark phase. The original P_c values were obviously not restored during the dark phase, because of a water shortage. This was also

reflected in an increase in the time needed for P_c recovery in the afternoon and at night (see enlargement in Fig. 5.2A and B). The turgor pressure recovery process starting in the afternoon could be approximated by an exponential function. The time constant, τ, of the exponential decreases of the P_p values increased from 54 min (just after watering) to 256 min, when the peak P_p value reached a maximum of *ca.* 95 kPa at the end of the light phase after 7 days (see the filled squares in Fig. 5.3). The increase of τ with ongoing non-irrigation could be fitted by an exponential function characterized by a time constant of 2.6 days.
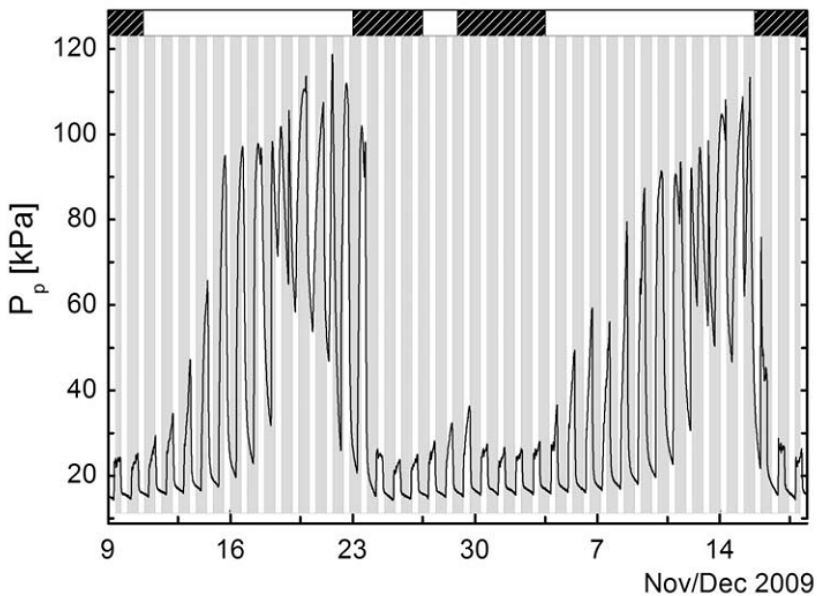
Fig. 5.1. Leaf patch clamp pressure probe measurements on a 2-m tall olive tree subjected to irrigation / non-irrigation cycles under well-defined laboratory conditions. The figure shows part of a 2-month recording of the output patch pressure, P_p. Irrigation was stopped several times (marked by white areas above the panel). Note that ongoing non-irrigation resulted in a dramatic increase of the P_p value during the dark phase and of the peak P_p value during the light phase after 4 days. Note further reversal in the diurnal P_p profiles after 7 days of non-irrigation. At this time, P_p takes maximum values during the dark phase and minimum values during the light phase. Upon irrigation, the original P_p

diurnal profiles are restored and measured again.
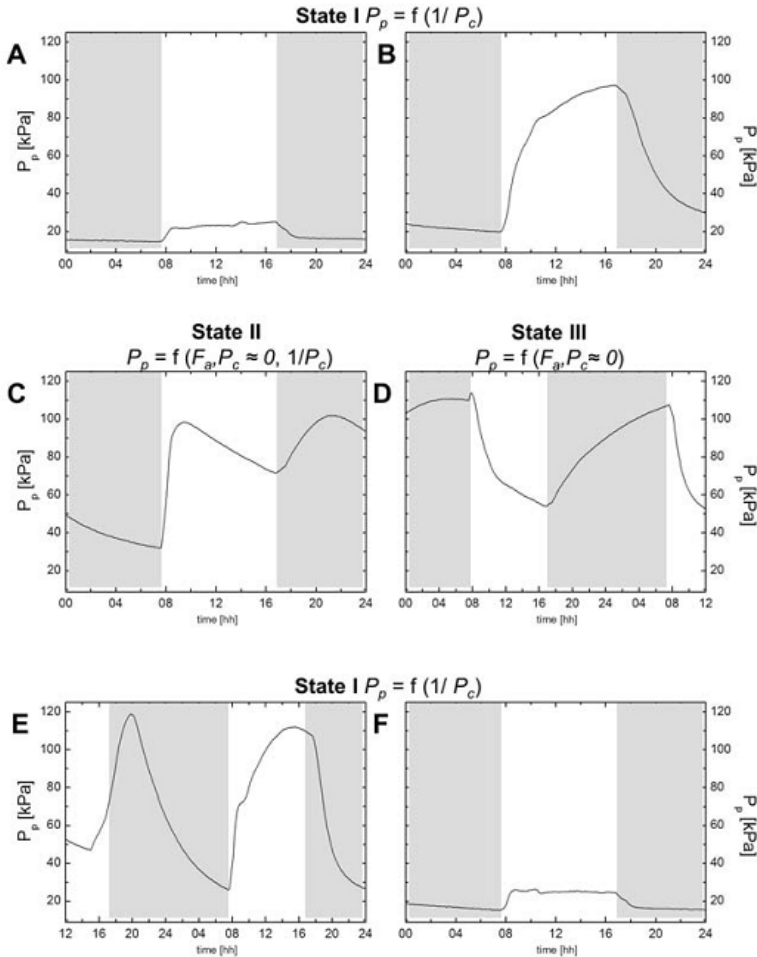
Fig. 5.2. Pressure transfer through the leaf patch under irrigation and non-irrigation conditions as predicted from Equation (5.1). *State I* (turgescent state; upper graphs): P_p is inversely coupled to P_c ($P_p = f (1 / P_c)$); the attenuation factor $F_{a,const}$ related to turgor pressure-independent structural elements (such as cuticle, cell walls and air-filled spaces) is practically constant. Thus, the magnitude of P_p peaking at noon and the night P_p values depends exclusively on P_c (A: well-watered leaf; B: leaf subjected to 4-day drought). *State II* (very low turgor pressure values; C): F_a is no longer constant because of an unfavorable ratio of air to water in the leaf. Thus, P_p becomes a linear function of $F_{a,pc\approx0}$, see Equation

(5.6), but still depends on P_c to some extent (P_p = f ($F_{a,Pc\approx0}$, 1 / P_c)). *State III* (turgor pressure values close to zero): P_p depends exclusively on F_a (P_p = f ($F_{a,Pc\approx0}$)) which assumes a minimum value during light phase (= large air spaces; maximum damping of pressure transfer) and a maximum value during dark phase (decrease of the air spaces by some water uptake and / or by a decrease in temperature: improvement of pressure transfer; D). Subsequent irrigation (arrow in E) resulted in an instant increase of the P_p values, followed by P_p decreasing during the dark phase and then by P_p peaking during the light phase (*state I*) on the following day (E). The amplitude of the P_p peaks decreased in the following 2 days, reaching the value measured under well-watered conditions (compare F with A).
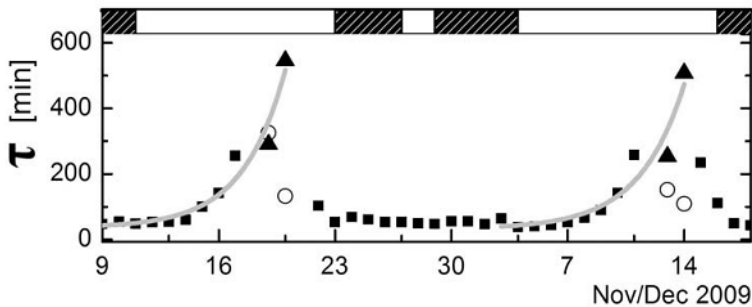
Fig. 5.3. Effects of non-irrigation / irrigation cycles on the time constant τ of the exponential P_p decrease measured in *state I* after switch off of the light (filled squares), as well as the exponential P_p decrease after switch on of the light (open circles) and the exponential P_p increase after switch off of the light measured in *state III* (for approximation of the P_p curves in *state III* by exponentials, see Fig. 5.5). Non-irrigation periods are marked as white areas above the panel. Note that upon irrigation, the original τ values of *state I* were always re-established within a few days. Note further that the filled square (*state I*) and filled triangle (*state III*) data points could by fitted with an exponential function (solid line; time constant = 2.6 day). For further explanations, see Discussion.

Cell turgor pressure probe measurements showed the well-known inverse relationship between P_p and P_c, taking into account the difficulties of P_c measurements on olive leaves. Inspection of the calibration curve in Fig.

5.4 reveals that a value of P_p = 95 kPa corresponded to a P_c value of *ca.* 50 kPa, providing evidence that the leaf cells were still turgescent. The turgor pressure range in which P_p = f (1 /P_c) holds is denoted as *state I* (Fig. 5.2).

On day 7 after stoppage of watering, the P_p profile changed dramatically (Figs. 5.1 and 5.2C). After switching on the light, the peak P_p value of 95 kPa was reached very rapidly compared to *state I* (3 h *versus* 11 h; Figs. 5.1 and 5.2) and then decreased until at the end of the light phase a minimum value was reached. In the following dark hours the P_p values increased again. A peak value was reached at midnight, then again a decrease of the P_p values was observed until the light was switched on at 07:30 h. This diurnal curve shape of the P_p values was also recorded qualitatively on the following day. Measurements on the next day showed (Fig. 5.2D) that this state was intermediate (termed *state II*), because the diurnal P_p curves overturned into a stable *state III* measured also in the following days of non-irrigation. This state was characterized by a continuous increase of the P_p values during the dark phase (non-transpiration) and a continuous decrease of the P_p values during the light phase (transpiration). Both curves could be approximated by exponential functions. The time constant, τ, in dependency of the time after reaching *state III*, are given in Fig. 5.3 for the decrease of the P_p values during the light phase and for the increase of the P_p values during the dark phase (open circles and filled triangles, respectively). It is obvious from the figure that the τ values of the dark phase in *state III* reached values of up to 600 min, whereas the τ values during the light phase were in the range measured for the τ values recorded during the turgor pressure recovery phase in *state I*. Subsequent irrigation (see Fig. 5.2E) resulted in an instant increase of the P_p values, followed by P_p decreasing during the dark phase and then peaking during the light phase on the following day. Peaking was nearly as high as observed the day before the overturning phenomena had started (compare Fig. 5.2E with 5.2B). After a further 2 days, the amplitude of the peak P_p values during the light phase was comparable to that

measured on the well-irrigated plants (Fig. 5.2F *versus* 5.2A). Similarly, the τ values decreased accordingly after re-watering and reached the original values of well-watered plants after 3 days (Fig. 5.3).
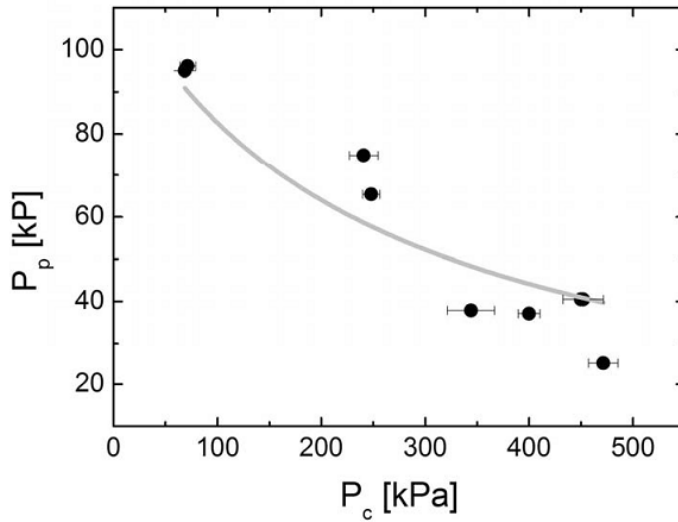
Fig. 5.4. Calibration of the leaf patch clamp pressure, P_p, measured in *state I* through short-term measurements of cell turgor pressure, P_c. Each P_c data point is an average turgor pressure value ($\pm$ SD) taken from a 2- to 5-min measurement; the corresponding P_p values represent the mean ($\pm$ SD) of at least three measuring points. Data were fitted using Equation (5.5), with $F_{a,const} = 0.29$, $P_{clamp} = 398$ kPa, $a = 1.0$, $b = 244$ kPa, $R^2 = 0.87$. The dependency of P_p on P_c was found for more than 30 cells measured on different days.

The phenomena described above were completely reversible, as shown by several irrigation/non-irrigation cycles, and were also found for different olive trees under field and laboratory conditions. It is also worthwhile to note that the reversal of the diurnal P_p curves upon severe drought could also be observed under field conditions; an example is given in Fig. 5.5. Whereas the leaves of the control trees remained in *state I* (Fig. 5.5A) over the summer period, trees that received only 60 % of the total irrigation

amount most of the time exhibited diurnal changes of P_p related to *state II* and *state III*, respectively (Fig. 5.5B).

Inspection of cross-sections of leaves subjected to severe drought, i.e. of leaves showing inverse diurnal P_p changes, had much larger areas of air spaces in the spongy mesophyll compared to well-watered leaves (0.5496 ± 0.012 μm^2 μm^{-2} *versus* 0.399 ± 0.008 μm^2 μm^{-2}; Fig. 5.6). This finding was supported by increased extraction of air from the leaves using the cell turgor pressure probe (a few microliters *versus* < 1 μl in well-watered leaves).

Changes in leaf thickness as a possible reason for the reversal of the P_p curves in response to ongoing drought could be excluded. Leaf thickness measurements on well-watered leaves showed P_p curves that were opposite to those depicted in Figs. 5.1 and 5.2. With ongoing drought, the P_p peaks decreased continuously towards their disappearance (data not shown).
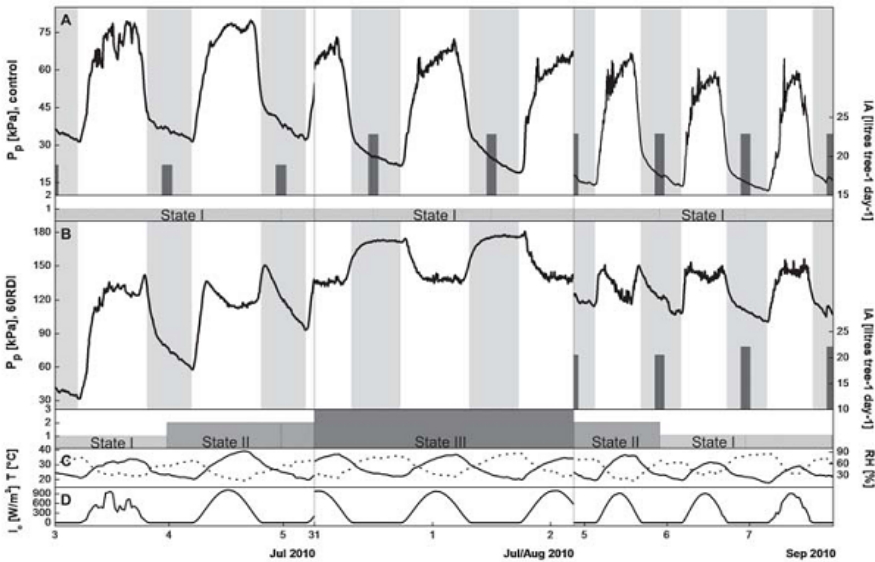
Fig. 5.5. Part of a long-term measurement of diurnal changes of P_p measured on east-oriented leaves of a control tree (A) and a 60RDI tree (B; RDI = regulated deficit irrigation) under field conditions. Irrigation amounts (IA) are denoted in grey bars; nocturnal hours are marked as grey columns. C: Ambient temperature (*T*; solid line) and

relative humidity (RH; dotted line). D: 30-min averages of solar global radiation (I_o). Note that below the curves the state of turgescence of the leaves is given: *State I* = turgor pressures > *ca.* 50 kPa (P_p peaking at noon, minimum P_p values during the night), *state II* = turgor pressures < *ca.* 50 kPa (half inverse state: second peaking in late afternoon) and *state III* = very low turgor pressures (inverse state: minimum P_p values at noon and maximum values during the night). For further details, see text.
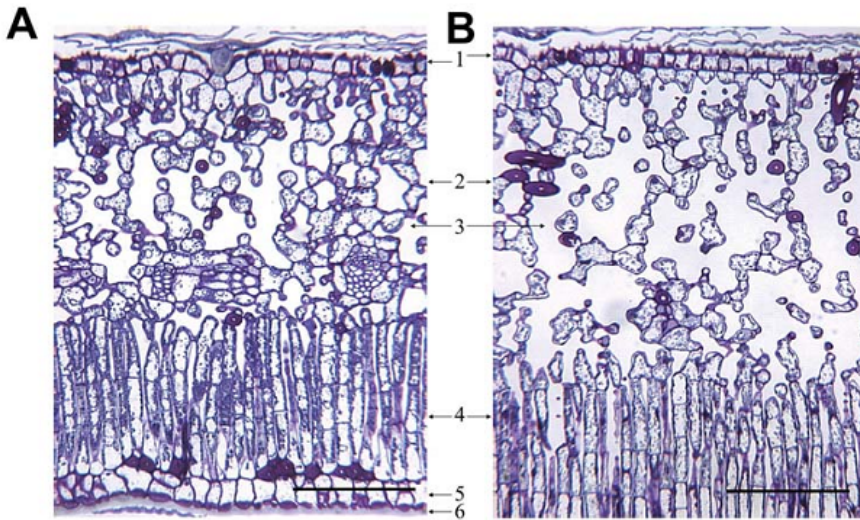
Fig. 5.6. Typical images of cross-sections of olive leaves under well-watered conditions (A; *state I*) and severe water stress (B; *state III*); bar = 100 μm. (1) Lower epidermis, (2) spongy mesophyll, (3) air space, (4) palisade mesophyll, (5) upper epidermis, (6) cuticle.

Theoretical

From a thermodynamic standpoint, the leaf patch can be considered as a black box consisting of turgescent cells and turgor-independent compressible structural elements, such as the cuticle, cell walls and air spaces. The output patch pressure P_p sensed by the sensor chip upon application of an external clamp pressure, P_{clamp}, is only determined by the

leaf transfer function, T_f (V), where V is the leaf patch volume (Zimmermann *et al.*, 2008; Westhoff *et al.*, 2009):

(5.1) $\quad P_p = T_f(V) F_{a,const} P_{clamp}$,

where $F_{a,const}$ is the leaf-specific attenuation factor that takes into account that only a fraction of P_{clamp} may arrive at the cell level due to P_c-independent pressure losses arising from the compressibility of the silicone used for the embedding of the sensor chip into the magnets and the leaf-specific structural elements.

$\quad$ T_f depends on the cellular volume of the leaf patch V, which, in turn, depends on P_c. The magnitude of volume changes upon changes in P_c is dictated by the average volumetric elastic modulus of the cells of the tissues, ε_P (Philip 1958):

(5.2) $\quad \left(\dfrac{\partial P_c}{\partial V} \right)_T = \dfrac{\varepsilon_P}{V}$.

ε_P is a function of P_c and is given by Equation (5.3) at constant temperature, T (Murphy & Ortega 1995):

(5.3) $\quad \varepsilon_p = \varepsilon_0 - (\varepsilon_0 - \varepsilon_\infty) e^{-kP_c}$,

where k is a constant, ε_0 and ε_∞ are the volumetric elastic moduli at $P_c \approx 0$ and $P_c \approx \infty$, respectively. According to Equation (5.3), ε_P reaches a plateau value for large P_c values. For smaller P_c values, i.e. $P_c < 1 / k$, ε_P can be approximated by a linear dependency on P_c:

(5.4) $\quad \varepsilon_p = aP_c + b$,

where $a = k\,(\varepsilon_\infty - \varepsilon_0)$ and $b = \varepsilon_0$. Both constants are equal or larger than unity. Combination of Equation (5.1) with Equation (5.2) and Equation (5.4) yields:

$$(5.5) \quad P_{\mathrm{p}} = \left(\frac{b}{aP_{\mathrm{c}} + b}\right)^{\frac{1}{a}} F_{\mathrm{a,const}} P_{\mathrm{clamp}}.$$

Equation (5.5) shows that P_{p} is a power function of P_{c}. This means that P_{p} increases more or less linearly with decreasing P_{c} over a large range of turgor pressures. However, at very low P_{c} (*ca.* < 100 kPa) values, P_{p} increases over-proportional with a further decrease in P_{c}, provided that the attenuation factor can still be assumed to be constant. Equation (5.5) describes *state I* quite well, as shown by fitting of the data in Fig. 5.4 using appropriate values for the elastic constants *a* and *b*. For $P_{\mathrm{c}} \approx 0$, Equation (5.5) becomes Equation (5.6):

$$(5.6) \quad P_{\mathrm{p}} = F_{\mathrm{a},P_{\mathrm{c}}\approx 0} P_{\mathrm{clamp}}.$$

In order to explain the experimental results, we have to assume that the attenuation factor in Equation (5.6), $F_{\mathrm{a},Pc\approx 0}$, is no longer constant and becomes a function of time, t, around $P_{\mathrm{c}} \approx 0$. The most likely reason for this is the diurnal variable accumulation of air in the leaf, as found experimentally (see Fig. 5.6). Thus, in the light of Equation (5.6), we are driven to the conclusion that P_{p} becomes a linear function of this parameter because there is no physical reason to assume that P_{clamp} is changing upon approaching $P_{\mathrm{c}} = 0$. *State II* (Fig. 5.2C) obviously reflects the transient pressure range below *ca.* 50 kPa, where changes in $F_{\mathrm{a},Pc\approx 0}$ start to contribute to P_{p}, thus partly compensating for the inverse effect of P_{c} on P_{p}.

Inspection of the P_{p} curves of *state III* (Fig. 5.2D) shows that the increase of P_{p} during the dark regime and the decrease of P_{p} during the light regime

can be approximated very well by assuming an exponential change of $F_{a,Pc\approx0}$ with time. The mathematical analysis yields, for the increase of P_p during the dark regime:

$$(5.7) \quad F_{a,P_c\approx0} = \left(F_{a,max} - F_{a,min}\right)\left(1 - e^{\frac{-t}{\tau_i}}\right) + F_{a,min} \, ,$$

and for the decrease of P_p during the light regime:

$$(5.8) \quad F_{a,P_c\approx0} = \left(F_{a,max} - F_{a,min}\right)\left(e^{\frac{-t}{\tau_d}}\right) + F_{a,min} \, ,$$

where $F_{a,max}$ and $F_{a,min}$ correspond to the maximum and minimum P_p values, respectively, and τ_i and τ_d are the time constants of the corresponding exponential functions. In light of the experimental results, there are some good reasons to assume that $F_{a,max}$ is equal or very similar to $F_{a,const}$.

Fig. 5.7A represents the theoretically expected change of $F_{a,Pc\approx0}$ with time using Equations (5.7) and (5.8), respectively, and Fig. 5.7B is the correlation between the P_p values and the corresponding $F_{a,Pc\approx0}$ values of Fig. 5.7A. Inspection of Fig. 5.7B shows that a linear correlation exists between these two parameters, as expected in light of Equation (5.6).
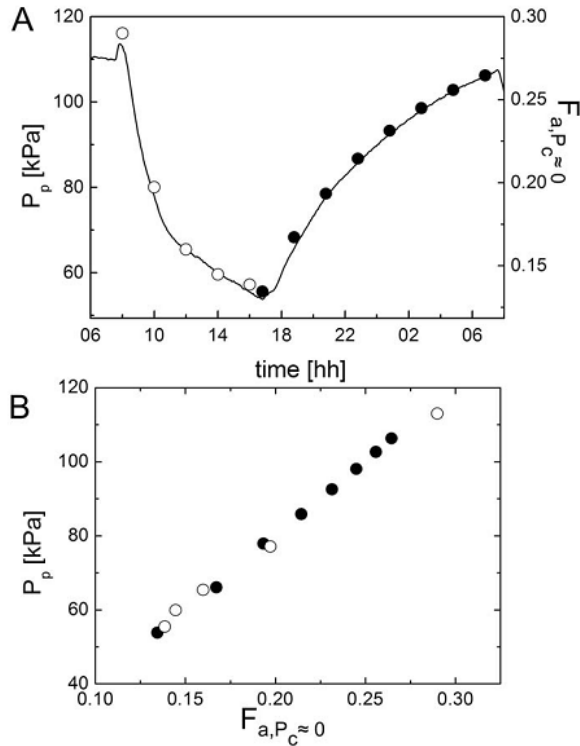
Fig. 5.7. Calculations of $F_{a,Pc\approx0}$ from P_p changes measured in *state III*. (A) Decrease of $F_{a,Pc\approx0}$ as a function of time between 07:00 h (beginning of the light phase) and 04:00 h (open circles; light phase; Equation 5.8) and increase of $F_{a,Pc\approx0}$ as a function of time between 04:30 h and 06:00 h of the following day (filled circles; dark phase; Equation 5.7). (B) Plots of the $F_{a,Pc\approx0}$ values *versus* the corresponding P_p values for the light and dark phases.

Discussion

Direct turgor pressure measurements on olive leaves using the cell turgor pressure probe have verified (Fig. 5.4) that the patch pressure P_p measured with the LPCP probe is inversely coupled to P_c over a large P_c range, as

predicted by Equation (5.5). This was also found for other plant species (see literature quoted above). In the P_c range where Equation (5.5) holds (termed *state I*; Figs. 5.1 and 5.2), P_p peaking occurs during the light phase (transpiration) and the minimum P_p values are recorded during the dark phase (non-transpiration).

We have demonstrated here for olive leaves that a reversal of the P_p curves occurred towards low turgor pressure values. The direct turgor pressure measurements have shown that the reversal of the diurnal P_p curves of olive leaves started below a turgor pressure, P_c, of about 50 kPa (*state III*). The transition from P_p peaking during the light phase (*state I*) to P_p peaking during the dark phase (*state III*) took place within 2 - 3 days (*state II*) under laboratory conditions. The reversal of the P_p curves was completely reversible after re-watering and was also found for olive trees under field conditions (Fig. 5.5).

Measurements of the pressure transfer function, and thus of P_c, require a uniform contact between the leaf patch and the pads of the magnetic probe. In the case of a non-uniform contact, mainly transpiration-induced changes in leaf thickness are recorded (Westhoff *et al.*, 2009). Leaf thickness assumes minimum values at high transpiration and *vice versa* maximum values at non-transpiration. Therefore, one possible explanation for the low-turgor pressure reversal of the P_p curves is that the probe is measuring changes in leaf thickness upon approaching $P_c \approx 0$ rather than the pressure transfer function of the leaf (Equation 5.1). However, this explanation is very unlikely. Changes in leaf thickness are only expected in response to dramatic turgor pressure changes, e.g. when P_c drops from *ca.* 500 kPa (well-watered conditions; Fig. 5.4) down to 50 - 100 kPa (water-stressed conditions; Fig. 5.4). P_c changes in a range between 50 kPa and a few kPa may be too small to affect leaf thickness (see also Burquez, 1987). Consistent with this, non-uniform clamping of the LPCP probe revealed (data not shown) that the changes in leaf thickness decreased and disappeared towards low turgor

pressures. This was also found for other plants (Amos Naor, personal communication) and is a reason why leaf thickness measurements have not found wide applications in the last two decades.

There were also no visual indications for changes in the uniform contact between the leaf and the probe upon approaching $P_c \approx 0$ that could explain the reversal of the P_p curves as outlined above. Evidence for a uniform contact even close to $P_c \approx 0$ also derived from the finding that after re-watering, P_p peaking during the light phase was re-established within 1 day (*state I*) without passing the transient *state II*. The amplitude of the P_p peaking during the light phase of the first day after watering was as high as the amplitude of P_p peaking measured just before the P_p reversal (compare Fig. 5.2E with 5.2B), indicating that there was a smooth transition from *state III* to *state I*. In the case of changes in the contact between the probe and the leaf patch, discontinuities after re-watering would be expected. More-over, in the following 2 days the P_p amplitude decreased to the original value of well-watered trees. The decrease was quite similar to that observed when re-watering started before the P_p reversal occurred. The above findings and observations are obviously only consistent with the assumption of a constantly uniform contact between the probe and the leaf over the entire turgor pressure range from 0 kPa up to the maximum P_c values of 500 kPa.

Analysis of changes in the time constants, τ, with ongoing non-irrigation depicted in Fig. 5.3 suggests that the reversal of the P_p curves is related to dramatic changes in leaf water status around $P_c \approx 0$. In *state I*, τ is the time constant of the exponential decrease of P_p after the light is switched off. This phase reflects the process of turgor pressure regeneration (e.g. Zimmermann *et al.*, 2009). As shown in Fig. 5.3, τ remains constant for about 3 days after stopping irrigation in order to increase then significantly with ongoing non-irrigation. The increase of τ can be described by an exponential function with a time constant of 2.6 days. Extrapolation of the

exponential curve of *state I* to *state III* shows (see Fig. 5.3) that the τ values of the P_p increase recorded during the dark phase (but not the τ values of the P_p decrease recorded during the light phase) can be fitted by the same function. This suggests that the P_p increase phase reflects the phase of some turgor pressure regeneration close to $P_c \approx 0$. The buildup of turgor pressure is obviously superimposed by a second, dominating process in the opposite direction.

This process is most likely initiated by the air in the leaves. Due to its high compressibility, air attenuates the pressure transfer through the leaf. Transpiring leaves will generally contain larger air spaces than non-transpiring ones (due to water uptake, and under field conditions due to lower temperatures during the night). Thus, attenuation of the external magnetic pressure will, in principle, be larger in transpiring plants than in non-transpiring ones. When the water supply of the leaves is sufficient and, in turn, the turgor pressure is quite high, the diurnal changes in the air amount in the leaves will be negligible. Thus, it is justified (and was verified experimentally) to assume that the attenuation factor, F_a, which takes – among other things – mainly pressure losses by compression of air spaces into account, is constant for a first and good approximation. However, the total amount of air within the leaf tissue is apparently increased dramatically with decreasing P_c below *ca.* 50 kPa. Support for this assumption was obtained from analysis of cross-sections through well-watered leaves and leaves subjected to severe drought. As shown in Fig. 5.6, the volume occupied by air increased considerably in leaves exhibiting inverse P_p curves (*state III*) compared to turgescent leaves (*state I*). Increased amounts of air were also found through extraction of air by using the cell turgor pressure probe.

As already mentioned above in the theoretical section, these findings and observations lead to the conclusion that the attenuation factor, F_a, can no longer be assumed to be constant at low P_c values. Since the contribution of

P_c to the P_p signals is practically negligible (see the denominator of Equation 5.5 and set $P_c = 0$), P_p becomes exclusively a linear function of $F_{a,Pc\approx0}$ when *state III* is reached (see Equation 5.6 and Fig. 5.7B). Theory and the experiments show consistently (Equations 5.7, 5.8 and Fig. 5.7A) that $F_{a,Pc\approx0}$ changes exponentially with time. $F_{a,Pc\approx0}$ reaches a maximum value (= minimum air-related losses of the external magnetic pressure) during the dark phase and a minimum value (= maximum air-related losses of the external magnetic pressure) during the light phase. The maximum $F_{a,Pc\approx0}$ value of 0.26 reached at the end of the dark phase corresponds quite well with the F_a value determined for $P_c > ca.$ 50 kPa, supporting the view that during the dark phase some turgor pressure is built up by water uptake through the roots or by water movement within the plants.

Conclusions

Taken together, the above considerations demonstrate that the turgor pressure information that can be deduced from LPCP probe measurements is not restricted to the normal turgor pressure range. Rather, the theory shows that valuable information about the water supply to the leaves can also be extracted from measurements at extremely low turgor pressures. The surprising finding that the P_p reversal phenomenon was completely reversible after re-watering suggests that the air spaces play an important role in the water supply of olive leaves under severe water stress. It is well-known (see the review article of Zimmermann *et al.*, 2004) that air spaces can create interfacial water flow (termed Marangoni streaming) through which water can still be shifted effectively to the leaf cells, even if the xylem is interrupted by gas bubbles due to cavitation. Future experiments must elucidate the proposed role of air spaces in more detail. Nevertheless, for agricultural water management, it is sufficient to point out that the P_p

reversal phenomenon can be used as a powerful indicator for determination of the water stress state of olive trees.

Chapter 6

Application of leaf patch pressure probes

to irrigation scheduling

Introduction

The global cropped area for the olive tree amounts to *ca.* 10.5 Mha, from which *ca.* 2.3 Mha are under irrigation (IOC, www.internationaloliveoil.org). Most of the irrigated olive orchards are in arid and semiarid areas, where deficit irrigation is compulsory. A common priority in these and other fruit tree orchards is to increase water productivity, i.e. the net income per unit water used (Kijne *et al.*, 2003). This can be achieved by both choosing a proper irrigation strategy and by an accurate irrigation control (Jones, 2004; Fereres & Soriano, 2007). A variety of methods for precise irrigation scheduling have been already tested. Most of these methods rely on plant-based measurements, mainly sap flow rates (Fernández *et al.*, 2008b) and trunk diameter variations (Fernández & Cuevas, 2010; Ortuño *et al.*, 2010). The potential of combining both methods to assess water stress has been evaluated for a variety of species (Steppe *et al.*, 2006; Sevanto *et al.*, 2008), including olive (Fernández *et al.*, 2011a). Other plant-based methods with a potential for scheduling irrigation are based on measurements of the water content in the stem (Nadler & Tyree, 2008; Nadler *et al.*, 2008), the plant electric potential (Gurovich & Hermosilla, 2009; Oyarce & Gurovich, 2011) and of the temperature of the leaves (Grant *et al.*, 2012). Although the findings reported in these and other publications have greatly increased our knowledge for a proper irrigation management, user-friendly indicators for irrigation scheduling based on clear thresholds have been rarely reported.

Pre-condition for optimization of current irrigation protocols of fruit trees is to understand the spatial and temporal variations in the flow-force relationships within the trees under well-watered as well as under water shortage conditions. Sap flow rates in tree stems can be reliably measured with a variety of methods (www.wgsapflow.com), provided that enough sensors and proper wound corrections are used (Fernández *et al.*, 2006b; 2008b). For fruit trees, including olive (Fernández *et al.*, 2001; 2006b), good results have been obtained with the t_z heat-pulse velocity method of Green

et al. (2003). The non-invasive leaf patch clamp pressure probe (LPCP probe or – commercial name – ZIM probe), recently introduced by Zimmermann and colleagues (Zimmermann *et al.* 2008; 2009) has been tested on olive by Ben-Gal *et al.* (2010), Fernández *et al.* (2011b) and Ehrenberger *et al.* (2012b). The leaf patch output pressure (P_p) measured by the LPCP probe is inversely correlated with the leaf turgor pressure, P_c (> *ca.* 50 kPa). Since turgor pressure is related with the leaf water potential and xylem pressure, respectively, one of the most important driving forces for sap flow can be studied over long periods of time. Multiple probe and sap flow recordings allow in principle the study of water transport over a range of scale spanning from the single leaf to the entire tree. In addition to that, comparative studies to evaluate the potential of the LPCP probe *versus* that of the pressure chamber for monitoring plant water status (Westhoff *et al.*, 2009; Rüger *et al.*, 2010a; Ben-Gal *et al.*, 2010) suggest that the LPCP probe can be used as a suitable indicator of water stress in vineyards and fruit tree orchards.

The aim of this work was to combine the t_z heat-pulse velocity method and the LPCP probe for (i) a better understanding of the daily and seasonal dynamics of water stress in olive trees under different water regimes, and (ii) for an evaluation of the potential of the P_p curves for irrigation scheduling. Measurements were made for an irrigation season, in a fully productive hedgerow 'Arbequina' olive orchard with 1667 trees ha^{-1}. Our hypothesis was that the LPCP probe has a great potential as a tool for irrigation scheduling. Furthermore, to test the potentiality of the LPCP probes for monitoring plant water status under field conditions, LPCP probe output signals and leaf water potential from the pressure chamber were concomitantly measured.

Materials and Methods

Orchard characteristics and irrigation treatments

The experiments were made in a hedgerow olive orchard located at 25 km to the west of Seville (37º 15′ N, −5º 48′ W), southwest Spain. Four year-old 'Arbequina' olive trees (2.40 m tall and 2.12 m wide) were planted in rows oriented north to south. Spacing between the trees was 1.5 m and between the rows 4 m (1667 trees ha^{-1}). Average soil textural values in the root zone (top 0.6 m) were 77.7 % sand, 2.2 % silt and 20.1 % clay. Volumetric soil water contents (θ_v) were 0.181 m^3 m^{-3} at field capacity (soil matric potential: $\Psi_m = -0.03$ MPa) and 0.089 m^3 m^{-3} at $\Psi_m = -1.5$ MPa. Standard management practices for high-density hedgerow olive orchards were applied (Rius & Lacarte, 2010). The soil was kept free of weeds by use of herbicides. Climate in the area is typically Mediterranean characterized by a mild, wet season from October to April and a hot, dry season during the rest of the year. Yearly average precipitation (*P*) and potential evapotranspiration (ET$_o$) were 535 mm and 1535 mm, respectively, for the 2002-2011 period. More details on the orchard conditions are given in Fernández *et al.* (2011b).

The irrigation season in 2010, the experimental year, lasted from May 18, day of year (DOY) 138 to November 2 (DOY 306), the harvesting day. All trees in the orchard were fully irrigated from May 18 to May 31. Two RDI treatments were established in the orchard from June 1 onwards. The 60RDI treatment was aimed at a total water supply of 60 % of the irrigation needs (IN), whereas the 30RDI treatment was aimed accordingly at 30 % of IN. Irrigation supplies were greater at the beginning of pit hardening and during the period of active oil accumulation in the fruits starting at late summer. During these two periods the olive tree is more sensitive to water stress. Water supplies were reduced at midsummer, because of the lower sensitivity of olive trees to water stress. We selected four 12 m × 16 m plots

per treatment which were distributed as a randomized block design. Each plot contained 24 border trees and 8 central trees on which the measurements were made. For reference, a Control plot was irrigated daily to replace 100% of IN. Irrigation needs were calculated as IN = $ET_c - P_e$, being ET_c the crop evapotanspiration and P_e the effective precipitation. We followed the crop coefficient approach (Allen *et al.*, 1998), i.e. $ET_c = K_c K_r ET_o$, being K_c the crop coefficient and K_r the coefficient related to the percentage of ground covered by the crop. For K_c we used the values determined by Fernández *et al.* (2006a). For K_r we used the approach of Fereres & Castel (1981). Values of ET_o were collected from a nearby standard weather station belonging to the Agroclimatic Information Network of the Junta of Andalucía. These stations use the FAO56 Penman-Monteith equation to calculate daily ET_c values. According to Orgaz & Fereres (1997), we assumed that P_e was 75 % of *P* recorded by the weather station in the orchard (see below). The irrigation system consisted of a lateral dripper line per tree row with a 2 L h^{-1} dripper every 0.5 m. A caudalimeter per irrigation sector recorded the irrigation amounts (IA) applied to each treatment. A 8N-3P-8K + 0.05 % B + 0.05 % Fe solution was injected into the irrigation system once a week throughout the irrigation season to cover the nutrient requirements.

Sap flow measurements

We used the t_z heat-pulse velocity (HPV) method of Green *et al.* (2003) to measure sap flow every 30 min in representative trees of each treatment, from June 2 (DOY 153) to November 2 (DOY 306). We used two sets of HPV probes (Tranzflo NZ Ltd., Palmerston North, New Zealand) per tree, installed on the east and west side of the stem at *ca.* 0.4 m above the soil. We instrumented one tree per plot, in three plots per RDI treatment. In the Control plot we instrumented three trees. Each set had two temperature probes located at 5 mm upstream and 10 mm downstream of a linear heater probe. Each temperature probe had four thermocouples, at 5, 12, 22 and 35

mm below the cambium. The system was controlled by a CR10X Campbell datalogger (Campbell Scientific Inc, North Logan, USA) powered by solar panels. Details on the analysis of the HPV outputs are described by Fernández *et al.* (2006b) who calibrated the method for olive trees. Sap flow rates (Q, L h^{-1}) were calculated after averaging the records from the two HPV sets of probes per tree. We assumed that the daily total Q value was equal to the daily tree water consumption (E_P, L tree^{-1} day^{-1}).

<div align="center">

The leaf patch clamp pressure probe

</div>

The principle of the magnetic leaf patch clamp pressure probe (LPCP probe) is described in detail elsewhere (Zimmerman *et al.*, 2008; 2009). Briefly, a small patch of an intact leaf is clamped between two metal pads in which two magnets are integrated. The external pressure exerted by the magnets on the leaf patch can be adjusted to the rigidity and elasticity of the leaf by using magnets of different strength or by proper adjustment of the distance between the two magnets. Leaf P_c is determined by measuring the pressure transfer function through the leaf. The attenuation of the applied external pressure and thus the output pressure signal, P_p, depends on the magnitude of the P_c which is oppositely directed to the magnetic pressure. High P_c attenuates the pressure transfer through the leaf patch and, in turn, P_p is small. By contrast, at very low P_c the attenuation of the transfer of the external pressure through the leaf tissue is less and P_p assumes large values. P_p is sensed by a pressure sensing chip integrated in one of the pads. For P_c values below *ca.* 50 kPa the magnitude of P_p is mainly determined by the proportion of intercellular air spaces in the spongy tissue of the leaf (Ehrenberger *et al.*, 2012b; see also below). The signals are sent wireless by transmitters (connected by cable with the probe) to a controller which transfers the data to a GPRS modem linked to an Internet server.

On April 26 (DOY 116) two LPCP probes in each of the trees instrumented with sap flow probes were installed. The probes were clamped on leaves of the east and of the west side of the canopy, at about 1.5 m

above ground. The clamping was made as recommended by Zimmermann *et al.* (2009) and others, i.e. soon after dawn at maximum leaf turgescence. The P_p output pressure signals were adjusted between 10 and 25 kPa by appropriate changing of the distance between the two magnets. The probes were clamped between the central nerve and the edge of the leaves in order to establish a uniform contact with the leaf tissue. The magnet containing the pressure sensor was placed on the abaxial side of the leaves. Fernández *et al.* (2011b) observed that the east side of the canopy was generally more stressed than the west side. The output pressure signals of the probes were collected every 5 min until November 2 (DOY 306). The probes and the Internet-based data transfer system were purchased from the company ZIM Plant Technology GmbH (Hennigsdorf, Germany). The system was powered by solar photovoltaic units. More details on the use of the probes in the field are given by Fernández *et al.* (2011b). Subjecting the probes to different pressure and temperature regimes under laboratory and field conditions showed that the readings of these probes were practically only affected by pressure, but not by temperature.

Other measurements

Time courses of both soil and plant water status, derived from θ_v, leaf water potential at predawn (Ψ_{pd}) and stem water potential at midday (Ψ_{stem}) measurements, are described in the Appendix III. The measurements of main meteorological variables carried out in the orchard were also described in the mentioned Appendix. Furthermore, a comparative study between P_p and Ψ_{leaf} were performed (see details in Appendix III).

Results

The effect of the irrigation treatments on atmospheric conditions and on both the soil and tree water status can be seen in Figs. 6.1 and 6.2. Basically, irrigation in the Control plot was enough to keep the soil close to field capacity conditions, all throughout the irrigation season. Consequently, the Control trees always showed low to moderate stress, depending on the atmospheric conditions. According to plant water potential or plant-based sensor signals, the 30RDI trees showed increasing water stress from DOY *ca.* 180 (June 29) to 220 (August 8). Measurements after the increase of irrigation from DOY 236 (August 24) showed a certain recovery of the trees' water stress reflected in the increase of both Ψ_{pd} and Ψ_{stem}, although full recovery was not observed prior to harvesting. Severe symptoms of water stress, such as fruit shrivelling and leaf rolling were observed on the 30RDI trees from around DOY 195 (mid July) to DOY 260 (mid September). For details on the time course of water stress on the 60RDI trees, see Fernández *et al.* (2011b).
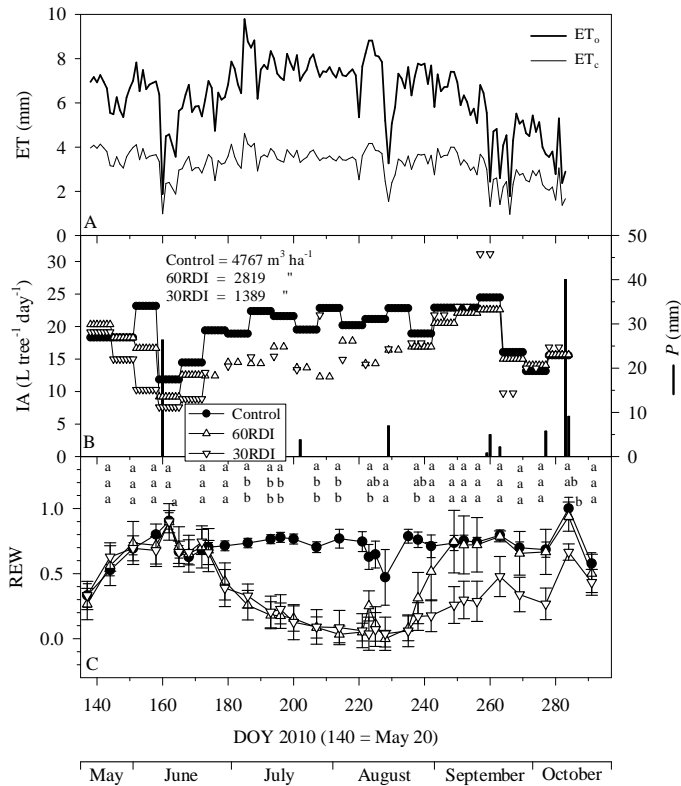
Fig. 6.1. Seasonal changes of (A) the potential (ET_o) and crop (ET_c) evapotranspiration, (B) the collected precipitation (P) and the irrigation amounts (IA) supplied during each irrigation treatment, and (C) the relative extractable water (REW) for each treatment. Vertical bars represent ± the standard error. Different letters indicate statistically significant difference ($P < 0.05$). DOY = day of year. See Fernández *et al.* (2011b) for details on the treatments and on ET_o, ET_c and REW calculations.
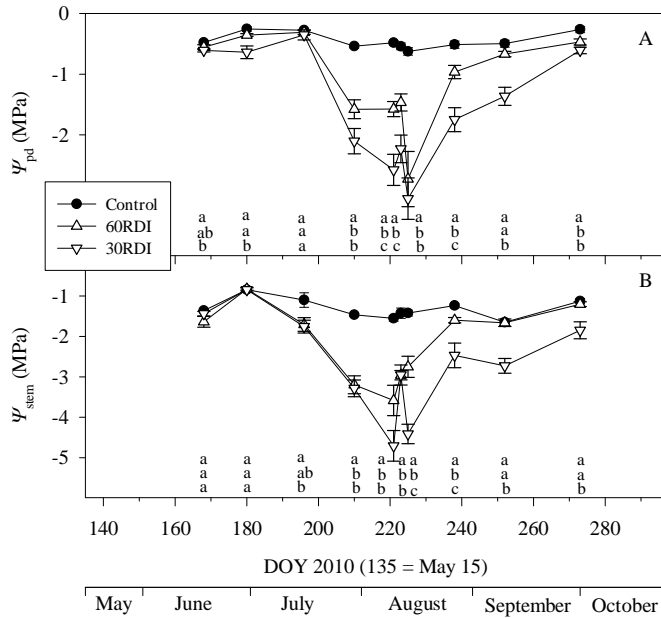
Fig. 6.2. Average values ($n = 8$) of (A) predawn leaf water potential (Ψ_{pd}) and (B) midday stem water potential (Ψ_{stem}) measured on representative trees of each treatment during the experimental period. Vertical bars represent $\pm$ the standard error. Different letters indicate statistically significant difference ($P < 0.05$). DOY = day of year.

Parts of a long-term Q and patch pressure P_p measurements on leaves of a Control tree recorded on the east side and two main driving variables for transpiration (D_a and R_s) are depicted in Fig. 6.3. The turgescent state termed *state I* according to the nomenclature of Ehrenberger *et al.* (2012b) is characterized by a reciprocal dependency of P_p on P_c. Consistent with this, upon sunrise and the onset of transpiration P_c decreased and correspondingly P_p increased up to a maximum value around noon. With progressive daytime P_c recovery occurred resulting in a decrease of P_p. During the night hours a minimum P_p value corresponding to a maximum P_c value was reached. The peak P_p values at noon and the night P_p values increased at the beginning of July and assumed these high values through

July and August. At the beginning of September the P_p values dropped down to values recorded during May (data not shown). On average, peaking of P_p occurred at 15:17 ± 2:09 h (8.6 ± 2.4 h after sunrise; CET – Central European Time) during the entire season. The seasonal changes in the P_p values were mostly induced by changes in atmospheric demand or air vapor pressure deficit (D_a) (see Fig. 6.3C and, for more details, Fernández *et al.* 2011b). On days of high D_a during midsummer the daily P_c loss increased and recovery of P_c during the night was incomplete, as shown by the P_p records (Fig. 6.3A and C, left and central graphs).
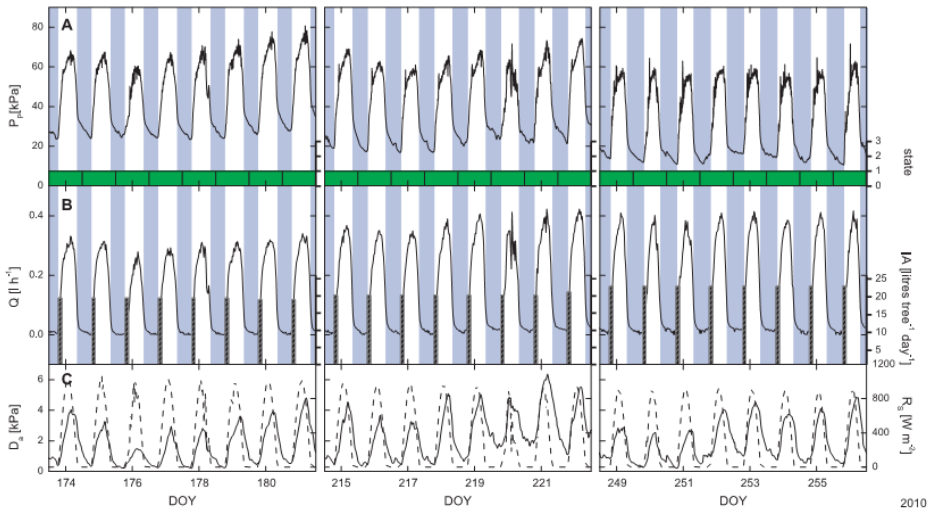
Fig. 6.3. Part of a long-term measurement of diurnal changes of the patch pressure P_p (A) and of the sap flow rate Q (B). The corresponding changes of vapour pressure deficit of the air (D_a; solid lines) and solar radiation (R_s; dashed lines) are given (C). P_p was measured on east-oriented leaves of a well-watered, Control tree. In (A) we give the state of turgescence of the leaves. The green colour indicates the turgescent *state I* (turgor pressures > *ca.* 50 kPa), at which P_p peaked at noon and showed minimum values during the night. The irrigation amounts (IA) are given by dashed bars in (B). Nocturnal hours are marked by blue columns; DOY = day of year: 174 = June 23; 215 = August 3; 249 = September 6.

As indicated in Fig. 6.3B, the diurnal pattern of Q and its dependency on D_a and R_s was comparable to that of P_p. The average peaking time of Q was at 15:04 ± 1:12 h (8.4 ± 1.5 h after sunrise). The mean of the maximum sap flow rates in the Control tree was 0.34 ± 0.06 L h^{-1} ($n = 149$).

There was usually a positive correlation between Q and P_p, i.e. an increase of Q was correlated on average with an increase of P_p and *vice versa* a decrease of P_p was generally correlated with a decrease in Q. However, it is important to note that Q peaking and P_p peaking did not always occurred at the same time. Often Q peaking occurred earlier or later than P_p peaking. The order of P_p and Q peaking did not always agree with those of D_a and R_s. This was the case for DOYs 217 (August 5) to 223 (August 11) (Fig. 6.3B, central graph), but it also occurred on DOYs 205 (July 25) to 209 (July 28) and DOYs 236 (August 24) to 245 (September 2), among other cases, when D_a was relatively high (data not shown). On those days, no relationship between the sequences of the occurrence of P_p- and Q-peaking could be found. Interestingly, the delay time between both parameters was subjected to large variations ranging from *ca.* 30 min to *ca.* 3 h. This is illustrated by the large standard deviation of the average values which were nearly identical for the case of P_p peaking preceding Q peaking (104 ± 65 min; $n = 51$) and for the case of Q peaking occurring earlier than P_p peaking (108 ± 67 min; $n = 57$). Fig. 6.4 shows a delayed peaking between Q and P_p and *vice versa* ranging from a few minutes to up to *ca.* 3 h. Fig. 6.4A represent a typical Q-P_p relationship for the case that Q peaking headed P_p peaking. The delay time between both variables was rather long (*ca.* 2 h). It is evident from Fig. 6.4A that P_p increased slightly after sunrise (06:35 h) whereas Q remained close to zero for the following *ca.* 1.5 h. Then a pronounced increase of Q was recorded. At the same time P_p increased significantly. Over the entire morning up to noon the increase of Q was linearly correlated with the increase of P_p. A linear relationship was also found for the decrease phase of Q and P_p during the afternoon independently of the time difference between peaking of the two variables. The hysteresis

between the increasing and decreasing phases was very small. Therefore, the data were pooled for calculation of the slope of the linear relationship between Q and P_p. The value of the slope was independent of the delay time between Q and P_p peaking (0.010 ± 0.000 L h^{-1} kPa^{-1}).
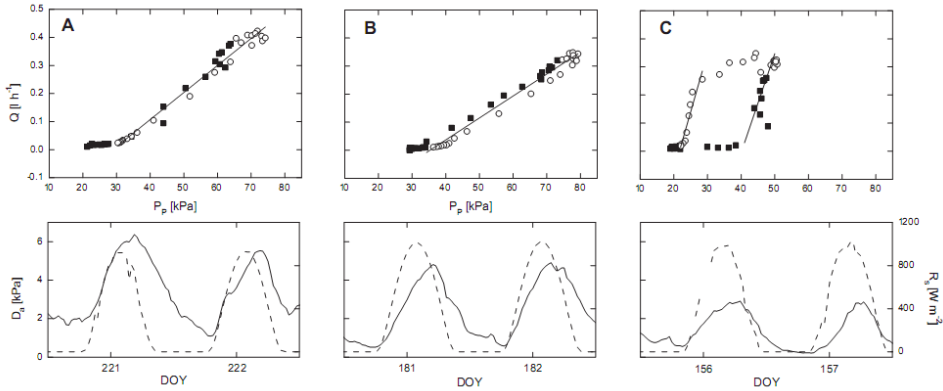
Fig. 6.4. Plots of diurnal changes of the Q values *versus* the corresponding diurnal changes of the P_p values together with vapour pressure deficit of the air (D_a; solid lines) and solar radiation (R_s; dashed lines) values recorded on the given day and the day before. Typical examples are given for Q peaking preceding P_p peaking (A) and for P_p peaking heading Q peaking (B and C). Data were measured on the same tree as in Fig. 6.3. (A) Measurements were performed on DOY 221 (August 9) and 222; the delay time between Q peaking and subsequent P_p peaking was *ca.* 2 h. (B) Measurements were performed on DOY 181 (June 30) and 182; the delay time between P_p peaking and subsequent Q peaking was *ca.* 10 min. (C) Measurements were performed on DOY 156 (June 5) and 157; the delay time between P_p peaking and subsequent Q peaking was *ca.* 2 h. Data measured after sunrise during the morning hours are denoted by squares and data measured from noon to midnight are denoted by circles.

Similar relationships between Q and P_p were found when P_p peaking occurred earlier than Q peaking, provided that the delay time between both parameters was not longer than *ca.* 30 min (Fig. 6.4B). Between sunrise and onset of sap flow P_p increased slightly and in the same order when Q was heading P_p (Fig. 6.4A). A pronounced increase of P_p together with a

significant increase of Q was observed 1.0 h to 1.5 h after sunrise. Consistent with the data in Fig. 6.4A, a linear relationship between both parameters existed during the morning and the afternoon hours. No hysteresis between the increasing and the subsequently decreasing phase of Q and P_p was observed. The value of the slope of $Q = f(P_p)$ was likewise to that measured for the case of Q heading P_p (0.008 ± 0.000 L h^{-1} kPa^{-1}). An increasing hysteresis between the morning and afternoon phase of $Q = f(P_p)$ was observed when the delay time between P_p and Q peaking increased further (Fig. 6.4C). Reason for this was obviously a strong increase of P_p between sunrise at 06:05 h and the onset of sap flow, that occurred much later (2.5 - 3.0 h) than in the case shown in Fig. 6.4A (1.5 h). With progressing time, Q increased linearly with P_p up to noon. The slope of the straight line (0.035 ± 0.013 L h^{-1} kPa^{-1}) was by a factor of *ca.* 4 larger than that measured at low delay times. By analogy to the early morning hours, after noon P_p decreased considerably whereas Q remained high (see Fig. 6.4C). The subsequent decrease of Q during afternoon was accompanied by a corresponding decrease of P_p. The slopes of the linear decreasing phases of P_p and Q were of the same order of magnitude (0.042 ± 0.010 L h^{-1} kPa^{-1}) as found for the increasing phase during the morning hours. It should be noted that these hysteresis phenomena occurred particularly during June, i.e. at the beginning of the demanding summer time.

Fig. 6.5 shows parts of long-term Q and P_p measurements on leaves of a 30RDI tree recorded on the east side. The tree was irrigated daily until DOY 173 (June 22). Then the tree was subjected to severe water stress during the following summer months, i.e. P_c dropped below *ca.* 50 kPa. From DOY 178 (June 27) to 184 (July 3) P_p curves showed *state II*, which, as detailed by (Ehrenberger *et al.*, 2012b), is characterized by half-reversal of the P_p curves, i.e. a P_p peak is recorded around noon and a second one at late afternoon (Fig. 6.5A, central graph). From DOY 185 (July 4) the diurnal P_p curves were in *state III*, i.e. fully inversed. This means that during the daytime a minimum P_p value and during the night a peak P_p value were

recorded (Fig. 6.5A, right graph). As discussed elsewhere (Ehrenberger *et al.*, 2012b) the reversal of the P_p curves upon severe water shortage is most likely due to the attenuation of the externally applied pressure by air and water vapour in the spongy mesophyll of the leaf. Under these conditions P_p is no longer a measure of P_c when being close to the plasmolytic point. In fact, *state III* is characteristic of a nearly turgorless state in the leaf. Under these conditions the attenuation of the applied external pressure is higher at noon, because of a large amount of air and water vapour accumulated in the leaf. Consequently minimum P_p values are recorded during the day. During the night the intercellular space in the mesophyll decreases due to some water uptake, which decreases the attenuation and a small increase of P_c occurs. In turn P_p increases. The *state II* and *III*, respectively, turned over into the turgescent *state I* upon watering or after rainfall (e.g. between DOY 282 (October 9) and DOY 285 (October 12), see Fernández *et al.*, 2011b).
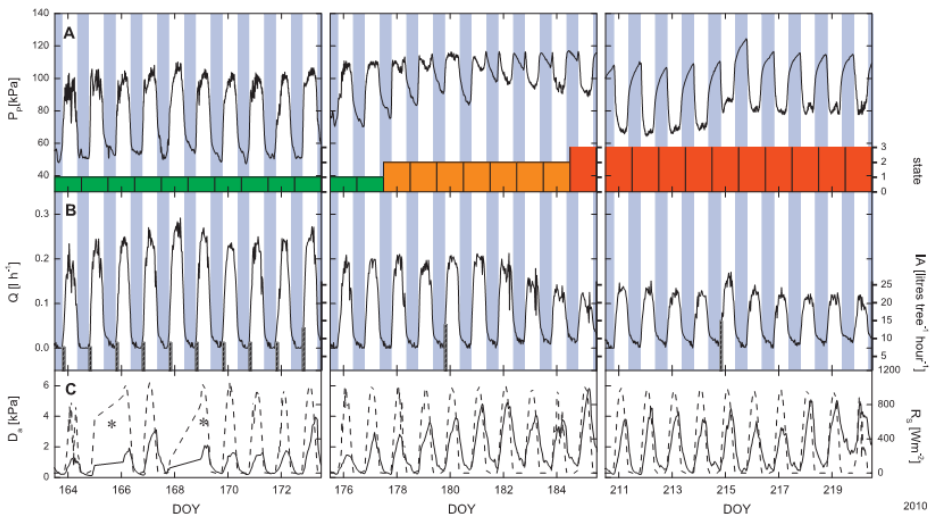
Fig. 6.5. Part of a long-term measurement of diurnal changes of the patch pressure P_p. (A) and of the sap flow rate Q (B). The corresponding changes of solar radiation (R_s; dashed lines) and vapour pressure deficit of the air (D_a; solid lines) are given (C). P_p was measured on east-oriented leaves of a 30RDI tree. In (A) we give the state of turgescence of the leaves. The green colour indicates turgescent *state I* (turgor pressures > *ca.* 50 kPa), at which

P_p peaked at noon and showed minimum values during the night; the orange colour means the half-inversed *state II* (turgor pressures < *ca.* 50 kPa), at which a second P_p peaking was observed at late afternoon; and the red colour means the inversed *state III* (turgor pressure close to zero), at which minimum P_p values were recorded at noon and maximum values during the night. The irrigation amounts (IA) are given by dashed bars in (B). Note that after a change from daily to weekly irrigation on DOY 173 a dramatic loss of P_c (< 50 kPa) occurred associated with a change of the shape of the diurnal P_p curves usually measured under turgescent conditions (*state I*; green coloured axis). After a transition state which started on DOY 178 and was characterised by half-inversed P_p curves (*state II*, orange coloured axis), completely inversed P_p curves were measured after DOY 184 (*state III*; red coloured axis). For further details, see text and Ehrenberger *et al.* (2012b). Nocturnal hours are marked by blue columns; DOY = day of year: 164 = June 13; 176 = June 25; 211 = July 30. Symbol *: lack of data transfer.

Fig. 6.5B shows the corresponding diurnal Q curves. It is obvious that under severe water stress the magnitude of Q decreased considerably. The transition of the P_p values from *state I* over *state II* into the inverted *state III* was not reflected in the Q values. Q decreased continuously without any irregularity until a nearly constant low value was reached after the leaves had entered *state III* from DOY 185 (July 4) (Fig. 6.6). On average, Q changed from 0.28 ± 0.02 L h^{-1} ($n = 9$; DOY 168 – June 17 – to 176 – June 25) to 0.09 ± 0.03 L h^{-1} ($n = 25$; DOY 185 – July 4 – to 209 – July 28). The shape of the Q curves did not change when the leaves entered the *state III*. Q peaking occurred still around noon (14:40 $\pm$ 1:30 h; 7.8 $\pm$ 1.7 h after sunrise) when the P_p values assumed minimum values, i.e. Q was negatively correlated with the P_p values. The average delay times showed also large variations and were in the same order of magnitude as found for the Control trees (Q peaking heading the P_p minimum: 120 $\pm$ 87 min, $n = 43$; P_p minimum heading Q peaking: 141 $\pm$ 85 min; $n = 22$). The delay time between Q peaking during the day and P_p peaking during the night when a small turgor pressure was built up was 474 $\pm$ 116 min indicating that P_p peaking in the night (*state III*) occurs by other mechanism than P_p peaking during the day (*state I*).
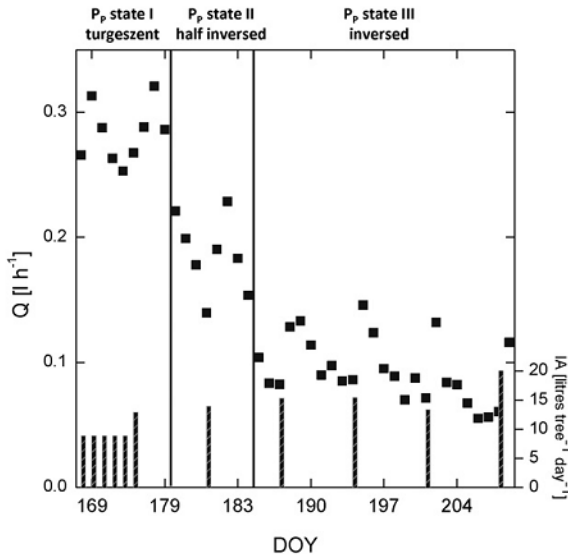
Fig. 6.6. Plot of the changes of daily maximum sap flow rates (Q) measured between DOY 168 (turgescent P_p state I) and DOY 209 (inversed P_p state III). Data were taken on a 30RDI tree. Note that Q decreased from state I to state III. Once the state III was achieved, the slope of Q vs. time decreased. DOY = day of the year: 168 = June 17; 209 = July 28; IA = irrigation amounts.

Plotting of the Q values *versus* the P_p values when the P_p curves were inverted (*state III*) yielded straight lines (Fig. 6.7) both for the case that Q peaking preceded the P_p minimum value (Fig. 6.7A) and for the case that P_p minimum value headed Q peaking (Fig. 6.7B). The slope of the lines ranged between -0.0026 and -0.0041 L h^{-1} kPa^{-1}, i.e. much lower than those found for these relationships under turgescent conditions. Furthermore, no hysteresis effects between the morning and afternoon curves were observed.

Comparable results as for the 30RDI trees were found for 60RDI trees (data not shown) even though the leaves of these trees were most of the time in *state II* during the summer season (see Fernández *et al.* 2011b).
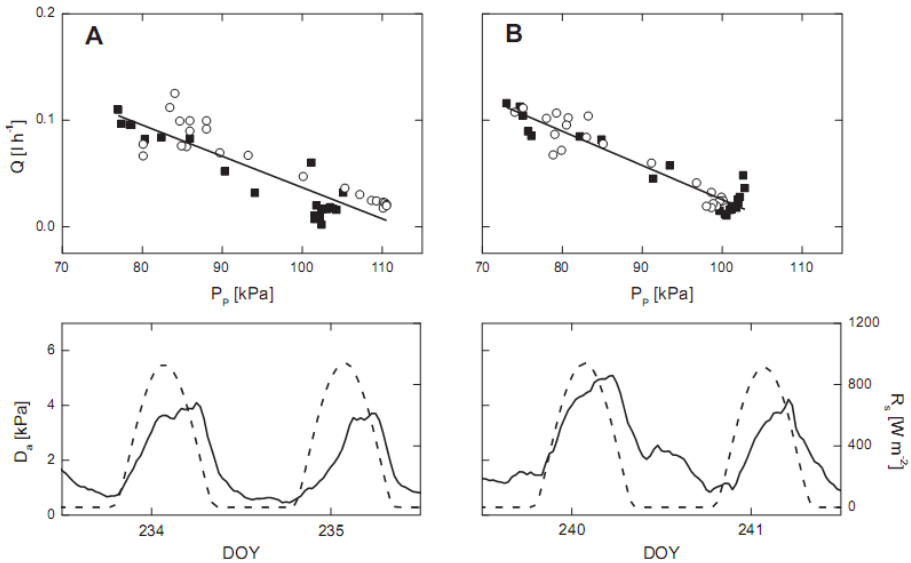
Fig. 6.7. Plots of diurnal - changes of the Q values *versus* the corresponding changes of the P_p values recorded on the 30RDI tree in Fig. 6.5 when the P_p curves became inverted (*state III*). Also shown are the vapour pressure deficit of the air (D_a; solid lines) and solar radiation (R_s; dashed lines) values measured on the given day and the day before. Typical examples are given for Q peaking preceding the P_p minimum value (A) and for P_p minimum value heading Q peaking (B). (A) Measurements were performed on DOY 234 (August 22) and 235, when Q peaking preceded the P_p minimum value with a delay time of *ca.* 3 h. (B) Measurements were performed on DOY 240 (August 28) and 241, when P_p minimum value headed Q peaking, with a delay time of *ca.* 2.5 h. Note that Q and P_p were negatively correlated with each other and that no hysteresis was observed. Values measured during the morning hours until noon, are denoted by squares, and those measured during the afternoon towards midnight are denoted by circles.

The diurnal changes of the output patch pressure (P_p) values and leaf water potential (Ψ_{leaf}) values recorded in parallel on June 23 and 24 as well as on September 9 by using the LPCP probe and the pressure chamber technique are presented in Fig. 6.8. The scatter of the Ψ_{leaf} data of the Control and RDI trees was sometimes quite high (particularly around noon). This is not surprising because the Ψ_{leaf} values reflect variations

181

between different leaves, while the P_p values reflect variations within the same leaf. Nevertheless, it is clear from Fig. 6.8 that the trend of the Ψ_{leaf} changes with progressing day was comparable with that measured for P_p. Plot of the P_p values *versus* the Ψ_{leaf} values (measured under the various irrigation treatment conditions) supports the view that there exists a linear dependency between both parameters despite the somewhat low values of the coefficient of determination which, for the P_p *versus* Ψ_{leaf} plots for the Control and 30RDI trees depicted in Fig. 6.9, ranged between 0.69 and 0.92. This can be traced back to the high sampling variability and to the sampling site (following the path of the sun). In the Control trees (Fig. 6.9A), the slope of the regression lines between the P_p *versus* the Ψ_{leaf} values of the June and the September measurements was similar. The same was observed for the 30RDI trees. In these trees, however, the Ψ_{leaf} values shifted in September to much lower values (Fig. 6.9B).
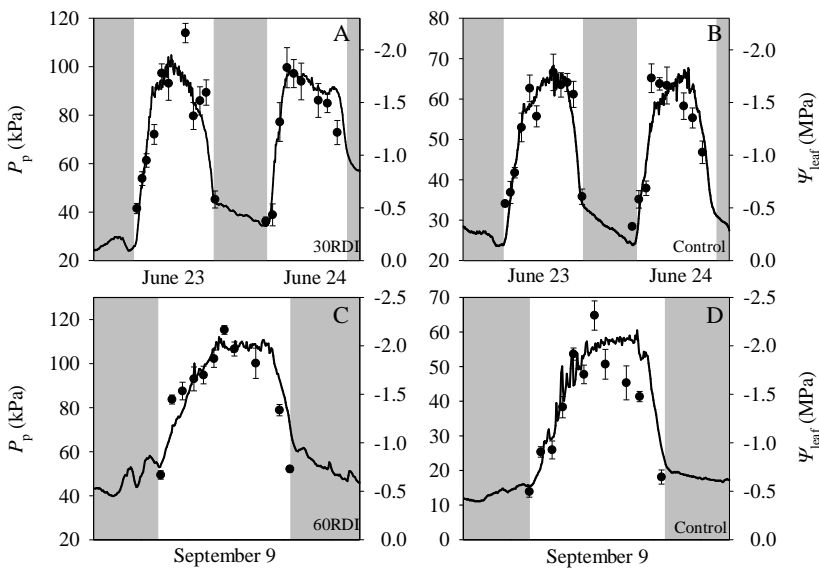
Fig. 6.8. Concomitant measurements of diurnal changes of P_p measured by a LPCP probe and of the leaf water potential Ψ_{leaf} (mean ± SE, $n = 8$) measured with a pressure chamber on representative 30RDI (A) and 60RDI (C) as well as on Control trees (B and D).

Measurements were performed before (A and B) and after (C and D) the summer months during which the highest atmospheric demands were recorded (Fig. 6.1A) and reduced irrigation amounts were applied to the RDI treatments (Fig. 6.1B). The shaded areas indicate nocturnal hours.
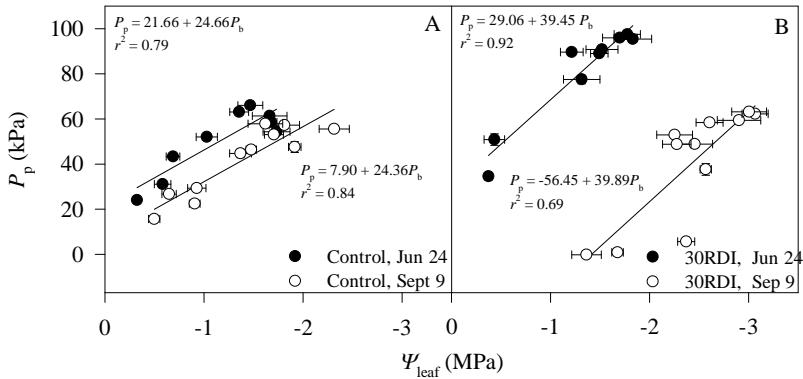
Fig. 6.9. Linear relationships between the output pressure P_p values and the leaf water potential Ψ_{leaf} values measured on Control (A) and 30RDI (B) trees on the same days as in Fig. 6.8.

Discussion

Concomitant measurements of Q and P_p on leaves of olive trees under field conditions have demonstrated that both parameters are closely correlated with each other over a wide range of P_p values, provided that the trees were well watered (Figs. 6.3 and 6.4). Even though Q and P_p peaking at noon did frequently not coincide (see below), it is clear that Q usually increased when P_p increased (for exceptions, see below). This was found for the Control trees over the entire summer period and also for the 60RDI and 30RDI trees until the end of June, i.e. before daily irrigation was stopped. Since P_p

is inversely coupled with the leaf P_c at values larger than *ca.* 50 kPa (*state I*; Ehrenberger *et al.*, 2012b) the finding of a positive correlation with Q and P_p suggests that the xylem pressure P_x and the turgor pressure P_c, respectively, in the leaves of olive trees and its changes upon transpiration dictates the magnitude of the sap flow rate.

Loss of P_c cannot be considered separated from the xylem vessels. Because of the rapid water exchange times between xylem and cells (see Zimmermann *et al.*, 2004) it can be assumed that along the xylem vessels local water equilibrium between the xylem and cell compartments exists. Therefore, the local xylem pressure P_x along the vessels must be equal to the leaf water potential Ψ_{leaf} at any height of the tree:

$$(6.1) \quad P_x = P_{c,a} - \pi_c ,$$

where $P_{c,a}$ is the average absolute hydrostatic pressure and π_c the average osmotic pressure in the tissue cells (Renner, 1915; Münch, 1930; Strugger, 1943; Hinckley *et al.*, 1978; Zimmermann *et al.*, 2004). On a daily basis the cellular osmotic pressure π_c can be assumed to be constant over the entire P_c range for a first approximation because of the large values of the volumetric elastic moduli of the tissue cells which minimize cell volume changes and of the very slow ion exchange time between the cells and the apoplast. Thus, a 1:1 relationship between P_x and P_c (= cellular hydrostatic pressure in relation to atmosphere) in the adjacent cells of the vessels is expected. This could be verified on several plant species using the xylem and cell turgor pressure probe technique (literature quoted in Zimmermann *et al.*, 2004).

Because of the tight hydraulic coupling between P_x and P_c we can, therefore, anticipate that the driving force for Q in the *ca.* 2.5 m tall, well-watered olive trees is ultimately a tension gradient generated in the xylem conduit by transpiration-induced changes in the leaf P_c. Taking the large distance between the measuring sites of sap flow and of the leaf patch clamp pressure probes into account, it seems likely that these xylem tension

gradients ranged from the roots (where the xylem pressure is obviously kept constant due to sufficient water supply) to the foliage (where negative xylem pressures are developed). This assumption implies that water lifting against gravity must occur through continuously water-filled vessels of well-watered olive trees. Under these circumstances maximum tension values of *ca.* 400 kPa at noon are expected (if water lifting in the roots against gravity is included into the considerations). Xylem tension values of this order of magnitude had been measured in many higher plants including the tropical liana *Epipremnum aureum* using the xylem pressure probe (Wistuba *et al.*, 2000; Zimmermann *et al.*, 2004). Concomitant flow-sensitive NMR imaging measurements on well watered *E. aureum* plants yielded also a linear 1:1 relationship between xylem tension and flow. However, in contrast to the finding here changes in xylem tension and flow in the several meters long liana occurred practically simultaneously upon changes in transpiration.

In the case of well-watered olive trees an increase in P_p was observed nearly instantaneously upon onset of transpiration after sunrise, whereas the onset of Q was always delayed, even when Q and P_p peaking at noon occurred more or less at the same time ($\pm$ 30 min; Fig. 6.4B). The delay time of the onset of Q after sunrise was usually *ca.* 1.5 h. The delayed occurrence of sap flow in the morning may be related to flow resistances, i.e. the xylem tension gradient has to exceed a certain threshold value in order to initiate sap flow. However, very frequently a significant increase of Q was only observed 2.5 h - 3 h after sunrise, even though significant xylem tension gradients should be built up after sunrise as suggested by the pronounced increase of P_p (see Fig. 6.4C). Later on with progressing morning, Q and P_p were linearly correlated, but the slope of the straight line was by a factor of *ca.* 4 larger than that measured when the delay time between sunrise and onset of sap flow was only *ca.* 1.5 h. On days which were characterized by vanishingly low Q values in the first 2 - 3 morning hours P_p peaking always occurred much earlier (by up to 2.5 h) than Q peaking. As a result, P_p was decreasing (i.e. P_c was increasing) in the

following 2 - 3 h after peaking due to the high Q values (Fig. 6.4C). After exceeding its maximum value at 15:04 $\pm$ 1:12 h, the subsequent decrease of Q was again linearly correlated with the decrease of P_p. The slope of the straight line was as high as during the morning hours.

These hysteresis Q/P_p phenomena, which were observed quite frequently in June, are not consistent with the assumption of long-distance xylem tension gradients and, in turn of continuously water filled vessels ranging from the roots to the leaves. Part of the effects described above could be explained by the atmospheric conditions. Thus, Fig. 6.4C shows that D_a, a main driving variable for Q, increased slowly at the early morning hours, when Q showed a great delay as compared to P_p. But Fig. 6.4C also shows P_p values over 40 kPa before significant sap flow rates were registered. Based on these results, we are driven to the conclusion that the leaves (but presumably also the branches) are partly disconnected by high resistances from the xylem conduit in the stem. The time lag observed between both variables would suggest that when plants are under water stress the role played by capacitance of storing tissues is of pivotal role in the maintenance of transpiration rates, and therefore stomatal opening. This is confirmed by the increase in the magnitude of maximum daily shrinkage of trunks reported in the trees of this orchard in other studies (Cuevas *et al.*, 2013).

Zimmermann *et al.* (2007) and Westhoff *et al.* (2009) investigated the cohesive/mobile water distribution in the xylem over the complete height of 30- to 60-m tall eucalyptus trees and 17- to 23-m tall birches using NMR imaging, jet-discharge methods for extraction of xylem sap and other techniques. These authors found that the stem and the branches were indeed interrupted by large air spaces from June onwards. The distribution of cohesive/mobile water pattern was quite inhomogeneous along the stem and the branches. The finding of these authors was consistent with the view that air resistances are bypassed (osmotic pressure-driven) through the

adjacent tissue cells and that stored water in the tissue (e.g. of the stem) is radially transported to the branches or to the leaves (Preston, 1952; Clark & Gibbs, 1957; Hinckley, *et al.* 1978; Zweifel, *et al.* 2000; 2001). Recently, by performing concomitant dendrometers and magnetic probe measurements on 1.5-m tall oak trees Ehrenberger *et al.* (2012a) have shown that the travelling time of water between stem and leaves increased by several hours upon ongoing drought suggesting the interruption of the xylem water pathways and thus of long-distance forces from the roots to the canopy.

In the light of these findings the diurnal changes of Q and P_p in Fig. 6.4C can easily be explained. In the early morning hours transpiration-induced short-distance tension gradients are built up between the reservoirs of stored water with the leaf xylem on the one hand and with the root xylem on the other hand. When the tension gradients between stem xylem and water storage reservoirs are large enough, sap flow occurs. Subsequently, when a continuous tension gradient is established between the stem and the leaves, a linear relationship between Q and P_p is observed, up to noon. Closure of the stomata results then in an increase of P_c (i.e. decreasing P_p values), but the sap flow in the stem is driven still by the tension gradients between root xylem and the water storage reservoirs for some time, before Q and P_p decrease again in parallel.

This scenario can also easily explain the frequent finding that Q peaking preceded P_p peaking at noon. We postulate that Q is driven primarily by short tension gradients existing already between stem xylem and the water storage reservoirs because of incomplete refilling during the night before. P_p increases (i.e. P_c and P_x in the leaves are decreasing) slowly depending on stomatal conductance. When the short distance tension gradients between the leaves and the water storage reservoirs exceed a certain threshold value and a continuous tension gradient between the stem and the leaves is established, a linear correlation between the P_p and Q changes is observed

up to noon. Since Q starts to decrease earlier than P_p, no hysteresis is expected to occur.

A dramatic increase in flow resistances was seen when the trees were subjected to severe water stress (Fig. 6.5). Water shortage was manifested in a reversal of the diurnal P_p curves, i.e. minimum values were recorded during the day and maximum values during the night (so-called *state III*). As briefly outlined above, this event occurs when leaf P_c is extremely small and a large amount of air and water vapour accumulated within the leaf. Close to the plasmolytic point P_p is obviously no longer a measure for turgor pressure; rather P_p is reflecting the diurnal fluctuations in the air and water vapour to water ratio of the leaf (Ehrenberger *et al.*, 2012b) thus leading to an apparent negative correlation between P_p and Q. Whereas 30RDI trees were during the summer time in *state III* (stem water potential below ca. – 1.70 MPa) at the most, half-inversed diurnal P_p curves were usually recorded on leaves of 60RDI trees (*state II*). Half-inversed P_p curves were only recorded for a few days on leaves of 30RDI trees after the stop of regular irrigation (Fig. 6.5A). The shape of the diurnal Q curves, however, was as usual (Fig. 6.5B). Q peaking still occurred during the day, when P_p assumed minimum values, i.e. both variables were negatively correlated with each other (Fig. 6.7). The delayed times between Q peaking and the minimum P_p values and *vice versa* were of the same order of magnitude as found for Q and P_p peaking in the turgescent *state I*. However, the maximum values of Q of the 30RDI trees were much smaller than under turgescent conditions. Most interestingly, the maximum Q value decreased continuously from *state I* over *state II* into *state III* (Fig. 6.6), but exhibited no irregularity. This is an important finding for setting of irrigation thresholds because a shift of the P_p curves from *state I* to *state II* or *state III* can be easily detected and monitored. The seasonal dynamics of different indices derived from Q values has been proven to have a potential to schedule irrigation in olive trees. An example is the D_{Ep} index, defined by Fernández *et al.* (2011a) as the daily difference for E_p between deficit irrigated and fully irrigated trees.

But clear thresholds for irrigation scheduling have not been derived yet from the Q values. On the other hand, Q records are still useful for irrigation scheduling even when the monitored trees are under severe water stress (Cuevas *et al.*, 2013). Our data clearly show that under severe water stress (P_c values below *ca.* 50 kPa) short-distance forces must be responsible for driving of the sap flow in the stem. At extremely low turgor pressures the water in the xylem of the leaves is most probably cavitated (Zimmermann *et al.*, 2004) and refilling of the vessels can occur only from storage water reservoirs that are linked to the stem or to the branches. Multiple sap flow measurements over the entire stem and branches together with multiple recordings of leaf patch pressure at various sites of the trees are needed to reveal the spatial and temporal dynamics of water relations of olive trees under different irrigation regimes. The most important points of such research are to quantify the storage capacity of different tissues within the tree and to quantify the amounts of water exchanged from various stores during the course of the day (Hinckley *et al.* 1978). Knowledge of this would pave the way to optimum irrigation protocols.

Changes in the P_p curves of the Control trees (in turgescent *state I* most of the time) showed that the turgor pressure during the night and the turgor pressure loss at noon were quite variable over the season because of the variable weather conditions. This detailed information on the dynamics of the daily water supply of the leaves was insufficiently reflected in the spot Ψ_{pd} and Ψ_{stem} measurements shown in Fig. 6.2, as expected. For the 30RDI trees the P_p measurements showed that the leaves of these trees were already in the half-inversed state (*state II*) on DOY 178 (June 27), when Ψ_{stem} began to decrease. The inversed *state III* was entered as early as on DOY 183 (July 2) which is consistent with the minimum Ψ_{pd} and Ψ_{stem} values registered around DOY 220 (August 8). Comparison of the data suggests that Ψ_{pd} and Ψ_{stem} values of *ca.* -0.5 MPa and *ca.* $-1.7\ \mathrm{MPa}$, respectively, are the threshold values for the olive trees. Below these values, turgor pressure

P_c is very low and compression of air-filled spaces becomes the dominant factor as mentioned above.

As for other plant species (Rüger *et al.*, 2010a), the correlation between Ψ_{leaf} and P_p could be verified here for olive trees (Fig. 6.8). Our results show that the diurnal changes of the Ψ_{leaf} values coincided with the diurnal changes in the P_p values, if the limited accuracy of the spot measurements of the balancing pressure values is taken into account. Plots of P_p *versus* Ψ_{leaf} yielded a linear correlation over the entire Ψ_{leaf} range (Fig. 6.9) regardless of the time of the year in which the measurements were performed. The slope of the regression lines at the measuring days in June and September was similar for both the control (Fig. 6.9A) and the RDI trees (Fig. 6.9B), even though the Ψ_{leaf} values were significantly lower in September than in June. In particular, in the case of the 30RDI trees, the decrease of the Ψ_{leaf} values was quite dramatic in September compared to June (Fig. 6.9B). Even though we cannot completely exclude effects of the unbalanced cell osmotic pressure on $\Psi_{leaf,}$ in the light of the considerations outlined above we are driven to the conclusion that the pressure chamber measures – like the LPCP probe –most likely relative changes in turgor pressure down to *ca.* 50 kPa. However, at turgor pressures below this value, pressure losses by compression of the large air-filled spaces become the dominant factor (i.e. the attenuation factor F_a is the relevant parameter at these low P_c values which determines the Ψ_{leaf} values). This suggests that the parameters Ψ_{leaf}, Ψ_{pd} and Ψ_{stem} reflect relative turgor pressure values or relative xylem pressure values ($\Delta\Psi = P_c - \Delta\pi$, being π the osmotic pressure; see e.g. Boyer, 1967; Koch *et al.*, 2004) and not absolute negative values of xylem pressure or absolute values of leaf water potential, as criticized by Zimmermann *et al.* (2004; 2007) and Rüger *et al.* (2010a).

The finding of a linear relationship between Ψ_{leaf} and P_p over a large range of turgor pressure values is still quite surprising. In the case of the

LPCP probe external pressure is applied to a "closed" system, i.e. to a leaf patch being in hydraulic contact to the surrounding tissue of an intact leaf. The external pressure is kept constant. Therefore, the LPCP probe measures the pressure transfer function of the leaf (Zimmermann *et al.*, 2008). By contrast, in case of the pressure chamber, increasing external pressure is applied to an "open" system consisting of an entire excised leaf. Thus, Ψ_{leaf} values must be *per se* much higher than P_p values, because large leaf areas are compressed and excessive pressure is needed for water shifting between the leaf compartments to the cut end of the leaf.

Our results might be explained from a conventional point of view based on the Cohesion-Tension theory (Holbrook & Zwieniecki, 2005; Tyree & Zimmerman, 2002). Linear correlation between Ψ_{leaf} and P_p values can be expected since changes either in volume or relative water content of leaf cells affect both Ψ and P_c. In fact, above the plasmolysis point most of the change in Ψ is due mostly to a change in P_c rather than in π (Jones, 1992). Therefore, and because P_p is highly related to P_c as Westhoff *et al.* (2009) in grapevine, and Ehrenberger *et al.* (2012b) in olive demonstrated, it is not surprising to find a high correlation between Ψ_{leaf} and P_p, as that shown in Fig. 6.9. The shift of Ψ_{leaf} to much lower values observed in September could be explained by the acclimation to drought occurring in most species of Mediterranean climate during summer (Galmes *et al.*, 2007; Serrano *et al.*, 2005). Thus, both active osmotic adjustment and increase in the bulk modulus of elasticity have been reported for olive under water stress conditions (Dichio *et al.*, 2003, 2006). Behind this response to water stress is the need of the plant to maintain high turgor pressure values, while its water potential decreases to allow for water uptake from the drying soil. The theoretical consequence of this seasonal adjustment would be the mentioned shift in the P_p *versus* Ψ_{leaf} relationship. The reason for the relationship keeping the same slope is that most of the changes in Ψ are due to changes in P_c.

The above considerations are interesting from a scientific viewpoint because they provide useful information for the ongoing debate about the magnitude of negative pressures that can exist in the xylem and are involved in long-distance water ascent. The above results suggest that the values of the xylem pressure in various plant species and trees may be much less than the values discussed in the literature on the basis of pressure chamber experiments. From a practical standpoint the use of Ψ values is still reasonable if these values are used as an indicator for setting of thresholds for irrigation. Equally P_p, which is also a relative parameter like Ψ, can be used for the selection of thresholds for irrigation.

Conclusions

When the olive trees are well watered the driving force for Q is the tension gradient generated in the xylem conduits by transpiration-induced changes in the leaf P_c. The increase in P_p was observed nearly instantaneously upon onset of transpiration after sunrise, whereas the onset of Q was delayed for *ca.* 1.5 h. This delay could be related to flow resistances, i.e. the xylem tension gradient has to exceed a certain threshold value to initiate sap flow. Q peaking during the day occurred earlier or later than P_p peaking, with a time difference of up to 3 h in both cases. At the beginning of the most demanding mid-summer period, we often observed hysteresis between the morning and afternoon phase of $Q = f(P_p)$, which usually increased when the delay time between P_p and Q increased. This hysteresis phenomena suggests that the outer parts of the canopy (leaves, shoots and perhaps branches) were partly disconnected by high resistances from the stem xylem. When the olive trees were severely stressed (P_c values below *ca.* 50 kPa or Ψ_{stem} below *ca.* −1.7 MPa), our data suggests that incomplete refilling occurs during the night and that the water in the xylem vessels of the leaves

is probably mostly cavitated. Under these conditions, refilling of the vessels would occur mostly from storage water reservoirs linked to the stem or to the branches. As stress progressed during the season, Q decreased continuously until a nearly constant low value was reached after the leaves entered *state III* (P_c < *ca.* 50 kPa). The shape of the P_p curves, however, clearly marked the leaves entering *state II* and *state III*, which can be considered as clear thresholds for irrigation scheduling. On the other hand, Q values have still a potential for irrigation scheduling when the trees are under severe water stress, while the P_p curves are inverted. Concomitant measurements of P_p values and Ψ_{leaf} values showed that the LPCP probe is an advantageous alternative to the pressure chamber for monitoring plant water status. Therefore, the automatic LPCP probe technology has a potential for improving irrigation management and for designing more rational irrigation strategies.

Chapter 7

General discussion

and

General conclussions

General discussion

Nowadays, optimization of irrigation strategies and techniques is an important issue that modern and precision agriculture has to deal with. The main objective of these strategies is to increment the crop water use efficiency and saving water. This cultural practice will become more and more compulsory in the near future since competition with other consumers of water resources is always increasing. In addition to this, predictions of the climate change (IPCC, 2013) and the continuous growth of human population are not favorable either. The limited water availability is exacerbated in arid and semi-arid areas, usually predominant in Mediterranean regions. Thus, regulated deficit irrigation (RDI) and precise irrigation scheduling in these areas become unavoidable for fruit tree orchards under drought conditions. To develop the best way to apply irrigation with saving water but without penalizing yield, two main factors have to be enhanced: (i) a better understanding of the physiological processes that occur during the life cycle of the cultivated plant species and (ii) reliable and sensitive plant indicators capable of continuously and automatically monitoring water stress in the field for long periods of time. This last Chapter tries to emphasize future research lines and opportunities on the view of the results obtained in this Thesis by using different methods to connect the emerging plant physiological knowledge with reliable plant sensors to monitor water stress. In the present Thesis, both process-based models and plant-based sensors have been used for improving our knowledge on the above factors (i) and (ii), and some conclusions can be highlighted from the studies carried out. Firstly, process-based models, focused on stomatal functioning in the present work, are a good option to improve our knowledge in the plant physiological mechanisms involved in the response to drought and environmental variables. Furthermore, their use allows the integration of the numerous processes implicated in those responses in a way that cannot be achieved experimentally. And secondly, plant-based sensors, in this study sap flow or leaf turgor pressure-related

probes, have been proven as potential tools for irrigation scheduling purposes since they integrate the response of soil and atmospheric effects on different scales of plant behavior. Still, different aspects are challenging in both approaches resulting in new horizons for future investigations. The use of plant-based sensors on their own has the difficulty of interpreting the output signals and relating them to specific physiological processes, since several and complex mechanisms are taking place and interacting in the plant response to water stress. Most of the effort has been put in testing several automatic plant-based sensors, like sap flow (Fernández *et al.*, 2001, 2008b; Intrigliolo & Castel, 2006a; Ortuño *et al.*, 2006; Conejero *et al.*, 2007), dendrometers (Fernández & Cuevas, 2010; Ortuño *et al.*, 2010; Intrigliolo & Castel, 2006b), infrared thermometry (Jones, 1999, 2002), etc., and in searching for thresholds and baselines which can be used for irrigation scheduling. Therefore, the focus has been oriented towards the question 'when' to irrigate. However, less attention has been paid to the regulatory mechanisms involved in the response observed in these plant-based sensors, or in other words in the 'why'. Thus, the unique use of those sensors helps to reflect different plant behaviors but, does not respond to the question of why these behaviors are achieved. Still, more profound analyses are needed to understand the mechanisms underlying the plant-based sensors functioning under different environmental conditions and water stress. On the other hand, process-based models are potent and integrating tools which, once calibrated, are able to predict the behavior of plants to any current and foreseen conditions from environmental variables. However, as we have seen in the preceding chapters, we still lack of knowledge to apply them for long periods of time. Seasonal or daily changes of the physiological parameters obtained from those mechanistic models cannot be only explained with simulation approaches since their fluctuations depend on many factors. Therefore, I suggest, in the light of the results obtained in this Thesis, the combined use of both plant mechanistic models and plant sensors are rising as a potential tool for irrigation scheduling in fruit tree orchards aiming to optimal water use efficiency. Hence, this novel

combined method would have a great potential for monitoring water stress in those orchards due to (i) models would predict which physiological parameters would play a more important role in the plant response to water stress in different situations and (ii) plant sensors would help us to comprehend how those parameters are varying according to the phenological period of the crop, the species or the diurnal environmental changes. Indeed, this is one of the research line in which our Irrigation and Crop Ecophysiology group in the IRNAS (CSIC) is currently involved, specially focused on the application on commercial orchards under regulated deficit irrigation.

The use of mechanistic models for a sustainable water management in fruit tree orchards considers altogether the plant responses to water stress and may help to elucidate the dynamic and physiological significance of plant-based sensors. In other ecophysiological studies, like those in forest species, the use of those models has been successfully applied to explain the adaptation mechanisms of different species to their environment (Sperry *et al.*, 2002), the physiology of the stomatal functioning (Buckley *et al.*, 2003) and the interaction mechanisms between the xylem and the phloem related to trunk diameter variation measurements (Steppe *et al.*, 2006). However, there are few attempts to apply these approaches in agricultural studies. In Chapter 2 the process-based models of Sperry *et al.* (1998, SACC model) and Buckley *et al.* (2003, BMF model) were assessed in a hedgerow olive tree orchard under regulated deficit irrigation. The results of that work are promising for understanding and interpreting the effects of deficit irrigation on the hydraulic limits imposed by both the soil and the plant, and on the mechanisms of the control of stomata. The SACC model was able to interpret the response in transpiration observed in our experimental site, which has a particular behavior induced by the shallow and sandy rhizosphere. The model was used further to simulate the optimal leaf area (controlled by pruning) and numbers of drippers (influencing the volume of wet rhizosphere) necessary to maintain the stomatal conductance at a given

level. Furthermore, seasonal patterns of the physiological parameters obtained – namely osmotic pressure, plant hydraulic resistance and sensitivity of guard cells to changes in turgor pressure – helped us to suggest long-term events occurred in the trees. To gain further insight into the regulation of stomatal conductance under drought, the Buckley *et al.* (2003, BMF) model was used in Chapter 3 to separate the role of hydraulic and non-hydraulic limitations. This novel approach informed us about the contribution of both factors in a more integrative way, leading to suggest daily patterns of those limitations. These seasonal and daily patterns help to generate new hypotheses about the dynamics of long and short-term hydraulic and biochemical signals. For example, the parameter $\chi\beta$, whose significance seems to be related with the effect of hormonal signals on stomatal behavior, like ABA (Buckley, 2005), was not exclusively regulated by changes in soil moisture (and hence, by ABA from droughted roots) since both water-stressed and well-irrigated olive trees presented similar evolutions during the season (Chapter 2). These results are in concert with studies about the closely effect of ABA synthesized in leaves, rather than in roots, on maintaining plant water status under changes in water availability (Holbrook *et al.*, 2002; Christmann *et al.*, 2005; Bauer *et al.*, 2013; Christmann *et al.*, 2013). Therefore, this suggestion opens the doors to continue investigating on the mechanisms which triggered the stomatal response to drought. Although isohydric behavior observed in almond (Chapter 3) was mainly explained by the decline in plant hydraulic conductance, the role of the increase in leaf ABA concentrations was hypothesized as a mediator affected, at least in part, the decline in hydraulic conductance. In fact, this hypothesis was demonstrated by Pantin *et al.* (2012) through a mechanism by modulating aquaporin activity. Moreover, the stomatal limitation analyses computed on that Chapter showed that non-hydraulic factors exerted little control over g_s during the middle of the day. Together, these results suggest the necessity of not only identifying the signaling pathways of ABA effects on stomatal control and their links with

hydraulic factors, but also studying their daily dynamics under different environmental and drought conditions.

A number of studies that explored the physiological responses of plants to drought identified plant hydraulics as one of the principal governors of gas exchange under water stress (Sperry, 2000; Meinzer, 2002; Brodribb & Cochard, 2009). The modeled seasonal pattern of plant hydraulics presented in Chapter 2 not only reflected the importance of increasing plant hydraulic resistance to deal with water stress of olive trees in a hedgerow orchard with a specific soil, but also pointed out that the equilibrium between leaf and root areas was critical to explain the results obtained. Although not studied in this Thesis, leaf hydraulic conductance seems to be a good candidate in future researches due to its dynamism. The relevance of plant hydraulics was also reflected in the study made in almond in Chapter 3 (see above). Although it was not the main goal of Chapter 4, the combined use of the BMF model and leaf turgor pressure-related probes in olive under different microenvironments (sun and shade) raised new insights into the regulation of hydraulic conductance and osmotic pressure. Both variables emerged as highly dynamic at the seasonal and diurnal scales suggesting an important role in the regulation of stomatal conductance, and hence transpiration and water status, of leaves under drought conditions. These results highlight the importance of considering those dynamical behaviors on mechanistic models of water use to adequately interpret the effects of drought. More complex and detailed models are needed to translate hypothesized mechanisms into testable predictions. Thus, other challenges in the quest to decipher the stomatal response to different factors are (i) to identify the mechanism for the red light effect and its connection to the CO_2 response and to photosynthesis, likely mediated by ABA (ii) to incorporate a mechanistic description of the blue light response and (iii) to disentangle the mechanism by which the decoupling of guard cell turgor from epidermal turgor in the response to humidity is achieved passively or if it requires active transport of solutes (Buckley & Mott, 2013). A detailed analysis about

future developments on stomatal modeling can be found in Damour *et al.* (2010).

Finally, the combination of the BMF model with the sap flow and water storage model of Steppe *et al.* (2006) and with the photosynthetic model of Farquhar *et al.* (1980) is a potential tool to evaluate the impact of changes in RDI strategies on crop transpiration and photosynthesis of fruit tree orchards. This modeling approach links basic physiological knowledge with plant-based sensors and it can be used to explore their physiological meaning as well as their long and short-term evolutions. In this context, the plant-based sensor presented in Chapter 4 (leaf turgor pressure-related probe) was compared with the turgor pressure output simulated with the BMF model, leading to a method of great value to understand the mechanisms involved in the regulation of leaf gas exchange and leaf water status under drought conditions. Chapters 5 and 6 are focused on the field applicability of this leaf turgor pressure-related probe whose potential for monitoring plant water status has been proved for a number of species (Westhoff *et al.*, 2009; Rüger *et al.*, 2010a; Fernández *et al.*, 2011b; Lee *et al.*, 2012; Bramley *et al.*, 2013). Although there are relevant indicators for irrigation scheduling resulted from the dynamics of these probe outputs, more experiments are still needed to elucidate the connection between those dynamic signals and their physiological bases. For example, detailed studies where leaf gas exchange, leaf hydraulic conductance, leaf osmotic pressure and other ecophysiological variables are measured concomitantly with leaf turgor pressure-related probe outputs might shed significant light on the physiological meaning of the probe output reversal phenomenon. Since this reversal signal output seems to be related to the increase of the intercellular air spaces in the leaf, cavitation into the leaf xylem vessels and turgor loss point events might be correlated with that phenomenon.

To sum up all this section, the simultaneous application of both process-based models and plant-based sensors in precision agriculture to increase

water use efficiency appears as a potential method for both irrigation scheduling and scientific research. A general conclusion that might describe the present investigation, and probably all the research in all sort of sciences, is a quote by Albert Einstein I always like to mention:

'The more we learn, the more we realize how much we don't know'.

Conclusiones generales

Las conclusiones generales que derivan de la presente Tesis son:

∴ El uso del modelo de las limitaciones hidráulicas al transporte de agua (el modelo SACC) nos llevó a identificar que la rizosfera de los árboles de nuestra parcela experimental, confinada al bulbo húmedo del suelo determinado por los goteros del sistema de riego, fue el principal factor limitante del uso del agua por estos olivos a medida que el suelo se secaba. El modelo mostró que esta limitación estuvo relacionada con el ratio entre las raíces el área foliar de los árboles y con el tipo de suelo de la zona de estudio. Manejos agrícolas, como la poda o el cambio del número de goteros, pueden ser usados para controlar ese ratio de una forma racional. La potencialidad del modelo radica en que puede ser utilizado para el manejo de cultivos de árboles frutales bajo diferentes condiciones de riego y suelo.

∴ La conductancia de la copa, derivada de medidas de flujo de savia, fue satisfactoriamente simulada por el modelo de conductancia estomática utilizado (el modelo BMF) en una gran variedad de días a lo largo del verano, y tanto en árboles bien regados como en árboles bajo riego deficitario. El ajuste osmótico fue similar en ambos tratamientos de riego, a pesar de las diferencias encontradas en el potencial hídrico de las hojas. El estrés hídrico afectó de una manera importante a la hidráulica de árboles bajo riego deficitario controlado. El potencial papel de señales reguladoras, diferentes a las puramente hidráulicas, fue evidente en ambos tratamientos, aunque nuestros datos sugieren que estas señales no estuvieron reguladas sólo por el estado hídrico del suelo.

∴ El desarrollo novel de un análisis cuantitativo de limitaciones del control estomático basado en el modelo BMF durante esta Tesis en

plantas de almendro permitió identificar que tanto señales hidráulicas como no hidráulicas estuvieron involucradas en el comportamiento isohídrico observado durante el estrés hídrico en suelo. Sin embargo, la caída de la conductancia estomática fue principalmente atribuible al descenso en la conductancia hidráulica y al efecto directo de la reducción en el estado hídrico del suelo, mientras que el parámetro del modelo que representa la señalización bioquímica en sequía explicó sólo el 7 % del cierre estomático. Además, el control de la conductancia estomática por factores no-hidráulicos se redujo bajo condiciones de luz saturante y alta demanda evaporativa al mediodía. Este novedoso abordaje del análisis de las limitaciones proporciona nuevas revelaciones no disponibles hasta la fecha debido al uso habitual de modelos que usan hipótesis mutuamente excluyentes.

∴ Las medidas con sondas relacionadas con la presión de turgencia en hojas (sondas LPCP) testadas en olivos se relacionó bien con la presión de turgencia derivada a partir del modelo BMF, confirmando su potencial para el seguimiento automático del estrés hídrico en condiciones de campo.

∴ El uso combinado del modelo BMF y las sondas LPCP permitió descubrir nuevos indicios sobre las evoluciones estacionales y diarias del potencial osmótico y la conductancia hidráulica. Estas variables demostraron ser muy dinámicas, y por lo tanto, la consideración de este dinamismo en la regulación de la conductancia estomática en condiciones de sequía es de gran importancia.

∴ El potencial de las sondas relacionadas con la presión de turgencia foliar (sondas LPCP) para monitorizar el estado hídrico de plantas de olivo bajo condiciones de laboratorio fue demostrado relacionando sus señales de salida con medidas reales a partir de sondas de potencial de

turgencia celular. Estos experimentos mostraron una curva diaria invertida cuando la presión de turgencia de la hoja caía por debajo de aproximadamente 50 kPa (estrés hídrico severo). Tras la reanudación del riego las curvas diarias originales se reestablecieron en 2-3 días. Las señales de salida de las sondas de olivos en el campo mostraron comportamientos de inversión similares durante la sequía, a pesar de las fluctuaciones en el microclima. Por tanto, la tecnología de las sondas automáticas LPCP se presenta con gran potencial para mejorar el manejo de riego y diseñar estrategias de riego más sostenibles.

∴ La explicación teórica para la inversión de las curvas observada en las hojas de olivo para valores de presión de turgencia de la hoja cercanos a cero es que se da un incremento de la proporción de aire y agua en los espacios intercelulares de la hoja.

∴ Por tanto, se evaluó la aplicabilidad agronómica de las sondas LPCP en un olivar en seto. La combinación de estas sondas con medidas de flujo de savia mostró que los cambios en la forma de las curvas obtenidas con las sondas LPCP se detectaron y monitorizaron de forma más sensible que los cambios de magnitud en la velocidad de flujo de savia. Para el ajuste de los umbrales de riego el hallazgo de estos cambios de la forma de la curva de salida durante estrés hídrico parece un indicador útil. Sin embargo, los valores de velocidad de flujo de savia siguen presentando potencial para la programación de riego cuando los árboles están bajo estrés hídrico severo, cuando las curvas relacionadas con la presión de turgencia de la hoja están invertidas.

∴ La combinación de estos dos sensores basados en medidas en plantas nos llevó a sugerir que tensiones de corto rango en el sistema vascular fueron los responsables de la elevación del agua por la planta y que la toma de agua a partir de los reservorios de la planta debe jugar un papel

importante en el abastecimiento de agua a las hojas. A medida que el estrés hídrico progresaba, las relaciones entre estos comportamientos y las señales obtenidas a partir de estos sensores fue cambiando. Estos resultados podrían ser importantes para cuantificar el papel de los reservorios de agua de la planta en la reorganización de los distintos elementos hidráulicos de la planta.

∴ Medidas simultáneas de valores de salida de las sondas LPCP y valores de potencial hídrico de hojas cercanas mostraron que la sonda LPCP es una ventajosa alternativa a la cámara de presión para monitorizar el estado hídrico de la planta. Sin embargo, esta relación no es constante en el tiempo y parece ser modulada por el ajuste osmótico realizado por las plantas.

General conclusions

The following general conclusions can be drawn from the present Thesis:

∴ The use of the model of hydraulic limitation of water transport (the SACC model) identified that the rhizosphere in the trees of our experimental farm, confined to the wet soil volume determined by the drippers, was the main limitation factor in the water use by these olive trees as soil dries. The model showed that this limitation was related to the root to leaf area ratio and to the very coarse soil of the study location. Canopy pruning or changing the number of drippers can be managed to control this ratio in a rational way. Potentially, the model can be used to manage fruit tree orchards of a single species growing under different soil and irrigation conditions.

∴ Actual canopy conductance, derived from sap flow measurements, was satisfactorily simulated by the model of stomatal conductance (the BMF model) on several dates through the summer, both in well-watered and water stressed trees. Osmotic adjustment occurred similarly in both irrigation treatments, despite differences found on leaf water potential. Water stress largely affected plant hydraulic conductivity of regulated deficit irrigated trees. A potential involvement of regulating signals, other than purely hydraulics, was evident in both treatments, although our data suggests that these signals were not regulated by the soil water status only.

∴ The novel model-based integrative approach developed for analyzing the limitations to stomatal control in almond plants suggested that both hydraulic and non-hydraulic influences were involved in the isohydric behaviour observed during soil drought. However, the decline in stomatal conductance was mainly attributable to the decline in hydraulic conductance and to the direct effect of reduced soil water status, whereas the model parameter that represents biochemical drought signalling explained only 7 % of that stomatal closure. Moreover, the control of stomatal conductance by non-hydraulic factors was reduced under saturating light and high evaporative demand at mid-day. This novel approach provides insights not available from an approach based on testing mutually exclusive alternative hypotheses.

∴ The leaf turgor pressure-related (leaf patch clamp pressure or LPCP) probe tested in olive trees was in good agreement with the leaf turgor pressure derived from the BMF model, confirming its potential for automatically monitoring leaf water status under field conditions.

∴ The use of both the BMF model and the LPCP probe raised new insights into the seasonal and daily evolutions of leaf osmotic pressure and hydraulic conductance. These variables emerged as highly dynamic and hence, their consideration into the regulation of stomatal conductance under drought conditions is of importance.

∴ The potentiality of LPCP probes to monitor plant water status was proved in olive plants under laboratory conditions relating their outputs to actual cell turgor pressure probe measurements. These experiments showed an inverted daily curve when leaf turgor pressure dropped below *ca.* 50 kPa (severe water stress). Upon watering, the original diurnal curves were reestablished within 2 - 3 days. Probe output signals from olive trees in the field showed similar reversal behaviors upon drought, despite pronounced fluctuations in microclimate. Therefore, the automatic LPCP probe technology has a potential for improving irrigation management and for designing more rational irrigation strategies.

∴ The theoretical explanation for the reversal curves observed in olive leaves close to zero leaf turgor pressure is due to an unfavorable air to water ratio in the intercellular leaf spaces.

∴ Then, the agronomical applicability of the LPCP probes was assessed in a hedgerow olive tree orchard. The combination of these probes with sap flow measurements showed that the shape changes in the LPCP output curves were detected and monitored more sensitively than changes in the magnitude of sap flow rates. For setting of irrigation thresholds the finding of these shape changes upon severe water stress seems to be a useful indicator. Nevertheless, sap flow rate values have still a potential for irrigation scheduling when the trees are

under severe water stress, while the leaf turgor pressure-related output curves are inverted.

∴ The combination of these two plant-based sensors led to suggest that short-range tension forces are responsible for water lifting in olive trees and that water uptake from water storage reservoirs must play an important role in the supply of the leaves with water. As water stress progressed, the relationships between these behaviors and the sensor outputs changed. This finding might be important to quantify the role of the water reservoirs in the rearrangement of the whole tree hydraulic elements.

∴ Concomitant measurements of LPCP output values and leaf water potential values showed that the LPCP probe is an advantageous alternative to the pressure chamber for monitoring plant water status. However, the correlation between leaf water potential and LPCP is not constant over time and it is modulated by osmotic adjustment.

Agradecimientos ~ Acknowledgements

Toda historia tiene un principio. Muchos de los que hayan empezado a leer este último apartado y me conozcan, pensarán: '*Ya estamos con las frasecitas…*'. Esta Tesis ha sido el resultado de innumerables acontecimientos que han ocurrido en mi vida durante estos últimos cuatro (mejor dicho, seis) años de andadura por el mundo de la investigación científica. Aunque el inglés ha sido el idioma en el que todas las secciones anteriores han sido escritas, me gustaría otorgarme el placer de escribir esta parte en español. Su importancia, al menos para mí, así lo merece. Resulta verdaderamente difícil agradecer con palabras todo el apoyo, ayuda y buenos momentos que tanta gente con la que me he ido encontrando me ha brindado. Me disculpo de antemano si me olvido de alguien. Haré un último gran esfuerzo para que esto no ocurra. Aunque también ha habido momentos no tan buenos y, por qué no decirlo, malos, considero que en la combinación de todos en su justa medida está la clave para encontrar el equilibrio personal.

Quiero comenzar agradeciendo a los ecólogos con los que empecé de 'pequeña' a entrenarme en el método científico. Gracias Sara, por esos preciosos viajes a la Flecha de El Rompido. Disfruté muchísimo de todos esos preciosos paisajes, que gracias a tu compañía hicieron de las salidas al campo un gran goce. Igualmente doy las gracias a María, Mari Cruz, Leonor y, muy especialmente, a Mari Paz, con quien pude compartir enriquecedores momentos. Con todas vosotras, espero seguir mucho tiempo en contacto. Mari Cruz, gracias también por esos *partiditos* de tenis que me ayudaron en su momento a descargar la tensión acumulada. Creo recordar que nunca llegué a ganarte ningún set. Cuando quieras, la revancha. También agradezco el trabajo que hicieron Jesús, Juanma y de nuevo Sara en aquel/las fantástico/as curso/jornadas sobre Espacios Naturales Protegidos. ¡Buen trabajo!

Después de esos 'aperitivos' en el mundo de la investigación, me pasé al campo de la agricultura de precisión. Y aquí fue cuando, en el verano de

2008, comencé realmente esta Tesis, aunque aún no lo supiera. Durante mi período de prácticas en el IFAPA de Alcalá del Río, tuve la oportunidad de cruzarme con muy buenos trabajadores y mejores personas. Isa, Ester, Jorge, José Antonio, José Luis, gracias a todos. Y por supuesto, Iván. Gracias a tu apoyo, enseñanzas, compañía y salidas al campo en busca del cítrico más estresado hídricamente. Contigo sé que seguiré manteniendo una fructífera relación profesional que seguirá alimentando nuestra amistad. Nunca olvidaré cómo en esas salidas al campo, junto con Jorge, José Antonio y, si mi memoria no me falla, Isa, me enseñaste a medir con la cámara de '*Scolapio*'. A través de la lupa tenía que ver cómo el xilema del peciolo de la hoja, previamente cortada y dispuesta dentro de la cámara, se humectaba a una presión determinada. ¿En serio…? Gracias por esos momentos. Marcaron mi principio en este *mundillo*.

Lo siguiente que llegó fue un 'almuerzo' de nueve meses en tierras murcianas. Allí, en el CEBAS de Murcia, tuve el gran placer de conocer a mucha y buena gente, con la que en los años posteriores pude reencontrarme en varias ocasiones. Arturo, gracias por la buena relación que llegamos a entablar, lo aprecio mucho. Sobre todo gracias por entender y respetar en todo momento mi elección de volver a mi tierra cuando me concedieron la última beca que he disfrutado. A mis compis de trabajo diario: Wenceslao, Carmen, Juan José Brito, Mª Fernanda, muchas gracias. No olvido los cortos pero muy buenos momentos que pasé con vosotros. Y a los cubanos que llegaron después, Jesús y Pedro, ¡muchas gracias chicos! Con vosotros también agoté innumerable horas en el campo y en el centro de trabajo, muchas veces hasta las tantas de la madrugada. Pero las risas lo curaban todo. Aún tengo pendiente el ir a visitaros. Después, con la gente con la que compartía el momento más feliz del día, la hora de la comida, les agradezco que hicieran muy ameno ese ratito. A vosotras, Carmen, Mª José, Mª Fernanda, Emma, gracias. A la gente del departamento, me alegro mucho de haberos conocido y haber compartido alguna que otra cena de departamento, de becarios… Emilio, Sara, Isabel, Juan José Alarcón, Mª

Carmen, Mª Jesús 'Quechu', Oussama, de algún u otro modo seguimos estando en contacto y seguramente en el futuro nos volvamos a cruzar. Espero no haber olvidado a nadie. Gracias a todos.

Y al final, llegó el momento del 'postre' y la vuelta a mi tierra andaluza. Aquí acabé en el IRNAS de Sevilla donde, cada día que ha pasado y sigue pasando, me he ido y me sigo alegrando de toda la gente de la que me he ido rodeando y he ido conociendo. En primer lugar, me gustaría hacer una mención especial a uno de mis directores, Antonio Díaz. Gracias por las incalculables horas que me has dedicado, por tu entusiasmo de cada día que me has contagiado, por querer hacer ciencia siempre lo mejor posible, por quitarte incluso horas de sueño para poder así enviar un artículo, por supuesto, el mismo día del *deadline* (siempre al límite…), por esas charlas en las que al final acababa con más dudas que cuando empezaban, y por los muy buenos viajes científicos que hemos podido compartir. Has sido un buen 'jefe' y compañero, y te has convertido en un gran amigo. Aún está pendiente ese partido de tenis que me prometiste…

Enrique, a ti también tengo muchísimo que agradecer. Gracias por tu búsqueda continua del trabajo bien hecho, por tu inagotable capacidad de trabajo, por ser tan buen 'padre' del grupo REC, y por saber tratar cualquier tipo de situación con la paciencia y la calma que se requiere. De ti he aprendido mucho y espero seguir aprendiendo.

A mis queridos compañeros desde el principio, Torres. Gracias por ser tan buen amigo desde nuestros años mozos en la facultad y por tu alegría. Al final terminamos trabajando juntos, y ha sido todo un placer. Gracias por enseñarme parte de los misterios de la hidráulica. Aún recuerdo mi primer Domingo de Ramos por el IRNAS en el laboratorio y rodeados de ramos de olivo, valga la redundancia. Y te agradezco aún más el que hayamos podido compartir 'eventos' colaterales de reuniones científicas. Alfonso, mi principito favorito, muchas gracias por hacer de cada momento una frase ingeniosa, por tu compañerismo y amistad, por tus detalles, por lo buen

trabajador que eres y por las risas contagiosas que surgen en el cuarto de la cuarta. Gracias también por aguantarme en tantos momentos de estrés que hemos tenido. Vicky, nuestra querida 'madre' del grupo. Gracias por tu carácter cariñoso y alegre, por tu apoyo y por tus excelentes cenas. Antonio Montero, gracias por tu inestimable ayuda. Tus trabajos merecen mi enorme gratitud, y creo que la de todo el grupo.

Y a todos los demás que habéis ido apareciendo en mi vida. Sheren, nuestra 'princesa' egipcia, gracias por los buenos momentos que hemos vivido, sobre todo por aderezarlas con tu especial sentido del humor. Después llegó Virginia, nuestra compi de 'Burgos'. Gracias por ser tan parecida a mí, disfruto cada día de risas como si fuera el primero, por ayudarme en momentos críticos, y por ser también tan buena trabajadora, compañera y amiga. Rafa, gracias por los fervientes debates que han surgido y siguen surgiendo de cualquier tema. María, gracias por tu ayuda en uno de los trabajos que tuve que entregar en los cursos de doctorado y por compartir con nosotros 'miles' de desayunos. Miriam, gracias igualmente por tus constructivas charlas en los desayunos. Y las nuevas incorporaciones, Lucía, gracias por tu ingenio y por las risas que contagias. Y Carmen, que aunque llevas poco tiempo entre nosotros, pareces una buena chica del norte.

A mis queridos amigos biólogos con los que, en cierta medida y menos de lo que quisiera, he seguido en contacto. Laura (todavía te debo una visita a Italia), Myriam 'osito', Ángela, Peck, Patri, Diana (gracias especialmente por acogerme en tu casa en Madrid), Sara, Elena, Inma, ¡gracias a todos!

A la gente del Área de Fisiología Vegetal. Empezaré especialmente dando las gracias a mi otro director, Alfonso De Cires. Gracias por creer en mí en todo momento, por tu apoyo y por tu amistad. Espero seguir manteniendo una fructífera relación contigo. Alfredo, gracias por tu ayuda en medidas de campo y por tus críticas constructivas para dar clases. Aunque no he podido pasar mucho tiempo con todos los demás, el que he

pasado ha sido el mejor. Vuestras comidas de departamento siempre me parecieron una maravilla. Sofía, Monre, Ana Belén, Cristina, Javi, Juan, Pilar, Eduardo, Nadja, Isa, Cire, Clara, gracias por los pequeños momentos que hemos podido compartir. Rosario, a ti quiero agradecerte especialmente que me enseñaras a preparar lo mejor posible unas prácticas, gracias por dedicarme tu tiempo.

Furthermore, in the two different short stays I could do abroad, I was very lucky to meet with very good scientists and better people. Tom, I want to thank you your patience with me to understand your lab gas exchange system, your hospitality, your friendliness and, of course, your dedication to science. This stay was personally and professionally very gratifying. I hope to keep in touch with you for a long time. Thanks to Heather, Laura, Kandis, Tanya, for your very good company. In the second stay, I had the pleasure to know Lawren. Thank you so much for allowing me to collaborate with you and your group to learn more about leaf hydraulics. Thanks to Christine, Megan, Grace, Marissa, Rodrigo, Molly, for your friendship and your support in the lab. Aquí además tuve la oportunidad de compartir alrededor de 3 meses con dos compañeros y amigos a los que aprecio y siempre recuerdo. Sebastìa, gracias por estar siempre al pie del cañón, estás hecho todo un 'currante', y por hacer de cada salida por Los Angeles una pequeña *aventurilla*. Alicia, ha sido todo un placer conocerte y trabajar contigo. Gracias por acogerme cuando me quedé sin 'hogar' y así dormir con Crick. Sigo echando de menos el *BrewCo* y las *Specials*. Espero que nos volvamos a reunir los tres 'mosqueperros' alguna vez.

Quiero dedicar un apartado especial a la persona que ha sufrido esta Tesis casi tanto como yo, o quizás más. Para ti, Luis, o como yo te llamo y te he llamado siempre, Gumba, va dedicado este apartado. Mi amigo, mi socio, mi compañero, mi amor. Cada día que he podido vivir contigo ha sido más enriquecedor que el anterior. Siempre admiro y admiraré tu capacidad de rozar la perfección y de superar cualquier obstáculo que se te cruce. Gracias por aguantar mis continuos cambios de humor, sobre todo

en esta última etapa. En parte, esta Tesis es también tuya. Gracias de nuevo por tu excelente trabajo. Gracias por los millones de consejos que me has dado y que han hecho de mí la que ahora comparte su vida contigo. Espero que este camino juntos siga siendo largo y que, aunque encontremos tramos intransitables, ideemos la manera de solventarlos.

Por último, quiero agradecer enormemente a mi familia el haber sido como es. A mis hermanos, Juan Fran y Nathalie, con los que he vivido un poco de casi todo. Gracias por compartir una de mis épocas más felices de mi vida, la infancia. Todo lo que pasó en esos días ha originado lo que soy hoy. Os quiero. A mi madre, la persona que siempre ha estado ahí, cuidándonos, enseñándonos los diferentes caminos de la vida y cuyo cariño y amor traspasó fronteras. Gracias por todo. Todo lo que soy, y llegaré a ser, os lo debo a ti y a papá. Te quiero. Y a mi padre, cuyo esfuerzo por sacarnos adelante en todo momento siempre admiraré. En homenaje a tu carácter de trabajador incansable y a tu espíritu luchador, te dedico esta Tesis. Gracias por haber sido tan buen padre. Nunca te olvido y siempre te querré.

Celia M.

218

Appendix I. Chapter 2.

30RDI, integrating 0.2-0-4 m depth, 90% IN, 10% OUT
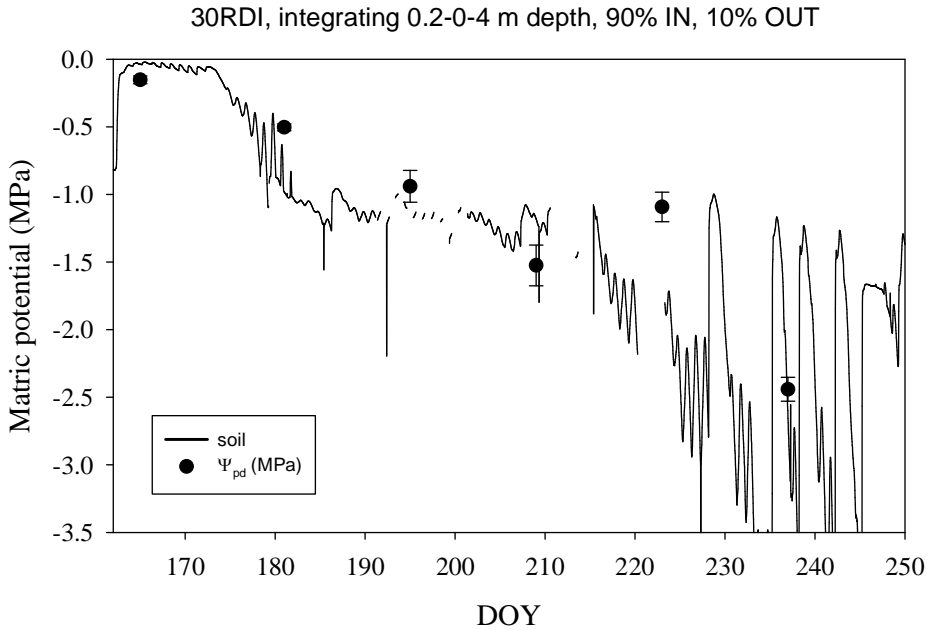
Extra Fig. 2.1. Agreement between soil matric potential (Ψ_s) and pre-dawn leaf water potential (Ψ_{pd}) along the season. Ψ_s was calculated from soil physical properties estimated from Rosetta software as mentioned in Chapter 2. In addition to this, in order to get a single value of Ψ_s, soil water content data had to be integrated as indicated in the chapter and above. All assumptions were inferred from measurements of root distribution, soil water content dynamics and confirmed with Ψ_{pd}. IN and OUT indicate the measurement of soil water content in the wet bulbs and outside bulbs, respectively. DOY = Day of year: 170 = June 19; 250 = September 7.

Appendix II. Chapter 3.

BMF model of stomatal conductance

The hydromechanical model proposed by Buckley, Mott & Farquhar (2003; hereafter, BMF) was based on the observation that stomatal conductance increases with guard cell turgor pressure (P_g) but decreases more strongly with epidermal cell turgor pressure (P_e):

$$(II.1) \quad g_s = \chi(P_g - mP_e),$$

where m, the mechanical advantage, is generally greater than unity. Equation (II.1) predicts stomatal opening when leaf water status declines, which is opposite to observations. Following Haefner *et al.* (1997), BMF thus hypothesized that guard cell osmotic pressure (π_g) was actively regulated in proportion to epidermal turgor, such that $\pi_g - \pi_a = BP_e$ at steady state (where π_a is apoplastic osmotic pressure and B is a proportionality factor). This is the 'hydroactive feedback hypothesis'. Based on an earlier model by Farquhar & Wong (1984), BMF further hypothesized that the proportionality constant B was itself proportional to the concentration of ATP in photosynthesizing cells (τ, which is a measure of the balance between the light and dark reactions of photosynthesis), so that $B = \beta\tau$, with β a scaling factor. Buckley *et al.* (2003) showed that β could be interpreted as the ratio of the specific rates of active ion uptake and passive ion efflux in guard cells; because abscisic acid (ABA) affects guard cells by stimulating passive efflux, one would expect β to decline as ABA concentration increases. Thus,

$$(II.2) \quad \pi_g = \pi_e + \beta\tau P_e.$$

When combined with a steady state model for liquid phase water flow from the soil to the epidermis ($E = K(\Psi_s - \Psi_e)$, where E is transpiration

rate, K is the effective leaf specific hydraulic conductance to the epidermis, and Ψ_s and Ψ_e are soil and epidermis water potentials, respectively), (II.1) and (II.2) lead to

$$(II.3) \quad g_s = \frac{\chi(\beta\tau - M)K(\Psi_s + \pi_e) + (\pi_e - \pi_a)}{K + \chi(\beta\tau - M + \rho)\Delta w},$$

where π_e is epidermal osmotic pressure, ρ is the ratio of effective epidermis-to-guard cell resistance and soil-to-epidermis resistance, and Δw is leaf to air water vapor mole fraction gradient. (Note that $K = 1/(r_{sx} + r_{xe}(f_e + f_g))$ where r_{sx} is the resistance from the soil to the point where water leaves the xylem in the leaf, r_{xe} is the resistance from that point to the epidermis, and f_e and f_g are the fractions of leaf transpiration that occur from the epidermis and guard cells, respectively. Thus, $\rho = f_g r_{eg} K$, where r_{eg} is the resistance from the epidermis to guard cells.) Buckley *et al.* (2003) defined the quantity $\beta\tau - M$ as the guard cell advantage, and gave it the symbol α:

$$(II.4) \quad \alpha = \beta\tau - M.$$

The quantity τ is simulated using the model of Farquhar & Wong (1984), which is based on the photosynthesis model of Farquhar *et al.* (1980). Different values of τ apply under carboxylation-limited conditions (denoted with a subscript 'c') and regeneration-limited conditions (denoted with a subscript 'j'):

$$(II.5) \quad \tau_c = \tau_m\left(1 - p' W_c / W_j\right), \text{ and}$$

$$(II.6) \quad \tau_j = \tau_m\left(1 - p'\right)(v - 1)/(vW_c/W_j - 1),$$

where W_c and W_j are the RuBP-saturated carboxylation rate and the carboxylation rate that can be sustained by the current rate of electron transport, respectively (defined below). The actual value of τ is then the

sum of either τ_c or τ_j and a basal level of ATP generated by non-photosynthetic processes, or τ_{np}:

(II.7) $\quad \tau = \tau_{np} + \begin{cases} \tau_c \\ \tau_j \end{cases} if \begin{array}{c} W_c < W_j \\ else \end{array}$.

The carboxylation rates W_c and W_j are given by

(II.8) $\quad W_c = \dfrac{V_m c_c}{c_c + K_c\left(1 + O/K_o\right)}$, and

(II.9) $\quad W_j = \frac{1}{4}\dfrac{Jc_c}{c_c + \Gamma^*}$,

where c_c is chloroplastic CO_2 partial pressure, V_m is the maximum carboxylation rate, J is the potential electron transport rate, K_c and K_o are the Michaelis constants for RuBP carboxylation and oxygenation, respectively, and Γ^* is the photorespiratory CO_2 compensation point. The net CO_2 assimilation rate is given by

(II.10) $\quad A = \left(1 - \Gamma^*/c_c\right) \cdot \min\{W_c, W_j\} - R_d$,

where R_d is the rate of non-photorespiratory CO_2 release in the light.

Simplifying the BMF model

Equation (II.3) is difficult to apply directly, because it contains many parameters whose estimation is not feasible on a broad scale. These include the sensitivity parameter β, the turgor-to-conductance scaling factor χ, the net epidermal mechanical advantage, M, and the resistance ratio ρ. β cannot be measured directly, and to estimate M and χ requires exceptionally difficult pressure probe measurements that are impractical for wide use (Franks *et al.*, 1998). We are unaware of any method to estimate ρ directly.

In the present chapter, we adopt four modifications that make the model far simpler to use, at little cost to accuracy. First, we modify the hydroactive feedback hypothesis to state that the osmotic gradient from guard to epidermal cells, not to the apoplast, is the target for active regulation (i.e., $\pi_g - \pi_e = BP_e$). Second, we assume $\rho \approx 0$; i.e., the resistance from epidermal to guard cells is negligible compared to the resistance from the soil to the epidermis. Third, we assume that epidermal osmotic pressure, π_e, is similar to bulk leaf osmotic pressure, π. Fourth, we assume that the steady state relationship between g_s and irradiance *in situ* is homogeneous (i.e., it goes through the origin), which implies that the non-photosynthetic component of α ($\beta\tau_{np}$) approximately cancels out the mechanical advantage ($\beta\tau_{np} \approx M$), with the result that $\alpha \approx \beta\tau$. Then Equation (II.3) can be written as

(II.11) $$g_s = \frac{\chi\beta\tau K(\Psi_s + \pi)}{K + \chi\beta\tau\Delta w} = \frac{naK(\Psi_s + \pi)}{K + na\Delta w},$$

where $n = \chi\beta\tau_m$ is a lumped parameter representing the non-hydraulic factors in the BMF model, and a is ATP concentration expressed relative to its maximum value:

(II.12) $n \equiv \chi\beta\tau_m$, and

(II.13) $a \equiv \tau/\tau_m$.

Thus, the product na is equal to the guard cell advantage ($na = \alpha$). Since the parameters χ, β and τ_m always appear as a product in Equation (II.11), they can be empirically fitted as a single parameter, n. This simplification effectively reduces the number of parameters in the model from five (K, π, χ, β and M) to three: K, π and n, which greatly facilitates fitting the model.

There is some rationale for the simplifications that underlie (II.11). The hypothesis that $\pi_g - \pi_e = BP_e$ is equivalent to $P_g = (B + 1)P_e$, which, in order

to represent a physiological process, would require a mechanism that could compare two turgor measurements in adjacent cells. This seems more physiologically plausible and parsimonious than $\pi_g - \pi_a = BP_e$, which would require a mechanism that could compare two osmotic pressure measurements and one turgor measurement across three locations (guard and epidermal cells and the adjacent apoplast). The assumption that $\rho \approx 0$ is difficult to test, but is supported by a wealth of empirical evidence previously summarized by Buckley & Mott (2002a, b) and Buckley (2005); see Buckley & Mott (2013) for a recent discussion of the merits of models based on $\rho = 0$ and $\rho \gg 0$. The assumption that $\pi_e \approx \pi$ has only been tested twice, to our knowledge: by Klein *et al.* (1996), who found that π_e and π were nearly identical in *Vicia faba*, and by Nonami & Schulze (1989), who found that π_e was around 20-40% smaller than mesophyll osmotic pressure, π_m, in *Tradescantia virginiana*. The latter result may reflect daytime accumulation of photosynthate in the mesophyll, or downregulation of π_e to help guard cells overcome the epidermal mechanical advantage during stomatal opening, as suggested by Franks & Farquhar (2007). The assumption that $\beta \tau_{np} \approx M$ is equivalent to the assumption that the relationship between g_s and irradiance is homogeneous, which is approximately correct for our study species, as shown in Extra Fig. 3.1.
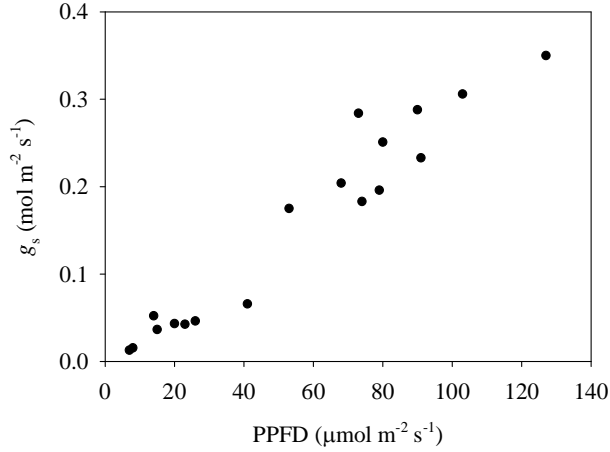
Extra Fig. 3.1. Measurements of stomatal conductance in relation to PPFD, validating the assumption that the response of g_s to irradiance is homogeneous in almond under field conditions. Measurements were made under similar Δw and plant water status.

Attributing changes in stomatal conductance to factors in the BMF model

An infinitesimal change in stomatal conductance, g_s, in the reduced BMF model (Equation II.11) can be parsed into contributions due to changes in the parameters and variables of the model, as follows:

(II.14) $\quad dg_s = \dfrac{\partial g_s}{\partial n}\,dn + \dfrac{\partial g_s}{\partial a}\,da + \dfrac{\partial g_s}{\partial K}\,dK + \dfrac{\partial g_s}{\partial \Psi_s}\,d\Psi_s + \dfrac{\partial g_s}{\partial \pi}\,d\pi + \dfrac{\partial g_s}{\partial \Delta w}\,d\Delta w$.

This may be approximated by an analogous expression based on finite differences rather than differentials:

(II.15) $\quad \delta g_s = \dfrac{\partial g_s}{\partial n}\,\delta n + \dfrac{\partial g_s}{\partial a}\,\delta a + \dfrac{\partial g_s}{\partial K}\,\delta K + \dfrac{\partial g_s}{\partial \Psi_s}\,\delta \Psi_s + \dfrac{\partial g_s}{\partial \pi}\,\delta \pi + \dfrac{\partial g_s}{\partial \Delta w}\,\delta \Delta w$.

We introduce the notation $\delta g_s(x)$ to denote the partial change in g_s attributable to some factor x, so that

(II.16) $\quad \delta g_s = \delta g_s(n) + \delta g_s(a) + \delta g_s(K) + \delta g_s(\Psi_s) + \delta g_s(\pi) + \delta g_s(\Delta w)$,

where $\delta g_s(n) = (\partial g_s/\partial n)\,\delta n$ and so forth. Finally, the proportional (or percent) contribution of each parameter can be estimated by dividing through by the sum of these changes. For example, the percent contribution due to non-hydraulic factors other than ATP (represented by n) is $-100 \cdot \delta g_s(n)/(\delta g_s(n) + \delta g_s(a) + \delta g_s(K) + \delta g_s(\Psi_s) + \delta g_s(\pi) + \delta g_s(\Delta w))$. (The negative sign ensures that the direction of each change is retained in the resulting percent changes; for example, if both $\delta g_s(K)$ and the overall change in g_s are negative, as they are in the example studied in the main text, the negative effect on g_s of a decline in K will be represented as a negative number.)

The partial derivatives in Equation (II.15) are easily computed by differentiating Equation (II.11) to give

(II.17) $\quad \dfrac{\partial g_s}{\partial n} = \left(\dfrac{K}{K + na\Delta w}\right)^2 (\Psi_s + \pi)a$,

(II.18) $\quad \dfrac{\partial g_s}{\partial a} = \left(\dfrac{K}{K + na\Delta w}\right)^2 (\Psi_s + \pi)n$,

(II.19) $\quad \dfrac{\partial g_s}{\partial K} = \left(\dfrac{na}{K + na\Delta w}\right)^2 (\Psi_s + \pi)\Delta w$,

(II.20) $\quad \dfrac{\partial g_s}{\partial \Psi_s} = \dfrac{naK}{K + na\Delta w}$,

(II.21) $\quad \dfrac{\partial g_s}{\partial \pi} = \dfrac{naK}{K + na\Delta w}$, and

(II.22) $\quad \dfrac{\partial g_s}{\partial \Delta w} = -\left(\dfrac{na}{K + na\Delta w}\right)^2 (\Psi_s + \pi)K$.

To apply these expressions to (II.15) and (II.16) in order to examine changes in g_s between two days in the WS treatment (21 and 31 Aug) at a given hour of the day, we used values of each parameter or variable in (II.17)-(II.22) corresponding to that time of day, but averaged between the two days (e.g., calculations for Equation II.17 applied at 1300h would use $\Delta w = 0.5(\Delta w(1300h, 21\ Aug) + \Delta w(1300h, 31\ Aug))$.

Temperature response of photosynthetic model parameters

Several parameters of the Farquhar *et al.* (1980) model of photosynthesis used in the present work and shown in Equations (II.8) and (II.9) have a high dependence on temperature. We used the values proposed by Bernacchi *et al.* (2002) for K_c, K_o and Γ^* obtained in tobacco *in vivo* in a c_c-basis.

(II.23) $Parameter = \exp\left(c - \Delta H_a / RT_k\right)$

where c is the scaling constant, ΔH_a the energy of activation, and T_k leaf temperature in °K. The specific temperature response of V_m, J and g_m in almond was obtained from Egea *et al.* (2011b)

(II.24) $Parameter = Parameter_{25} \dfrac{\exp\left(c - \Delta H_a / RT_k\right)}{1 + \exp\left(\dfrac{\Delta S T_k - \Delta H_d}{RT_k}\right)}$

where $Parameter_{25}$ is the value of the parameter at 25 °C, ΔH_d the energy deactivation and ΔS an entropy term. Values of the parameters in (II.27) and (II.28) used in this chapter are given in Extra Table 3.1.

Extra Table 3.1. Parameter values used in this chapter for responses of photosynthetic parameters to temperature.

	c	ΔH_a	ΔH_d	ΔS
K_c	38.28	80.99		
K_o	14.68	23.72		
Γ^*	13.49	24.46		
V_m	31.57	78.05	155.20	0.5
J	14.03	34.75	189.79	0.6
g_m	19.94	49.43	431.12	1.37

Appendix III. Chapter 6.

Other measurements

For each plot profiles of θ_v were measured 1-2 times per week using a Profile probe (Delta-T Devices Ltd, Cambridge, UK). The Profile probe was calibrated *in situ*, by comparing the soil permittivity (ε) values derived from the Profile probe readings with θ_v values measured with time domain reflectometry (TDR) probes. The resulting calibration curve was: $(\varepsilon)^{0.5} = 2.177 + 6.66\ \theta_v$, $r^2 = 0.72$. At the plots which were subjected to the RDI treatments we installed two access tubes per plot, in a distance of 0.5 m from the tree trunk and of 0.01 m and 0.04 m, respectively, from the dripper. In the Control plot we placed six access tubes, three at a distance of 0.01 m and three at a distance of 0.04 m from the dripper. Measurements in each access tube were made at 0.1, 0.2, 0.3, 0.4, 0.6 and 1.0 m depths. The

θ_v values in the rootzone, i.e. down to 0.6 m, were used to derive (according to Granier, 1987) a depth equivalent of water expressed as the level of relative extractable water (REW) (Extra Figure 6.1C).

The time course of the water status of the trees was monitored by measuring the leaf water potential at predawn (Ψ_{pd}) and the midday stem water potential (Ψ_{stem}), once every two weeks during the whole irrigation season. Measurements were made with a Scholander-type pressure chamber (PMS Instrument Company, Albany, Oregon, USA). For the RDI treatments we sampled one leaf per tree from two representative trees per plot ($n = 8$). In the Control plot we sampled two leaves per tree from four trees in order to have the same number of replicates. For Ψ_{pd} we sampled the 4th or 5th leaf apart from the apex of peripheral twigs at about 1.5 - 1.9 m height above the ground. For Ψ_{stem} we sampled leaves from the inner part of the canopy. The leaves were wrapped in aluminium foil *ca.* 2 h before the measurements. Comparative measurements of P_p and leaf water potential (Ψ_{leaf}) were performed on June 23 and 24 as well as on September 9, i.e. before and after the period of severe water restrictions suffered by the RDI trees at midsummer. At these days, we measured Ψ_{leaf} of each treatment every hour taking at least 8 replicates from dawn to sunset. Leaves were sampled as described for Ψ_{pd} following the path of the sun.

Thirty minute average values of the main meteorological variables were recorded by a Campbell weather station (Campbell Scientific Ltd., Shepshed, UK) located in the centre of the area covered by the experimental plots. We used a pole for installing all meteorological sensors between 2 m and 3 m height above the canopies.

References

Ache P, Bauer H, Kollist H, Al-Rasheid KAS, Lautner S, Hartung W, Hedrich R. **2010**. Stomatal action directly feeds back on leaf turgor: new insights into the regulation of the plant water status from non-invasive pressure probe measurements. *The Plant Journal* **62**: 1072 - 1082.

AEA. **2011**. Anuario de Estadística Agraria. Ministerio de Agricultura, Alimentación y Medio Ambiente. España.

Alder NN, Sperry JS, Pockman WT. **1996**. Root and stem xylem embolism stomatal conductance, and leaf turgor in *Acer grandidentatum* populations along a soil moisture gradient. *Oecologia* **105**: 293 - 301.

Allen RG, Pereira LS, Raes D, Smith M. **1998**. Crop evapotranspiration. Guidelines for computing crop water requirements. *Irrigation and Drainage* paper 56. FAO, Rome, Italy.

Angeles G, *et al*. 2004. The Cohesion-Tension Theory. Letters. *New Phytologist* **163**: 451 - 452.

Aranda I, Forner A, Cuesta B, Valladares F. **2012**. Species-specific water use by forest tree species: from the tree to the stand. *Agricultural Water Management* **114**: 67 - 77.

Ball JT, Woodrow IE, Berry JA. **1987**. A model predicting stomatal conductance and its contribution to the control of photosynthesis under different environmental conditions. In: *Progress in Photosynthesis Research* (ed. J. Biggens), pp. 221 - 224. Martinus Nijhoff Publishers, The Netherlands.

Barranco D. **2001**. Variedades y patrones. En: *El Cultivo del olivo.* 4ª Edición, pp. 63 - 88. Barranco D., Fernández-Escobar R. & Rallo L. Ed. Mundi-Prensa, Junta de Andalucía.

Barros PM, Gonçalves N, Saibo NJM, Oliveira MM. **2012**. Cold acclimation and floral development in almond bud break: insights into the regulatory pathways. *Journal of Experimental Botany* **63**: 4585 - 4596.

Bartlett MK, Scoffoni C, Ardy R, Zhang Y, Sun S, Cao K, Sack L. **2012**. Rapid determination of comparative drought tolerance traits: using an osmometer to predict turgor loss point. *Methods in Ecology and Evolution* **3**: 880 - 888.

Bauer H, Ache P, Lautner S, Fromm J, Hartung W, Al-Rasheid K a S, Sonnewald S, Sonnewald U, Kneitz S, Lachmann N, Mendel R, Bittner F, Hetherington AM, Hedrich R. **2013**. The stomatal response to reduced relative humidity requires guard cell-autonomous ABA synthesis. *Current Biology* **23**: 53 - 57.

Beikircher B, Mayr S. **2009**. Intraspecific differences in drought tolerance and acclimation in hydraulics of *Ligustrum vulgare* and *Viburnum lantana*. *Tree Physiology* **29**: 765 - 775.

Ben-Gal A, Kool D, Agam N, van Halsema GE, Yermiyahu U, Yafe A, Presnov E, Erel R, Majdop A, Zipori I. **2010**. Whole-tree water balance and indicators for short-term drought stress in non-bearing "Barnea" olives. *Agricultural Water Management* **98**: 124 - 133.

Bernacchi CJ, Portis AR, Nakano H, von Caemmerer S, Long SP. **2002**. Temperature response of mesophyll conductance. Implications for the determination of Rubisco enzyme kinetics and for limitations to photosynthesis in vivo. *Plant Physiology* **130**: 1992 - 1998.

Blank K, Lamersdorf N, Dohrenbusch A, Murach D. **1995**. Response of a Norway spruce forest ecosystem to drought ∕ rewetting experiments at Solling, Germany. *Water, Air and Soil Pollution* **85**: 1251 - 1256.

Boyer JS. **1967**. Leaf Water Potentials Measured with a Pressure Chamber. *Plant Physiology* **42**: 133 - 137.

Boyer JS. **1982**. Plant productivity and environment. *Science* **218**: 443 - 448.

Boyer JS. **1996**. Advances in drought tolerance in plants. *Advances in Agronomy* **56**: 187 - 218.

Bramley H, Ehrenberger W, Zimmermann U, Palta JA, Rüger S, Siddique KHM. **2013**. Non-invasive pressure probes magnetically clamped to leaves to monitor the water status of wheat. *Plant and Soil* **369**: 257 - 268.

234

Bramley H, Turner NC, Turner DW, Tyerman SD. **2007**. Comparison between gradient-dependent hydraulic conductivities of roots using the root pressure probe: the role of pressure propagations and implications for the relative roles of parallel radial pathways. *Plant, Cell & Environment* **30**: 861 - 874.

Brodribb TJ, Cochard H. **2009**. Hydraulic failure defines the recovery and point of death in water-stressed conifers. *Plant Physiology* **149**: 575 - 584.

Brodribb TJ, Holbrook NM. **2003**. Stomatal Closure during Leaf Dehydration, Correlation with Other Leaf Physiological Traits. *Plant Physiology* **132**: 2166 - 2173.

Brodribb TJ, Holbrook NM. **2004**. Diurnal depression of leaf hydraulic conductance in a tropical tree species. *Plant, Cell & Environment* **27**: 820 - 827.

Brodribb TJ, McAdam SAM. **2011**. Passive origins of stomatal control in vascular plants. *Science* **331**: 582 - 585.

Brodribb TJ, McAdam SAM. **2013**. Abscisic Acid mediates a divergence in the drought response of two conifers. *Plant Physiology* **162**: 1370 - 1377.

Buckley TN, Mott KA, Farquhar GD. **2003**. A hydromechanical and biochemical model of stomatal conductance. *Plant, Cell & Environment* **26**: 1767 - 1785.

Buckley TN, Mott KA. **2002a**. Dynamics of stomatal water relations during the humidity response: implications of two hypothetical mechanisms. *Plant, Cell & Environment* **25**: 407 - 419.

Buckley TN, Mott KA. 2002b. Stomatal water relations and the control of hydraulic supply and demand. *Progress in Botany* **63**: 309 - 325.

Buckley TN, Mott KA. **2013**. Modelling stomatal conductance in response to environmental factors. *Plant, Cell & Environment* **36**: 1691 - 1699.

Buckley TN. **2005**. The control of stomata by water balance. *The New Phytologist* **168**: 275 - 292.

Burgess SSO, Adams MA, Bleby TM. **2000**. Measurement of sap flow in roots of woody plants: a commentary. *Tree Physiology* **20**: 909 - 913.

Burquez A. **1987**. Leaf thickness and water deficits in plants: a tool for field studies. *Journal of Experimental Botany* **38**: 109 - 114.

Callister AN, Arndt SK, Adams MA. 2006. Comparison of four methods for measuring osmotic potential of tree leaves. *Physiologia Plantarum* **127**: 383 - 392.

Campbell GS. **1985**. Soil physics with BASIC - Transport models for soil-plant systems. In: Developments in Soil Science 14. Elsevier, New York.

Cardon ZG, Mott KA, Berry JA. **1994**. Dynamics of patchy stomatal movements, and their contribution to steady-state and oscillating stomatal conductance calculated using gas-exchange techniques. *Plant, Cell & Environment* **17**: 995 - 1007.

Carr MKV. **2013**. The water relations and irrigation requirements of olive (*Olea europaea* L.): a review. *Experimental Agriculture* **49**: 597 - 639.

Cermák J, Kucera J, Bauerle WL, Phillips N, Hinckley TM. **2007**. Tree water storage and its diurnal dynamics related to sap flow and changes in stem volume in old-growth Douglas-fir trees. *Tree Physiology* **27**: 181 - 198.

Chalmers DJ, Mitchell PD, van Heek L. **1981**. Control of peach tree growth and productivity by regulated water supply, tree density and summer pruning. *Journal of the American Society for Horticultural Science* **106**: 307 - 312.

Chaves MM, Pereira JS, Maroco J, Rodrigues ML, Ricardo CPP, Osório ML, Carvalho I, Faria T, Pinheiro C. **2002**. How plants cope with water stress in the field? Photosynthesis and growth. *Annals of Botany* **89**: 907 - 916.

Choat B, Drayton WM, Brodersen C, Matthews MA, Shackel KA, Wada H, McElrone AJ. **2010**. Measurement of vulnerability to water stress-induced cavitation in grapevine: a comparison of four techniques applied to a long-vesseled species. *Plant, Cell & Environment* **33**: 1502 - 1512.

Christmann A, Grill E, Huang J. **2013**. Hydraulic signals in long-distance signaling. *Current Opinion in Plant Biology* **16**: 293 - 300.

Christmann A, Hoffmann T, Teplova I, Grill E, Müller A. **2005**. Generation of active pools of abscisic acid revealed by in vivo imaging of water-stressed *Arabidopsis*. *Plant Physiology* **137**: 209 - 219.

Christmann A, Weiler EW, Steudle E, Grill E. 2007. A hydraulic signal in root-to-shoot signalling of water shortage. *The Plant Journal* **52:** 167 - 174.

Cifre J, Bota J, Escalona JM, Medrano H, Flexas J. **2005**. Physiological tools for irrigation scheduling in grapevine (*Vitis vinifera* L.). *Agriculture, Ecosystems & Environment* **106**: 159 - 170.

Clark J, Gibbs RD. **1957**. Studies in tree physiology. IV. Further investigations of seasonal changes in moisture content of certain Canadian forest trees. *Canadian Journal of Botany* **35**: 219 - 253.

Cochard H, Barigah ST, Kleinhentz M, Eshel A. **2008**. Is xylem cavitation resistance a relevant criterion for screening drought resistance among *Prunus* species? *Journal of Plant Physiology* **165**: 976 - 982.

Comstock JP, Mencuccini M. 1998. Control of stomatal conductance by leaf water potential in *Hymenoclea salsola* (T. & G.), a desert subshrub. *Plant, Cell & Environment* **21:** 1029 - 1038.

Conejero W, Alarcón JJ, García-Orellana Y, Nicolás E, Torrecillas A. **2007**. Evaluation of sap flow and trunk diameter sensors for irrigation scheduling in early maturing peach trees. *Tree Physiology* **27**: 1753 - 1759.

Connor DJ. **2005**. Adaptation of olive (*Olea europaea* L.) to water-limited environments. *Australian Journal of Agricultural Research* **56**: 1181 - 1189.

Cornwell WK, Bhaskar R, Sack L, Cordell S, Lunch CK. **2007**. Adjustment of structure and function of Hawaiian *Metrosideros polymorpha* at high *vs* low precipitation. *Functional Ecology* **21**: 1063 - 1071.

Cowan IR, Farquhar GD. **1977**. Stomatal function in relation to leaf metabolism and environment: stomatal function in the regulation of gas exchange. In *Integration of Activity in the Higher Plant* (ed. D.H. Jennings), pp. 471 - 505. Cambridge University Press, Cambridge, UK.

Cuevas MV, Martín-Palomo MJ, Diaz-Espejo A, Torres-Ruiz JM, Rodriguez-Dominguez CM, Perez-Martin A, Pino-Mejías R, Fernández JE. **2013**. Assessing water stress in a hedgerow olive orchard from sap flow and trunk diameter measurements. *Irrigation Science* **31**: 729 - 746.

Cuevas MV, Torres-Ruiz JM, Álvarez R, Jiménez MD, Cuerva J, Fernández JE. **2010**. Assessment of trunk diameter variation derived indices as water stress indicators in mature olive trees. *Agricultural Water Management* **97**: 1293 - 1302.

Damour G, Simonneau T, Cochard H, Urban L. **2010**. An overview of models of stomatal conductance at the leaf level. *Plant, Cell & Environment* **33**: 1419 - 1438.

David TS, Ferreira MI, Cohen S, Pereira JS, David JS. **2004**. Constraints on transpiration from an evergreen oak tree in southern Portugal. *Agricultural and Forest Meteorology* **122**: 193 - 205.

Davies W, Zhang J. **1991**. Root Signals And The Regulation Of Growth And Development Of Plants In Drying Soil. *Annual Review of Plant Physiology and Plant Molecular Biology* **42**: 55 - 76.

De Herralde F, Biel C, Savé R. **2003**. Leaf photosynthesis in eight almond tree cultivars. *Biologia Plantarum* **46**: 557 - 561.

Delplancke M, Alvarez N, Benoit L, Espíndola A, I Joly H, Neuenschwander S, Arrigo N. **2013**. Evolutionary history of almond tree domestication in the Mediterranean basin. *Molecular Ecology* **22**: 1092 - 1104.

Dewar RC. **2002**. The Ball-Berry-Leuning and Tardieu-Davies stomatal models: synthesis and extension within a spatially aggregated picture of guard cell function. *Plant, Cell & Environment* **25**: 1383 - 1398.

Diaz-Espejo A, Buckley TN, Sperry JS, Cuevas MV, de Cires A, Elsayed-Farag S, Martin-Palomo MJ, Muriel JL, Perez-Martin A, Rodriguez-Dominguez CM, Rubio-Casal AE, Torres-Ruiz JM, Fernández JE. **2012**. Steps toward an improvement in process-based models of water use by fruit trees: A case study in olive. *Agricultural Water Management* **114**: 37 - 49.

Diaz-Espejo A, Fernández JE, Palomo MJ, Moreno F. **2002**. Are we managing correctly the canopy o four olives trees? pp. 263 - 264 in: *Proceedings of the European Society for Agronomy. VII Congress of the European Society for Agronomy*. Córdoba, Spain.

Diaz-Espejo A, Walcroft AS, Fernández JE, Hafidi B, Palomo MJ, Girón IF. **2006**. Modeling photosynthesis in olive leaves under drought conditions. *Tree Physiology* **26**: 1445 - 1456.

Dichio B, Xiloyannis C, Angelopoulos K, Nuzzo V, Bufo SA, Celano G. **2003**. Drought-induced variations of water relations parameters in Olea europaea. *Plant and Soil* **257**: 381 - 389.

Dichio B, Xiloyannis C, Sofo A, Montanaro G. **2006**. Osmotic regulation in leaves and roots of olive trees during a water deficit and rewatering. *Tree Physiology* **26**: 179 - 185.

Dichio B, Xiloyannis C, Sofo A, Montanaro G. **2007**. Effects of post-harvest regulated deficit irrigation on carbohydrate and nitrogen partitioning, yield quality and vegetative growth of peach trees. *Plant and Soil* **290**: 127–137.

Dodd IC. **2005**. Root-to-shoot signalling: assessing the roles of 'up' in the up and down world of long-distance signalling in planta. *Plant and Soil* **274**: 251–270.

Dodd IC. **2013**. Abscisic acid and stomatal closure: a hydraulic conductance conundrum? *The New Phytologist* **197**: 6 - 8.

Dodd IC, Egea G, Davies WJ. **2008**. Abscisic acid signalling when soil moisture is heterogeneous: decreased photoperiod sap flow from drying roots limits abscisic acid export to the shoots. *Plant, Cell & Environment* **31**: 1263 - 1274.

Dodd IC, Egea G, Watts CW, Whalley WR. **2010**. Root water potential integrates discrete soil physical properties to influence ABA signalling during partial rootzone drying. *Journal of Experimental Botany* **61**: 3543 - 3551.

Egea G, Nortes PA, González-Real MM, Baille A, Domingo R. **2010**. Agronomic response and water productivity of almond trees under contrasted deficit irrigation regimes. *Agricultural Water Management* **97**: 171 - 181.

Egea G, González-Real MM, Baille A, Nortes PA, Diaz-Espejo A. **2011a**. Disentangling the contributions of ontogeny and water stress to photosynthetic limitations in almond trees. *Plant, Cell & Environment* **34**: 962 - 979.

Egea G, Verhoef A, Vidale PL. **2011b**. Towards an improved and more flexible representation of water stress in coupled photosynthesis-stomatal conductance models. *Agricultural and Forest Meteorology* **151**: 1370 - 1384.

Ehrenberger W, Rüger S, Fitzke R, Vollenweider P, Günthardt-Goerg M, Kuster T, Zimmermann U, Arend M. **2012a**. Concomitant dendrometer and leaf

patch pressure probe measurements reveal the effect of microclimate and soil moisture on diurnal stem water and leaf turgor variations in young oak trees. *Functional Plant Biology* **39**: 297 - 305.

Ehrenberger W, Rüger S, Rodriguez-Dominguez CM, Diaz-Espejo A, Fernández JE, Moreno J, Zimmermann D, Sukhorukov VL, Zimmermann U. **2012b**. Leaf patch clamp pressure probe measurements on olive leaves in a nearly turgorless state. *Plant Biology* **14**: 666 - 674.

Escalona JM, Flexas J, Medrano H. **1999**. Stomatal and non-stomatal limitations of photosynthesis under water stress in field-grown grapevines. *Australian Journal of Plant Physiology* **26**: 421 - 433.

Ethier GJ, Livingston NJ. **2004**. On the need to incorporate sensitivity to CO_2 transfer conductance into the Farquhar-von Caemmerer-Berry leaf photosynthesis model. *Plant, Cell & Environment* **27**: 137 - 153.

FAO (Food and Agriculture Organization of the United Nations). **2012**. FAOSTAT 2012: FAO Statistical Databases: Agriculture. Available from http://faostat.fao.org/.

Farquhar GD, Caemmerer S, Berry JA. **1980**. A biochemical model of photosynthetic CO_2 assimilation in leaves of C3 species. *Planta* **149**: 78 - 90.

Farquhar GD, Wong SC. **1984**. An empirical model of stomatal conductance. *Australian Journal of Plant Physiology* **11**: 191 - 210.

Fereres E, Castel JR. **1981**. Drip Irrigation Management. Division of Agricultural Sciences, University of California (Leaflet 21259).

Fereres E, Evans RG. **2006**. Irrigation of fruit trees and vines: an introduction. *Irrigation Science* **24**: 55 - 57.

Fereres E, Goldhamer DA, Parsons LR. **2003**. Irrigation Water Management of Horticultural Crops. *HortScience* **38**: 1036 - 1042.

Fereres E, Soriano MA. **2007**. Deficit irrigation for reducing agricultural water use. *Journal of Experimental Botany* **58**: 147 - 159.

Fernández JE, Cuevas MV. **2010**. Irrigation scheduling from stem diameter variations: a review. *Agricultural and Forest Meteorology* **150**: 135 - 151.

Fernández JE, Diaz-Espejo A, d'Andria R, Sebastiani L, Tognetti R. **2008a**. Potential and limitations of improving olive orchard design and management through modelling. *Plant Biosystems* **142**: 130 - 137.

Fernández JE, Diaz-Espejo A, Infante JM, Durán P, Palomo MJ, Chamorro V, Girón IF, Villagarcía L. **2006a**. Water relations and gas exchange in olive trees under regulated deficit irrigation and partial rootzone drying. *Plant and Soil* **284**: 273 - 291.

Fernández JE, Durán PJ, Palomo MJ, Diaz-Espejo A, Girón IF. **2006b**. Calibration of sap flow estimated by the compensation heat pulse method in olive, plum and orange trees: relationships with xylem anatomy. *Tree Physiology* **26**: 719 - 728.

Fernández JE, Green SR, Caspari HW, Diaz-Espejo A, Cuevas MV. **2008b**. The use of sap flow measurements for scheduling irrigation in olive, apple and Asian pear trees and in grapevines. *Plant and Soil* **305**: 91 - 104.

Fernández JE, Moreno F, Cabrera F, Arrue JL, Martín-Aranda J. **1991**. Drip irrigation, soil characteristics and the root distribution and root activity of olive trees. *Plant and Soil* **133**: 239 - 251.

Fernández JE, Moreno F, Girón IF, Blázquez OM. **1997**. Stomatal control of water use in olive tree leaves. *Plant and Soil* **190**: 179 - 192.

Fernández JE, Moreno F, Martín-Palomo MJ, Cuevas MV, Torres-Ruiz JM, Moriana A. **2011a**. Combining sap flow and trunk diameter measurements to assess water needs in mature olive orchards. *Environmental and Experimental Botany* **72**: 330 - 338.

Fernández JE, Moreno F. **1999**. Water Use by the Olive Tree. *Journal of Crop Production* **2**: 101 - 162.

Fernández JE, Palomo M, Diaz-Espejo A, Clothier B, Green S, Girón I, Moreno F. **2001**. Heat-pulse measurements of sap flow in olives for automating irrigation: tests, root flow and diagnostics of water stress. *Agricultural Water Management* **51**: 99 - 123.

Fernández JE, Palomo M-J, Díaz-Espejo A, Girón I-F. **2003**. Influence of partial soil wetting on water relation parameters of the olive tree. *Agronomie* **23**: 545 - 552.

Fernández JE, Perez-Martin A, Torres-Ruiz JM, Cuevas MV, Rodriguez-Dominguez CM, Elsayed-Farag S, Morales-Sillero A, García JM, Hernandez-Santana V, Diaz-Espejo A. **2013**. A regulated deficit irrigation strategy for hedgerow olive orchards with high plant density. *Plant and Soil* **372**: 279 - 295.

Fernández JE, Rodriguez-Dominguez CM, Perez-Martin A, Zimmermann U, Rüger S, Martín-Palomo MJ, Torres-Ruiz JM, Cuevas MV, Sann C, Ehrenberger W, Diaz-Espejo A. **2011b**. Online-monitoring of tree water stress in a hedgerow olive orchard using the leaf patch clamp pressure probe. *Agricultural Water Management* **100**: 25 - 35.

Fernández JE, Romero R, Montaño JC, Diaz-Espejo A, Muriel JL, Cuevas MV, Moreno F, Girón IF, Palomo MJ. **2008c**. Design and testing of an automatic irrigation controller for fruit tree orchards based on sap flow measurements. *Australian Journal of Agricultural Research* **59**: 589 - 598.

Fernández JE. **2014a**. Plant-based sensing to monitor water stress: Applicability to commercial orchards. *Agricultural Water Management*, **142**: 99 - 109.

Fernández JE. **2014b**. Understanding olive adaptation to abiotic stresses as a tool to increase crop performance. *Environmental and Experimental Botany* **103**: 158 - 179.

Fichot R, Barigah TS, Chamaillard S, Le Thiec D, Laurans F, Cochard H, Brignolas F. **2010**. Common trade-offs between xylem resistance to cavitation and other physiological traits do not hold among unrelated *Populus deltoids* × *Populus nigra* hybrids. *Plant, Cell & Environment* **33**: 1553 - 1568.

Flexas J, Diaz-Espejo A, Gago J, Gallé A, Galmés J, Gulías J, Medrano H. **2013**. Photosynthetic limitations in Mediterranean plants: A review. *Environmental and Experimental Botany* doi: 10.1016/j.envexpbot.2013.09.002.

Flexas J, Medrano H. **2002**. Drought-inhibition of Photosynthesis in C3 Plants: Stomatal and Non-stomatal Limitations Revisited. *Annals of Botany* **89**: 183 - 189.

Flora LL, Madore MA. **1993**. Stachyose and mannitol transport in olive (*Olea europaea* L.). *Planta* **189**: 484 - 490.

Franks PJ, Buckley TN, Shope JC, Mott KA. **2001**. Guard cell volume and pressure measured concurrently by confocal microscopy and the cell pressure probe. *Plant Physiology* **125**: 1577 - 1584.

Franks PJ, Cowan IR, Farquhar GD. **1998**. A study of stomatal mechanics using the cell pressure probe. *Plant, Cell & Environment* **21**: 94 - 100.

Franks PJ, Farquhar GD. **2007**. The mechanical diversity of stomata and its significance in gas-exchange control. *Plant Physiology* **143**: 78 - 87.

Franks PJ. **2004**. Stomatal control and hydraulic conductance, with special reference to tall trees. *Tree Physiology* **24**: 865 - 878.

Franks PJ. **2013**. Passive and active stomatal control: either or both? *The New Phytologist* **198**: 325 - 327.

Fuchs EE, Livingston NJ. **1996**. Hydraulic control of stomatal conductance in Douglas fir [*Pseudotsuga menzlesii* (Mirb) Franco] and alder [*Alnus rubra* (Bong)] seedlings. *Plant, Cell & Environment* **19:** 1091 - 1098.

Galmes J, Flexas J, Save R, Medrano H. **2007**. Water relations and stomatal characteristics of Mediterranean plants with different growth forms and leaf habits: responses to water stress and recovery. *Plant and Soil* **290**: 139 - 155.

Galvez-Valdivieso G, Fryer MJ, Lawson T, Slattery K, Truman W, Smirnoff N, Asami T, Davies WJ, Jones AM, Baker NR, *et al.* 2009. The high light response in Arabidopsis involves ABA signaling between vascular and bundle sheath cells. *The Plant Cell* **21**: 2143 - 2162.

Gao Q, Zhao P, Zeng X, Cai X, Shen W. **2002**. A model of stomatal conductance to quantify the relationship between leaf transpiration, microclimate and soil water stress. *Plant, Cell & Environment* **25**: 1373 - 1381.

García JM, Cuevas MV, Fernández JE. **2013**. Production and oil quality in "Arbequina" olive (*Olea europaea*, L.) trees under two deficit irrigation strategies. *Irrigation Science* **31**: 359 - 370.

Giorio P, Sorrentino G, D'Andria R. **1999**. Stomatal behaviour, leaf water status and photosynthetic response in field-grown olive trees under water deficit. *Environmental and Experimental Botany* **42**: 95 - 104.

Girma FS, Krieg DR. **1992**. Osmotic Adjustment in Sorghum: I. Mechanisms of Diurnal Osmotic Potential Changes. *Plant Physiology* **99**: 577 - 582.

Girona J, Mata M, Marsal J. **2005**. Regulated deficit irrigation during the kernel-filling period and optimal irrigation rates in almond. *Agricultural Water Management* **75**: 152 - 167.

Goldhamer D, Fereres E. **2001**. Irrigation scheduling protocols using continuously recorded trunk diameter measurements. *Irrigation Science* **20**: 115 - 125.

Goldhamer DA, Viveros M, Salinas M. **2006**. Regulated deficit irrigation in almonds: effects of variations in applied water and stress timing on yield and yield components. *Irrigation Science* **24**: 101 - 114.

Goldhamer DA, Viveros M. **2000**. Effects of preharvest irrigation cutoff durations and postharvest water deprivation on almond tree performance. *Irrigation Science* **19**: 125 - 131.

Gómez-Cadenas A, Pozo OJ, García-Augustín P, Sancho JV. 2002. Direct analysis of abscisic acid in crude plant extracts by liquid chromatography-electrospray/tandem mass spectrometry. *Phytochemical Analysis* **13:** 228 - 234.

Gómez-del-Campo M. **2013**. Summer deficit-irrigation strategies in a hedgerow olive orchard cv. "Arbequina": effect on fruit characteristics and yield. *Irrigation Science* **31**: 259 - 269.

González-Altozano JR, Castel P. **2003**. Riego deficitario controlado en "Clementina de Nules". I. Efectos sobre la producción y la calidad de la fruta. *Spanish Journal of Agricultural Research* **1**: 81 - 92.

Graham JB, Aguilar NM, Dudley R, Gans C. **1995**. Implications of the late Palaeozoic oxygen pulse for physiology and evolution. *Nature* **375**: 117 - 120.

Granier A. **1987**. Evaluation of transpiration in a Douglas-fir stand by means of sap flow measurements. *Tree Physiology* **3**: 309 - 320.

Grant OM, Davies MJ, James CM, Johnson AW, Leinonen I, Simpson DW. **2012**. Thermal imaging and carbon isotope composition indicate variation amongst strawberry (*Fragaria × ananassa*) cultivars in stomatal conductance and water use efficiency. *Environmental and Experimental Botany* **76**: 7 - 15.

Grassi G, Magnani F. **2005**. Stomatal, mesophyll conductance and biochemical limitations to photosynthesis as affected by drought and leaf ontogeny in ash and oak trees. *Plant, Cell & Environment* **28**: 834 - 849.

Green S, Clothier B, Jardine B. **2003**. Theory and Practical Application of Heat Pulse to Measure Sap Flow. *Agronomy Journal* **95**: 1371 - 1379.

Gurovich L, Hermosilla P. **2009**. Electric signaling in fruit trees in response to water applications and light-darkness conditions. *Journal of Plant Physiology* **166**: 290 - 300.

Gutschick VP, Simonneau T. **2002**. Modelling stomatal conductance of field-grown sunflower under varying soil water content and leaf environment: comparison of three models of stomatal response to leaf environment and coupling with an abscisic acid-based model of stomatal response to soil drying. *Plant, Cell & Environment* **25**: 1423 - 1434.

Guyot G, Scoffoni C, Sack L. **2012**. Combined impacts of irradiance and dehydration on leaf hydraulic conductance: insights into vulnerability and stomatal control. *Plant, Cell & Environment* **35**: 857 - 871.

Hacke UG, Sperry JS, Ewers BE, Ellsworth DS, Schafer KVR, Oren R. **2000**. Influence of soil porosity on water use in *Pinus taeda. Oecologia* **124**: 495 - 505.

Haefner JW, Buckley TN, Mott KA. **1997**. A spatially explicit model of patchy stomatal responses to humidity. *Plant, Cell & Environment* **20**: 1087 - 1097.

Hetherington AM, Woodward FI. **2003**. The role of stomata in sensing and driving environmental change. *Nature* **424**: 901 - 908.

Hetherington AM. **2001**. Guard Cell Signaling. *Cell* **107**: 711 - 714.

Higgins SS, Larsen FE, Bendel RB, Radamaker GK, Bassman JH, Bidlake WR, Alwir A. **1992**. Comparative gas-exchange characteristics of potted,

glasshouse-grown almond, apple, fig, grape, olive, peach and Asian pear. *Scientia Horticulturae* **52**: 313 - 329.

Himmelsbach W, Treviño-Garza EJ, González-Rodríguez H, González-Tagle MA, Gómez Meza MV, Aguirre Calderón OA, Eduardo Estrada Castillón A, Mitlöhner R. **2011**. Acclimatation of three co-occurring tree species to water stress and their role as site indicators in mixed pine-oak forests in the Sierra Madre Oriental, Mexico. *European Journal of Forest Research* **131**: 355 - 367.

Hinckley TM, Lassoie JP, Running SW. **1978**. Temporal and spatial variations in the water status of forest trees. *Forest Science* **24**: 1 - 72.

Holbrook NM, Shashidhar VR, James RA, Munns R. **2002**. Stomatal control in tomato with ABA-deficient roots: response of grafted plants to soil drying. *Journal of Experimental Botany* **53**: 1503 - 1514.

Holbrook NM, Zwieniecki MA. **2005**. Vascular Transport in Plants. Academic Press, Amsterdam, 564 pp.

Hothorn T, Bretz F, Westfall P. **2008**. Simultaneous inference in general parametric models. *Biometrical Journal* **50**: 346 - 363.

Hu FB. **2003**. The Mediterranean diet and mortality-olive oil and beyond. *The New England Journal of Medicine* **348**: 2595 - 2596.

Hummel I, Pantin F, Sulpice R, Piques M, Rolland G, Dauzat M, Christophe A, Pervent M, Bouteillé M, Stitt M, Gibon Y, Muller B. **2010**. Arabidopsis plants acclimate to water deficit at low cost through changes of carbon usage: an integrated perspective using growth, metabolite, enzyme, and gene expression analysis. *Plant Physiology* **154**: 357 - 372.

Hutmacher RB, Nightingale HI, Rolston DE, Biggar JW, Dale F, Vail SS, Peters D. **1994**. Growth and yield responses of almond (*Prunus amygdalus*) to trickle irrigation. *Irrigation Science* **14**: 117 - 126.

Iniesta F, Testi L, Orgaz F, Villalobos FJ. **2009**. The effects of regulated and continuous deficit irrigation on the water use, growth and yield of olive trees. *European Journal of Agronomy* **30**: 258 - 265.

Intrigliolo DS, Castel JR. **2006a**. Performance of various water stress indicators for prediction of fruit size response to deficit irrigation in plum. *Agricultural Water Management* **83**: 173 - 180.

Intrigliolo DS, Castel JR. **2006b**. Usefulness of diurnal trunk shrinkage as a water stress indicator in plum trees. *Tree Physiology* **26**: 303 - 311.

Intrigliolo DS, Castel JR. **2010**. Response of plum trees to deficit irrigation under two crop levels: tree growth, yield and fruit quality. *Irrigation Science* **28**: 525 - 534.

IOC. International Olive Council, http://www.internationaloliveoil.org.

IPCC. **2013**. Climate Change 2013: The Physical Science Basis. Contribution of Working Group I to the Fifth Assessment Report of the Intergovernmental Panel on Climate Change. Cambridge University Press, New York.

Irvine J, Perks MP, Magnani F, Grace J. **1998**. The response of Pinus sylvestris to drought: stomatal control of transpiration and hydraulic conductance. *Tree Physiology* **18**: 393 - 402.

ISHS. Working Group on Sap Flow, http://www.wgsapflow.com

Jacobsen S-E, Jensen CR, Liu F. **2012**. Improving crop production in the arid Mediterranean climate. *Field Crops Research* **128**: 34 - 47.

Jarvis AJ, Davies WJ. **1998**. The coupled response of stomatal conductance to photosynthesis and transpiration. *Journal of Experimental Botany* **49**: 399 - 406.

Jarvis PG, McNaughton KG. **1986**. Stomatal control of transpiration: scaling up from leaf to region. *Advances in Ecological Research* **15**: 1 - 49.

Jarvis PG. **1976**. The interpretation of the variations in leaf water potential and stomatal conductance found in canopies in the field. *Philosophical Transactions of the Royal Society of London. Series B* **273**: 593 - 610.

Jiang M, Zhang J. **2001**. Effect of abscisic acid on active oxygen species, antioxidative defense system and oxidative damage in leaves of maize seedlings. *Plant and Cell Physiology* **42**: 1265 - 1273.

Johnson DM, Woodruff DR, McCulloh KA, Meinzer FC. **2009**. Leaf hydraulic conductance, measured in situ, declines and recovers daily: leaf hydraulics, water

potential and stomatal conductance in four temperate and three tropical tree species. *Tree Physiology* **29**: 879 - 887.

Jones HG, Tardieu F. **1998**. Modeling water relations of horticultural crops: A review. *Scientia Horticulturae* **74**: 21 - 46.

Jones HG 1985. Partitioning stomatal and non-stomatal limitations to photosynthesis. *Plant, Cell & Environment* **8:** 95 - 104.

Jones HG. **1990**. Physiological aspects of the control of water status in horticultural crops. *HortScience* **25**: 19 - 26.

Jones HG. **1992**. Stomata. In Plants *and Microclimate: A Quantitative Approach to Environmental Plant Physiology* (ed. H.G. Jones) pp. 131 - 162. Cambridge University Press, Cambridge, UK.

Jones HG. **1999**. Use of infrared thermometry for estimation of stomatal conductance as a possible aid to irrigation scheduling. *Agricultural and Forest Meteorology* **95**: 139 - 149.

Jones HG. **2002**. Use of infrared thermography for monitoring stomatal closure in the field: application to grapevine. *Journal of Experimental Botany* **53**: 2249 - 2260.

Jones HG. **2004**. Irrigation scheduling: advantages and pitfalls of plant-based methods. *Journal of Experimental Botany* **55**: 2427 - 2436.

Jones HG. **2007**. Monitoring plant and soil water status: established and novel methods revisited and their relevance to studies of drought tolerance. *Journal of Experimental Botany* **58**: 119 - 130.

Kijne JW, Barker R, Molden DJ. **2003**. Water Productivity in Agriculture: Limits and Opportunities for Improvement. CABI, IWMI, Wallingford, UK.

Klein I, Esparza G, Weinbaum SA, DeJong TM. **2001**. Effects of irrigation deprivation during the harvest period on leaf persistence and function in mature almond trees. *Tree Physiology* **21**: 1063 - 1072.

Klein M, Cheng G, Chung M, Tallman G. **1996**. Effects of turgor potentials of epidermal cells neighbouring guard cells on stomatal opening in detached leaf epidermis and intact leaflets of *Vicia faba* L. (faba bean). *Plant, Cell & Environment* **19**, 1399 - 1407.

Koch GW, Sillett SC, Jennings GM, Davis SD. **2004**. The limits to tree height. *Nature* **428**: 851 - 854.

Kolb KJ, Sperry JS. **1999**. Transport constraints on water use by the Great Basin shrub, *Artemisia tridentata*. *Plant, Cell & Environment* **22**: 925 - 935.

Kozlowski TT, Pallardy SG. **2002**. Acclimation and Adaptive Responses of Woody Plants to Environmental Stresses. *The Botanical Review* **68**: 270 - 334.

Kramer PJ, Boyer JS. **1995**. Water Relations of Plants and Soils. Academic Press, San Diego, CA, USA.

Le Roux X, Grand S, Dreyer E, Daudet F-A. **1999**. Parameterization and testing of a biochemically based photosynthesis model for walnut (*Juglans regia*) trees and seedlings. *Tree Physiology* **19**: 481 - 492.

Lee KM, Driever SM, Heuvelink E, Rüger S, Zimmermann U, de Gelder A, Marcelis LFM. **2012**. Evaluation of diel patterns of relative changes in cell turgor of tomato plants using leaf patch clamp pressure probes. *Physiologia Plantarum* **146**: 439 - 447.

Leuning R. **1990**. Modelling Stomatal Behaviour and Photosynthesis of Eucalyptus grandis. *Australian Journal of Plant Physiology* **17**: 159 - 175.

Leuning R. **1995**. A critical appraisal of a combined stomatal-photosynthesis model for C3 plants. *Plant, Cell & Environment* **18**: 339 - 355.

Lo Gullo MA, Nardini A, Trifilò P, Salleo S. **2005**. Diurnal and seasonal variations in leaf hydraulic conductance in evergreen and deciduous trees. *Tree Physiology* **25**: 505 - 512.

Lopez-Zamora I, Falcao N, Comerford NB, Barros NF. **2002**. Root isotropy and an evaluation of a method for measuring root distribution in soil trenches. *Forest Ecology and Management* **166**: 303 - 310.

Maherali H, DeLucia EH. **2000**. Xylem conductivity and vulnerability to cavitation of ponderosa pine growing in contrasting climates. *Tree Physiology* **20**: 859 - 867.

Marchi S, Tognetti R, Minnocci A, Borghi M, Sebastiani L. **2008**. Variation in mesophyll anatomy and photosynthetic capacity during leaf development in a

deciduous mesophyte fruit tree (*Prunus persica*) and an evergreen sclerophyllous Mediterranean shrub (*Olea europaea*). *Trees* **22**: 559 - 571.

Marigo G, Peltier JP. **1996**. Analysis of the diurnal change in osmotic potential in leaves of Fraxinus excelsior L. *Journal of Experimental Botany* **47**: 763 - 769.

Martínez-Vilalta J, Prat E, Oliveras I, Piñol J. **2002**. Xylem hydraulic properties of roots and stems of nine Mediterranean woody species. *Oecologia* **133**: 19 - 29.

Matos MC, Rebelo E, Lauriano J, Semedo J, Marques N, Campos PS, Matos A, Vieira-Da-Silva J. **2004**. CO_2 Assimilation and Water Relations of Almond Tree (*Prunus amygdalus* Batsch) Cultivars Grown Under Field Conditions. *Photosynthetica* **42**: 473 - 476.

McAdam SAM, Brodribb TJ. **2012**. Stomatal innovation and the rise of seed plants. *Ecology Letters* **15**: 1 - 8.

McBurney T. **1988**. A temperature-controlled plant psychrometer. *Plant and Soil*, **109**: 271 - 275.

McCarthy MG. **1997**. The effect of transient water deficit on berry development of cv. Shiraz (*Vitis vinifera* L.). *Australian Journal of Grape and Wine Research* **3**: 2 - 8.

McDowell N, Pockman WT, Allen CD, Breshears DD, Cobb N, Kolb T, Plaut J, Sperry JS, West A, Williams DG, *et al.* **2008**. Mechanisms of plant survival and mortality during drought: why do some plants survive while others succumb to drought? *The New phytologist* **178**: 719 - 739.

Meinzer FC. **2002**. Co-ordination of vapour and liquid phase water transport properties in plants. *Plant, Cell & Environment* **25**: 265 - 274.

Messinger SM, Buckley TN, Mott KA. **2006**. Evidence for involvement of photosynthetic processes in the stomatal response to CO2. *Plant Physiology* **140**: 771 - 778.

Miranda JD, Padilla FM, Martínez-Vilalta J, Pugnaire FI. **2010**. Woody species of a semi-arid community are only moderately resistant to cavitation. *Functional Plant Biology* **37**: 828 - 839.

Mitchell PD, Chalmers DJ. **1982**. The effects of reduced water supply on peach tree growth and yield. *Journal of the American Society for Horticultural Science* **107**: 853 - 856.

Möller M, Alchanatis V, Cohen Y, Meron M, Tsipris J, Ostrovsky V, Sprintsin M, Cohen S. **2007**. Use of thermal and visible imagery for estimating crop water status of irrigated grapevine. *Journal of Experimental Botany* **58**: 827 - 838.

Monteith JL. **1995**. A reinterpretation of stomatal responses to humidity. *Plant, Cell & Environment* **18**: 357 - 364.

Moreno F, Fernández JE, Clothier BE, Green SR. **1996**. Transpiration and root water uptake by olive trees. *Plant and Soil* **184**: 85 - 96.

Moriana A, Orgaz F, Pastor M, Fereres E. **2003**. Yield responses of a mature olive orchard to water deficits. *Journal of the American Society for Horticultural Science* **128**: 425 - 431.

Moriana A, Villalobos FJ, Fereres E. **2002**. Stomatal and photosynthetic responses of olive (*Olea europaea* L.) leaves to water deficits. *Plant, Cell & Environment* **25**: 395 - 405.

Morison JIL, Baker NR, Mullineaux PM, Davies WJ. **2008**. Improving water use in crop production. *Philosophical Transactions of the Royal Society of London. Series B, Biological Sciences* **363**: 639 - 658.

Mott KA, Parkhurst DF. **1991**. Stomatal responses to humidity in air and helox. *Plant, Cell & Environment* **14**: 509 - 515.

Mott KA. **1988**. Do Stomata Respond to CO_2 Concentrations Other than Intercellular? *Plant Physiology* **86**: 200 - 203.

Münch E. **1930**. Die Stoffbewegungen in den Pflanzen. Gustav Fischer, Jena, Germany.

Murphy R, Ortega JKE. **1995**. A new pressure probe method to determine the average volumetric elastic modulus of cells in plant tissues. *Plant Physiology* **107**: 995 - 1005.

Nadler A, Raveh E, Yermiyahu U, Green SR. **2003**. Evaluation of TDR use to monitor water content in stems of lemon trees and soils and their responses to water stress. *Soil Science Society of America Journal* **67**: 437 - 448.

Nadler A, Raveh E, Yermiyahu U, Green SR. **2006**. Stress-induced water content variations in mango stem by time domain reflectometry. *Soil Science Society of America Journal* **70**: 510 - 520.

Nadler A, Raveh E, Yermiyahu U, Lado M, Nasser A, Barak M, Green S. **2008**. Detecting Water Stress in Trees Using Stem Electrical Conductivity Measurements. *Soil Science Society of America Journal* **72**: 1014 - 1024.

Nadler A, Tyree MT. **2008**. Substituting Stem's Water Content by Electrical Conductivity for Monitoring Water Status Changes. *Soil Science Society of America Journal* **72**: 1006 - 1013.

Naor A, Gal Y, Peres M. **2006**. The inherent variability of water stress indicators in apple, nectarine and pear orchards, and the validity of a leaf-selection procedure for water potential measurements. *Irrigation Science* **24**: 129 - 135.

Naor A, Naschitz S, Peres M, Gal Y. **2008**. Responses of apple fruit size to tree water status and crop load. *Tree Physiology* **28**: 1255 - 1261.

Nardini A, Pedá G, Salleo S. **2012**. Alternative methods for scaling leaf hydraulic conductance offer new insights into the structure - function relationships of sun and shade leaves. *Functional Plant Biology* **39**: 394 - 401

Neill S. **2007**. Interactions between abscisic acid, hydrogen peroxide and nitric oxide mediate survival responses during water stress. *New Phytologist* **175**: 4 - 6.

Netzer Y, Yao C, Shenker M, Bravdo B, Schwartz A. **2009**. The use of crop coefficients for skilled irrigation of table grapes trained to a large trellis system. *Irrigation Science* **27**: 109 - 120.

Neumann P. **2008**. Coping mechanisms for crop plants in drought-prone environments. *Annals of Botany* **101**: 901 - 907.

Nonami H, Schulze ED. **1989**. Cell water potential, osmotic potential, and turgor in the epidermis and mesophyll of transpiring leaves. *Planta* **177**, 35 - 46.

Nortes PA, Gonzalez-Real MM, Egea G, Baille A. **2009**. Seasonal effects of deficit irrigation on leaf photosynthetic traits of fruiting and non-fruiting shoots in almond trees. *Tree Physiology* **29**: 375 - 388.

Oren R, Sperry JS, Katul GG, Pataki DE, Ewers BE, Phillips N, Schafer KVR. 1999. Survey and synthesis of intra- and interspecific variation in stomatal sensitivity to vapour pressure deficit. *Plant, Cell and Environment* **22**: 1515 - 1526.

Orgaz F, Fereres E. **1997**. Riego. In: Barranco, D., Fernandez-Escobar, R., Rallo, L. (Eds.), *El cultivo del olivo*. Mundi Prensa, Madrid, pp. 251 - 272.

Orgaz F, Testi L, Villalobos FJ, Fereres E. **2006**. Water requirements of olive orchards II: determination of crop coefficients for irrigation scheduling. *Irrigation Science* **24**: 77 - 84.

Ortuño MF, Conejero W, Moreno F, Moriana A, Intrigliolo DS, Biel C, Mellisho CD, Pérez-Pastor A, Domingo R, Ruiz-Sánchez MC. **2010**. Could trunk diameter sensors be used in woody crops for irrigation scheduling? A review of current knowledge and future perspectives. *Agricultural Water Management* **97**: 1 - 11.

Ortuño MF, García-Orellana Y, Conejero W, Ruiz-Sánchez MC, Alarcón JJ, Torrecillas A. **2006**. Stem and leaf water potentials, gas exchange, sap flow, and trunk diameter fluctuations for detecting water stress in lemon trees. *Trees* **20**: 1 - 8.

Ounapuu E, Sellin A. **2013**. Daily dynamics of leaf and soil-to-branch hydraulic conductance in silver birch (*Betula pendula*) measured in situ. *Plant Physiology & Biochemistry* **68**: 104 - 110.

Oyarce P, Gurovich L. **2011**. Evidence for the transmission of information through electric potentials in injured avocado trees. *Journal of Plant Physiology* **168**: 103 - 108.

Palomo M, Moreno F, Fernández J, Díaz-Espejo A, Girón I. **2002**. Determining water consumption in olive orchards using the water balance approach. *Agricultural Water Management* **55**: 15 - 35.

Pantin F, Monnet F, Jannaud D, Costa JM, Renaud J, Muller B, Simonneau T, Genty B. **2012**. The dual effect of abscisic acid on stomata. *The New Phytologist* **197**: 65 - 72.

Pardossi A, Incrocci L. **2011**. Traditional and new approaches to irrigation scheduling in vegetable crops. *HortTechnology* **21**: 309 - 313.

Patakas A, Noitsakis B. **1999**. Mechanisms Involved in Diurnal Changes of Osmotic Potential in Grapevines under Drought Conditions. *Journal of Plant Physiology* **154**: 767–774.

Peak D, Mott KA. **2011**. A new, vapour-phase mechanism for stomatal responses to humidity and temperature. *Plant, Cell & Environment* **34**: 162 - 178.

Pérez-Pérez JG, Romero P, Navarro JM, Botía P. **2008**. Response of sweet orange cv. "Lane late" to deficit irrigation in two rootstocks. I: water relations, leaf gas exchange and vegetative growth. *Irrigation Science* **26**: 415 - 425.

Perks MP, Irvine J, Grace J. **2002**. Canopy stomatal conductance and xylem sap abscisic acid (ABA) in mature Scots pine during a gradually imposed drought. *Tree Physiology* **22**: 877 - 883.

Philip JR. **1958**. The Osmotic Cell, Solute Diffusibility, and the Plant Water Economy. *Plant Physiology* **33**: 264 - 271.

Pinheiro J, Bates D, DebRoy S, Sarker D. 2012. R Development Core Team. nlme: Linear and Nonlinear Mixed Effects Models. R package version 2.15.0.

Pires RCM, Bodine JD, Sakai E, Villa HL, da Silva TJA, Arruda FB. **2011**. Effect of trickle irrigation on root development of the wet bulb and 'Pera' orange tree yield in the state of Sao Paulo, Brazil. *Engenharia Agricola* **31**: 1096 - 1103.

Preston RD. **1952**. Movement of water in higher plants. In: Frey-Wyssling, A. (Ed.), *Deformation and Flow in Biological Systems*. North Holland Pub. Co., pp. 257–321.

Rapopport HF. **2001**. Botánica y morfología. En: *El Cultivo del olivo.* 4ª Edición, pp. 37 - 59. Barranco D., Fernández-Escobar R. & Rallo L. Ed. Mundi-Prensa, Junta de Andalucía.

Reidel EJ, Rennie EA, Amiard V, Cheng L, Turgeon R. **2009**. Phloem loading strategies in three plant species that transport sugar alcohols. *Plant Physiology* **149**: 1601 - 1608.

254

Renner O. **1915**. Theoretisches und experimentelles zur kohäsionstheorie der wasserbewegung. *Jahrbücher für wissenschaftliche Botanik* **56**: 617 - 667.

Rennie EA, Turgeon R. **2009**. A comprehensive picture of phloem loading strategies. *Proceedings of the National Academy of Sciences of the United States of America* **106**: 14162 - 14167.

Rius X, Lacarte JM. **2010**. La revolución del olivar. El cultivo en seto. COMGRAFIC, S.A., Barcelona, 340 pp.

Rodriguez-Dominguez CM, Ehrenberger W, Sann C, Rüger S, Sukhorukov V, Martín-Palomo MJ, Diaz-Espejo A, Cuevas MV, Torres-Ruiz JM, Perez-Martin A, Zimmermann U, Fernández JE. 2012. Concomitant measurements of stem sap flow and leaf turgor pressure in olive trees using the leaf patch clamp pressure probe. *Agricultural Water Management* **114**: 50 - 58.

Romero P, Botia P, Garcia F. **2004a**. Effects of regulated deficit irrigation under subsurface drip irrigation conditions on vegetative development and yield of mature almond trees. *Plant and Soil* **260**: 169 - 181.

Romero P, Botia P, Garcia F. **2004b**. Effects of regulated deficit irrigation under subsurface drip irrigation conditions on water relations of mature almond trees. *Plant and Soil* **260**: 155 - 168.

Romero P, Botía P. **2006**. Daily and seasonal patterns of leaf water relations and gas exchange of regulated deficit-irrigated almond trees under semiarid conditions. *Environmental and Experimental Botany* **56**: 158 - 173.

Romero P, Navarro JM, García F, Botía Ordaz P. **2004c**. Effects of regulated deficit irrigation during the pre-harvest period on gas exchange, leaf development and crop yield of mature almond trees. *Tree Physiology* **24**: 303 - 312.

Rouhi V, Samson R, Lemeur R, Damme P Van. **2007**. Photosynthetic gas exchange characteristics in three different almond species during drought stress and subsequent recovery. *Environmental and Experimental Botany* **59**: 117 - 129.

Rudall PJ, Hilton J, Bateman RM. **2013**. Several developmental and morphogenetic factors govern the evolution of stomatal patterning in land plants. *The New Phytologist* **200**: 598 - 614.

Rüger S, Ehrenberger W, Arend M, Geßner P, Zimmermann G, Zimmermann D, Bentrup F-W, Nadler A, Raveh E, Sukhorukov VL. **2010a**. Comparative monitoring of temporal and spatial changes in tree water status using the non-invasive leaf patch clamp pressure probe and the pressure bomb. *Agricultural Water Management* **98**: 283 - 290.

Rüger S, Netzer Y, Westhoff M, Zimmermann D, Reuss R, Ovadiya S, Gessner P, Zimmermann G, Schwartz A, Zimmermann U. **2010b**. Remote monitoring of leaf turgor pressure of grapevines subjected to different irrigation treatments using the leaf patch clamp pressure probe. *Australian Journal of Grape and Wine Research* **16**: 405 - 412.

Ruiz-Sanchez M, Domingo R, Castel JR. **2010**. Review. Deficit irrigation in fruit trees and vines in Spain. *Spanish Journal of Agricultural Research* **8**: S5 - S20.

Sack L, Holbrook NM. **2006**. Leaf hydraulics. *Annual Review of Plant Biology* **57**: 361–381.

Santesteban LG, Miranda C, Royo JB. **2011**. Regulated deficit irrigation effects on growth, yield, grape quality and individual anthocyanin composition in *Vitis vinifera* L. cv. "Tempranillo." *Agricultural Water Management* **98**: 1171 - 1179.

Sauter A, Davies WJ, Hartung W. **2001**. The long-distance abscisic acid signal in the droughted plant: the fate of the hormone on its way from root to shoot. *Journal of Experimental Botany* **52**: 1991 - 1997.

Schaap MG, Leij FJ, van Genuchten MT. **2001**. Rosetta: a Computer Program for Estimating Soil Hydraulic Parameters With Hierarchical Pedotransfer Functions. *Journal of Hydrology* **251**: 163 - 176.

Schachtman DP, Goodger JQD. **2008**. Chemical root to shoot signaling under drought. *Trends in Plant Science* **13**: 281 - 287.

Scholander PF, Bradstreet ED, Hemmingsen EA, Hammel HT. **1965**. Sap Pressure in Vascular Plants: Negative hydrostatic pressure can be measured in plants. *Science* **148**: 339 - 346.

Serrano L, Peñuelas J, Ogaya R, Savé R. **2005**. Tissue-water relations of two co-occurring evergreen Mediterranean species in response to seasonal and experimental drought conditions. *Journal of Plant Research* **118**: 263 - 269.

Sevanto S, Nikinmaa E, Riikonen A, Daley M, Pettijohn JC, Mikkelsen TN, Phillips N, Holbrook NM. **2008**. Linking xylem diameter variations with sap flow measurements. *Plant and Soil* **305**: 77 - 90.

Shackel K, Lampinen B, Sibbett S, Olson W. **2000**. The relation of midday stem water potential to the growth and physiology of fruit trees under water limited conditions. *Acta Horticulturae* **537**: 425 - 430.

Smith BD. **2001**. Documenting plant domestication: the consilience of biological and archaeological approaches. *Proceedings of the National Academy of Sciences of the United States of America* **98**: 1324 - 1326.

Smith DM, Allen SJ. **1996**. Measurement of sap flow in plant stems. *Journal of Experimental Botany* **47**: 1833 - 1844.

Sperry JS, Adler FR, Campbell GS, Comstock JP. **1998**. Limitation of plant water use by rhizosphere and xylem conductance: results from a model. *Plant, Cell & Environment* **21**: 347 - 359.

Sperry JS, Hacke UG, Oren R, Comstock JP. **2002**. Water deficits and hydraulic limits to leaf water supply. *Plant, Cell & Environment* **25**: 251 - 263.

Sperry JS, Tyree MT. **1988**. Mechanism of water stress-induced xylem embolism. *Plant Physiology* **88**: 581 - 587.

Sperry JS. **2000**. Hydraulic constraints on plant gas exchange. *Agricultural and Forest Meteorology* **104**: 13 - 23.

Stahlberg R, Van Volkenburgh E, Cleland RE. **2001**. Long-distance signaling within *Coleus × hybridus* leaves; mediated by changes in intra-leaf CO_2? *Planta* **213**: 342 - 351.

Steppe K, De Pauw DJW, Lemeur R, Vanrolleghem PA. **2006**. A mathematical model linking tree sap flow dynamics to daily stem diameter fluctuations and radial stem growth. *Tree Physiology* **26**: 257 - 273.

Steudle E. **2001**. The Cohesion-Tension mechanism and the acquisition of water by plant roots. *Annual Review of Plant Physiology and Plant Molecular Biology* **52**: 847 - 875.

Strugger S. **1943**. Der aufsteigende saftstrom in der pflanze. *Naturwissenschaften* **31**: 181 - 194.

Taiz L, Zeiger E. **2010**. *Plant physiology*. Fifth Edition. Sinauer Associates, Inc., Sunderland, Massachusetts, USA.

Tardieu F, Davies WJ. 1992. Stomatal response to ABA is a function of current plant water status. *Plant Physiology* **98:** 540 - 545.

Tardieu F, Simonneau T. 1998. Variability among species of stomatal control under fluctuating soil water status and evapo- rative demand: modelling isohydric and anisohydric behaviours. *Journal of Experimental Botany* **49:** 419 - 432.

Testi L, Villalobos FJ, Orgaz F, Fereres E. **2006**. Water requirements of olive orchards: I simulation of daily evapotranspiration for scenario analysis. *Irrigation Science* **24**: 69 - 76.

Teviotdale BL, Goldhamer DA, Viveros M. **2001**. Effects of deficit irrigation on hull rot disease of almond trees caused by *Monilinia fructicola* and *Rhizopus stolonifer*. *Plant Disease* **85**: 399 - 403.

Tognetti R, Giovannelli A, Lavini A, Morelli G, Fragnito F, d'Andria R. **2009**. Assessing environmental controls over conductances through the soil-plant-atmosphere continuum in an experimental olive tree plantation of southern Italy. *Agricultural and Forest Meteorology* **149**: 1229 - 1243.

Tomlinson KW, Poorter L, Sterck FJ, Borghetti F, Ward D, de Bie S, van Langevelde F. **2013**. Leaf adaptations of evergreen and deciduous trees of semi-arid and humid savannas on three continents (H Cornelissen, Ed.). *Journal of Ecology* **101**: 430 - 440.

Torrecillas A, Ruiz-Sánchez MC, del Amor F, León A. **1988**. Seasonal variations on water relations of *Amygdalus communis* L. under drip irrigated and non irrigated conditions. *Plant and Soil* **106**: 215 - 220.

Torres-Ruiz JM, Diaz-Espejo A, Morales-Sillero A, Martín-Palomo MJ, Mayr S, Beikircher B, Fernández JE. **2013a**. Shoot hydraulic characteristics, plant water status and stomatal response in olive trees under different soil water conditions. *Plant and Soil* **373**: 77 - 87.

Torres-Ruiz JM, Diaz-Espejo A, Perez-Martin A, Hernandez-Santana V. **2013b**. Loss of hydraulic functioning at leaf, stem and root level and its role in the stomatal behavior during drought in olive trees. *Acta Horticulturae* **991**: 333 - 339.

Tyerman SD, Tilbrook J, Pard C, Kotula L, Sullivan W, Steudle E. **2004**. Direct measurement of hydraulic properties in developing berries of *Vitis vinifera* L. cv. Shiraz and Chardonnay. *Australian Journal of Grape and Wine Research* **10**: 170 - 181.

Tyree MT, Cochard H, Cruizat P, Sinclair B, Ameglio T. **1993**. Drought-induced leaf shedding in walnut: evidence for vulnerability segmentation. *Plant, Cell and Environment* **16**: 879 - 882.

Tyree MT, Dixon MA. **1986**. Water stress induced cavitation and embolism in some woody plants. *Physiologia Plantarum* **66**: 397 - 405.

Tyree MT, Vargas G, Engelbrecht BMJ, Kursar TA. **2002**. Drought until death do us part: a case study of the desiccation-tolerance of a tropical moist forest seedling-tree, *Licania platypus* (Hemsl.) Fritsch. *Journal of Experimental Botany* **53**: 2239 - 2247.

Tyree MT, Zimmerman MH. **2002**. Xylem Structure and the Ascent of Sap. Springer, New York, 304 pp.

USDA. 2010. Keys to soil taxonomy (11th Edition). United States Department of Agriculture, Natural Resource Conservation Service, 334.

Vico G, Porporato A. **2008**. Modelling C3 and C4 photosynthesis under water-stressed conditions. Plant and Soil 313, 187–203.

Villalobos FJ, Orgaz F, Mateos L. **1995**. Non-destructive measurement of leaf area in olive (*Olea europaea* L.) trees using a gap inversion method. *Agricultural and Forest Meteorology* **73**: 29 - 42.

Warren CR, Dreyer E. **2006**. Temperature response of photosynthesis and internal conductance to CO_2: results from two independent approaches. *Journal of Experimental Botany* **57**: 3057 - 3067.

Westhoff M, Reuss R, Zimmermann D, Netzer Y, Gessner A, Gessner P, Zimmermann G, Wegner LH, Bamberg E, Schwartz A, Zimmermann U.

2009. A non-invasive probe for online-monitoring of turgor pressure changes under field conditions. *Plant Biology* **11**: 701 - 712.

Wistuba N, Reich R, Wagner H-J, Zhu JJ, Schneider H, Bentrup F-W, Haase A, Zimmermann U. **2000**. Xylem Flow and its Driving Forces in a Tropical Liana: Concomitant Flow-Sensitive NMR Imaging and Pressure Probe Measurements. *Plant Biology* **2**: 579 - 582.

Woodward FI. **1998**. Do plants really need stomata? *Journal of Experimental Botany* **49**: 471 - 480.

Xu S-M, Liu L-X, Woo KC, Wang D-L. **2007**. Changes in photosynthesis, xanthophyll cycle, and sugar accumulation in two North Australia tropical species differing in leaf angles. *Photosynthetica* **45**: 348 - 354.

Yao C, Moreshet S, Aloni B. **2001**. Water relations and hydraulic control of stomatal behaviour in bell pepper plant in partial soil drying. *Plant, Cell & Environment* **24:** 227 - 235.

Zeder MA. **2008**. Domestication and early agriculture in the Mediterranean Basin: origins, diffusion, and impact. *Proceedings of the National Academy of Sciences of the United States of America* **105**: 11597 - 11604.

Zimmermann D, Reuss R, Westhoff M, Gessner P, Bauer W, Bamberg E, Bentrup F-W, Zimmermann U. **2008**. A novel, non-invasive, online-monitoring, versatile and easy plant-based probe for measuring leaf water status. *Journal of Experimental Botany* **59**: 3157 - 3167.

Zimmermann D, Westhoff M, Zimmermann G, Gessner P, Gessner A, Wegner LH, Rokitta M, Ache P, Schneider H, Vásquez JA, *et al.* 2007. Foliar water supply of tall trees: evidence for mucilage-facilitated moisture uptake from the atmosphere and the impact on pressure bomb measurements. *Protoplasma* **232**: 11 - 34.

Zimmermann U, Rüger S, Shapira O, Westhoff M, Wegner LH, Reuss R, Gessner P, Zimmermann G, Israeli Y, Zhou A, *et al.* 2009. Effects of environmental parameters and irrigation on the turgor pressure of banana plants measured using the non-invasive, online monitoring leaf patch clamp pressure probe. *Plant Biology* **12**: 424 - 436.

Zimmermann MH. **1983**. Xylem Structure and the Ascent of Sap. Springer, Berlin.

Zimmermann U, Schneider H, Wegner LH, Haase A. **2004**. Water ascent in tall trees: does evolution of land plants rely on a highly metastable state? *New Phytologist* **162**: 575 - 615.

Zufferey V, Cochard H, Ameglio T, Spring J-L, Viret O. **2011**. Diurnal cycles of embolism formation and repair in petioles of grapevine (*Vitis vinifera* cv. Chasselas). *Journal of Experimental Botany* **62**: 3885 - 3894.

Zweifel R, Item H, Häsler R. **2000**. Stem radius changes and their relation to stored water in stems of young Norway spruce trees. *Trees* **15**: 50 - 57.

Zweifel R, Item H, Häsler R. **2001**. Link between diurnal stem radius changes and tree water relations. *Tree Physiology* **21**: 869 - 877.